Parametric Investigation of Flow-Sound Interaction Mechanism of Circular Cylinders in Cross-Flow

by

Omar Afifi

A Thesis Submitted in Partial Fulfillment of the Requirements
for the Degree of

Masters of Applied Science in Mechanical Engineering

Faculty of Engineering and Applied Science

University of Ontario Institute of Technology

December, 2016

Abstract

Flow-excited acoustic resonance in heat exchangers has been an ongoing issue for the past century. The main challenge in this issue, is in the actual prediction of the resonance occurrence. This is due to the complexity of the flow-sound interaction mechanism that takes place between the packed cylinders. Most of the research lately has therefore shifted focus to simpler geometries that resemble the same mechanisms of flow-sound interaction found in actual heat-exchangers. The research presented hereafter summarizes an extensive experimental parametric work performed on multiple simple configurations such as single, tandem and side-by-side cylinders in cross-flow. The main objective of the research is to identify the critical parameters that should be included in the damping criteria to reliably predict the occurrence of acoustic resonance in tube bundles. Special attention is given to the geometrical characteristics of the duct (i.e. cross-sectional area) and how they affect the acoustic resonance. To achieve this; more than one hundred experiments have been performed in three different wind-tunnels of different cross-sectional areas. The research is motivated by the fact that most of the criteria developed to date, fail to predict the destructive phenomena of acoustic resonance in 30-40% of the cases.

I would like to dedicate this thesis to my super parents,

Dr. Marwa & Dr. Mohamed,

and my beloved siblings

Dr. Salma & Amjad

Without your support and love, I would not have been where or who I am today

Please forgive me for what I have done to you, as I have definitely made your lives harder with my selfish decisions

May God protect you and fill your lives with happiness

Acknowledgments

First and foremost, I would like to extend a deep and sincere acknowledgment to my supervisor Dr. Atef Mohany, for his continuous support and mentorship throughout the time-frame of this work and well before. Thank you for accepting me to work under your supervision during my undergraduate and graduate academic years. I learned a lot from your expertise every single day.

Secondly, I would like to thank the research team and the head of the Aeroacoustics and Noise Control Laboratory (ANCL) at the University of Ontario Institute of Technology for their continuous help and support in every stage of this research.

Thirdly, I would like to thank all my colleagues and friends; Nadim, Mahmoud, Moamen, Mohamed, Omar, Bashar, Maged, Mirai, Mirna, Hammad and Mina for their continuous academic and moral support. Thank you all for your help and friendship, and thank you for taking the time to listen to me talking about my problems. Without this support, I would not have been able to finish my Masters.

Moreover, I would like to also thank Mr. Hidayat Shahid from the Faculty of Engineering and Applied Science at the University of Ontario Institute of Technology, for his technical support and for allowing me to borrow some of the hardware that I have used. Lastly, I would like to acknowledge the financial support provided by the Natural Sciences and Engineering Research Council (NSERC), which helped in the successful completion of this work.

Table of Contents

Acknowledgments iv

Table of Contents v

List of Tables ix

List of Figures x

Nomenclature xix

Chapter 1 1

1 Introduction 1

1.1 Motivation 1

1.2 Scope of Work and Objectives 3

1.3 Novelty and Contribution 4

1.4 Thesis Outline 5

Chapter 2 6

2 Literature Review 6

2.1 Flow Over Single Cylinder 6

2.1.1 Vortex Formation and Flow Regions 6

2.1.2 Strouhal Number 7

2.1.3 Reynolds Number 9

2.1.4 Relationship Between Strouhal Number and Reynolds Number 12

2.2 Flow Over a Pair of Cylinders 18

2.2.1 Wake Interference and Flow Patterns 19

2.2.2 Flow Patterns: Tandem Cylinders 21

2.2.3 Flow Patterns: Side-by-Side Cylinders 25

2.2.4 Strouhal Number: Tandem Cylinders 26

2.2.5 Strouhal Number: Side-by-Side cylinders 30
2.3 Aerodynamic Noise 31
2.4 Flow-excited Acoustic Resonance 36
2.4.1 Duct Acoustics 37
2.4.2 Acoustic Damping/Attenuation in Ducts 38
2.4.3 Flow-excited Acoustic Resonance: Single Cylinder 43
2.4.4 Flow-excited Acoustic Resonance: Tandem Cylinders 48
2.4.5 Flow-exited Acoustic Resonance: Side-by-Side Cylinders 50
2.4.6 Damping Criteria in Tube Bundles of Heat Exchangers 55
2.5 Summary and Research Needs 69
Chapter 3 71
3 Experimental Setup & Methodology 71
3.1 Experimental Setup 71
3.2 Experiments Design 76
3.3 Data Acquisition and Instrumentation 79
3.3.1 Data Acquisition 79
3.3.2 Instrumentation 80
3.4 Experimental Procedure 84
Chapter 4 85
4 Aeroacoustic Response of Single Cylinder in Cross-Flow 85
4.1 Introduction 85
4.2 Typical Response 87
4.3 Single Cylinder at Centerline (Y/H = 0) 92
4.3.1 Effect of Diameter 92
4.3.2 Effect of Height 98

4.3.3 Effect of Blockage Ratio (D/H) 101
4.3.4 Comparison with the Literature 106
4.3.5 Analogy Between Mechanical & Acoustic Systems 109
4.3.6 Damping of The Acoustic Systems 114
4.3.7 Effect of the Constant Parameters on the Acoustic Damping 116
4.3.8 Normalization Scheme and Important Scaling Parameters 119
4.4 Single Cylinder Shifted from Centerline (Y/H = 0.25) 121
4.4.1 Effect of Location 121
4.4.2 Effect of Height 128
4.4.3 Effect of Blockage Ratio (D/H) 130
4.4.4 Comparison with the Literature 132
4.5 Special Case: Isolated Cylinders (Y/H = -0.25 and 0.25) 133
4.5.1 Effect of Diameter and T/D 137
4.6 Conclusion 139
Chapter 5 141
5 Aeroacoustic Response of Tandem Cylinders in Cross-Flow 141
5.1 Introduction 141
5.2 Typical Response 144
5.3 Origin of Pre-Coincidence Resonance 148
5.4 Effect of Reynolds Number on Strouhal Number 150
5.5 Effect of Diameter and Height on Pre-Coincidence Resonance 151
5.6 Effect of Height on Intensity of Resonance 161
5.7 Effect of Blockage Ratio (D/H) 165
5.8 Comparison with the Literature 168
5.9 Conclusion 171

Chapter 6 174

6 Conclusions & Recommendations 174

6.1 Conclusions 174

6.2 Future Work and Recommendations 176

References 178

List of Tables

Table 1 : Approximation for visco-thermal attenuation in ducts, English (2010)..... 41

Table 2 : Comparison of Strouhal number, velocity at resonance and sound pressure level for single cylinder cases in duct height 203mm (8”) 96

List of Figures

Figure 2-1 : Flow regions of disturbed flow as suggested by Zdravkovich (1997)..... 7

Figure 2-2 : Regimes of flows around cylinders in cross-flow, Lienhard (1966)..... 11

Figure 2-3 : The setup used by Relf (1921) for water experiments..... 12

Figure 2-4 : The setup used by Relf (1921) for air experiments..... 13

Figure 2-5 : Relationship between the dimensionless parameters for the water and air experiments, Relf (1921) 14

Figure 2-6 : Results obtained for different diameters (Kovàsznay, 1949)..... 15

Figure 2-7 : Strouhal number and Reynolds number relationship (Roshko, 1961)..... 16

Figure 2-8 : Schematic of free shear layers past a cylinder in cross-flow 17

Figure 2-9 : Schematic of tandem, side-by-side and staggered configurations 18

Figure 2-10 : Classifications of interference regions, Zdravkovich (1985)..... 20

Figure 2-11 : Classifications of interference regions II, (Zdravkovich 1987) 20

Figure 2-12 : Flow patterns classifications, Igarashi (1981)..... 23

Figure 2-13 : Flow patterns sketch, Igarashi (1981) 24

Figure 2-14 : PIV image of two side-by-side cylinders at different spacing ratios a) T/D = 1.5, b) T/D = 2.0. a) shows the biased flow pattern behavior, Sumner D. et al. (1999b) . 26

Figure 2-15 : Classification of flow Regimes in side-by-side and tandem arrangements for stationary cylinders, Zdravkovich (1985) 26

Figure 2-16 : Strouhal number map for two tandem smooth cylinders, Okajima (1979). 28

Figure 2-17 : Igarashi map for Strouhal number for tandem configuration, Igarashi (1981) 29

Figure 2-18 : Strouhal number data for two side-by-side cylinders at different pitch-to-diameter ratios and at different Reynolds number ratios from 55 – 2.8 x 10^4, Sumner (2010) 30

Figure 2-19 : Directivity pattern, in far field of a compact dipole, Blake (1986) 33

Figure 2-20 : Dipole sound fields due to fluctuating lift and drag on a cylinder in cross-flow, Etkins (1956) 35

Figure 2-21 : Schematic of a simple closed-closed duct geometry 37

Figure 2-22 :Dependency of sound attenuation on the pipe diameter and the Mach number for smooth pipes with turbulent flow , (a) predicted downstream attenuation coefficient , (b) Theoretically calculated upstream attenuation coefficient , Ingard and Singhal (1974) 40

Figure 2-23 : Comparison of measured damping coefficient at three different velocities compared to the theoretical prediction by Kirchhoff model, Golliard et al. (2013) 42

Figure 2-24 : Schematic of the coincidence between the acoustic cross-modes and the vortex shedding frequency for different arbitrary duct heights and diameters 44

Figure 2-25 : Typical aeroacoustic response for single bare cylinder, Mohany and Ziada (2005) 46

Figure 2-26 : Aeroacoustic response for tandem cylinders, Mohany and Ziada (2005) ... 50

Figure 2-27 : Out of phase vortex shedding from two tandem cylinders at large spacing ratio, off-resonance, Sumner (1999b) 52

Figure 2-28 : Schematic of the synchronized vortex shedding pattern at the wake of two side-by-side cylinders with large spacing ratios , at resonance conditions, Hanson et al. (2009) 52

Figure 2-29 : Aeroacoustic response of two side-by-side cylinders with spacing ratio of T/D = 1.25 and D = 21.8 mm for the first acoustic mode, Hanson et al. (2009) 53

Figure 2-30 : Comparison of the aeroacoustic responses of multiple cylinders, D = 12.7mm. Cylinders are positioned at the acoustic particle velocity antinodes, Arafa and Mohany (2015) 55

Figure 2-31 : Different theories proposed for tube bundles excitation mechanism , (a) Karman vortex streets shedding, Chen and Young (1968) (b) turbulent buffeting, Owen (1965) 56

Figure 2-32 : Comparison of data from X, Grotz and Arnold (1956), ▽, Fitzpatrick and Donaldson (1977) , +, Baylac et al. (1973) and o, Jaudet et al. (1971), with the damping criterion proposed by Grotz and Arnold (1956). The figure is taken from Fitzpatrick (1985). 60

Figure 2-33 : Comparison of data from X, Grotz and Arnold (1956), ▽, Fitzpatrick and Donaldson (1977) , +, Baylac et al. (1973) and o, Jaudet et al. (1971), with the damping criterion proposed by Chen (1968). Figure is taken from Fitzpatrick (1985) 61

Figure 2-34 : Revised Fitzpatrick criterion compared with data from X, Grotz and Arnold (1956), ▽, Fitzpatrick and Donaldson (1977) , +, Baylac et al. (1973) and o, Jaudet et al. (1971), with the damping criterion proposed by Chen (1968). Figure is taken from Fitzpatrick (1985) 62

Figure 2-35 : In-line tube-bundle criterion Ziada et al. (1989b) 64

Figure 2-36 : Staggered tube bundle criterion, Ziada et al. (1989b) 66

Figure 2-37 : comparison of input energy parameter proposed by Blevins with other parameters in literature, Fenestra et al. (2006) 69

Figure 3-1 : Isometric CAD view of the wind-tunnel assembly at the Aeroacoustics and Noise Control Laboratory (UOIT) 72

Figure 3-2 : Test section without the middle side windows 75

Figure 3-3 : Cylinder fixation inside the test section 75

Figure 3-4 : Bellmouth for one of the used test sections 76

Figure 3-5 : Typical data acquisition layout (courtesy of National Instruments) 79

Figure 3-6 : Outside and inside view of the insertion ports for the microphones 81

Figure 3-7 : Acoustic pressure amplitude measured from the top wall as a function of microphone position 82

Figure 4-1 : Schematic of the test section used showing the position of measurement devices as well as the acoustic pressure distributions inside the duct (all dimensions in mm) 87

Figure 4-2 : Typical pressure spectrum (frequency domain) at any arbitrary velocity (U) , where U is any velocity at off-resonance condition, D=28.5 mm (1”), H=305mm (12”), Y/H=0 88

Figure 4-3 : 3D waterfall plot, D = 28. 5 mm (1.125”), H = 305mm (12”) for Y/H=0 88

Figure 4-4 : Pressure response of single cylinder D = 10.5 mm (0.416”) , H = 254mm (10”), Y/H = 0 91

Figure 4-5 : Frequency response of single cylinder D = 10.5 mm (0.416”) , H = 254mm (10”), Y/H = 0 91

Figure 4-6 : Effect of diameter on acoustic pressure, H = 203mm (8”), Y/H = 0. 93

Figure 4-7 : Effect of diameter on the excitation frequency at resonance (numerical), H = 203 mm (8”), Y/H = 0. 94

Figure 4-8 : Effect of diameter on frequency response , H= 203 mm (8”), Y/H = 0..... 95

Figure 4-9 : Pressure drop measured across the cylinder over L = 504 (20”), H = 203 (8”), Y/H = 0. 97

Figure 4-10 : Coefficient of pressure over L = 504 (20”), H = 203 (8”), Y/H = 0. 97

Figure 4-11 : Acoustic response of a single cylinder in different test section height, D = 21.05mm (0.8”) 100

Figure 4-12 : Frequency response of a single cylinder in different duct heights D = 21.05mm (0.8”) 100

Figure 4-13 : Effect of height on acoustic pressure amplitude for small diameters, D = 15.9 mm (0.6") 101

Figure 4-14 : Schematic of duct mode frequency and vortex shedding frequencies 102

Figure 4-15 : Effect of blockage ratio (D/H) on the velocity at coincidence 104

Figure 4-16 : Pressure response for blockage ratio (D/H) of 6.25% 105

Figure 4-17 : Effect of blockage ratio (D/H) on the maximum acoustic pressure for single cylinder, 1st acoustic mode (Y/H = 0) 106

Figure 4-18 : Comparison with empirical formula related to duct geometry and dynamic head of the flow for 1st cross-mode, (Y/H = 0) 108

Figure 4-19 : Comparison with empirical formula related to input energy parameter, for 1st cross-mode, (Y/H = 0) 109

Figure 4-20 : schematic of a damped Mass-Damper-Spring (MDS) system 110

Figure 4-21 : Amplitude response as a function of the frequency ratio and amplification ratio 112

Figure 4-22 : Theoretical Kirchhoff damping coefficient (α) as a function of the frequency and duct height 115

Figure 4-23 : Effect of the speed of sound on the damping coefficient for the case of D = 0.5”, H = 10” (theoretical). 118

Figure 4-24 : Schematic of the test section showing relative position of cylinder away from centerline at Y/H = 0.25 122

Figure 4-25 : Acoustic pressure response of single cylinder at two different locations, D = 15.9 mm (0.6”) , H = 254 mm (10”) 124

Figure 4-26 : Frequency response of single cylinder at two different duct locations D = 15.9mm (0.6”), H = 254 mm (10”) 124

Figure 4-27 : Sound pressure levels of single cylinder at two different duct locations D = 15.9mm (0.6”), H = 254 mm (10”) 125

Figure 4-28 : Static pressure drop of single cylinder at two different duct locations D = 15.9mm (0.6”), H = 254 mm (10”) 126

Figure 4-29 : Static pressure drop of single cylinder at two different duct locations D = 15.9mm (0.6”), H = 305 mm (12”) 126

Figure 4-30 : Static pressure drop of single cylinder at two different duct locations D = 15.9mm (0.6”), H = 203 mm (8”) 127

Figure 4-31 : Acoustic pressure response of D = 12.7mm (0.5") in different duct heights 128

Figure 4-32 : Frequency response of D = 12.7mm (0.5") in different duct heights 129

Figure 4-33 : All diameters tested for location (Y/H = 0.25), 2nd mode..... 130

Figure 4-34 : Pressure response of D/H = 0.075 for different diameters and cylinders at Y/H = 0.25, 2nd mode..... 131

Figure 4-35 : Effect of blockage ratio (D/H) on the acoustic pressure response for single cylinders at Y/H = 0.25, 2nd mode 132

Figure 4-36 : Comparison with empirical formula related to input energy parameter for 2nd acoustic mode (Y/H = 0.25) 133

Figure 4-37 : Schematic of wind-tunnel for side-by-side experiment 134

Figure 4-38 : Pressure response of diameter 19 mm (0.75") in H = 305 mm (12") relative to the cylinder position in duct..... 136

Figure 4-39 : Frequency response of diameter 19 mm (0.75") in H = 305 mm (12") relative to the cylinder position in duct..... 136

Figure 4-40 : Pressure drop of diameter 19 mm (0.75") in H = 305 mm (12") relative to the cylinder position in duct..... 137

Figure 4-41 : Effect of diameter on acoustic pressure of side-by-side cylinders; H = 305 mm (12") 138

Figure 4-42 : Effect of diameter on frequency response of side-by-side cylinders , H = 305 mm (12") 139

Figure 5-1 : Schematic of cylinders in tandem arrangement (L) is the length between the center of the two diameters and (D) is the diameter of the cylinder. 142

Figure 5-2 : Pre-coincidence resonance for tandem configuration (D = 28.5mm , L/D = 2.0, H = 305mm) 145

Figure 5-3 : 3D waterfall plot of cylinders in tandem arrangement (D = 28.5mm , L/D = 2.0, H = 305mm) 145

Figure 5-4 : Pressure response of two tandem cylinders for D = 28.5mm , L/D = 2, H= 305mm 147

Figure 5-5 : Frequency response of two tandem cylinders for D = 28.5mm , L/D = 2, H= 305mm 147

Figure 5-6 : Strouhal numbers for pre-coincidence, coincidence, and vortex shedding. ■, St. number for pre-coincidence, ▲, St. number for coincidence, ○, St. number for vortex shedding, (Mohany and Ziada, 2005). ■, St. number for coincidence, ●, St. number for pre-coincidence, ♦, St. number for vortex shedding, Current study. All Strouhal numbers are based on the frequency of vortex shedding and the spacing (L) between the cylinders. 149

Figure 5-7 : Comparison between the sound pressure level for tandem cylinders with spacing ratio L/D = 2.0 and in-line tube bundles with X_L (L/D) = 2.0. ●, Ziada & Oengoren (1992) in-line tube bundle X_L = 2.0. ○, Current experiment L/D = 2.0, D = 25.4 mm, H = 305 mm.▲, Current experiment L/D = 2.0, D = 28.5mm, H = 305 mm. ▬, Current experiment L/D = 2.0, D = 21 mm, H = 254 mm. 150

Figure 5-8 : Effect of Reynolds number on the Strouhal number of vortex shedding from two tandem cylinders for spacing ratios of L/D = 1.5 and 2.0. ×, Igarashi (1981) L/D = 2.06. ▬, Mohany et al. (2005), L/D = 1.2. ●, Mohany et al. (2005), L/D = 2. 0. ▲, Current experiments L/D =2.0, H = 305mm. □, Current experiments L/D = 1.5, H = 254mm. 151

Figure 5-9 : Acoustic pressure response of two tandem cylinders D = 15.8 mm (0.625”) in H = 254 mm (10") - L/D = 1.5..... 154

Figure 5-10: Frequency response of two tandem cylinders D = 15.8 mm (0.625”) in H = 254 mm (10") - L/D = 1.5..... 154

Figure 5-11 : Acoustic pressure response of two tandem cylinders D = 25.4 mm (1”) in H = 254mm (10") - L/D = 1.5..... 155

Figure 5-12 : Frequency response of two tandem cylinders D = 25.4 mm (1”) in H = 254 mm (10") - L/D = 1.5..... 155

Figure 5-13 : Static Pressure Drop Across Tandem Cylinders at H = 254mm, L/D = 1.5 156

Figure 5-14 : Acoustic response of different cylinders in H = 245 mm (10") - L/D = 2.0 157

Figure 5-15 : Pressure response for D = 10.56 mm (0.416”) , H = 254 mm (10”), L/D = 2.0..... 159

Figure 5-16 : Frequency response for D = 10.56 mm (0.416”) , H = 254 mm (10”), L/D = 2.0..... 159

Figure 5-17 : Acoustic pressure response of two tandem cylinders D = 12.7 mm (0.5”) in H = 305mm (12") - L/D = 1.5..... 160

Figure 5-18 : Frequency response of two tandem cylinders D = 12.7 mm (0.5”) in H = 305mm (12") - L/D = 1.5..... 160

Figure 5-19 : Acoustic pressure response of diameter D = 19 mm (0.75") in different duct heights – L/D = 2.0 162

Figure 5-20 : Frequency response of diameter D = 19 mm (0.75") in different duct heights – L/D = 2.0 162

Figure 5-21 : Normalized acoustic pressure distribution for the first mode along the top wall of the duct , tandem cylinders of diameter D = 19 mm (0.75") , H = 203 mm (8") and 305 mm (12") - L/D = 1.5..... 164

Figure 5-22 : Acoustic response for D/H = 0.093 , L/D = 1.5, ▲, H = 305 mm (12”), ■, H = 203 mm (8”)..... 167

Figure 5-23 : Frequency response for D/H = 0.093 , L/D = 1.5, ▲, H = 305 mm (12”), ■, H = 203 mm (8”)..... 167

Figure 5-24 : Static pressure drop across the cylinders, for D/H = 0.093 , L/D = 1.5, ▲, H = 305 mm (12”), ■, H = 203 mm (8”) 168

Figure 5-25 : Comparison of tandem cylinder cases at L/D = 1.5 with the empirical formula suggested by Blevins and Bressler in terms of input energy parameter..... 170

Nomenclature

Letter Symbol	*Quantity*	*Dimension*
c	Speed of Sound	$m \cdot s^{-1}$
C_p	Pressure coefficient	[-]
D	diameter	m or mm
f	frequency	s^{-1}
I	sound Intensity	W/m^2
M	Mach number	[-]
P	pressure	$kg \cdot m^{-1} \cdot s^{-2}$
Pr	Prandtl number	[-]
Re	Reynolds number	[-]
St	Strouhal number	[-]
t	time	s
U	velocity	$m \cdot s^{-1}$

Greek Symbols

Letter Symbol	*Quantity*	*Dimension*
α	damping co-efficient	m^{-1}
γ	ratio of specific heats	[-]
ζ	mechanical damping ratio	[-]
μ	dynamic viscosity	$kg \cdot m^{-1} \cdot s^{-2}$
ν	kinematic viscosity	$m^2 s^{-1}$
ρ	density	$kg \cdot m^{-3}$
φ	phase angle	radian

Chapter 1

1 Introduction

1.1 Motivation

Bluff bodies in cross-flow tend to shed vortices in their wakes as a result of boundary layer separation. At certain conditions, vortex shedding could cause flow-induced vibrations and/or flow-excited acoustic resonance. Flow-excited acoustic resonance occurs when both the vortex shedding frequency from the enclosed body matches one or more of the natural acoustic frequencies of the enclosure (duct) and when the energy in the flow is high enough to overcome the acoustic damping of the system. The topic of flow-excited acoustic resonance in industrial applications has gained a lot of attention in the past century due to its harmful effects. In the past 70 years, a lot of this research was focused mainly on the flow-excited acoustic resonance occurrence in tube bundles of heat exchangers. Although preventive measures are always considered in industrial set-ups, there have been multiple numbers of incidents in which mechanical systems such as the tube bundles failed as a direct result of the flow-excited acoustic resonance.

Multiple damping criteria, to predict the occurrence of acoustic resonance in heat exchangers, have been developed over the past years. However, none of the proposed criteria to date is reliable in predicting the occurrence of flow-excited acoustic resonance in tube bundles. This is mainly due to the complexity of the flow-sound interaction

mechanism that occurs between the packed cylinders, as it involves many parameters, and is not yet fully understood, for the full-sized heat exchangers.

The flow-sound interaction mechanism from tandem cylinders is found to exhibit similar characteristics as the in-line tube bundles of heat exchangers, Mohany (2007). Therefore, many of the research have been focused on the simplified models of single, tandem and side-by-side cylinders to better understand the basic phenomena of flow-sound interaction mechanism before applying it to the full-sized heat exchangers. However, although the configurations of single, tandem and side-by-side cylinders in ducts are considered to be the *simplest* forms of tube-bundle-like configurations to study, the full characterization of flow-sound interaction mechanism for them is not yet possible and some gaps are still found in the literature even with the simplified models.

For example; all of the developed damping criteria focused on including the parameter of the spacing ratios between the cylinders as opposed to the diameters of the cylinders themselves in the damping criteria. However, just recently; a series of studies conducted by Mohany et al. (2005, 2009a, 2009b, 2011) have revealed that the excitation of the pre-coincidence acoustic resonance in two tandem cylinders, which is similar to the acoustic resonance in in-line tube bundles, depends significantly on the cylinder diameter and not just the spacing ratio between the cylinders (i.e. for a given spacing ratio when the cylinder diameter increases the pre-coincidence acoustic resonance appears).This means that the diameter, which was previously overlooked, is actually a very important parameter that needs to be included in any damping criterion for tube bundles.

Similarly, most of the work done in literature to investigate the flow-excited acoustic resonance from the simple cases of single, tandem and side-by-side cylinders seem to neglect the effect of the test section dimensions. Although it is very important to include the geometrical parameters since the test section dimensions (i.e. height and width) will affect the duct acoustic natural frequency, which will, in turn, affect the frequency of resonance, the acoustic noise radiated and the acoustic energy lost from the test section.

The experimental parametric work presented in this thesis is therefore motivated by the fact that the flow-sound interaction mechanism of the simplified models is not yet fully characterized. A lot of investigation in terms of both predicting the occurrence of acoustic resonance and estimating the magnitude of the acoustic pressure at resonance is still required. Fully understanding the mechanism of the flow-sound interactions in basic geometries and identifying the most important parameters that affect the mechanism can lead to the full understanding and characterization of the more complex configurations like full-size tube bundles.

1.2 Scope of Work and Objectives

The objective of this work is to perform a comprehensive parametric study to identify the effect of different parameters on the flow-sound interaction mechanism in simple configurations to further enhance the understanding of the flow-sound interaction in more complex geometries such as in tube bundles of heat exchangers. The objectives can, therefore, be summarized in the following main points: -

1. Investigate the effect of the duct height on the flow-sound interaction of circular cylinders in cross-flow for different configurations.

2. Investigate the effect of the location of cylinders in the duct on flow-sound interaction for different duct heights and different cylinder diameters.
3. Inspect the currently proposed prediction (damping) criteria to try and identify their shortcomings in terms of prediction of acoustic resonance as well as estimation of acoustic pressure amplitudes at resonance.
4. Identify the most important parameter(s) that affect the aeroacoustic response of cylinders in ducts

1.3 Novelty and Contribution

The work performed in this thesis provides a better understanding of the mechanism of flow-sound interaction for circular cylinders in cross-flow. The novelty of the work lies in the approach of the study as well as the design and number of experiments performed. The experimental design allowed for multiple different parameters, such as the height of the duct, the diameter of the cylinder, and the spacing ratios between the cylinders, to be isolated and tested independently for various configurations. The final results and conclusions show that the height of the duct is a very crucial parameter that has been over-looked in the past, and might be the reason why the prediction (damping) criteria fails to predict acoustic resonance excitation in some geometries. Further contributions of the work presented here can be summarized in the following key points.

1) It was shown that the height of the duct greatly affects the acoustic pressure amplitudes, because it changes the damping capacity of the system.

2) The relative location of the cylinder within the duct affects the aeroacoustic response of the system, and might excite different acoustic modes depending of the

location with respect to the acoustic particle velocity distribution. The effect of the duct height on the acoustic response is observed across all the modes.

3) The special cases of D/H for the single and tandem cylinders shows that scaling the acoustic pressure with the dynamic head of the flow ($0.5\ \rho\ U^2$) may be misleading. This is valid for single and tandem configurations.

4) The currently used damping (prediction) criteria overlooks the geometrical effect of the duct (i.e. the height), and including the damping as an exclusive parameter in the damping criteria should be done.

1.4 Thesis Outline

The remaining part of the thesis is divided into five main chapters. The second chapter is a literature review of the current state of science related to the topics covered in the thesis. The literature review covers three broad topics of vortex formation from single and multiple cylinders in cross-flow, the generation of aerodynamic sound, and flow-excited acoustic resonance in rectangular ducts. The third chapter provides an overview of the experimental setup used, as well as the methodology that was followed in performing the experiments. The fourth and fifth chapters discuss the main findings and results from the experiments performed. The main findings are compared with similar experiments and studies found in the literature. Lastly; a concluding chapter that outlines the main findings of the work and the recommendations for future studies in extension to this thesis.

Chapter 2

2 Literature Review

2.1 Flow Over Single Cylinder

2.1.1 Vortex Formation and Flow Regions

Bluff and streamlined bodies in cross-flow often experience fluid disturbances as a result of the fluid-solid interaction between the flowing fluid and the solid boundaries of the body. These disturbances vary in magnitude depending on the size, shape, and orientation of the body encountering the flow. The shape of the body greatly affects the mechanism by which the flow separates from the body surface. For instance; streamlined bodies such as airfoils tend to delay surface separation of the fluid compared to bluff bodies. The delayed separation results in weaker vortex shedding and turbulence in the wake. On the other hand, bluff bodies such as flat plates, triangular, and circular cylinders cause more oscillation and disturbances in the downstream flow. Mainly, the disturbance in the flow is characterized by the local velocity variations in magnitude, direction and time.

One of the simplest cases of fluid-solid interactions is a cylinder immersed in a fluid. The distribution of the disturbed flow regions around a cylinder as well as the velocity difference from the mainstream flow velocity at different regions is shown is **Figure 2-1**. The main four disturbed flow regions as suggested by Zdravkovich (1997) are; retarded flow region, boundary region attached to the cylinder surface, displaced and accelerated

flow region in the sideways direction, and separated flow or “wake” region. Vorticities, or eddies, are locally spiraling fluid motion. In turbulent flows, the vorticity is the main reason for relatively intense fluid motions and mixing, Blake (1986). Vorticity is mainly generated due to the high velocity and pressure gradients between the wake of the cylinder, and the upper and lower outside region. The velocity gradient forces the vorticity to initiate at the down crossing points of the upper and lower sides of the shear layer and then “roll-up” and progress downstream the cylinder. Additional velocity gradients induced to the system causes the vorticity perturbations to amplify, Williamson and Roshko (1988).

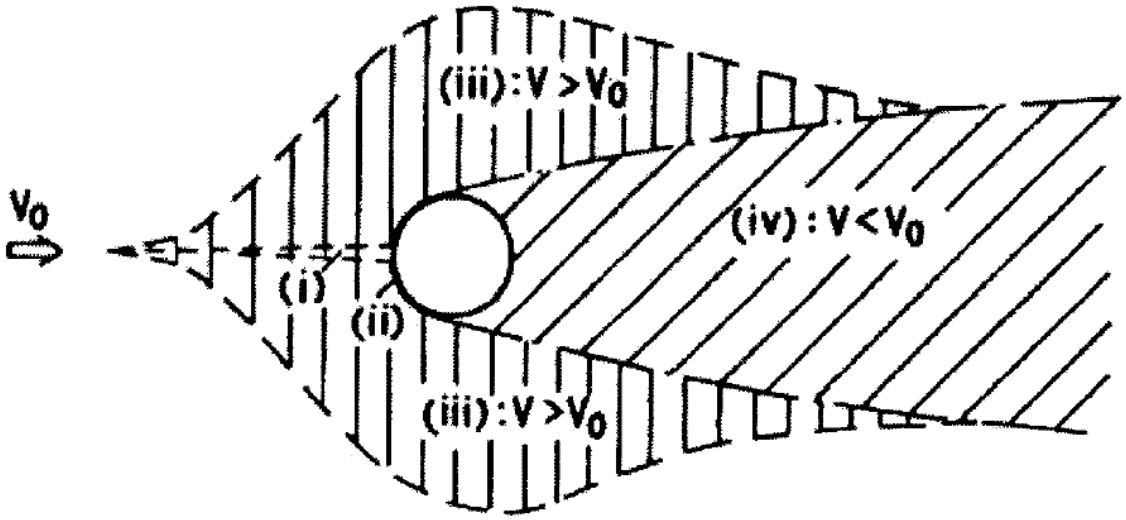

Figure 2-1 : Flow regions of disturbed flow as suggested by Zdravkovich (1997)

2.1.2 Strouhal Number

Vortex shedding from cylinders usually occurs in an oscillating and synchronized manner from the upper and lower separation points of the cylinder surface. The vortex shedding frequency depends on both the velocity of the oncoming fluid and the cylinder

diameter. A dimensionless parameter that describes this oscillating flow mechanism is the Strouhal number. The Strouhal number relates the vortex shedding frequency to the cross-flow velocity and the diameter of the cylinder according to **Equation 2.1**

$$\mathrm{St} = \frac{\mathrm{fl}}{\mathrm{U}} \tag{2.1}$$

where *f* is the frequency of vortex shedding, *L* is a characteristic length (such as diameter *D*) and *U* is the free-stream velocity. The physical representation of the Strouhal number can be interpreted as the ratio between the inertial forces due to flow instability to the velocity changes. The Strouhal number for a single cylinder in subcritical cross-flow has a constant value of 0.2 over a wide range of Reynolds number. For cylinders in tandem, side-by-side or staggered configurations, and rectangular or triangular shaped cylinders, the Strouhal number is not constant and depends on various factors such as the bluffness of the body and the Reynolds number of the flow.

Historically, the origin of the Strouhal number dates back to 1878, when Vincent Strouhal observed the Aeolian tones generated from hung wires due to air flow, Strouhal (1878). Strouhal altered many parameters of the wire such as the tension, length, diameter and material; however, he observed that the produced tones were only dependent on the wire diameter and the speed of the flow. The different tones produced resulted from the vortex shedding; though, at the time Strouhal concluded that only intuitively and did not formulate the relationship into its current format. Years after, studies performed by researchers like Kovàsznay (1949), Roshko (1961) and others further explored the different parameters in this relationship, and subsequently formulated the well-known Strouhal number in

Equation (2.1). The constant in the equation was named after the Czech physicist to honor his fundamental contributions.

2.1.3 Reynolds Number

Flow regimes or patterns over cylinders immersed in the fluid are characterized mainly by a dimensionless quantity called the Reynolds number (Re). Initially, the concept was introduced by George Gabriel Stokes in 1851 but was later adopted and popularized by Osborne Reynolds (1883). The physical interpretation of the Reynolds number is that it describes the ratio between the inertial forces to the viscous forces of the fluid. Reynolds number can be calculated as follows:

$$\mathrm{Re} = \frac{\rho \mathrm{UL}}{\mu} \qquad \textbf{(2.2)}$$

where ρ is the density of the fluid, U is the free-stream velocity, L is any characteristic length (diameter usually for a cylinder), μ is the dynamic viscosity of the fluid. Lienhard (1966) classified the major flow regimes expected in the wake of single cylinders, as shown in **Figure 2-2**, to the following :-

I. **Re < 5:** the flow is usually very slow and can be observed to almost stick to the surface of the cylinder. The flow is said to be creeping since the advection inertial fluid forces are very low compared to inertial forces and no separation occurs at the boundary layer of the cylinder.

II. **5-15 < Re < 40:** the steady separation region, where a pair of symmetric Föppl vortices can be observed symmetrically in the wake of the cylinder.

III. **40 < Re < 90 and 90 < Re <150:** periodic laminar region, in which two regimes of vortex street shedding are observed in the wake. The first range is governed by the wake instability while the second range is governed by the vortex shedding phenomena.

IV. **150 < Re < 300 & 300 < Re < 300,000:** this region is the transiting region between the laminar and the transient regions to the turbulent region. At the smaller range, the transition takes place to turbulent vortex shedding, while at the larger range the vortex shedding becomes fully turbulent.

V. **300,000 < Re < 3,500,000:** turbulence starts to be introduced to the actual boundary layer of the cylinder. This region is characterized by a narrower and more disorganized wake regions. No vortex streets appear in the wake of the cylinder in this range.

VI. **Re > 3,500,000:** in this region, the vortex streets start to appear again with a thinner wake. The boundary layer is fully turbulent and appears in a similar fashion to the vortex streets experienced in the range of 300 < Re < 300,000.

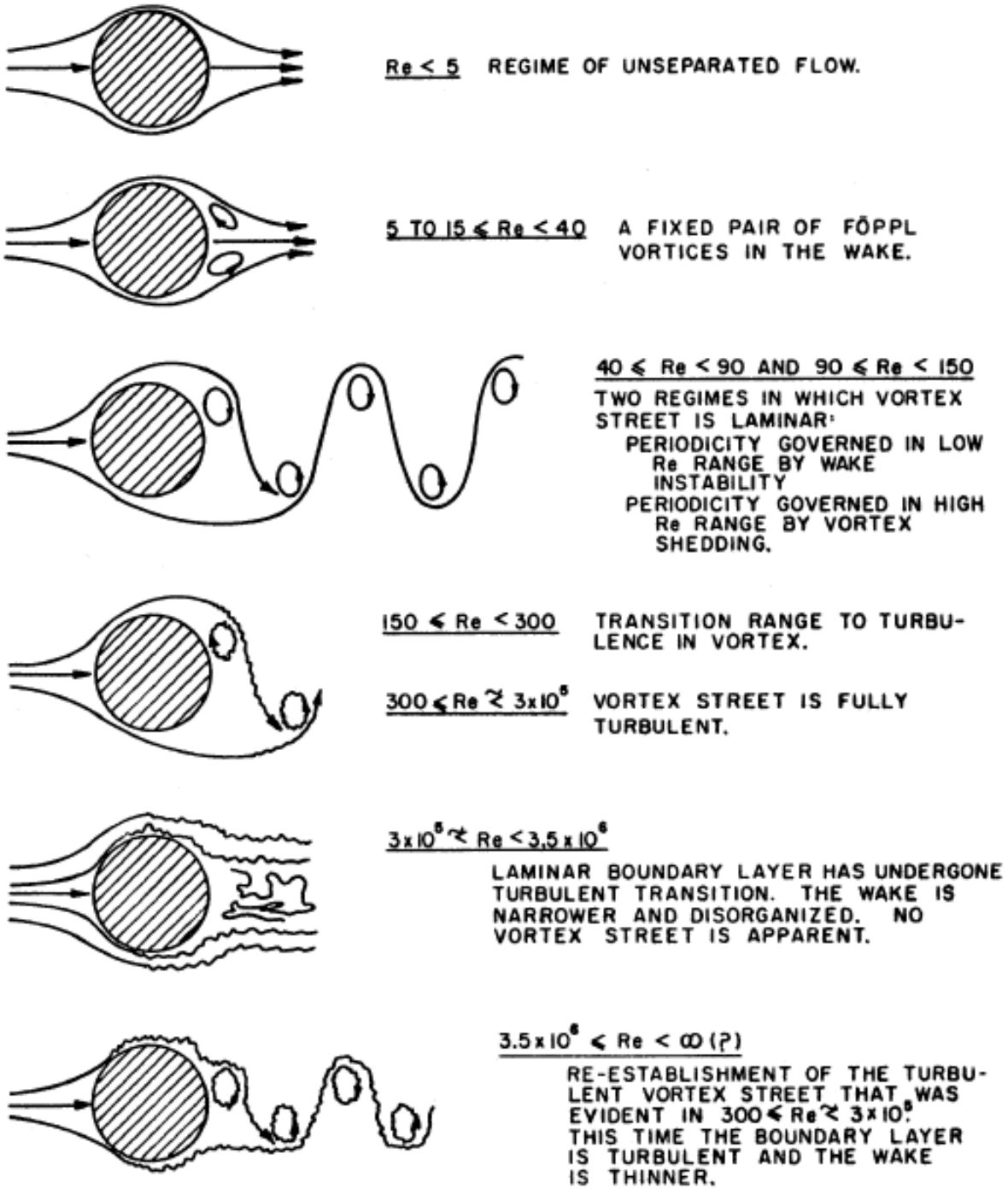

Figure 2-2 : Regimes of flows around cylinders in cross-flow, Lienhard (1966)

2.1.4 Relationship Between Strouhal Number and Reynolds Number

Since the work of Vincent Strouhal (1878) and John William Strut, Baron Rayleigh (1879), there has been a number of research considering the topic of noise generation from bluff bodies. The early studies conducted in the 1950s focused more on building upon what Strouhal had found; those studies focused on quantifying the generated sound and relating the sound parameters, (i.e. frequency), to flow quantities, (i.e. Strouhal and Reynolds numbers). The earliest of those studies, known to the reader, was a study performed by Relf (1921) to investigate the "musical tones" generated from circular wires. Relf performed two experiments to investigate the cause of the produced sound when wires were placed in a cross-flow. The first experiment was performed in a water test section (5x3"), with velocities of up to 1 inch/second, and with different cylinder diameters. The period of eddy formation (i.e. the frequency) was recorded using a fine piece of paper (3/16 in^2) that was fixed behind the cylinder with a fine strip of metal. The simple setup used is shown in **Figure 2-3.**

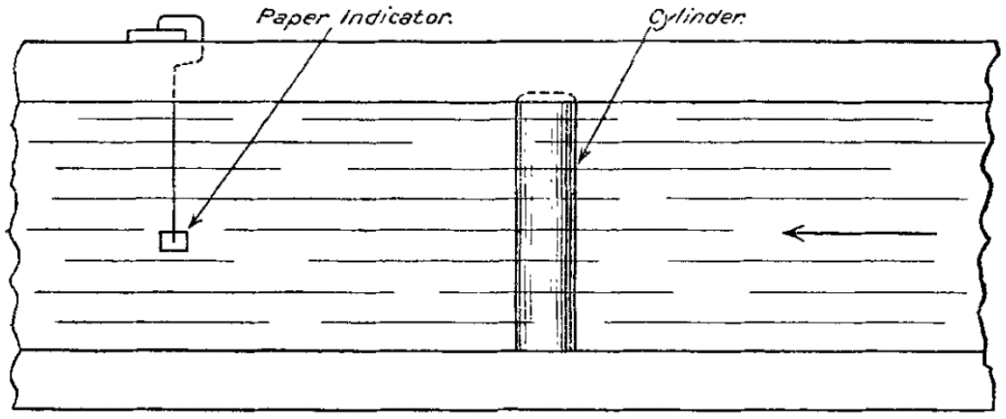

Figure 2-3 : The setup used by Relf (1921) for water experiments

A second similar experiment was performed on fine wires moving in an air medium. The wire was hung between two cross-pieces and attached to a shaft that moved using an electrical motor. When the motor rotated, the wire moved in a circular motion of known diameter. The velocity of the wire was correlated with the known rotational speed of the motor. **Figure 2-4** shows the setup used by Relf in performing the air experiments.

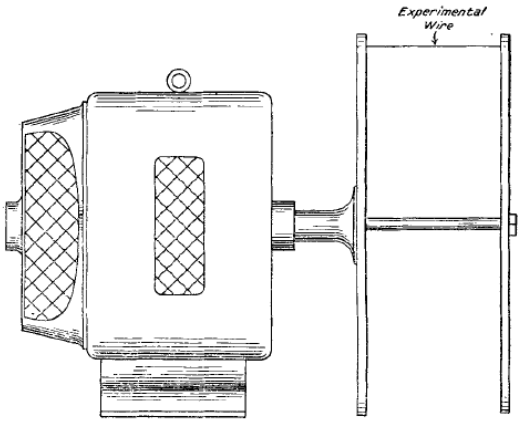

Figure 2-4 : The setup used by Relf (1921) for air experiments

Relf calculated the frequencies of the wire rotation and reported that they varied between 1000 and 4000 rotations per second. After applying dimensional analysis, he concluded that the frequency of the eddies is related to the wires diameter and the speed of rotation by **Equation 2.3**.

$$n = \frac{V}{D}\, f\, \left(\frac{VD}{\nu}\right) \qquad \textbf{(2.3)}$$

where n is the number of eddies formed per second, V is the velocity, D is the wire diameter, ν is the kinematic viscosity of the fluid, and f indicated a function that is yet to be identified.

The dimensionless quantities ($\frac{nD}{V}$, $\frac{VD}{\nu}$) were plotted against each other and the first Strouhal and Reynolds number relation was obtained. **Figure 2-5** shows the results of the Strouhal and Reynolds number calculated from the water and air experiments.

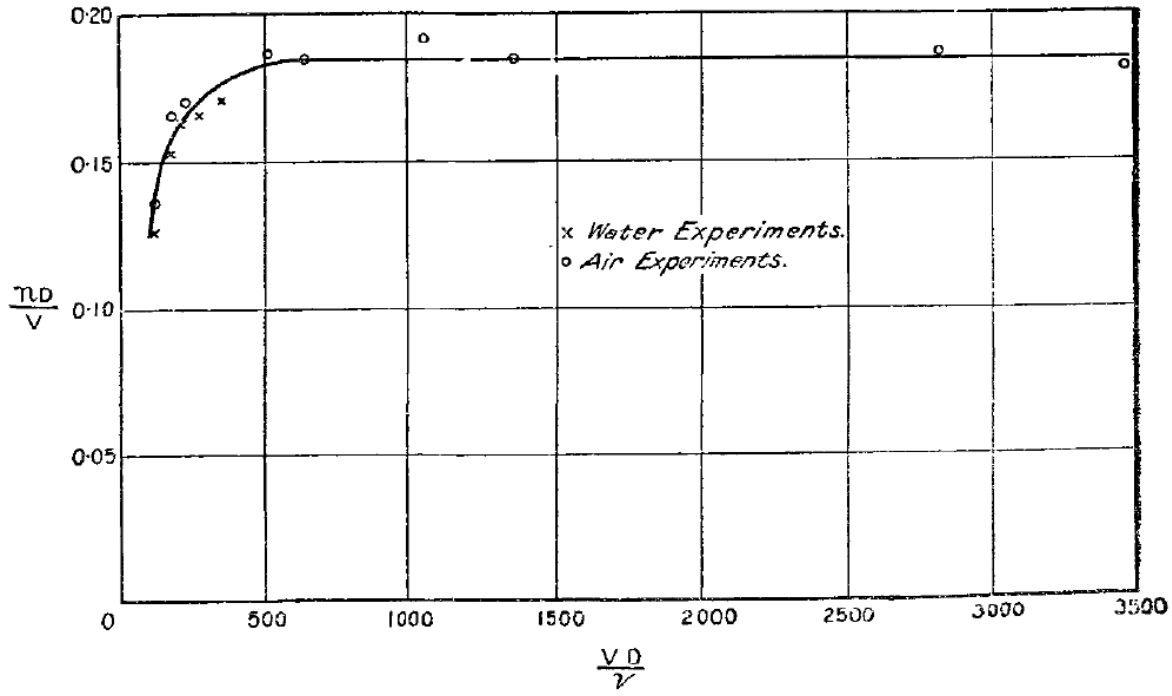

Figure 2-5 : Relationship between the dimensionless parameters for the water and air experiments, Relf (1921)

Relf found that all the results from the air and water experiments lied on a single graph. He reported that at values above *VD/v* = 500 the other quantity *nD/V* remained constant causing the frequency of the emitted noise to become directly proportional to the velocity of the medium and inversely proportional to the diameter of the wire.

Years after, Kovàsznay (1948) used a hot-wire anemometer to investigate the wake behind circular cylinders at low Reynolds numbers, and reported several key characteristics related to the flow. The results of the study were reported in terms of the dimensionless parameters

of Strouhal and Reynolds numbers for cylinders with different diameters ranging from *0.040* to *0.800* cm. **Figure 2-6** shows the results reported by Kovàsznay for different diameters tested.

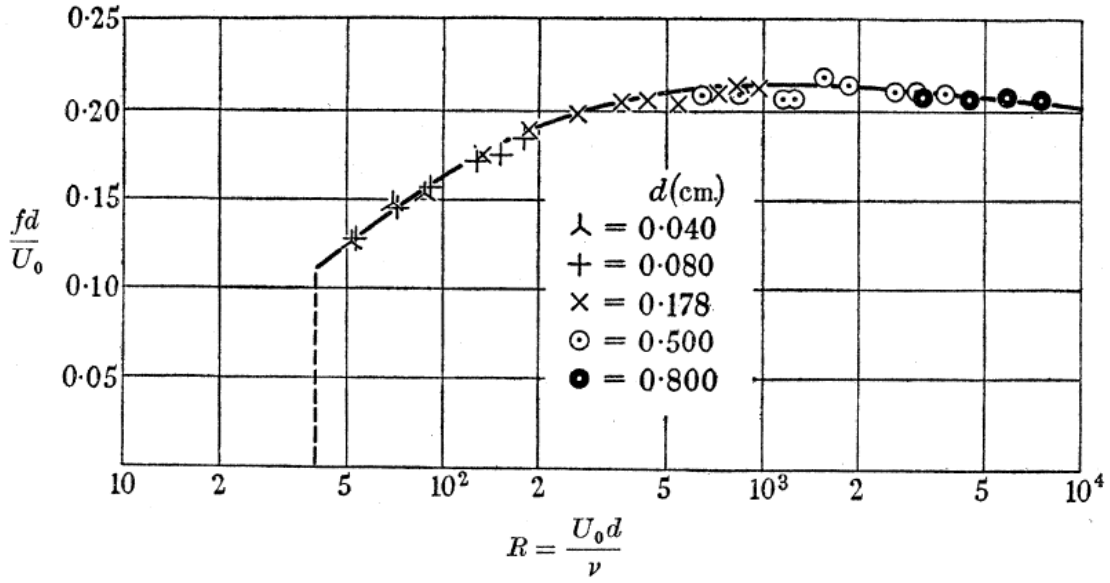

Figure 2-6 : Results obtained for different diameters (Kovàsznay, 1949)

Relf and Kovàsznay both concluded that there seems to be a strong relation between the Reynold and Strouhal numbers beyond a critical value for Reynolds number (Relf reported 500, while Kovàsznay reported 40). However, all experiments were performed in relatively low Reynolds number and the exact relation could not, yet, be characterized.

In 1954, Anatol Roshko performed a more extensive and generalized study on the wake development and velocity fluctuations behind circular cylinders using hot-wire measurements. Unlike previous studies, Roshko covered a wider range of Reynolds number (40 to 10,000). **Figure 2-7** shows Roshko's data in terms of Reynolds and Strouhal number.

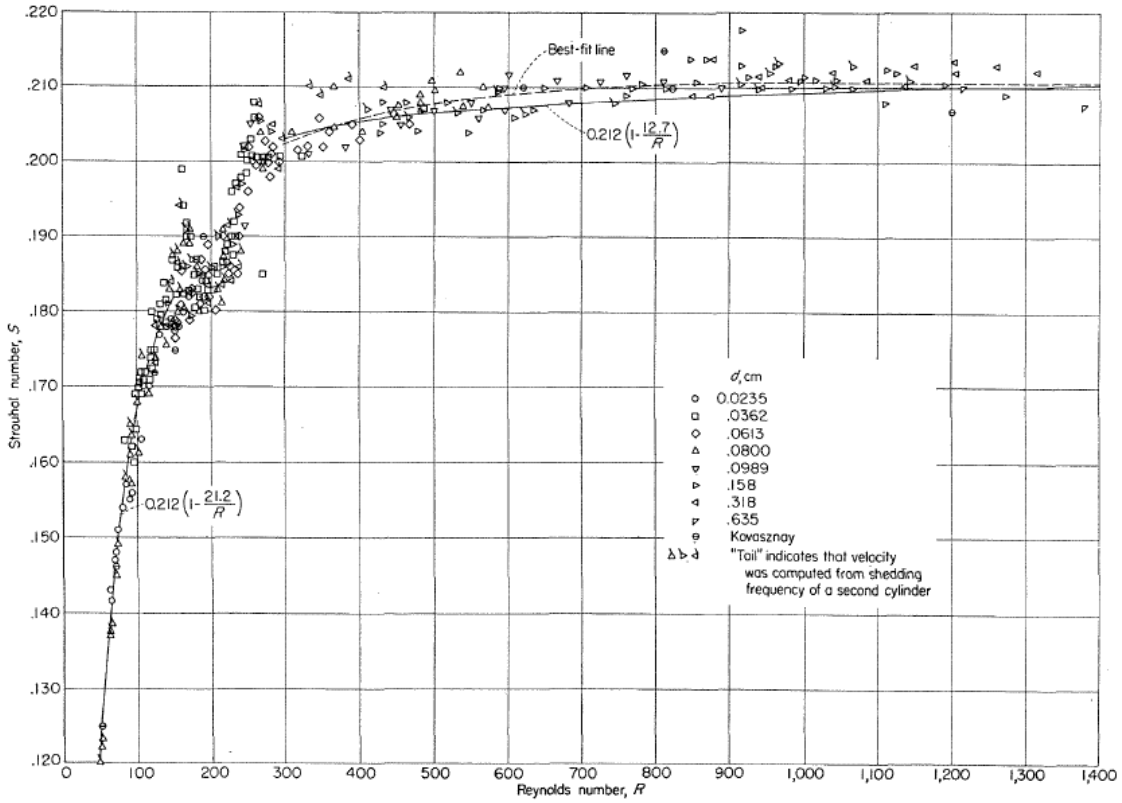

Figure 2-7 : Strouhal number and Reynolds number relationship (Roshko, 1961)

Roshko concluded that there exist two distinct vortex shedding regimes depending on the Reynolds number. A stable range *(40 < R < 150),* an irregular range *(300 < R < 10,000+)* and a mid-range that he called "transition range" *(150 < R <300).* The three distinct ranges had different features not only in nature of the velocity fluctuations but also in their Strouhal-Reynolds relationship. The stable region was characterized by stable vortex shedding and a linearly rising S(R) behavior. The irregular region was characterized by an irregular but detectable vortex shedding at a single frequency as well as a constant Strouhal number value. The transition range in between could not be characterized well as the frequency signal was highly irregular and unreadable, according to Roshko. Moreover, the Strouhal-Reynolds relation for the transition region was highly unstable. The unknown

nature of this range was used to explain the jump in the S(R) plot. Roshko concluded that the different behaviors of the three distinct regions suggest that there exist two distinct regimes of periodic wake phenomena, and a middle range that was deemed as a "transition range". Roshko defined the Strouhal numbers based on the Reynolds number for the two distinct regimes as follows:

$$S = 0.212\left(1 - \frac{21.2}{R}\right) 50 < R < 150 \qquad \textbf{(2.4a)}$$

$$S = 0.212\left(1 - \frac{12.7}{R}\right) 300 < R < 2{,}000 \qquad \textbf{(2.4b)}$$

Roshko also suggested a new, more generalized Strouhal number based on the distance (*d'*) between the free vortex layers instead of the diameter (*d*) of the cylinder. The new number was called the universal Strouhal number and gave it a value of S' = 0.28. **Figure 2-8** shows a schematic of the free shear layers past a cylinder in cross-flow with the proposed *d'* parameter.

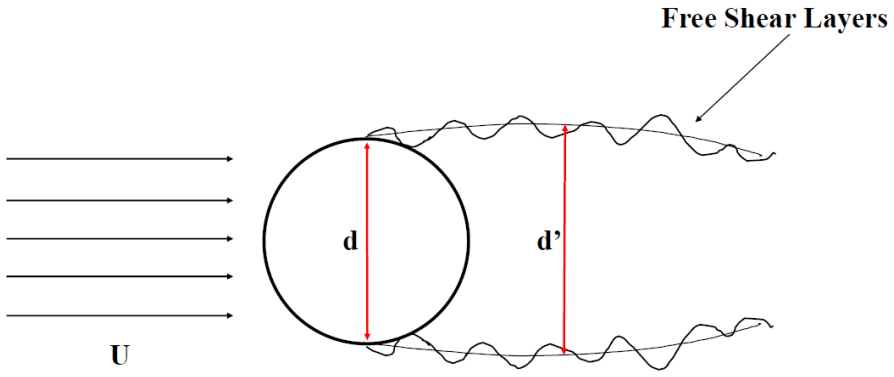

Figure 2-8 : Schematic of free shear layers past a cylinder in cross-flow

2.2 Flow Over a Pair of Cylinders

The Flow field and regimes around a pair of cylinders within the proximity of one another involves more complex interactions of flow separation, flow reattachment, vortex impingement, and vortex recirculation, Zhou, and Yiu (2006). The simplest configurations for pairs of cylinders in cross-flow are tandem, side-by-side and staggered.

A tandem configuration is when two cylinders are placed in-line parallel to the oncoming flow. Side-by-side configuration refers to two cylinders that are on top of each other, both facing oncoming flow. A staggered configuration refers to when both cylinders are at a relative angle between each other. The angle is between 0 degrees (tandem) and 90 degrees (side-by-side). The cylinders usually have equal diameters (D) and are separated by either center-to-center longitudinal spacing (L) for tandem configuration or center-to-center transverse spacing (T) for side-by-side arrangements. In analysis, the longitudinal and transverse spacing are usually non-dimensionalised by the diameter of the cylinders, and the terms longitudinal pitch ratio (L/D) and transverse pitch ratio (T/D) are used accordingly. **Figure 2-9** shows a schematic of the tandem, side-by-side and staggered configurations and the associated general nomenclature. Only the tandem and side-by-side configurations will be discussed in this literature review.

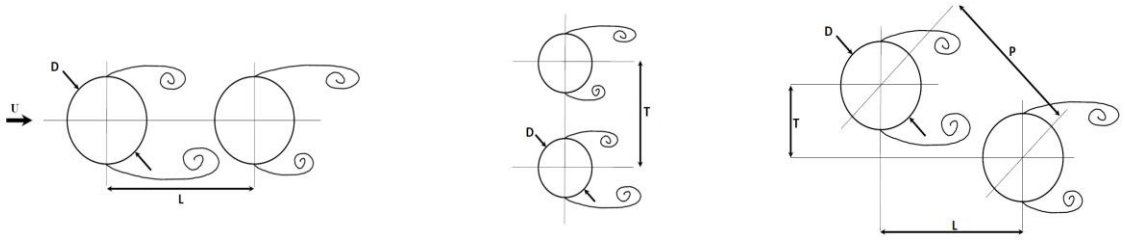

Figure 2-9 : Schematic of tandem, side-by-side and staggered configurations

Most of the studies in the literature are concerned with two cylinders of the same diameter However, some studies such as those performed by Hiwada et al (1979), Igarashi (1982), Lam et al. (1993), Alam and Zhou (2008), and others involved two cylinders of different diameters. For this thesis, tandem arrangements of equal diameters will be discussed. Topics covered in the literature review will be limited to studies most relevant to acoustic resonance and noise generation, thus discussion will be limited to topics of wake interference, flow regimes, vortex shedding, Strouhal number and the flow-excited acoustic resonance.

2.2.1 Wake Interference and Flow Patterns

Wake interference refers to the interaction between the wakes of two or more cylinders when they are within the vicinity of each other. The wake interference is a crucial concept, as it affects other important parameters such as the vortex shedding frequencies and the forces acting on the cylinders, which will, in turn, affect the noise radiated from the cylinders. Studies of wake patterns and vortex shedding behind pairs of rigid cylinders have been mainly conducted by Zdravkovich and Igarashi in the 1970s and 1980s. Studies involving cylinders under forced oscillations were also performed, examples are studies done by Mahir and Rockwell (1996a, 1996b).

Zdravkovich (1985, 1987), classified the fluid behavior and the wake interactions for two pairs of fixed cylinders in terms of the longitudinal and transverse pitch ratios. **Figure 2-10** shows a graphical map representation for the first classification proposed by Zdravkovich (1985). The proposed map can be interpreted for a tandem, side-by-side, and staggered pairs of cylinders.

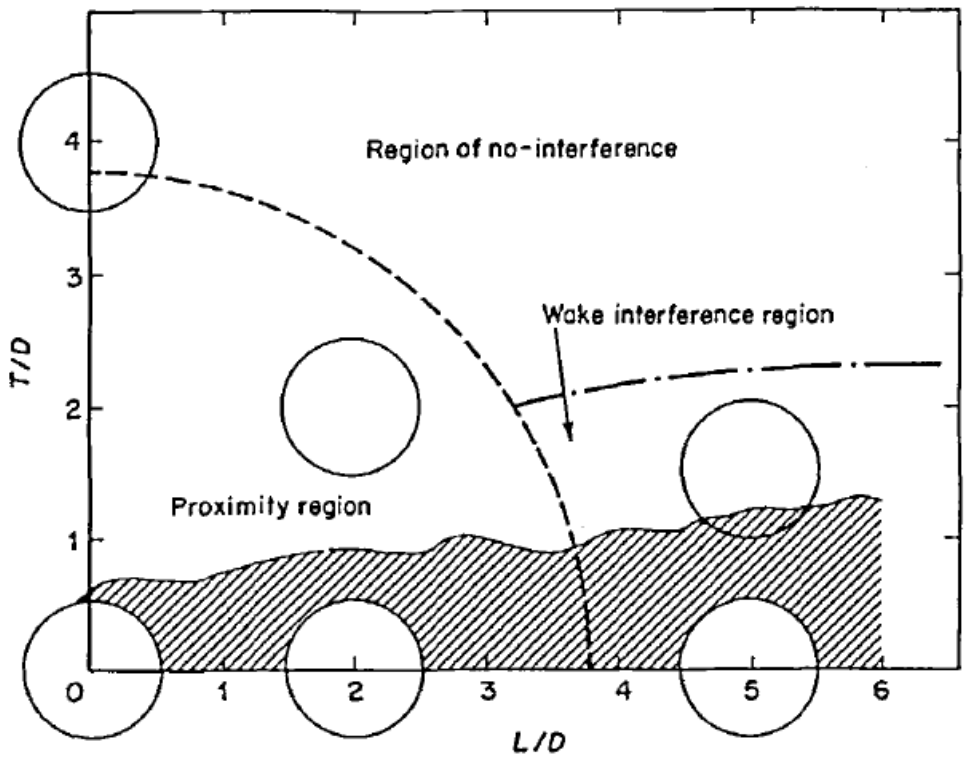

Figure 2-10 : Classifications of interference regions, Zdravkovich (1985)

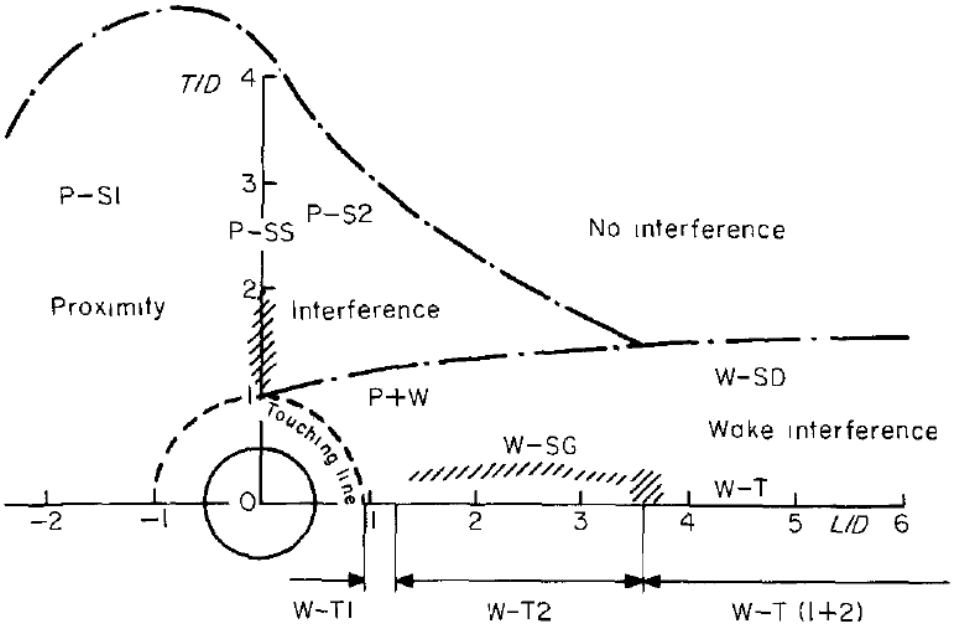

Figure 2-11 : Classifications of interference regions II, (Zdravkovich 1987)

Furthermore; in 1987 Zdravkovich proposed another, more detailed representation of the flow interferences (**Figure 2-11**). Zdravkovich classification can be summarized into four main regions; proximity interference region (P), wake interference region (W), P+W region, and no interference region. The first region is the proximity interference region (P) which occurs when the two cylinders are close to each other but none of them is totally submerged in the wake of the other. This region only applies for staggered and side-by-side configurations and is further classified into three sub-regions (P-SS, for side by side), (P-S1, for an upstream cylinder in staggered arrangements), (P-S2, for a downstream cylinder in staggered arrangement). The second region is the wake interference region (W) occurs when one cylinder is completely in the wake of the other cylinder. The wake interference region applies for the tandem and staggered configurations and is further classified into two sub-regions (W-T, for tandem) and (W-S, for staggered). The third region is the combination of proximity and wake regions (P+W), it consists of a mixture of the two regions and is characterized by extreme variations in magnitudes of the forces acting on the cylinders. This region applies for a tandem, side-by-side and staggered configurations. The fourth region is the no interference region; which refers to the region where the interference between the cylinders' wakes is negligible. Wakes from the cylinders in this region are identical to wake structure experienced for single cylinders.

2.2.2 Flow Patterns: Tandem Cylinders

The flow patterns around the tandem cylinders are highly dependent on the longitudinal spacing ratio (L/D) between the two cylinders and the Reynolds number. The two fundamental classifications proposed by Zdarvkovich (1985) and Igarashi

(1981,1982), will be presented here. Recently, some researchers have also proposed flow patterns classifications such as Zhou and Yiu (2006).

Igarashi (1981) performed an excellent research regarding the characteristics of flow around two tandem cylinders, of equal diameters. Flow visualization using smoke and force measurements were done on a wide set of tandem cylinders. The Reynolds number for the study varied between 8700 to 52000 and the longitudinal spacing ratios were varied between the ranges of $1.03 \leq L/D \leq 5.0$. Igarashi found that up to the spacing ratio of L/D = 3.5, the changes in the flow structure were observed at discrete spacing ratios of L/D = 1.1, 1.6, 2.3 and 3.1. The dependency of the regimes on the Reynolds number was observed only in the range of $1.1 \leq L/D \leq 2.0$.

Figure 2-12 shows the proposed flow patterns classifications, as a function of the spacing ratio (L/D) and the Reynolds number. **Figure 2-13** shows the sketches associated with each pattern. The seven recognized patterns behaviors are summarized as follows: -

1. **Pattern A:** no reattachment of the separated shear layers from the upstream cylinder, on the downstream cylinder, occurs, and the two cylinders act more as a single cylinder with a slender shape.
2. **Pattern B:** Synchronized shear layer vortex formation and vortex shedding on to the near wake of the downstream cylinder is observed, with a constant frequency regardless of the velocity.
3. **Pattern C:** quasi-static vortices are formed in the gaps between the cylinders.
4. **Pattern D:** unstable and random vortices start to appear and vortex shedding becomes more detectable.

5. **Pattern E:** bi-stable flow pattern is observed, where the separated shear layer from the upstream cylinder rolls up in front of the downstream one. This region is considered a transitional region between patterns D and F.
6. **Pattern E'**: a bi-stable flow similar to that observed in (E) remains for a longer period of time.
7. **Pattern F:** full-vortices are formed and completely rolled up in front of the downstream cylinder
8. **Pattern G:** a transition pattern of unstable flow between the patterns of A, B, and C.

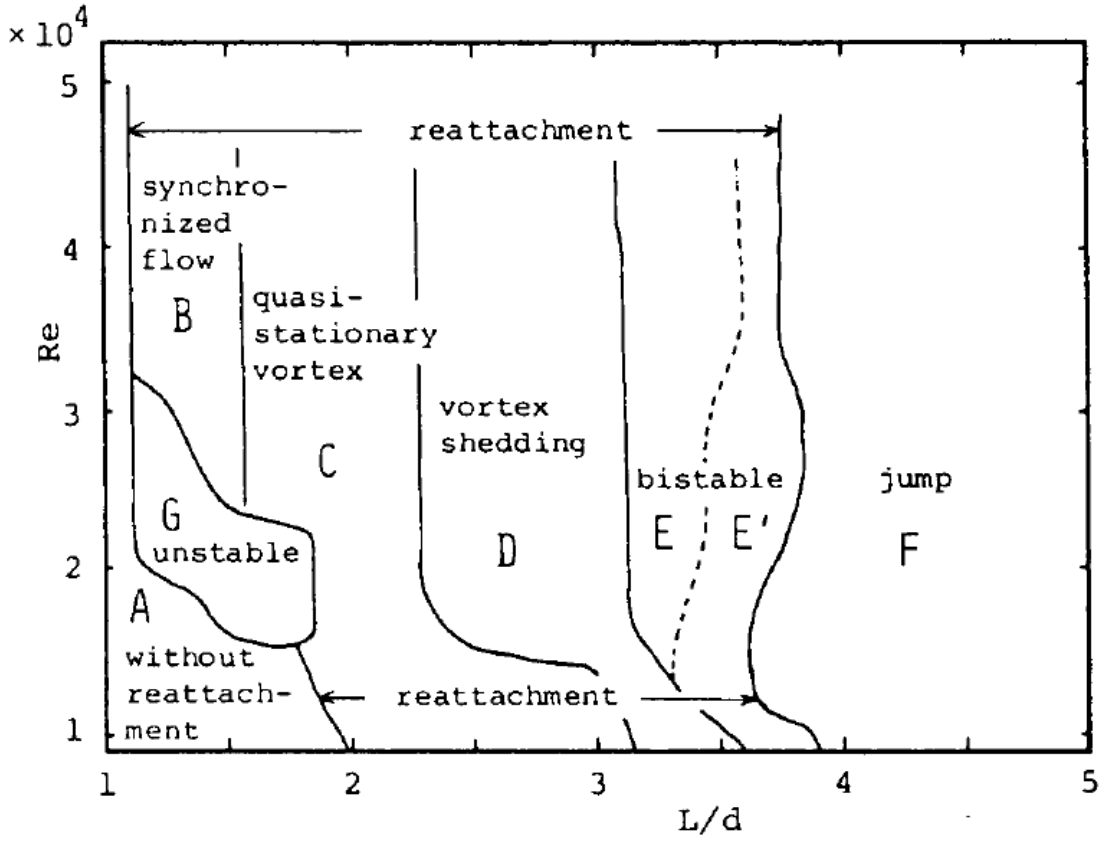

Figure 2-12 : Flow patterns classifications, Igarashi (1981)

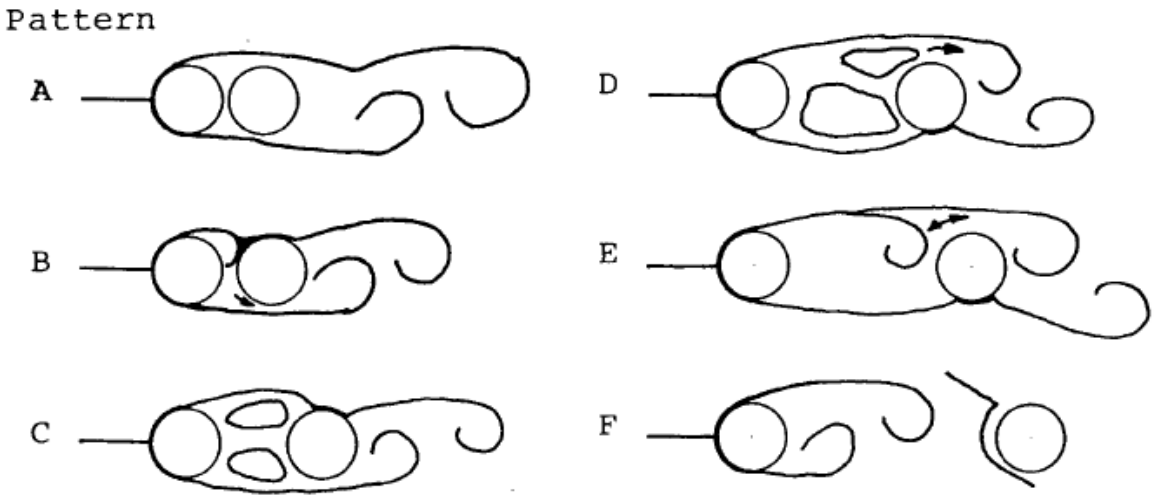

Figure 2-13 : Flow patterns sketch, Igarashi (1981)

Zdravkovich (1985) sub-divided the first regime (one vortex street) for tandem cylinders proposed by Igarashi, according to the flow changes in the gap between the cylinders into more detailed regions as follows (refer to **Figure 2-12** visualizations): -

1. **L/D < 1:** the two cylinders act as a single body, with a high Strouhal number (body becomes more like an elliptical shape). In this region, the shear layer that separates from the upstream cylinder does not reattach on the downstream one.
2. **1.1 ≤ L/D < 1.6:** a synchronized vortex shedding occurs on the front side of the rear cylinder as a result of the vortex shedding from the upstream one.
3. **1.6 < L/D < 2.4:** quasi-steady reattachment of separated shear layer from the upstream cylinder is observed on the downstream one.
4. **L/D > 2.5:** no regular vortex shedding is observed behind the downstream cylinder.
5. **L/D > 3.8**: where 3.5 is the critical spacing ratio, Zdravkovich (1977), beyond which, vortex shedding starts to occur behind the upstream cylinder. At L/D > 3.8, the tandem cylinders act as isolated cylinders and von Karman vortex streets are observed behind each cylinder.

2.2.3 Flow Patterns: Side-by-Side Cylinders

For the side-by-side configuration, Zdravkovich (1985) divided the proximity interference region ($0 < T/D < 3.8$) similarly into the following:

1. **$1 \leq T/D < 1.2$:** small spacing ratio, with a single vortex shedding formed downstream the two cylinders. The two cylinders act as a single bluff body.
2. **$1.2 \leq T/D$ 2.2:** a biased gap flow is observed (leaning towards one cylinder), narrow and wide wakes are formed. A bi-stable nature is also observed for the biased gap shedding, where the narrow and wide wakes are intermittently changed between the two cylinders. Different vortex shedding frequencies are measured for the wakes. **Figure 2-14** shows a PIV image of the biased flow pattern observed by Sumner et al. (1999b) for side-by-side cylinders within this region.
3. **$T/D > 2.2$:** two vortex shedding are observed behind the cylinders; the vortex shedding is coupled in an out-of-phase mode.
4. **$T/D > 4$:** coupling between the shedding further decreases until the two cylinders act as two isolated cylinders.

The flow regimes classifications outlined above for both tandem and side-by-side configurations can be summarized as per **Figure 2-15** , Zdravkovich (1985).

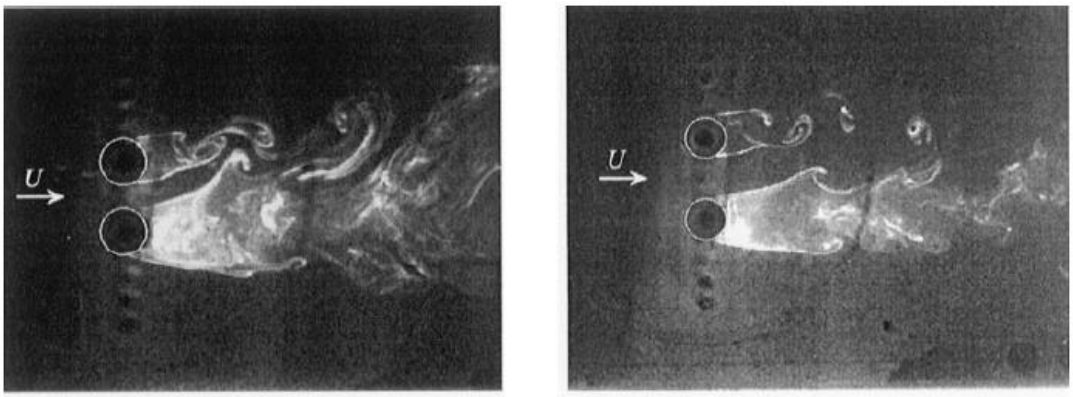

Figure 2-14 : PIV image of two side-by-side cylinders at different spacing ratios a) T/D = 1.5, b) T/D = 2.0. a) shows the biased flow pattern behavior, Sumner D. et al. (1999b)

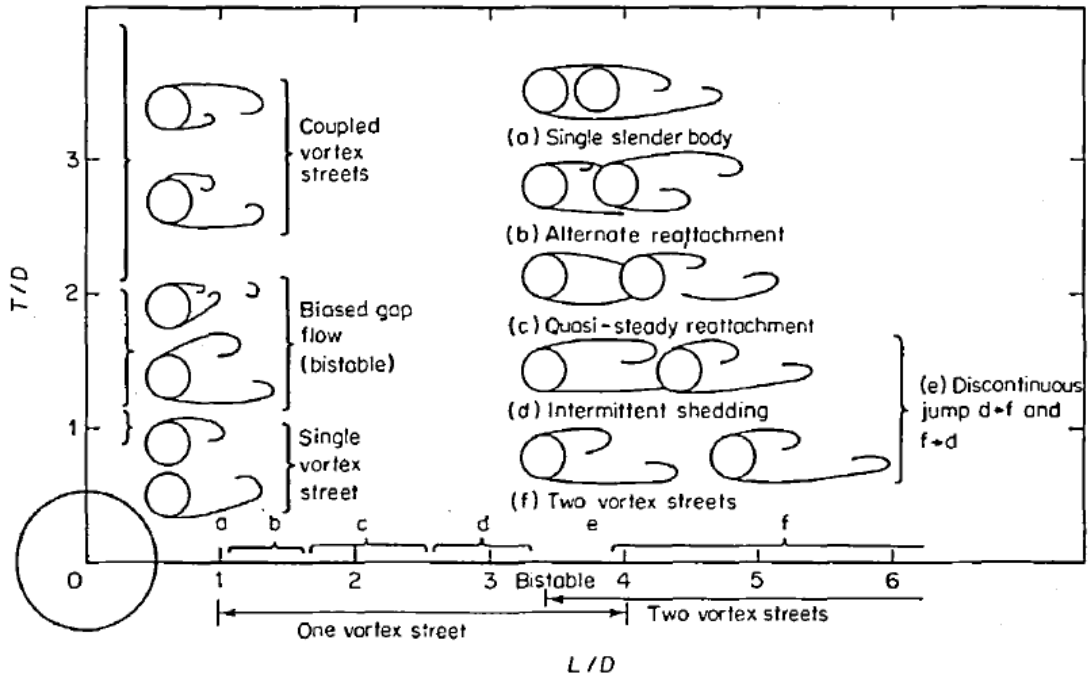

Figure 2-15 : Classification of flow Regimes in side-by-side and tandem arrangements for stationary cylinders, Zdravkovich (1985)

2.2.4 Strouhal Number: Tandem Cylinders

Vortex shedding and Strouhal number for the case of pairs of cylinder are a crucial piece of information. For a single cylinder, the value of the Strouhal number is constant for a wide range of Reynolds number and is equal to 0.2. For pairs configuration, however, the

case is different and the Strouhal number varies depending on the Reynolds number and the spacing ratios between the cylinders. The vortices formed from pairs of cylinders usually occur at higher Strouhal numbers than that of single cylinders, Sumner (2010).

Many studies such as those conducted by Okajima (1979), Igarashi (1981), Arie et al. (1983) and Zhou and Yiu (2006) have focused on generating maps of Strouhal numbers for different cases of pairs of cylinders (with similar diameters) in terms of pitch ratios (L/D and T/D) and for a wide range of Reynolds number. Other research focused on Strouhal maps for multiple in-line cylinders or staggered configurations such as Fitzhugh (1973), Igarashi (1984), Blevins and Bressler (1987), Alam and Sakamoto (2005), Fenestra and Weaver (2006), and others. For cylinders with different diameters; the work done by Novak (1975), Igarashi (1982), Alam et al (2003b), and Alam and Zhou (2008) can be referred to. The Strouhal number is usually obtained from the frequency spectrum of the vortex shedding or via hotwire measurements.

Okajima (1979) performed experiments with very high Reynolds number flows (above critical point) on two tandem cylinders. He measured the Strouhal number for cylinders in tandem configuration of equal diameter. The Strouhal number measurement was taken at two locations (St_1) in the middle distance between the two cylinders and (St_2) at 4 diameters downstream the furthest cylinder downstream. **Figure 2-16** shows the Strouhal number map proposed by Okajima; it was based on two longitudinal spacing ratios (L/D = S/D = 2 and 4) and was reported against the Reynolds number.

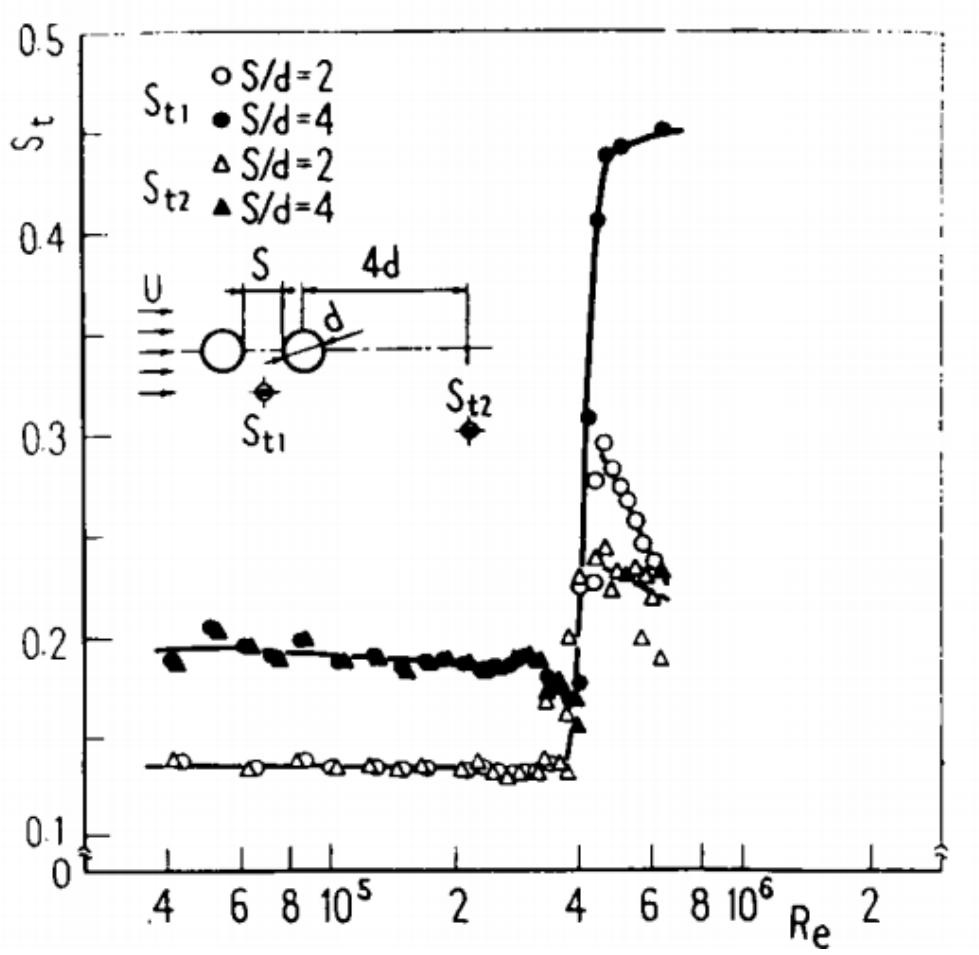

Figure 2-16 : Strouhal number map for two tandem smooth cylinders, Okajima (1979)

At the spacing ratio of 4 (above the critical spacing ratio of 3.5), the two cylinders act as single bodies with each shedding its own vortices, at a discrete frequency and with a Strouhal number of 0.2. When the Reynolds number reaches a value of about 4×10^6, the first Strouhal number (St_1), between the cylinders, jumps to almost 0.45. For the spacing ratio of L/D = 2, the Strouhal number becomes approximately equal to 0.14, measured at both locations over the entire range of the Reynolds number up to 4×10^6.

Later in 1982, Igarashi developed another Strouhal number map covering more spacing ratios for two tandem cylinders. The spacing ratios ranged from 1 –5, and measurements were taken at two different Reynolds numbers of Re = 2.2 x 10^4 and Re = 3.5 x 10^4. **Figure 2-17** shows the map developed by Igrashi (1982). Unlike the value for the single cylinder the value of the Strouhal number is highly dependent on the spacing ratio L/D for all the cases. The dependency of the Strouhal number on Reynolds number is most pronounced in the range of $1.1 \leq L/D \leq 2$. Igarashi's map was in good agreement with that provided by Okajima (1979).

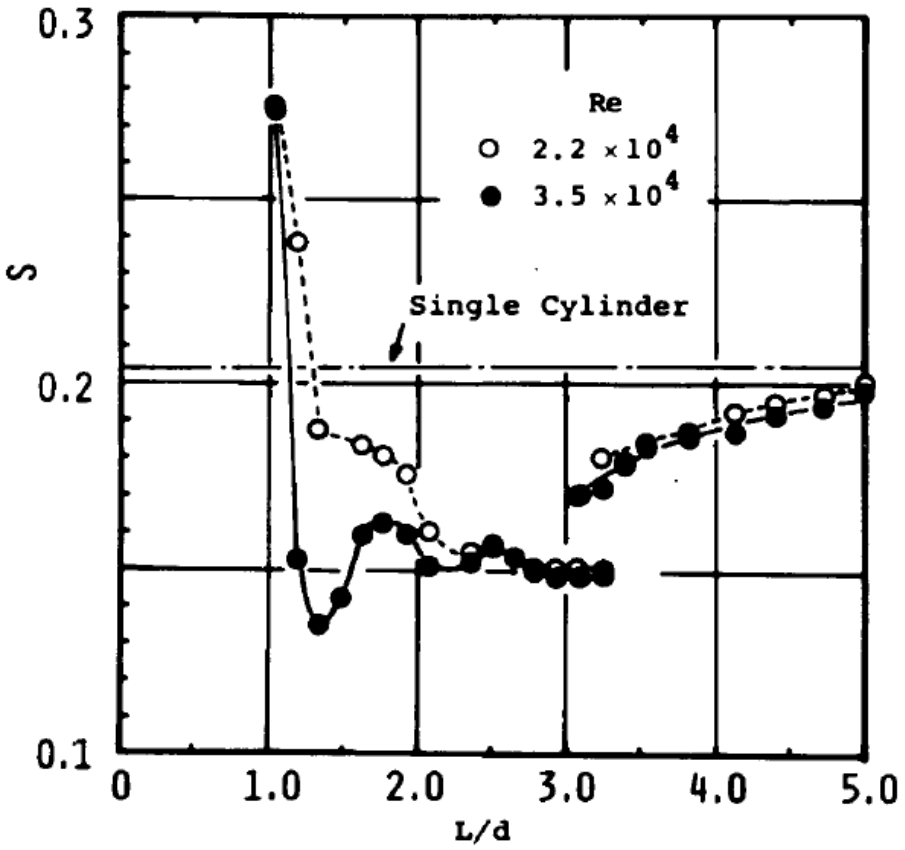

Figure 2-17 : Igarashi map for Strouhal number for tandem configuration, Igarashi (1981)

2.2.5 Strouhal Number: Side-by-Side cylinders

Similarly, in the case of side-by-side cylinders, the Strouhal number shows great dependency on both the Reynolds number and the pitch-to-diameter ratio. **Figure 2-18** shows an extensive map for the effect of spacing ratio T/D on the Strouhal number and Reynolds number taken from Sumner (2010). For the small pitch ratios, the Strouhal number is less than 0.2, although in terms of vortex shedding, at this small pitch-ratios the two cylinders act as a single bluff body. This shows the great dependency on both the Reynolds number and the pitch ratio. As the pitch ratio increases to higher values, the Strouhal number measured starts to become closer to that of the single cylinder (i.e. 0.2), which implies that the two cylinders wakes are not affected by each other.

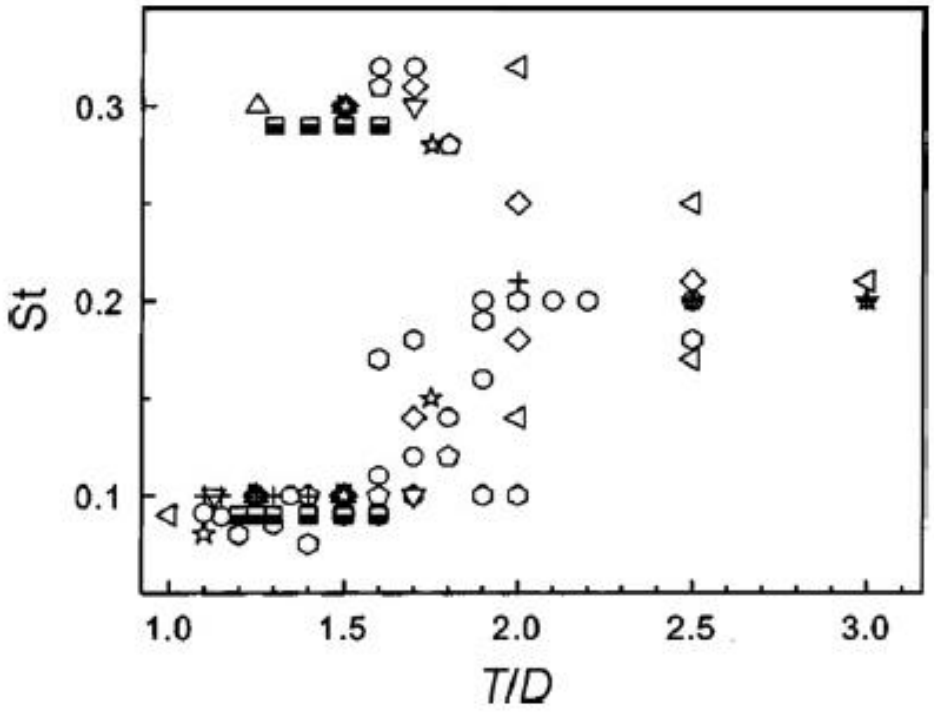

Figure 2-18 : Strouhal number data for two side-by-side cylinders at different pitch-to-diameter ratios and at different Reynolds number ratios from 55 – 2.8 x 10^4, Sumner (2010)

2.3 Aerodynamic Noise

Aerodynamic noise refers to the sound generated due to turbulence in fluid flow. The turbulence is usually a result of the fluid-solid interaction or flow instabilities. Many researchers have investigated the effect of turbulence and vortex formulation on the actual generation of sound, since the 1950s.

One of the pioneer scholars in the field of aerodynamic noise generation is James Lighthill; who published a series of extensive papers in the 1950s where he discussed the sound generated aerodynamically (as a by-product of fluid flow). His approach, however, was different than other scholars during that time (i.e. Roshko and Kovàsznay), since he related the sound intensity to the actual details of the flow rather than the frequency and Reynolds number. Lighthill (1952) characterized the noise generated from fluctuating fluid flow through first analyzing the actual details of the flow, and then deducing the sound field from it. This was done by transforming the Navier-Stokes and continuity equations to form an exact, inhomogeneous wave equation, whose source terms are only important within the turbulence region, Howe (2002).

Such methodology basically explained how the kinetic energy of the flow was changed to sound energy and subsequently, how it intensified and progressed. Lighthill approach was very mathematical in nature and was heavily based on the conservation of momentum equations and momentum flux tensors with the assumption of a uniform flow and acoustic mediums. He suggested that the density of fluctuations in a real flow must be exactly equal to the fluctuations that would occur in a uniform acoustic medium experiencing an external stress of the same magnitude. The difference between the effective stresses in the real flow and the stresses in the uniform acoustic medium produced was given by **Equation 2.5**.

$$T_{ij} = \rho v_i v_j + p_{i_j} - a_o^2 p \delta_{ij} \quad \textbf{(2.5)}$$

Where T_{ij} is the momentum flux tensor, $\rho v_i v_j$ are fluctuating Reynolds stresses, which accounts for turbulent fluctuations in flow, p_{i_j} are real stresses made up of hydrostatic pressure and viscous stresses, and a_o^2 is the square of speed of sound. The sound radiated is produced by static distribution of acoustic *quadrupoles* sources. Lighthill's analogy of sound generation was revolutionary and formed the basis of noise generation studies for many applications such as acoustics and aeronautical engineering. The only major limitation to Lighhill's analogy was that it was specific for sound radiated in unbounded, free field flows. It was noted by Lighthill (1954) that the solid boundaries in some cases play an important role in the sound radiation from a source. For example, fluctuating lift in case of rigid circular cylinders in a uniform flow.

This encouraged Curle (1955) to work on extending the work of Lighthill (1952) and derive a formal solution to incorporate the effect of wall boundaries. Incorporating the solid boundaries effects meant that the sound waves generated will experience reflections and diffractions at the walls. Moreover, the solid boundaries presence limited the *quadrupole* effect of the emitted sound, previously suggested by Lighthill, to a *dipole* one. The fundamental frequency of the emitted sound also changed a result and became one-half of the quadrupole source. **Figure 2-19** shows the directivity patterns of dipole sources around a cylinder.

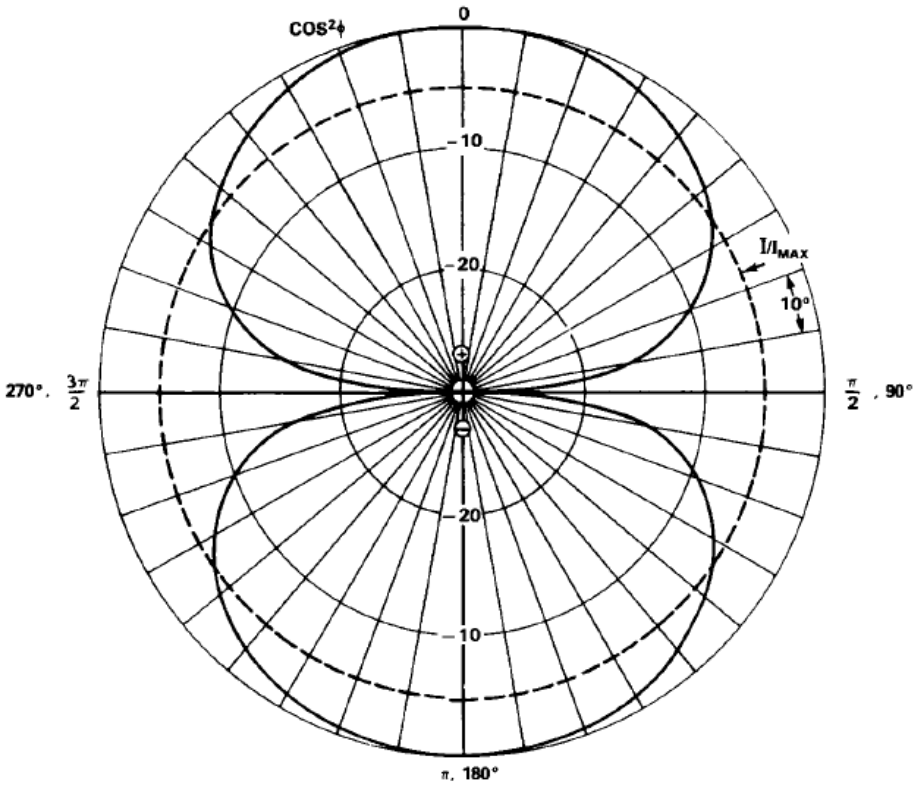

Figure 2-19 : Directivity pattern, in far field of a compact dipole, Blake (1986)

Curle worked on Lighthill's equation and included terms such as zero normal velocities at the boundaries (no slip condition) to account for the effect of the walls. Using dimensional analysis, he deduced that the intensity of sound generated from a dipole source (I), is proportional to the following expression (**Equation 2.6**) at a far distance. Where U_o is the typical flow velocity, L is the typical body length, a_o is the velocity of sound in the medium, and x is the point of observation.

$$I \alpha \frac{U_0^6 L^2}{a_0^2 x^2} \qquad \textbf{(2.6)}$$

Later, Gerrard (1955), performed measurements for sound emitted from circular cylinders in air streams. In his study, Gerrard experimentally investigated the frequency and intensity of the sound produced as a result of placing a circular cylinder in an air stream, at Reynolds numbers in which the periodic vortex shedding was expected. His results agreed well with those of Lighthill and Curle in terms of the directionality of the sound emitted (i.e. dipole sound source) and the source of the emitted sound (fluctuating forces). He suggested that the intensity of the sound measured at the plane perpendicular to the cylinder axis can be expressed using the following **Equation 2.7**.

$$I = \frac{\overline{P^2}}{\rho_o a_o} = \frac{\rho_o U^4}{a_o}\frac{l^2}{r^2}\cos^2\theta\, f(R) \qquad \textbf{(2.7)}$$

Where P^2 is the mean square sound pressure, ρ_o is the density of air, a_o is the velocity of sound in air, U is the velocity of the fluid, l is the length of the cylinder, r is the point of measurement, and R is the Reynolds number based on diameter and viscosity.

Etkins (1956), performed a wide range of tests on various cylinders in cross-flow to investigate the Aeolian tones produced as a result of the fluid forces acting on the cylinders. He concluded that the sound field produced was mainly a result of the fluctuating lift and drag forces acting on the rigid cylinder. The frequency of the sound field emitted due to the fluctuating lift was found to be equal to the frequency of the vortex shedding from the cylinder, while the frequency of the fluctuating drag was found to be 2 times larger.

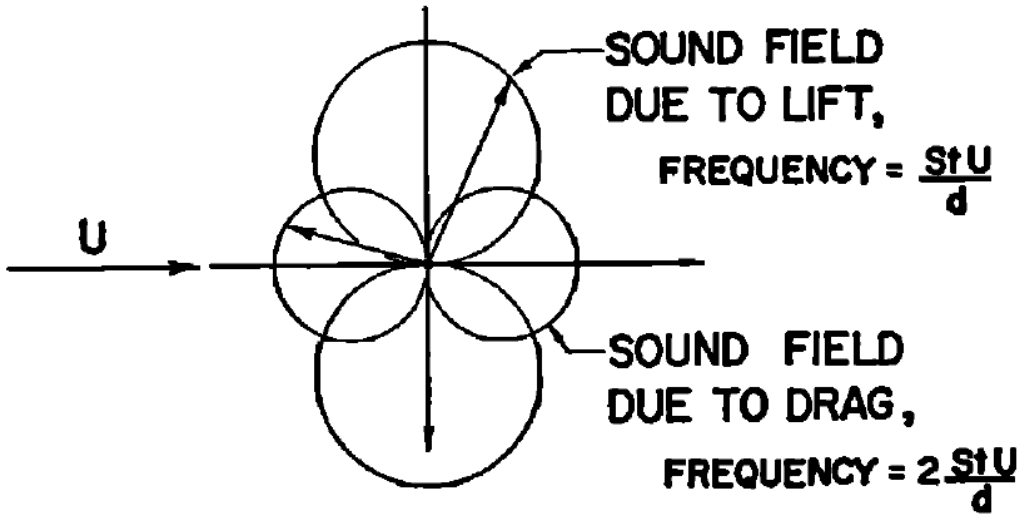

Figure 2-20 : Dipole sound fields due to fluctuating lift and drag on a cylinder in cross-flow, Etkins (1956)

Although the work done by Lighthill and Curle was revolutionary and very extensive, it did not specify exactly how the vortices from the bluff-bodies generated the sound in the first place. It was not until Alan Powell (1964), developed a mathematical relation to show how the aerodynamic sound generated as a result of the moving vortices behind a bluff body or due to turbulence. Powell's theory was particularly suited for estimating sound intensity from flow in terms of vorticity strength.

Howe (1975 and 1980) extended the work done previously by Lighthill, Curle, Ffocus Williams and Powell developed a simple expression (Howe's integrand) for the dissipation of sound from a trailing edge as a result of a flow. Howe's integrand expressed by **Equation 2.8** is simply a triple product, that determines the instantaneous acoustic power generated by a vorticity in a flow.

$$\prod = -\rho \int \omega \cdot \left(v_p \, x \, U\right) dV \qquad \textbf{(2.8)}$$

Where ω is the vorticity vector, v_p is the particle velocity vector, U is the flow velocity vector, ρ is the fluid density, and V is the volume over which the integrand in calculated. Acoustic energy is generated when the integral yields a positive number and is absorbed when the integrand yields a negative number. Howe's integrand provides an excellent estimation for the acoustic power, and forms the basis of fluid-acoustic coupling studies.

2.4 Flow-excited Acoustic Resonance

Acoustic resonance is one of the flow-induced vibration mechanisms experienced in industrial applications, Rodarte (2001). The acoustic resonance occurrence as a result of bounded bluff body in a flow, is applicable to many industrial applications such as tube and shell heat exchangers, boilers, street poles, underwater corrugated pipes, and many others. Flow-excited acoustic resonance is usually associated with high tonal noises and excessive vibrations. Sound pressure levels of up to (173 dB) have been reported in the literature, Blevins and Bressler (1987). This high level of noise and vibration, if untreated, can be damaging to mechanical equipment. An example of mechanical failures due to resonance and vibration is the breakdown of the steam dryer, NRC (2003) and the damage of the pressure tubes in Darlington nuclear station in 1991. Even when the structural failure is not a problem, high tonal noises may be damaging to human ears and may exceed the allowable federal/provincial noise regulations. Therefore, flow-excited acoustic resonance is an important phenomenon that needs to be fully understood and characterized, and most importantly treated.

2.4.1 Duct Acoustics

Acoustic resonance in ducts containing single cylinder is considered the most basic and fundamental configuration to study. In order to better understand the resonance excitation mechanism of this case, it is useful to first understand some basic concepts and parameters related to duct acoustics. For that, consider a simple duct of a rectangular cross section, with arbitrary dimensions of width, depth and height denoted by (w), (d), and (d) respectively, as presented in the schematic shown in **Figure 2-21.**

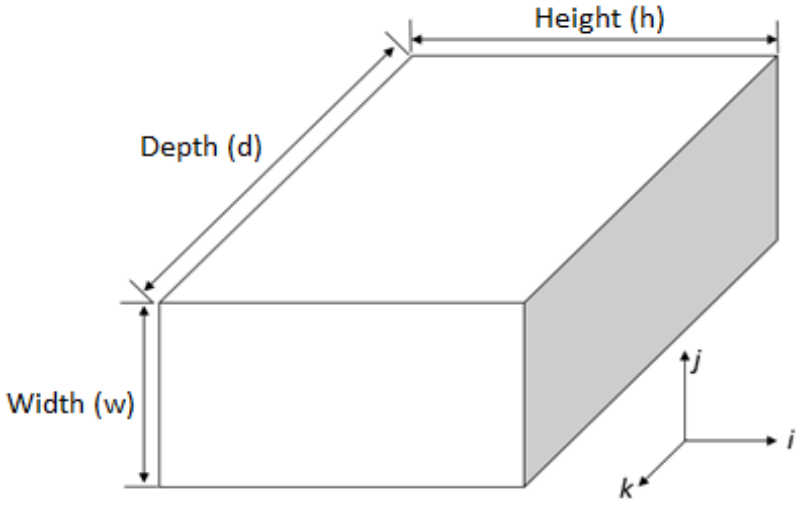

Figure 2-21 : Schematic of a simple closed-closed duct geometry

The natural frequencies for the first three acoustic modes of this closed-closed duct can be calculated as follows, Blevins (2005): -

$$f_{a(i,j,k)} = \frac{c}{2}\left(\frac{j^2}{L_w^2} + \frac{i^2}{L_h^2} + \frac{k^2}{L_d^2}\right)^{\frac{1}{2}} \quad \textbf{(2.9)}$$

Where *i, j, k* are indexes that correspond to the modes in *h, w, l* components respectively, L_w, L_h, L_d are lengths of the duct in the width, height and depth directions, and *c* is the speed of sound in air.

For the experiments covered in this thesis, the frequency and mode of interest is that in the direction perpendicular to the cylinder length and duct width. (i.e. i-direction, height). Thus the above general equation can further be simplified to: -

$$f_{a(h)} = \frac{ic}{2L_h} = \frac{ic}{2h} \quad \textbf{(2.10)}$$

2.4.2 Acoustic Damping/Attenuation in Ducts

Attenuation or damping of sound propagating in ducts occurs due to many energy loss mechanisms such as viscosity, heat conduction, turbulence, and convection, Rodarte (2000). However, viscous and heat conduction losses at the duct boundaries are the most dominant contributors to the total attenuation of sound. Mainly, viscous and thermal losses occur in the acoustic viscous and thermal boundary layers near the walls of ducts and are responsible for the natural attenuation of the sound wave, Mikhail et al. (1993). The attenuation of sound inside the duct is a purely acoustic matter that involves many parameters such as, viscosity and heat related parameters. Therefore, theoretically estimating the damping or attenuation of a certain duct geometry is a complex and tedious task, and many approximations are usually required to obtain accurate results.

A considerable amount of research has been conducted and many theoretical relations have been developed in order to quantify the amount of sound damping in ducts. Most of the research conducted assumed a plane 1-D acoustic wave propagating in the duct for

simplification. The wave equation for a plane acoustic pressure wave propagating inside a duct is described by a second order partial differential as follows:

$$\frac{\partial^2 p}{\partial x^2} = \left(\frac{1}{c_o^2}\right)\left(\frac{\partial^2 p}{\partial t^2}\right) \quad \textbf{(2.11)}$$

Where p is the acoustic pressure, c_o is the speed of sound in the medium and x is the position along the duct. Ingard and Singhal (1974) performed experiments in a duct with flow velocity of 0 to 170 m/s, and measured the attenuation of the positive and negative acosutic waves propagating at different duct diameters. The sound source in their experiment was located on one side of the duct at the center. The upstream and downstream values of the attenuation were determined by using two pressure transducers on either side of the sound source.

Figure 2-22 shows the dependency of the sound attenuation in smooth pipes on the Mach number and the duct diameter for downstream and upstream directions. It can be seen that the sound attenuation is more pronounced in the upstream direction than the downstream. The attenuation is almost independent of the Mach number at low flow velocities, however, for Mach numbers above 0.25 the dependency is quite pronounced, and seems to decrease with the increasing pipe diameter.

For the quasi-static approximation adapted, Ingard and Singhal concluded that the visco-thermal attenuation in ducts is proportional to the square root of the acoustic frequency, while the contribution caused by the turbulence is independent of the frequency. Table 1 shows four of the commonly used relations for the visco-thermal attenuation coefficient, English (2010). Moreover, it was highlighted by, English (2010), that the attenuation increases with the increasing Helmholtz number (ka). Where the Helmholtz number is

defined based on the angular frequency, the speed of sound and the radius of the duct. In the case of rectangular ducts, the diameter can be substituted with the hydraulic diameter, if needed.

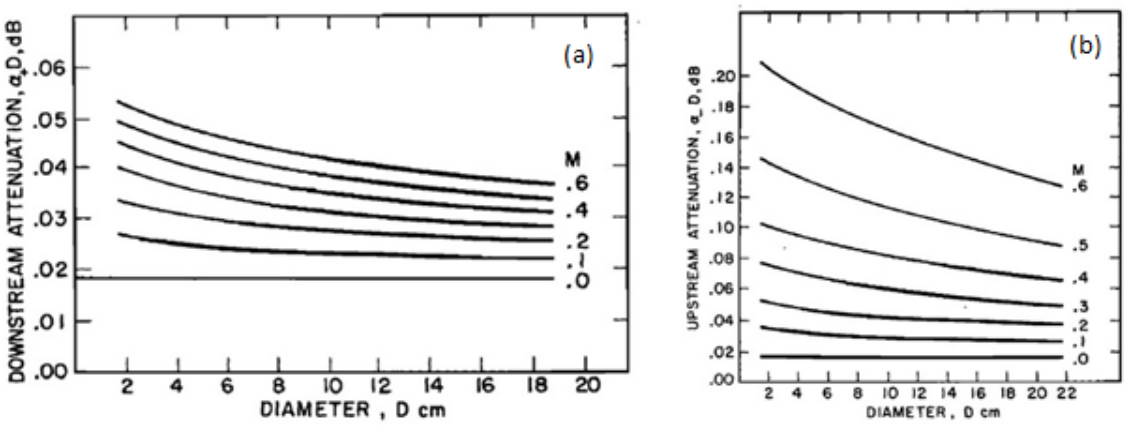

Figure 2-22 :Dependency of sound attenuation on the pipe diameter and the Mach number for smooth pipes with turbulent flow , (a) predicted downstream attenuation coefficient , (b) Theoretically calculated upstream attenuation coefficient , Ingard and Singhal (1974)

Table 1 : Approximation for visco-thermal attenuation in ducts, English (2010)

Helmholtz (1863)	$\boldsymbol{\alpha_h = \frac{\omega}{c\sqrt{2}\,Sh}}$
Kirchhoff (1868)	$\alpha_K = \frac{\omega}{c}\left(\frac{1}{\sqrt{2}\,Sh}\left(1+\frac{\gamma-1}{\sqrt{Pr}}\right) + \frac{1}{Sh^2}\left(1+\frac{\gamma-1}{\sqrt{Pr}}-\frac{\gamma}{2}\frac{\gamma-1}{\sqrt{Pr}}\right)\right)$
Rayleigh (1896)	$\alpha_R = \frac{\omega}{c}\left(\frac{2\sqrt{\gamma}}{Sh}\right)$
Ingard (1974)	$\alpha_{Ingard} = \frac{\omega}{c}\frac{2-\frac{3}{2}}{Sh}\left(1+\frac{1}{\sqrt{Pr}}\right)$

Where *Sh* is the shear wave number, *Pr* is the Prandtl number, γ is the ratio of specific heats, *c* is the speed of sound in the medium and ω is the angular frequency. The inclusion of these parameters shows the great dependency of the acoustic attenuation on the viscosity, the heat conduction and the frequency of the acoustic mode. Recently, Golliard et al. (2013), adapted the Kirchhoff model along with the linearized relation between the pressure drop and the friction coefficient factor proposed by Ingard and Singhal, (1974) to theoretically predict the damping coefficient in smooth and corrugated pipes. The acoustic damping in smooth and corrugated pipes was estimated both theoretically and experimentally to help treat the acoustic resonance phenomena in subsea pipes and natural gas pipes. **Figure 2-23** shows the experimental values for damping coefficient at three different velocities and the comparison with the theoretical damping model.

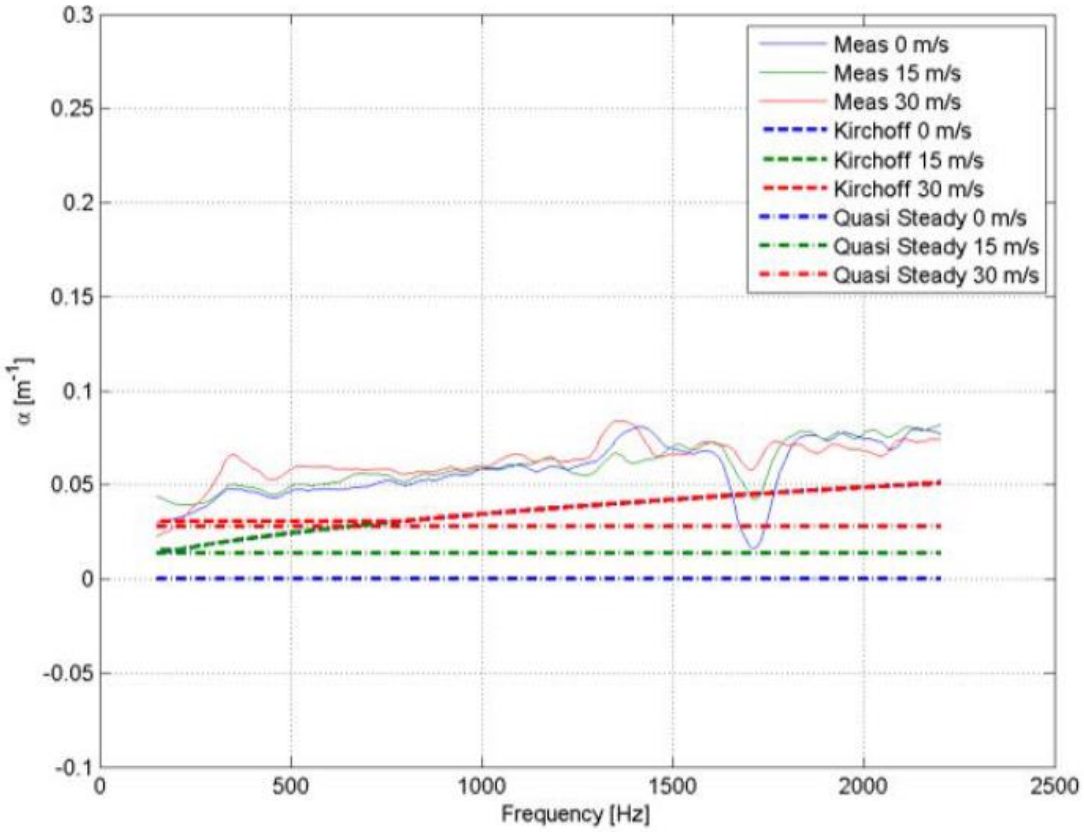

Figure 2-23 : Comparison of measured damping coefficient at three different velocities compared to the theoretical prediction by Kirchhoff model, Golliard et al. (2013)

Results presented by, Joachim Golliard and his colleagues at TNO, showed reasonably well agreement between the experimental values and the theoretical model. Although the experimental were 40% higher than the theoretical model, the dependency of the damping on the frequency was captured quite well.

The acoustic behavior of any flow duct system can be accurately modeled without considering the actual manner by which the sound was excited, Davies (1988). Thus it is reasonable to assume that although the relations derived for duct attenuation were developed for simple and generalized cases, they are applicable to other complex cases and can give an overall implication of the damping/attenuation of the system. For instance, the

model proposed by Kirchoff was mainly for a homogeneous medium in absence of mean flow, however, when adapted by Golliard et al. (2013), it showed good agreement with experimental results in cases of smooth pipes and corrugated pipes with the mean flow for dry and wetted gasses.

2.4.3 Flow-excited Acoustic Resonance: Single Cylinder

Single cylinders in rectangular ducts are considered the simplest case of flow-excited acoustic resonance in ducts containing bluff bodies. Fundamentally, understanding the acoustic behavior of single cylinders is necessary to further understand acoustic resonance in more complex arrangements such as heat exchangers. Although it is considered a relatively simple case, the noise field generated by single cylinders inside ducts is complex compared to noise generated in the free field. The presence of the duct wall can absorb or reflect acoustic waves inside, and affect the acoustic field. Thus the acoustic field inside ducts varies significantly and depends on multiple parameters such as the noise source frequency, the source position, the source strength, the size/ shape of the enclosure and the wall acoustic impedance, Rodarte (2000).

Figure 2-24 shows a schematic for the relation between the natural acoustic frequency of a duct, the vortex shedding frequency, and the upstream velocity. This schematic emerges as a useful tool to estimate the acoustic resonance occurrences (visually) for ducts of different heights. The horizontal lines represent the constant duct acoustic natural frequency (f_a) for two ducts of different heights, while the slanted lines represent the vortex shedding frequencies (f_v). The vortex shedding frequency increases linearly with the upstream velocity until it coincides with one of the acoustic modes of the duct. When it coincides, acoustic resonance may occur at a corresponding velocity at resonance peak is

U_1. In special cases, such as when $f_v = f_a$ and $f_{v2} = f_{a2}$, acoustic resonance may occur for two different diameters/heights at the same velocity (U_2).

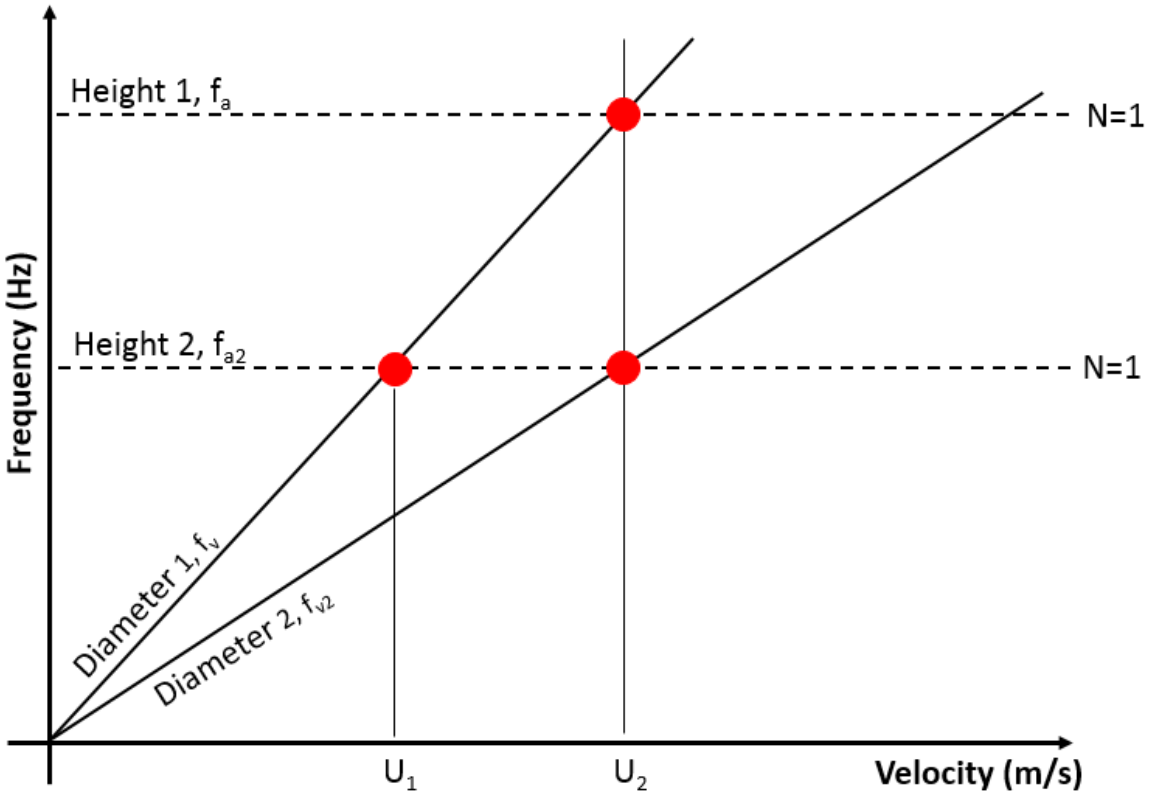

Figure 2-24 : Schematic of the coincidence between the acoustic cross-modes and the vortex shedding frequency for different arbitrary duct heights and diameters

The onset of acoustic resonance is initiated practically when the frequencies are within a small range of each other. In order for acoustic resonance to materialize, there should be enough energy in the system to overcome the acoustic damping of the duct. The acoustic resonance is caused by a feedback cycle in which the vortex shedding from the cylinder acts as a sound source that excites an acoustic standing wave, which further enhances the shedding process, Mohany (2007).

Figure 2-25 shows a typical aeroacoustic response of a single cylinder in a duct experiencing resonance, Mohany and Ziada (2005). When resonance starts, the pressure amplitudes start to increase with the increasing velocity (energy), this increase usually reaches a peak value commonly referred to as $P_{rms,\ max.}$ The acoustic pressure amplitude starts to decrease with further increase in the velocity beyond this point. In the frequency response before resonance, the frequency of vortex shedding increases linearly with the velocity (U) acting on the cylinder until it coincides with the duct frequency. The two frequencies remain locked together for a certain range of velocity depending on the cylinder diameter and duct damping. After a period of time, the lock-in region breaks and the frequency of vortex shedding starts to increase linearly again with the velocity. The slope of the increasing line for single cylinders is 0.2, which corresponds to the Strouhal number. Few number of studies have performed work related to noise generated from single cylinders in resonating conditions, Blevins and Bressler (1987, 1993), Rodarte (2001), Mohany and Ziada (2005, 2011), Eid and Ziada (2011), Arafa and Mohany (2014, 2015a and 2015b).

The related study to the current work in literature is that of Blevins and Bressler (1993). Blevins and Bressler performed a wide variety of experiments on ducts containing single tubes and tube arrays at resonance. The main purpose of the work was to correlate the maximum acoustic pressure amplitude recorded at resonance to the geometrical parameters of the duct/cylinder and the fluid properties of the fluid.

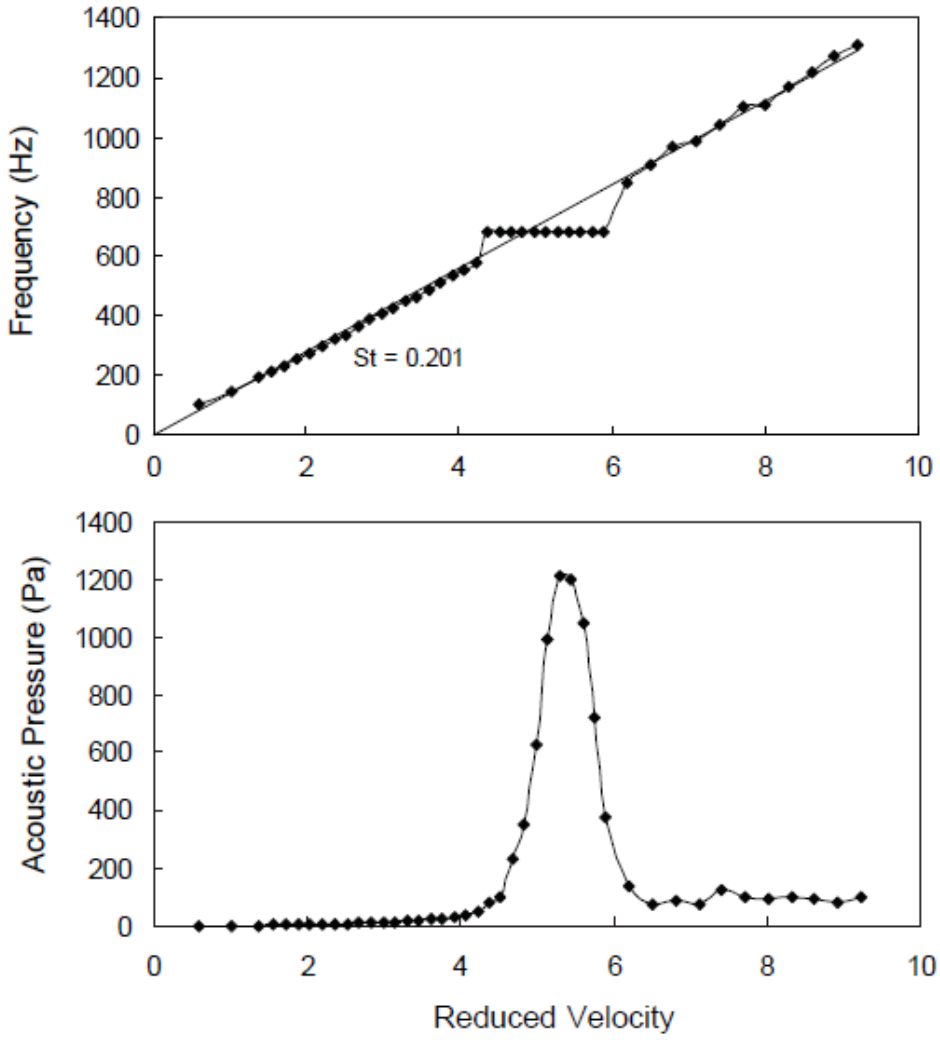

Figure 2-25 : Typical aeroacoustic response for single bare cylinder, Mohany and Ziada (2005)

Blevins performed sixteen experiments on single cylinders and fitted his data to correlate the maximum acoustic pressure amplitude to the dynamic head, Mach number, blockage ratio, static pressure drop and the input energy parameter (MΔP). He suggested that the maximum acoustic pressure can be calculated using the following two equations, for a single cylinder and for multiple rows of cylinders. Equation (2.12b) could also be applied to a row of cylinders.

$$P_{rms,\max} = 12.5\,\rho\frac{U^2}{2}\left(\frac{U}{C}\right)\left(\frac{D}{B}\right) \quad \textbf{(2.12a)}$$

$$P_{rms,\max} = 12.5\left(\frac{U}{C}\right)\Delta P_{static} \quad \textbf{(2.12b)}$$

Blevins and Bressler claim that the equations work within 26% error margin in the range of 0.02 < M <0.5 , 5 <ΔP_{static} < 50 (in H_2O) and 2000 < Re < 300000. The suggested equations were later found to lack accuracy, even within the data of Blevins and Bressler themselves. For example, it was reported that the absolute error is 26% and 3dB. However, some of the experimental data varied by about 57%. More importantly the equations proposed do not account for the effect of the enclosure damping. Moreover, the motor capabilities limited the testing of the proposed equations by Blevins and Bressler (1993) to only the first acoustic mode. It is not known if the equations are accurate in predicting maximum acoustic amplitudes at the higher modes of resonance (2^{nd} and 3^{rd} acoustic modes).

Arafa and Mohany (2015) have performed experimental investigation dealing with the aeroacoustic response of isolated cylinders in cross-flow. The experiments were conducted to analyze the effect of the cylinder position along the duct height, on the excitation levels of acoustic pressure amplitudes. Single cylinders were placed at different heights along the duct and the aeroacoustic responses were compared in terms of frequency of vortex shedding and acoustic pressure amplitudes. The study concluded that the position of the cylinder relative to the acoustic particle velocity distribution across the duct dictated the acoustic pressure amplitude and the dominating mode of resonance. The study however was done on one duct height only.

Other studies performed for single cylinders in rectangular ducts at resonance, focused mainly on either changing the diameter of the cylinder and/or changing the geometry of the cylinder by adding fins, Rodarte (2001), Eid and Ziada (2011), Mohany and Ziada (2009), Arafa and Mohany (2015). None of the investigation done focused on the effect of the duct height on the flow-sound interaction and acoustic resonance excitation for single cylinders.

2.4.4 Flow-excited Acoustic Resonance: Tandem Cylinders

Tandem cylinders placed in a duct is considered to be a more advanced configuration that involves separation and reattachment of shear layers and a complex interaction between the wakes of the cylinders. Various studies have been conducted to study the interaction of the wakes of cylinders in tandem arrangements, and investigate the wake patterns. However, only a few number of researchers have done experiments on tandem cylinders in ducts at *self-excited* resonance conditions, Mohany and Ziada (2005, 2009a, 2009b) and Shaaban and Mohany (2015). None of the work done investigated the effect of the duct height on the excitation mechanism of tandem arrangement.

Tandem cylinders are known to experience a different aeroacoustic response during resonance. Mohany and Ziada (2005 and 2009) performed experimental work on tandem cylinders in ducts at acoustic resonance conditions and compared them to single cylinder tests, in terms of aeroacoustic responses. Eleven different spacing ratios within the range of L/D = 1.2 – 4.5 were tested for wind speeds of up to 120 m/s to see the effect of the gap and diameter on the excitation mechanism of the acoustic resonance. Mohany and Ziada found that the aeroacoustic response for the tandem cylinders is very different from that of the single cylinder, especially for cases with large cylinder diameters.

The resonance for tandem cylinders differed from the single cylinders in the range of velocity excitation and the nature of the resonance mechanism itself. It was found that for two tandem cylinders within the proximity region (L/D < 3.5) the acoustic resonance occurred over two different velocity ranges. The first resonance is called *"pre-coincidence"* and is excited by the shear layer instability in the gaps between the cylinders, and is similar to the acoustic resonance occurring in the case of cavity flows. The second resonance is called *"coincidence"* and is similar to the acoustic resonance experienced for single cylinders (i.e. due to natural vortex shedding process). The resonance phenomenon for the tandem cylinders is thus referred to as a *"dual-resonance"* phenomenon. **Figure 2-26** shows the different behavior of the acoustic resonance of tandem cylinders (compare with **Figure 2-25**).

The acoustic resonance of tandem cylinders was found to greatly depend on the diameter of the cylinders as well as the spacing ratio between the cylinders. Cylinders with spacing ratios more than 3.5, were found to act as single cylinders because no wake interaction occurs between the two bodies.

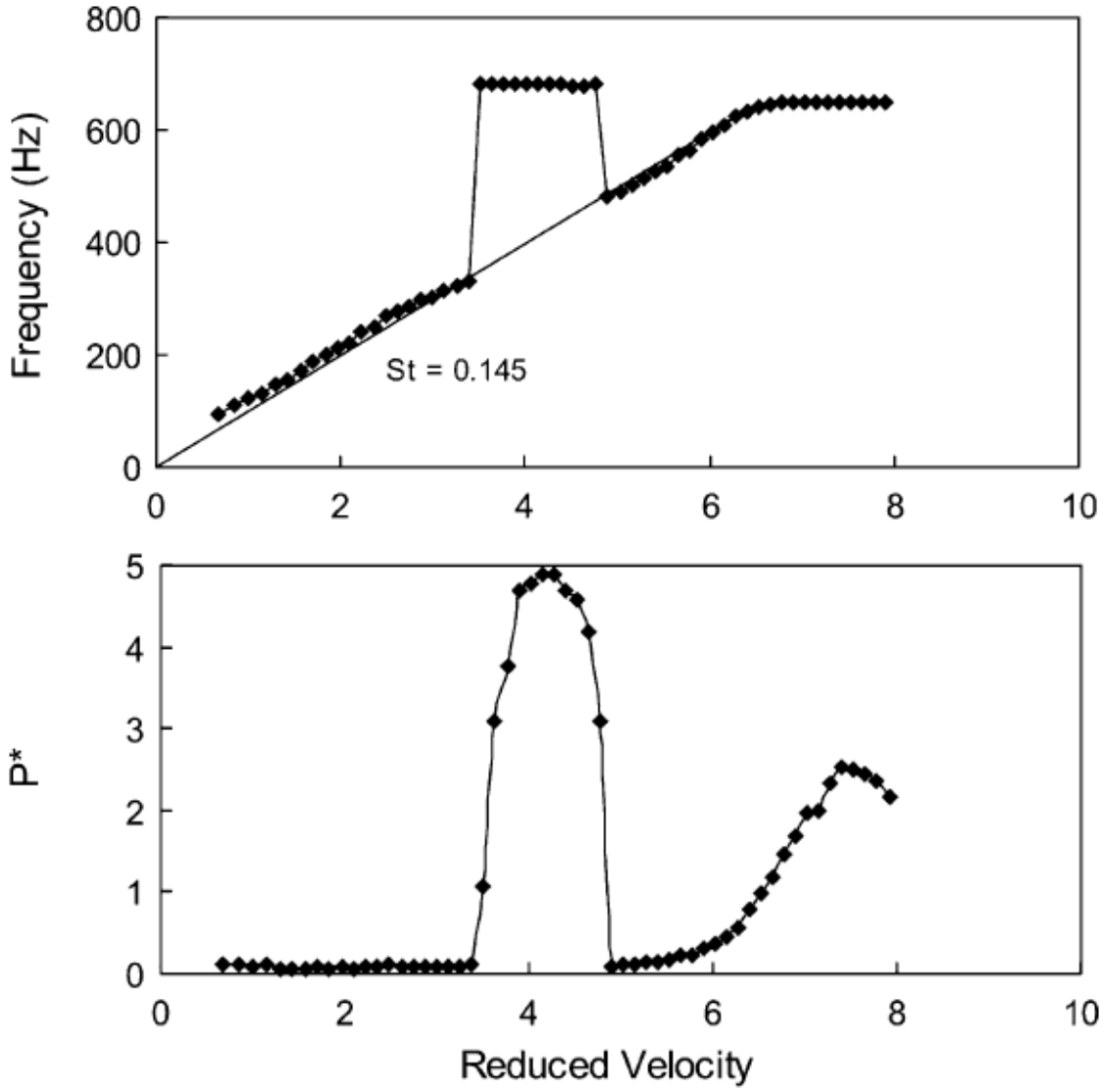

Figure 2-26 : Aeroacoustic response for tandem cylinders, Mohany and Ziada (2005)

2.4.5 Flow-exited Acoustic Resonance: Side-by-Side Cylinders

Flow excited acoustic resonance of two side-by-side cylinders in rectangular ducts has been investigated in only two studies to date, Hanson et al. (2009) and Arafa and Mohany (2016). Hanson et al. (2009) performed an experimental study on two side-by-side cylinders at six different spacing ratios in the range of T/D = 1.25 – 3. The main objective of the study was to investigate the effect of the gap between the cylinders on the

aeroacoustic response. Special attention in this study was given to the close spacing ratios, where the bi-stable vortex shedding regime is expected. **Figure 2-27** shows the anti-phase vortex shedding from two side-by-side cylinders at large spacing ratios during off-resonance conditions. The wake structure of two side-by-side cylinders before and during self-excited acoustic resonance was recently visualized by Mohany et al. (2014) for a spacing ratio of 2.5. Hanson et al. (2009) found that the occurrence of the acoustic resonance synchronized the wakes of both cylinders, which eliminates the bi-stable vortex shedding regime; moreover, the vortex shedding in both wakes became of comparable strength. **Figure 2-28** shows a schematic of the synchronized vortex shedding from both cylinders during resonance conditions.

Hanson et al. (2009) concluded that for large spacing ratios the side-by-side cylinders behaves very similarly to single cylinders, while cylinders in the small and intermediate spacing ratio regions (T/D <2.2) two Strouhal numbers were observed before the onset of acoustic resonance, however, the acoustic resonance was excited at an intermediate Strouhal number range between the two. The intermediate Strouhal number was found to be of value 0.2.

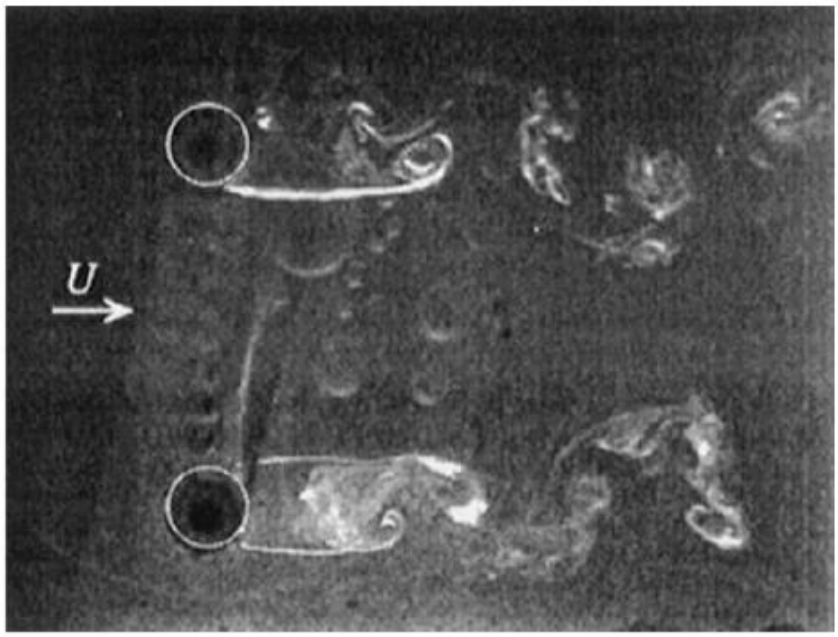

Figure 2-27 : Out of phase vortex shedding from two tandem cylinders at large spacing ratio, off-resonance, Sumner (1999b)

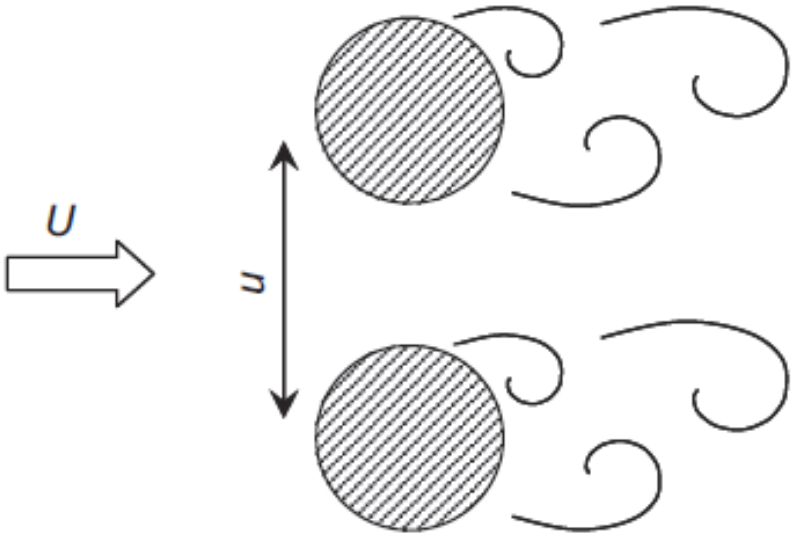

Figure 2-28 : Schematic of the synchronized vortex shedding pattern at the wake of two side-by-side cylinders with large spacing ratios , at resonance conditions, Hanson et al. (2009)

Figure 2-29 shows the aeroacoustic response of two tandem cylinders at the small spacing ratio. The three Strouhal numbers are clearly seen in the frequency response. In terms of aeroacoustic response, the two side by side cylinders at all the tested spacing ratios were found to exhibit higher acoustic pressure amplitudes and wider lock-in regions compared to single cylinders of similar diameters. However, the onset and offset of acoustic resonance occurred at the same reduced velocities as the single cylinder cases.

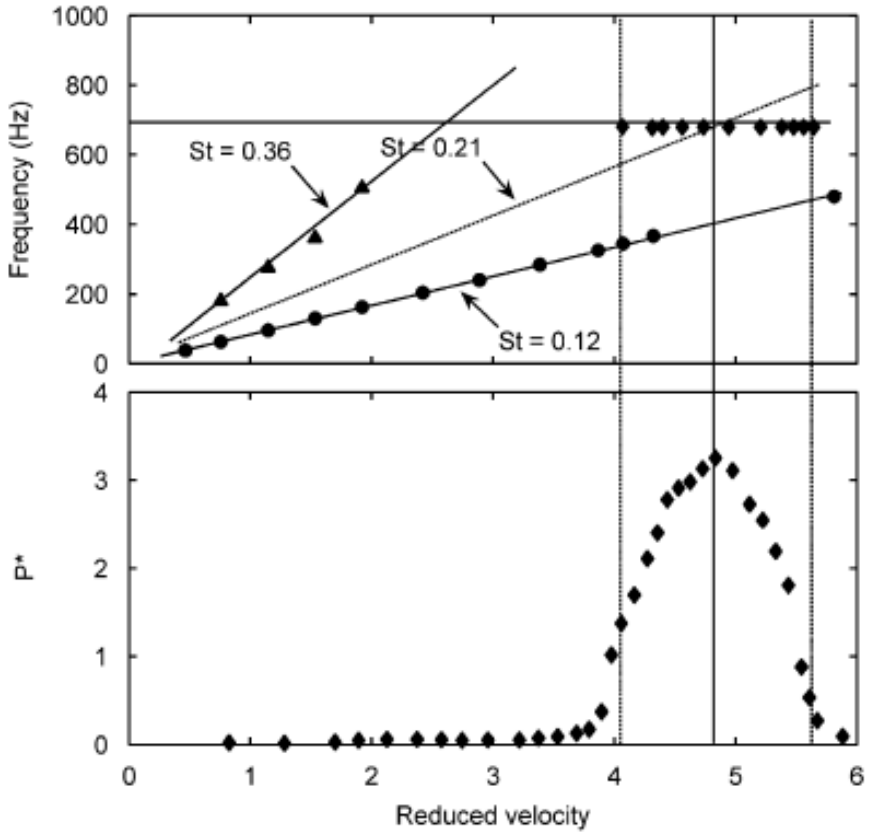

Figure 2-29 : Aeroacoustic response of two side-by-side cylinders with spacing ratio of T/D = 1.25 and D = 21.8 mm for the first acoustic mode, Hanson et al. (2009)

The second study was conducted by Arafa and Mohany (2015) for two side-by-side cylinders at large spacing ratio (T/D > 3.5) during resonance conditions. The experiments

were done mainly to investigate the effect of the cylinders position within the rectangular test section on the flow-excited acoustic resonance. It was concluded that when the two cylinders are positioned at the two nodes of the second acoustic cross-mode, the acoustic resonance was not a result of the linear superposition of individual cases. The acoustic resonance in the case of the two side-by-side cylinders was found to produce higher acoustic pressure due to the reduction in the radiation losses.

Arafa and Mohany also concluded that the location of the cylinder within the duct relative to the acoustic particle velocity distribution has a drastic effect on the excitation frequency at resonance. It was found that moving the cylinder away from the acoustic particle velocity anti-node of a specific acoustic mode, decreases the level of generated noise (relative ot this mode). The variation in the acoustic pressure amplitude followed the theoretical sinusoidal distribution of the acoustic particle velocity. Whenever the cylinder is placed at an acoustic particle velocity node of a certain cross-mode this mode is never excited at resonance. **Figure 2-30** shows the acoustic pressure amplitude for a cylinder of similar diameter tested at various locations of acoustic particle velocity antinodes.

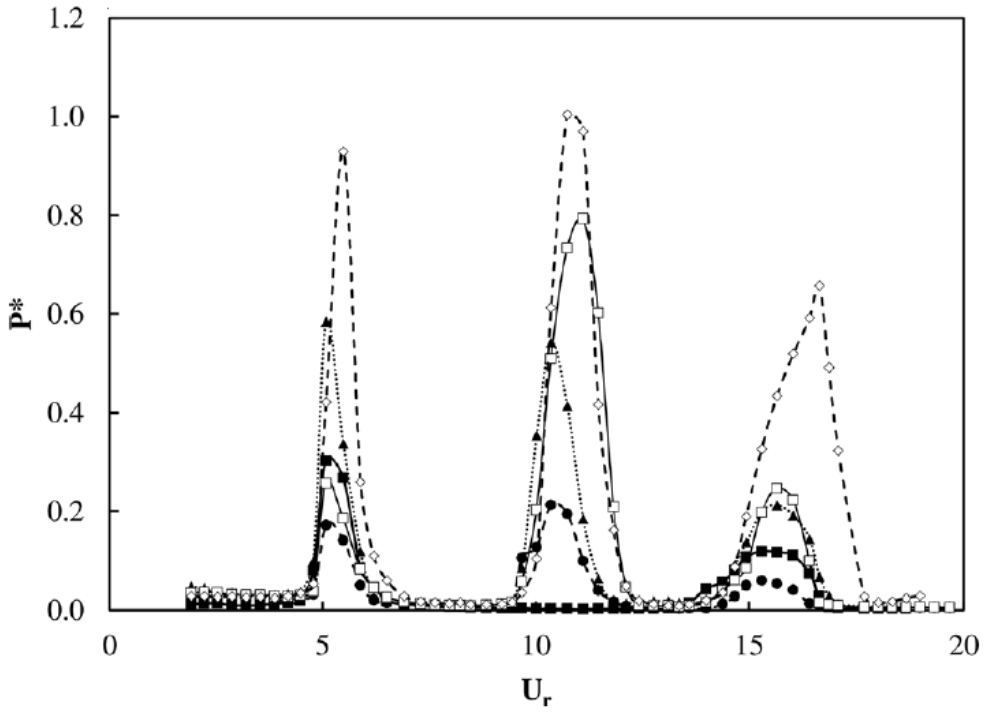

Figure 2-30 : Comparison of the aeroacoustic responses of multiple cylinders, D = 12.7mm. Cylinders are positioned at the acoustic particle velocity antinodes, Arafa and Mohany (2015)

2.4.6 Damping Criteria in Tube Bundles of Heat Exchangers

The first to observe and report flow induced noise in tube bundles of heat exchangers was Baird (1954), where he observed the buckling of superheater unit tubes. The excessive vibrations resulted as a direct consequence of flow-excited acoustic resonance.

Two theories were proposed at the time, one indicating that the resonance in tube bundles occurs as a result of normal vortex shedding, and the other was that the resonance occurrs as a result of turbulent buffeting. The latter theory was proposed by Owen (1965) who argued that discrete vorticity like the ones experienced for single cylinders is impossible in the case of heat exchangers, thus the source of vibration (structural, or gaseous), is due to

the randomly fluctuating forces imposed on the tubes by the turbulent eddies (turbulent buffeting). The second theory was proposed by Chen and Young (1968) who claimed that in heat exchangers, every tube sheds vortices downstream in a manner similar to the single cylinder shedding. The wake of each cylinder was considered to be a potential noise source, and the acoustic resonance materialized when the overall frequency of the resultant pressure fluctuations matched one of the acoustic modes of the ducts. Despite the change in point of views regarding the reason of acoustic resonance, the mechanism by which the resonance initiated (i.e. frequency coincidence) was supported similarly by both. Each theory was supported by different scholars at that time. **Figure 2-31** shows the difference between the proposed theories of Chen and Owen. Later, Fitzpatrick (1985) attributed the noise source in tube bundles to vortex shedding, turbulent buffeting and broadband buffeting simultaneously.

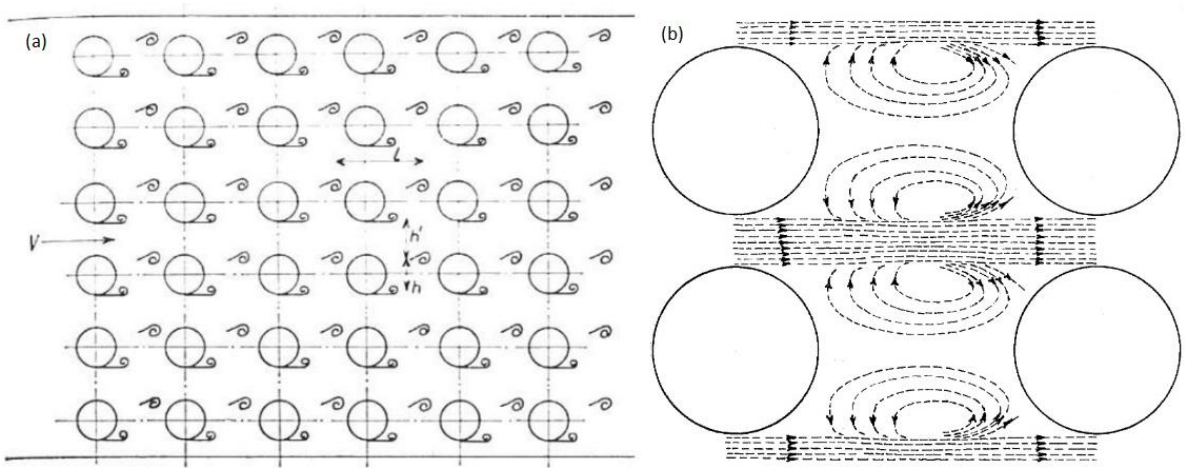

Figure 2-31 : Different theories proposed for tube bundles excitation mechanism , (a) Karman vortex streets shedding, Chen and Young (1968) (b) turbulent buffeting, Owen (1965)

Many criteria have been developed in order to predict the occurrence of the acoustic resonance in tube bundles. Research has been done on actual heat exchangers and scaled laboratory models and hundreds of experiments were conducted, yet the problem still persists. In almost 30-40% of the cases in which acoustic resonance is expected to occur, it does not**,** Blevins and Bressler (1993).

The inaccurate prediction of resonance may lead to catastrophic consequences such as the breakdown of the tube bundles inside the heat exchangers., which may cause mechanical failures to the overall structures. Even when the structural failure is not a concern, the high tonal noise produced from acoustic resonance may be damaging to human ears and/or exceed federal/provincial governing laws.

The following six prediction criteria (damping criteria) are considered the fundamental ones proposed since 1950.

The first damping criterion referred to as the "slenderness ratio" criterion, was developed by Grotz and Arnold (1956) to predict the occurrence of acoustic resonance in in-line tube bundles. The damping criterion is described by **Equation 2.13.**

$$\Gamma = \frac{H/D}{\left(\frac{L}{D}-1\right)i} < 62 \text{ or } 80 \qquad \textbf{(2.13)}$$

Where *H* is the duct height, and *L* is the spacing between any two consecutive cylinders, *D* is the diameter of the cylinders, and *i* is the acoustic mode of interest.

It is based on the assumption that the disturbance in the tube wake will need to be sustained by the pressure disturbances reflected from the walls of the duct. Based on their

experimental evidence, they set up the upper boundaries to the value of 62 or 80, after which the acoustic resonance will not occur. Blevins and Bressler (1993) questioned the validity of this model for staggered configurations.

The second criterion was proposed by Chen (1968) based on experimental data collected in an "ideal" laboratory setting. The Chen damping criterion for acoustic resonance is defined as follows: -

$$\Psi = \left(\frac{R_{cr}}{S}\right)\left(\frac{L-d}{L}\right)^2\left(\frac{d}{T}\right) > 600 \qquad \textbf{(2.14)}$$

Where R_{cr} is the critical Reynolds number, S is the Strouhal number, T is the transverse spacing. The equation is used for in-line tube bundles. For staggered configuration ($2L$) should be used instead. Chen, however, did not provide any information regarding how the threshold value was obtained. The threshold value of 600 is defined for tube banks without fins, in 1973 however, this critical value was revised and raised to Ψ = 2000. The reason being is that the 600 value was assumed for laboratory controlled "ideal" case but when the criterion was tested in actual tube banks of heat exchanger units, it failed to predict resonance until the 2000 mark. The reason for this according to Chen was due to the degree of uniformity of the velocity distribution over the test section. In the actual heat exchanger unit, the flow is not as organized and ideal as it is in the lab setting, thus the system becomes chaotic which introduces more damping to the system, Chen (1968), Chen and Young (1974).

Fitzpatrick (1982, 1985), analyzed the damping criteria proposed by Grotz & Arnold and Chen and compared them to experimental data from other studies performed by Fitzpatrick and Donaldson (1977), Baylac et al. (1973) and Jaudet et al. (1971). The data compared

together had the same tube diameter, duct size, and longitudinal pitch ratio. The difference was in the transverse pitch to diameter ratio (X_L). **Figure 2-32** and **Figure 2-33** shows the comparison taken from the study conducted by Fitzpatrick (1985) with the criterion proposed by Grotz and Arnold (1956) and Chen (1968), respectively. Fitzpatrick concluded that the damping criterion proposed by Grotz and Arnold gave better prediction guidance than the criterion proposed by Chen. The main issue in the Chen criterion according to Fitzpatrick is that it is geometrically incompatible (i.e. does not account for geometrical scaling). For example, if the diameter of the tubes were doubled at a constant spacing ratio and resonance frequency, the critical velocity at which resonance will occur will be also doubled, because of the constant value of the Strouhal number. This will cause the critical Reynolds number value to increase by 4 times, which may give misleading predictions. The discrepancy due to geometric scaling problem, can be observed clearly by the extreme points in the figures, Ziada (1989a, 1989b).

To construct a reasonable prediction criterion and overcome this inconsistency, Fitzpatrick included the Reynolds number to the form of (Grotz & Arnold) and developed his own criterion as follows: -

$$\Delta^* = \left(\frac{Re^{0.5}}{M_{cr}S}\right)\left\{\frac{1}{2(X_L-1)(X_D)}\right\} \qquad \textbf{(2.15)}$$

Where $M_{cr} = V_{Cr}/c_o$ is the critical Mach number. The inclusion of the Reynolds number served to account for the geometrical scaling. Fitzpatrick compared his modified damping version against the previously published data. The criterion showed a promising reduction in scattering the data. The data was clearly bounded by two distinct lines representing the upper and lower resonance boundaries **Figure 2-34**. The upper boundary represents the high damping of the system after which the energy in the system is weak compared to the

damping, thus resonance will not occur. The lower boundary represents higher acoustic mode frequencies that overcomes the turbulent energy present in the system at this frequency.

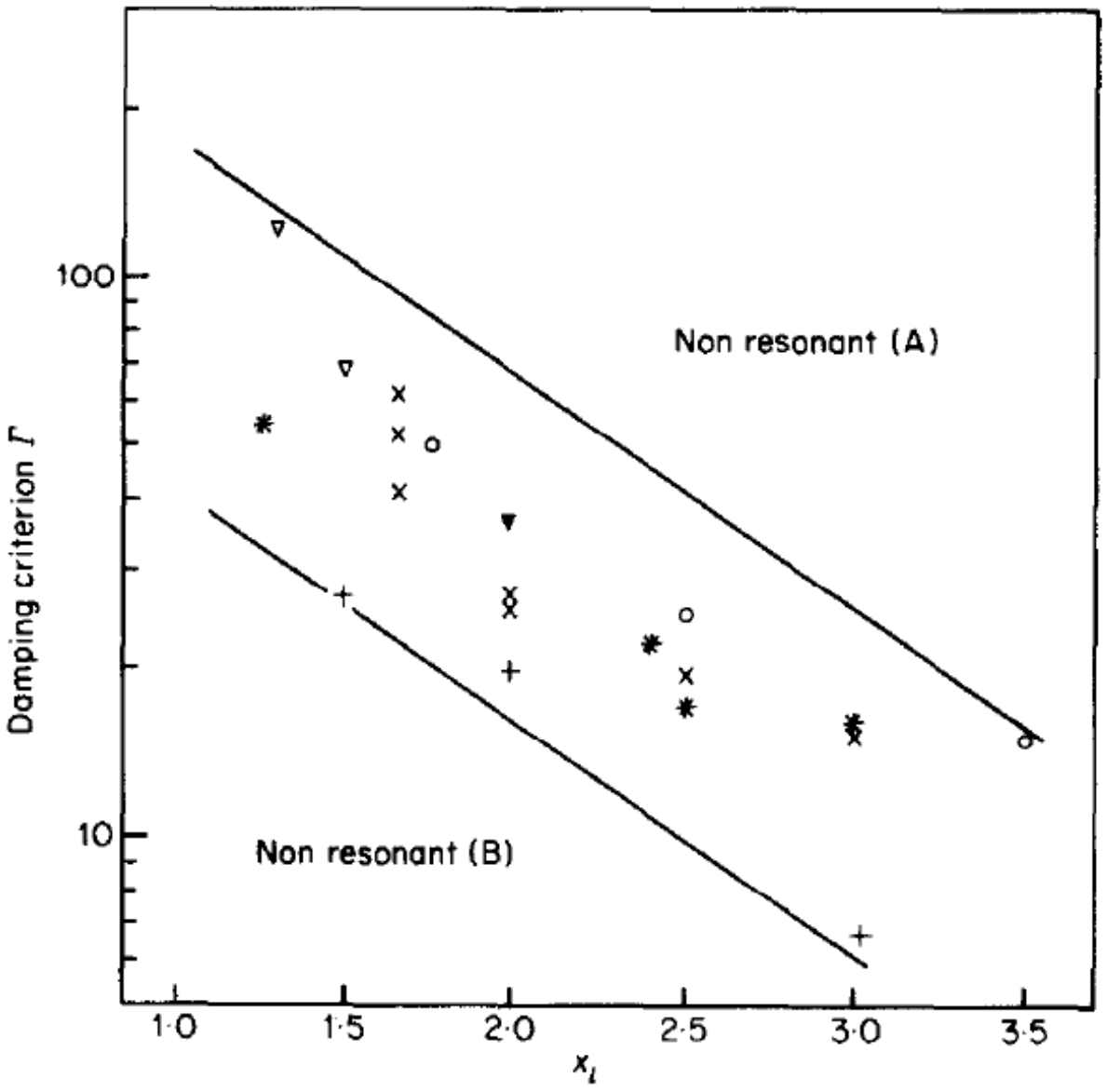

Figure 2-32 : Comparison of data from X, Grotz and Arnold (1956), ▽, Fitzpatrick and Donaldson (1977) , +, Baylac et al. (1973) and o, Jaudet et al. (1971), with the damping criterion proposed by Grotz and Arnold (1956). The figure is taken from Fitzpatrick (1985).

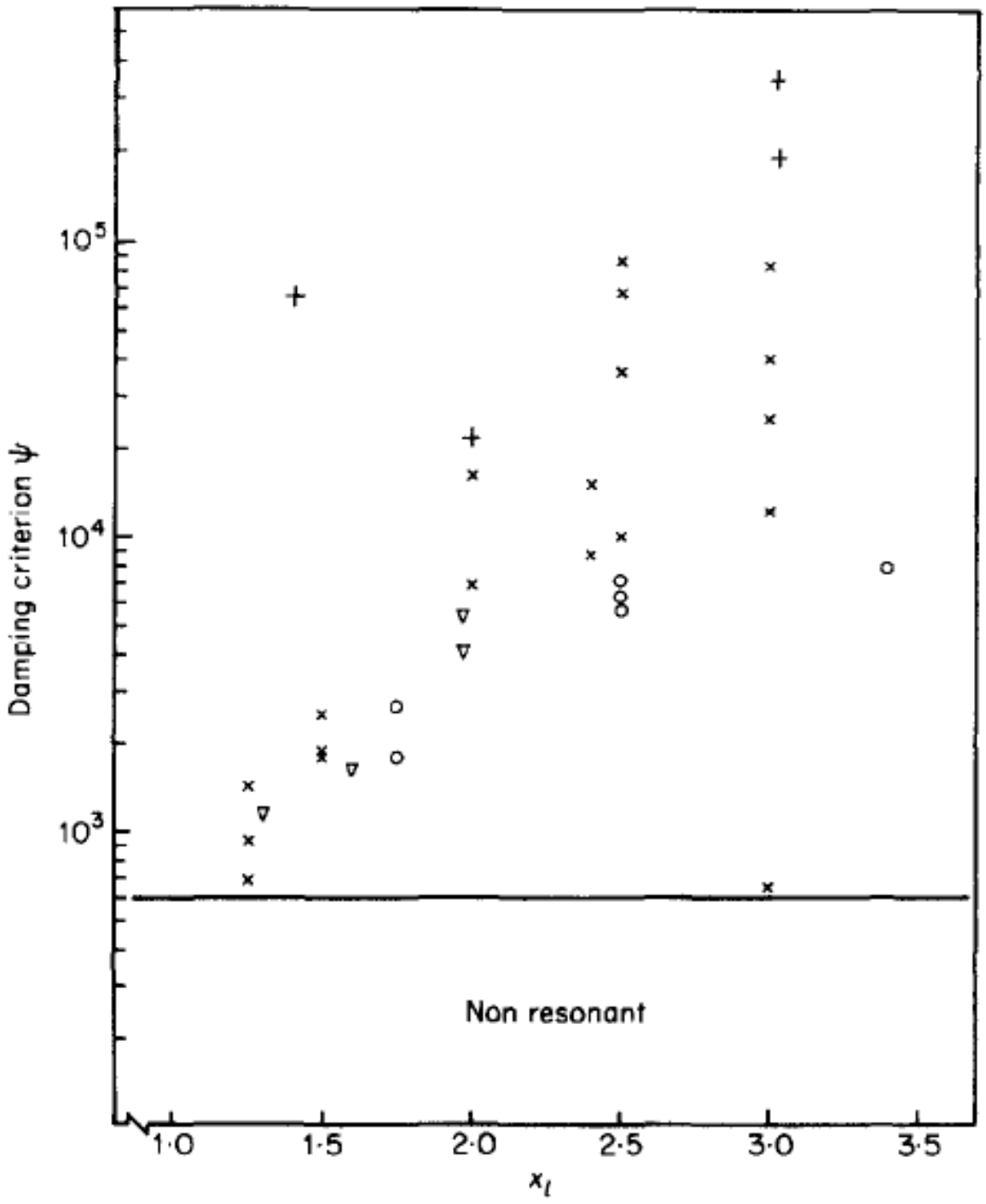

Figure 2-33 : Comparison of data from X, Grotz and Arnold (1956), ▽, Fitzpatrick and Donaldson (1977) , +, Baylac et al. (1973) and o, Jaudet et al. (1971), with the damping criterion proposed by Chen (1968). Figure is taken from Fitzpatrick (1985)

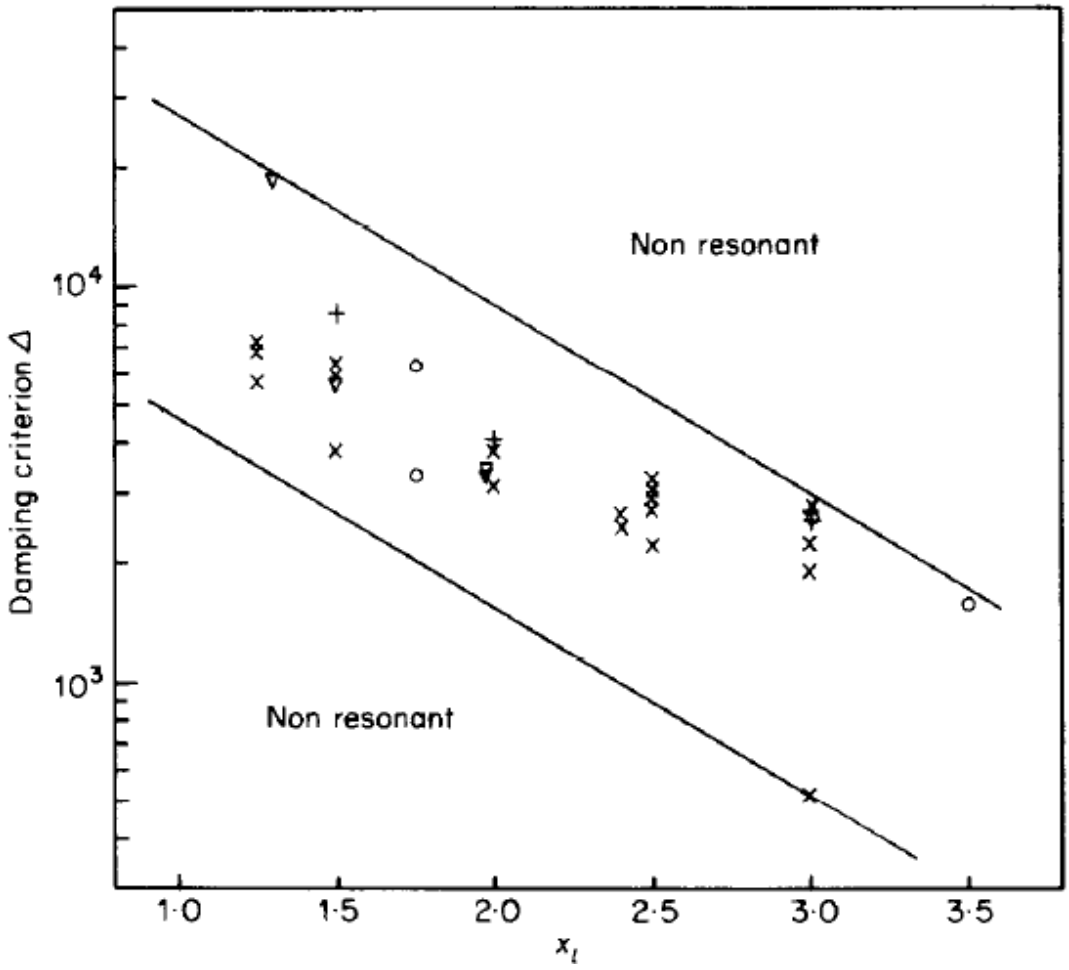

Figure 2-34 : Revised Fitzpatrick criterion compared with data from X, Grotz and Arnold (1956), ▽, Fitzpatrick and Donaldson (1977) , +, Baylac et al. (1973) and o, Jaudet et al. (1971), with the damping criterion proposed by Chen (1968). Figure is taken from Fitzpatrick (1985)

Ziada et al. (1989a, 1989b) performed extensive research in regards to the acoustic resonance in tube bundles of heat exchangers. A general damping criteria for in-line and staggered tube bundles was proposed to overcome the limitations found in previous criteria, to account for geometrical scaling as well as gas properties, and to include both resonance and non-resonance cases.

Several tests were performed in wind and water tunnel facilities, with variable duct heights, different configurations, and different tube diameters. Staggered and in-line arrays of closely packed tubes with various tube diameters were tested in order to investigate resonating cases. Cases where the condition of frequency coincidence is satisfied but the acoustic resonance is not materialized, were still included in analysis. Flow visualization was performed at different Reynolds number in the water channel since they are free of resonance effects, thus the flow structure will be representative for off-resonance cases. The damping criterion provided by Ziada et al. covered a wide range of tubes of diameters 1.65 to 63 mm, frequencies (17 to 800 Hz), speeds of sound (345 to 600 m/s) and kinematic viscosities ($1.6x10^{-5}$ to $12x10^{-5}$ m^2/s). This wide range of spacing ratios and test conditions meant that most of the industrial scenarios could be mimicked easily (including the effect of gas properties).

Ziada et al. (1989a, 1989b) used data points from all the experimental studies performed at the time and added their own data to them to cover as many scenarios as possible. Parametric studies were performed to obtain the distinct relationships between the Reynolds number, the spacing ratios and the acoustical Reynolds number according to the configuration (in-line or staggered). The following resonance criterion was developed to predict acoustic resonance in in-line tube bundles.

$$G_i = Re_{cr}^{0.5}(X_T)\left(\frac{v}{cD}\right) \qquad \textbf{(2.16)}$$

Figure 2-35 shows the curve of the criterion against experimental data points from Ziada and others. It can be observed that the criterion distinguishes well between the resonating and non-resonating cases.

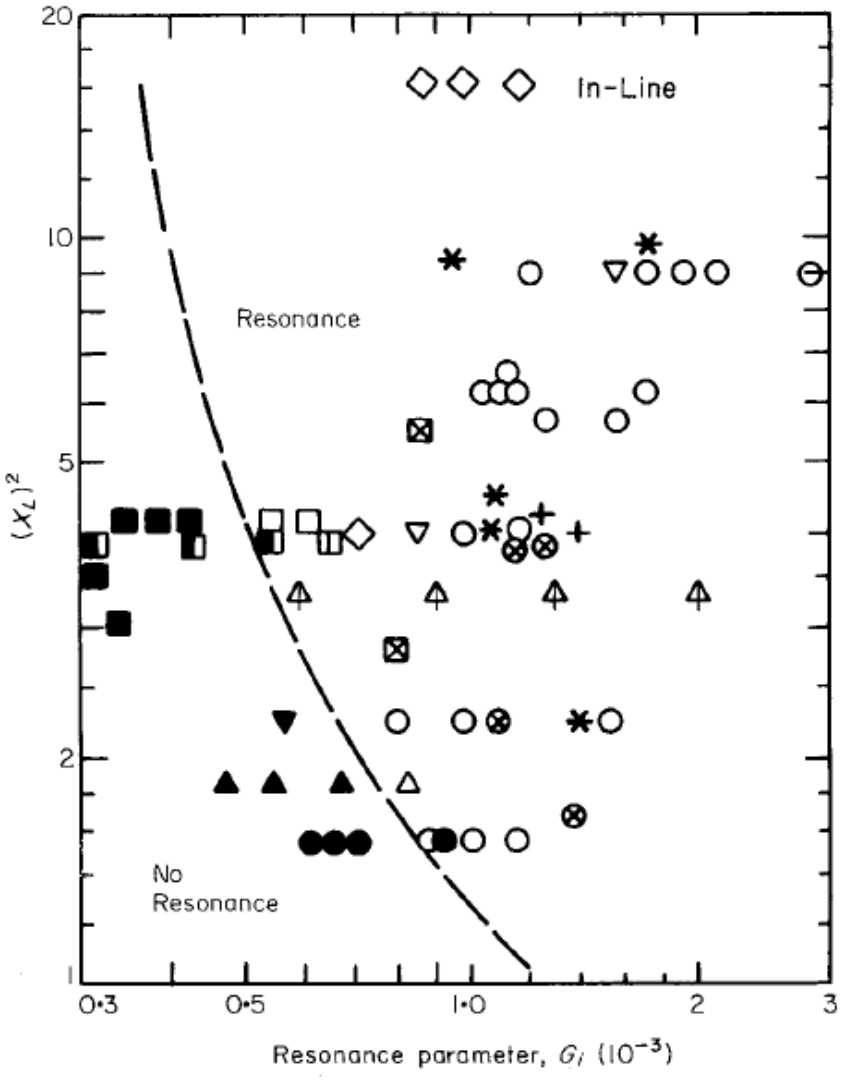

Figure 2-35 : In-line tube-bundle criterion Ziada et al. (1989b)

For the staggered arrangement the following criterion was developed, and the comparison with the literature is depicted in **Figure 2-35**. It is worth noting that for the staggered arrangement not all the diameters were tested (only those in the range of 19 to 31 mm) and

also all the data points compared were from laboratory tests and none were from actual industrial units.

$$G_s = Re_{Cr}^{0.5} \left(\frac{\sqrt{X_L(X_T-1)}}{(X_L-1)}\right)\left(\frac{v}{cD}\right) \quad \textbf{(2.17)}$$

The comparison with experimental data performed by other scholars against the proposed criteria by Ziada et al. (1989) showed promising results for both configurations. Finally, Ziada et al. (1989) provided a design procedure to predict and suppress the acoustic resonance in tube bundles based on his criteria. The procedure consisted of three steps as follows: -

1) Estimation of the acoustical frequency of the duct and the effective speed of sound proportional to the solidity ratio.
2) Estimation of the critical velocity (with a safety margin of 20%) based on the relationship with the Strouhal number. The Strouhal number for every spacing ratio is different, and are provided in different tables.
3) Estimation of the resonance parameter whether G_i for inline tube bundles or G_s for staggered tube bundles.

However, one major limitation of the proposed criteria is that they do not provide any information about the level of the broadband noise produced. Thus in some cases according to the criteria a unit might be in a no- resonance condition, where in fact it is experiencing resonance and is very loud and unpleasant to the operator.

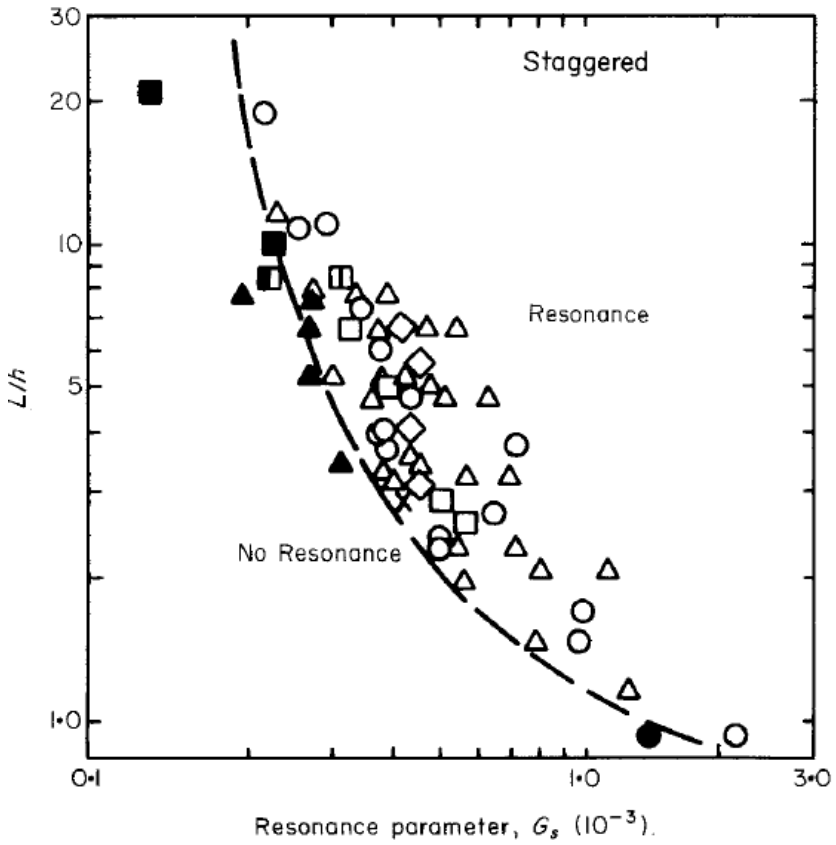

Figure 2-36 : Staggered tube bundle criterion, Ziada et al. (1989b)

Blevins and Bressler (1987) performed a series of experiments on a simulated heat exchanger unit with nine different tube patterns. Measurements were done for the sound pressure levels, the pressure drop across the heat exchanger and the turbulence. At first, they proposed a damping criterion and charts for in-line and staggered tube bundles. The criterion was based solely on the spacing ratios between the cylinders and disregarded the effects of important parameters such as the Reynolds number, the tube parameters and gas properties, Ziada et al. (1989a, 1989b). This omission resulted in the inaccurate prediction of resonance occurrence for closely packed (small spacing ratios) tube bundles. For example, according to the first proposed criterion, the closely packed tube bundles would

not resonate, however in some reported cases in the literature, acoustic resonance for closely packed tubes was observed.

In 1993, Blevins and Bressler extended their study and complemented the results with more experiments on single cylinders and tube arrays. Sixteen experiments were performed for the single cylinder cases in a test section of variable height. Six diameters in the range of 3.17 – 25.4 mm were tested. As for the tube bundles, only a single diameter was tested (19.05 mm). Blevins and Bressler revisited the old criterion and developed two criteria that correlate the maximum acoustic pressure amplitude (P_{rms}) at resonance in the case of single cylinders and tube bundles.

The criterion for the single cylinder is described by Equation 2.12a. It relates the maximum acoustic pressure at resonance to the Mach number, the dynamic head of the flow and the geometrical properties of both the cylinder (diameter) and the duct (height). As for the rows and arrays, they provided a different formula Equation 2.12b to relate the maximum sound pressure levels at resonance with the so-called input energy parameter, which is the multiplication of the Mach number and the static pressure drop across the tube bundle. Resonance is expected if $U/f_a D > 2$. Blevins and Bressler (1993) indicated that the equation may also be used to predict the maximum acoustic pressure for a single cylinder.

Lastly, Eisinger et al. (1996), proposed a criterion for the prediction of resonance in tube bundles of heat exchangers based on the input energy parameter (proposed by Blevins and Bressler) and the dimensionless acoustic particle velocity of the acoustic mode. The

criterion also included the effect of the acoustic duct frequency (variable heights) and the acoustic damping of the fluid inside the banks. The criterion was based on actual industrial measurements taken during operation as well as 60 laboratory tests with cold air flow. The following is the guideline proposed by Eisinger to predict resonance.

1. Input energy parameter $M\Delta P_i$ is compared with input energy parameters related to acoustic pressure $M\Delta P_{p,i}$ or acoustic particle velocity $M\Delta P_{v,i}$
2. Dimensionless acoustic particle velocity at resonance $\left({v_p}/{v}\right)_i$ is compared to limit value $\left({v_p}/{v}\right)_p$
3. Use graphical map provided by Eisinger et al. (1996) to predict if vibration (resonance) will occur or not

The data from the experimental results of Fenestra et al. (2006) as well as other data from literature were compared against the criteria of Blevins and Bressler. **Figure 2-37** shows the comparison between the maximum acoustic pressure versus the input energy parameter as specified by Blevins. The comparison shows that the suggested equation by Blevins greatly under-predicts the actual maximum acoustic pressure in case of full-scale heat exchangers.

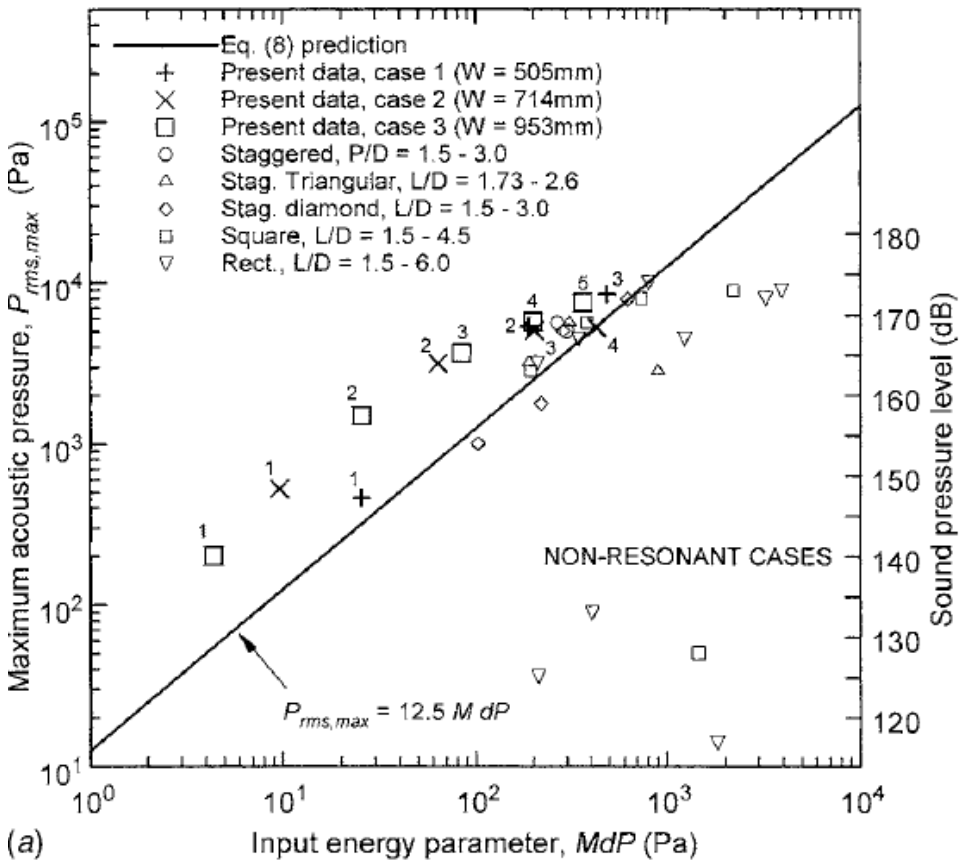

Figure 2-37 : comparison of input energy parameter proposed by Blevins with other parameters in literature, Fenestra et al. (2006)

2.5 Summary and Research Needs

The extensive literature review conducted provided an in-depth analysis of the current state of knowledge in regards to the flow-sound interaction of circular cylinders in cross-flow. A great amount of work has been completed in the past century to try and understand the interaction phenomena that occurs between the tubes in the tube- bundles of heat exchangers. Although the fundamental phenomenon of the flow-excited acoustic resonance is well understood and documented in terms of the condition necessary to initiate and sustain an acoustic resonance, accurately predicting the resonance occurrence,

especially in tube bundles of heat exchangers still remains a challenge. Very few research has been done on simpler configurations such as single, side-by-side and tandem cylinders during acoustic resonance conditions, although the fundamental understanding of simple geometries is necessary to fully characterize the phenomena in more complex designs. Moreover, some cases have been identified in literature where the proposed design guidelines and criteria fails to predict acoustic resonance occurrence and pressure amplitude for very basic geometries such as single cylinders.

Finally, most of the research found in literature, whether for complex or simple configurations focuses on changing parameters related to the enclosed body such as the diameter of the cylinder, the geometry of the cylinder (i.e. finned), the spacing between the cylinders, the orientation of the cylinders and the flow conditions. No attention has been given to the actual physical or acoustical properties of the duct, and the influence of duct parameters such as the height on the flow-sound interaction mechanism has not been investigated.

The purpose of this research is, therefore, to perform a comprehensive parametric study to identify the effect of different parameters on the flow-sound interaction mechanism of circular cylinders in cross-flow. The effects of the duct height, acoustic damping and the location of the cylinder inside the duct will be experimentally investigated in simple configurations like a single cylinder, tandem and side-by-side. It is believed that the findings of this research will help further enhance the understanding of flow-sound interaction in more complex geometries such as in tube bundles of heat exchangers. In doing so, it will be easier to develop more reliable damping criteria to prevent, or at least expect the flow-excited acoustic resonance in tube bundles of heat exchangers.

Chapter 3

3 Experimental Setup & Methodology

3.1 Experimental Setup

This chapter describes the experimental setup and testing procedures used to perform the experiments of the present work. In the first section, the currently existing wind tunnel setup, at the Aeroacoustics and Noise Control Laboratory (Oshawa, ON), and motor capabilities are described in detail. In the second section, the design of the experiments and the rationale behind each experimental set is presented. The third section discusses the instrumentation tools and data acquisition techniques adapted to perform the experiments. Lastly, the testing procedures that were followed to conduct the experiments are briefly outlined.

An isometric view of the fully-assembled experimental setup used in the experiments is shown in **Figure 3-1**. The test rig is an open-loop wind tunnel facility made up of various parts. The test sections used for the experiments were connected to the existing setup shown in **Figure 3-1** at the diffuser point. For every built test section, a bell mouth intake was customized to fit the internal dimensions of the test section. A contraction or an expansion cone at the downstream end of the test section had to be customized for every test section as well. The contraction/expansion cone serves to fit any test section with a varying height to the currently existing wind tunnel dimensions *127x254 mm (5”x10”)*.

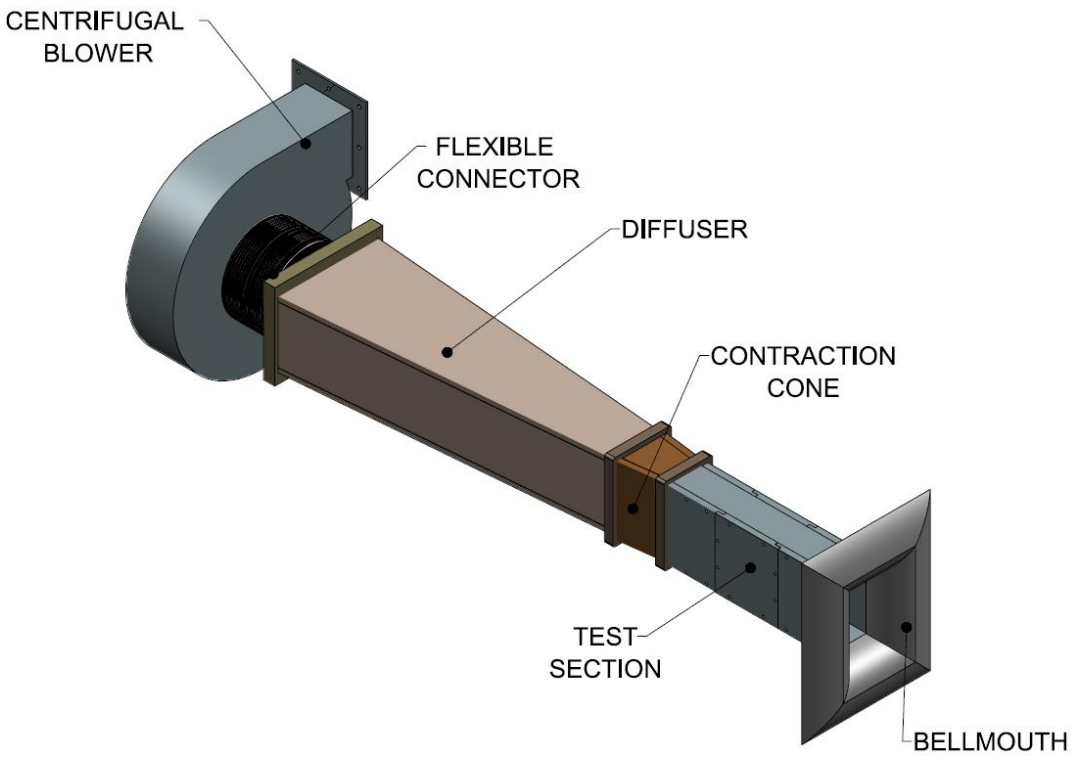

Figure 3-1 : Isometric CAD view of the wind-tunnel assembly at the Aeroacoustics and Noise Control Laboratory (UOIT)

The test rig in **Figure 3-1** consists of the following sub-parts.

1. **Centrifugal blower, motor and flexible connector:** a centrifugal blower is connected to an electric motor with a variable frequency driver (VFD). The motor that drives the blower is a 75HP 3-Phase electric motor with a maximum rating of *1780 RPM* (maximum velocity is *165m/s, M = 0.48)*. The VFD serves to control the velocity of the blower by changing the frequency supplied to the electrical motor. The frequency going to the motor can be changed by increments as small as *0.05 Hz* within the range of *0 Hz to 60 Hz*. This allowed for actual velocity increments of *0.5m/s* to be achieved. The blower structure along with the motor is rigidly fixed to the floor over a concrete

slab to absorb any vibrations induced from the blower. The flexible connector installed between the diffuser and the blower ensures that there are no vibrations transmitted from the test section to the blower or vice versa.

2. **Diffuser:** the wooden diffuser serves to connect the blower to the test section. The diffuser is made up of hard Russian birch plywood of thickness *19 mm (0.75")*. The diffuser is long enough to ensure that negligible pressure drops are experienced along the test section depth.
3. **Contraction/expansion cones:** contraction and expansion cones were manufactured for every test section exclusively to account for the height change. The cones were built with a smooth gradual increase/decrease along their lengths with a maximum included angle of *7°*. These precautions ensured that negligible pressure drops (if any) will occur over the test section as a result of sudden expansion or contraction.
4. **Test sections:** three test sections with different heights of *203, 254, 305 mm (8", 10" and 12")* were built for the experiments performed in this thesis. The width and depth of all test sections were fixed to *127 mm (5") and 762mm (30")* respectively. All the test sections were built in a systematic manner using hard Russian birch plywood of thickness *19mm (0.75").* The sides were made by assembling three wood sides of the same size. Then two *127x762 mm (5x30")* wooden plates were bolted at the top and bottom of the sides to create a full rectangular test section. The rigidity of the structure was maintained by utilizing *50.8x50.8mm (2x2")* cross-section wood frames on the top and bottom pieces, and by using *101x50mm (4x2")* hardwood frames on the inlet and outlet. **Figure 3-2** shows one of the fully built test sections without one of the side windows installed. The different support beams and frames to ensure the rigidity of the

structure can be clearly observed in the figure. The side windows are installed as per the experiment requirements (i.e. single or tandem configuration). The windows were cut exactly to the window dimensions to fit in the size and avoid any spaces on the side. The windows are then bolted with four screws to the wooden support beam at the top and bottom of the test section. Prior to the installation of the side windows, weather strips are glued at the top and bottom to ensure that no leakage occurs. **Figure 3-3** shows an example of the cylinder fixation for different configurations. It can be seen that when the cylinders are enclosed inside the duct, no gaps or spaces are observed due to the tight tolerance. Leakage at all connection points and critical locations were always checked using smoke prior to experiments to ensure a well-sealed experimental setup. All the cylinders used are tapped and drilled from the sides for $5/16^{th}$' – 18 bolts. To fix the cylinders in the middle windows, bolts and spacers are used on the outside and tightened to the cylinders and wooden side.

Figure 3-2 : Test section without the middle side windows

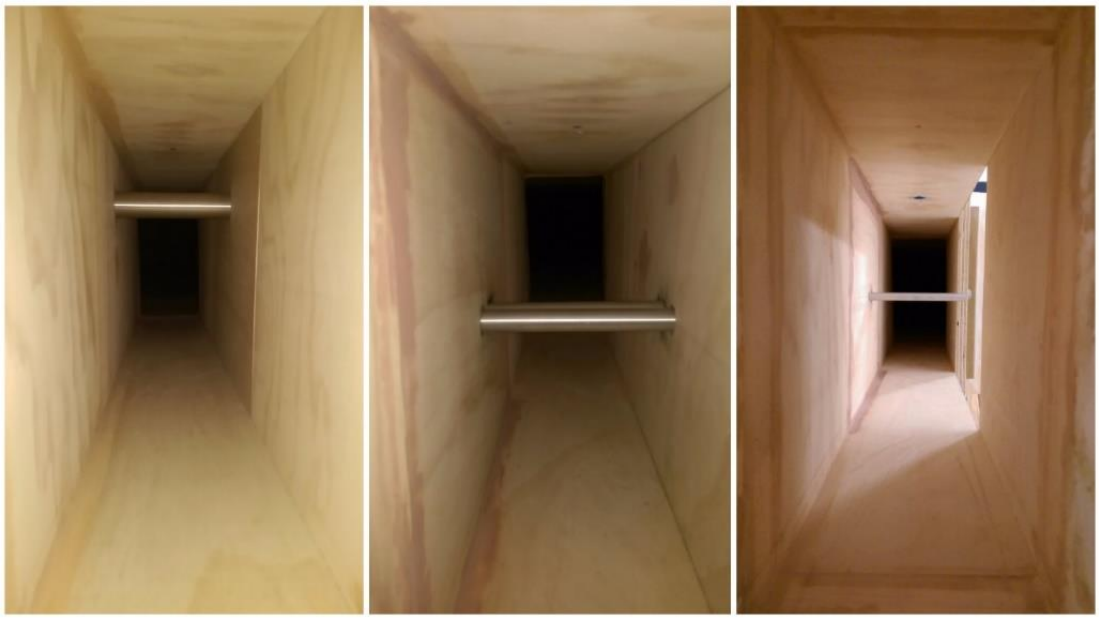

Figure 3-3 : Cylinder fixation inside the test section

5. **Bell-mouth:** for every test section, a different bell mouth as shown in **Figure 3-4** with the required internal dimensions was built. All the outer surfaces were coated with acrylic paint to ensure surface smoothness. The bell mouth had rounded parabolic leading edges to ensure the full flow of air with minimal disturbance at the inlet. The turbulence intensity inside the test sections was less than 1%.

Figure 3-4 : Bellmouth for one of the used test sections

3.2 Experiments Design

In order to fully analyze and understand the effect of the duct's geometry on the aeroacoustic response of cylinders in cross-flow, multiple experiments have been conducted to identify the parameters that have the most impact on the cylinders' acoustic behavior. For the presented work, more than 100 experiments were performed, each of which contained at least 60 data points. Each data point corresponds to a certain acoustic state of the system at a specific velocity and for a specific case. Seven smooth aluminum cylinders with varying diameters in the range of *10.6 – 25.0 mm (0.4 - 1.125")* were used in the present work. For tandem arrangements at different spacing ratios two cylinders of

the same diameter were used. To ensure that various scenarios are covered, different configurations for cylinders enclosed in ducts were tested. The four main configurations tested are as follows:

1) Single cylinders located at duct centerline **(Y/H = 0)**
2) Single cylinders shifted away from duct centerline **(Y/H = 0.25)**
3) Side-by-side cylinders at different transverse spacing ranges **T/D = 5.33 - 14.32**
4) Tandem configuration at two different longitudinal spacing ratios of **L/D = 1.5, 2**

To investigate the effect of the height; three different test sections of different heights *203, 254, 305 mm (8", 10" and 12")* were customized to fit the wind tunnel setup in the Aeroacoustics and Noise Control Laboratory at the University of Ontario Institute of Technology (Oshawa, ON).As the main objective of this work is to investigate the effect of the duct geometry on the aeroacoustic response of single and tandem cylinders in cross-flow, four different experimental sets were designed specifically to test for certain parameters of interest. The experiment sets were designed as follows:

1. The first experimental set focuses on testing all the cylinders in different heights to investigate the effect of the diameter (D), height (H), the combined effect of D and H, the blockage ratio (D/H) on the pressure amplitude of acoustic resonance and the frequency response. For this set, the cylinders were placed at the center of the duct, to excite the first acoustic cross mode of the duct. Special cases were considered where the blockage ratio (D/H) and the velocity at coincidence (U) were equal for different cases but the frequency at resonance was not.
2. The second set of measurements was designed to investigate the effect of the duct height on single cylinders shifted away from the centerline, and positioned at a

relative duct height of Y/H = 0.25. This position relative to the duct height was chosen to excite the 2nd acoustic cross-mode of the duct. In this set, the effects of the cylinder location, diameter and test section height were investigated.

3. The third set aims to extend the scope of the work by investigating the special cases of similar (D/H) and (U) but different pressure amplitude and frequency of excitation, on a more advanced configuration. Tandem configuration at two different spacing ratios L/D = 1.5 and 2, within the proximity region, were tested in the three duct heights. The effect of the height on the response of the tandem cylinders in the special cases of (D/H) was analyzed.

4. Lastly, in the tallest test section, two cylinders are placed in a side-by-side arrangement for transverse spacing ratios in the range of 5.33 – 14.32. Cylinders in these transverse spacing ratios are known to behave as isolated cylinders in terms of vortex shedding. Acoustically both cylinders should act as source/sink in terms of acoustic power, however, it seems that they both enhance the resonance instead, and the acoustic pressure amplitudes are magnified. The effect of the test section height on the aeroacoustic response of two side-by-side cylinders are investigated for this set. The Reynolds number (calculated based on the diameter) for the experiments ranged from (6.0 x 10 3 – 3.0 x 10 5), and the Mach number which ranged from 0.034 to 0.47.

3.3 Data Acquisition and Instrumentation

3.3.1 Data Acquisition

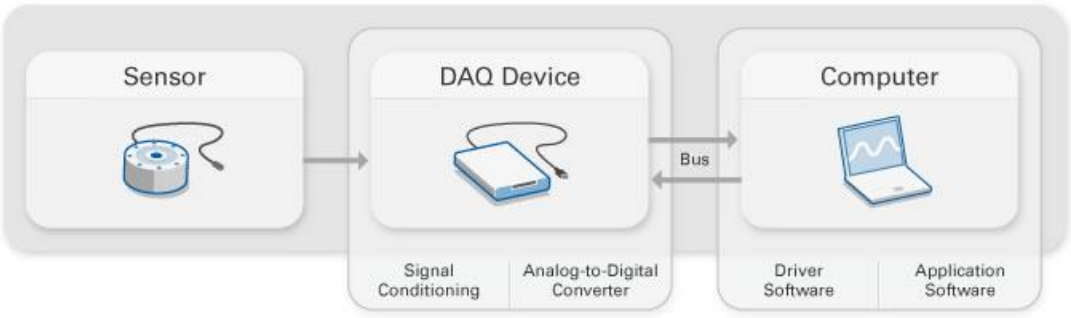

Figure 3-5 : Typical data acquisition layout (courtesy of National Instruments)

Figure 3-5 shows a typical data acquisition scheme similar to the scheme utilized in the experiments. The data acquisition consisted of a sensing element (pressure microphone), a signal conditioner, data acquisition card, and a computer software package for data analysis. For the experiments presented in this thesis, a pressure field microphone flush-mounted in the duct through insertion ports was used. The pressure field microphone is designed to directly measure the sound in front of the diaphragm with a constant phase and magnitude regardless of the orientation. The type of microphone used was carefully selected as it is mainly designed for high speed ducted flows. When the microphone senses the pressure perturbations that occurs inside the duct, the signal is then fed into a signal conditioner that amplifies and filters it in preparation for next steps. The DAQ card then receives the amplified and filtered signal and converts it from an analog to a digital signal to be read by the computer software and later the user. The final step in the data acquisition system is usually the software package on the computer, where the user gets to observe a representable form of the data for further analysis. For the experiments performed in this

thesis, the software used for the analysis are LabVIEW and Matlab with in-house developed codes to perform Fast Fourier transformation (FFT) and other spectral analysis on the signal. The hardware instrumentation used for the experiments are outlined briefly in the next section.

3.3.2 Instrumentation

DAQ Device The DAQ card used in the experiments is a high-quality multifunction data acquisition device manufactured by National Instruments of type (BNC-2110). The DAQ device serves to simplify the connections between the sensor (microphone) and the computer used to make it in a readable format for further analysis.

Signal Conditioner: The signal conditioner used is manufactured by PCB Piezotronics, model number 482C05. It is a basic four-channel signal conditioner designed to be used specifically with the sensors of ICP input type, which is similar to the microphones used. The signal conditioner provides an adjustable current source (0 to 20mA) to power the ICP sensors connected to it.

Microphone: The microphone (pressure transducer) used for the experiments is a pre-polarized ¼ inch pressure microphone manufactured by PCB Piezotronics model (378C10). This microphone is well suited for high velocity ducted flows. The frequency range of the microphone can reach up to 5KHz (±2dB.), which covers the entire frequency range required for the experiments. The sensitivity of the microphone, as reported by the manufacturer, is 1.0mv/Pa (±3dB).

The microphone was rigidly fixed and flush-mounted at the top wall of the test section through special insertion ports. The ports were made by drilling a hole slightly larger than

the microphone's mean diameter and then fixing a connecting brass nibble fitting to the wood. The microphone would then slide smoothly inside the brass union fitting and gets fixed from the top by the compression nut. This ensures that the microphone is rigidly mounted and flush with the inside top wall. **Figure 3-6** shows the different insertion ports positions at the top wall of one of the test section as well as the brass union used. The unused holes were filled with wax and completely plugged from inside and outside to avoid leakage.

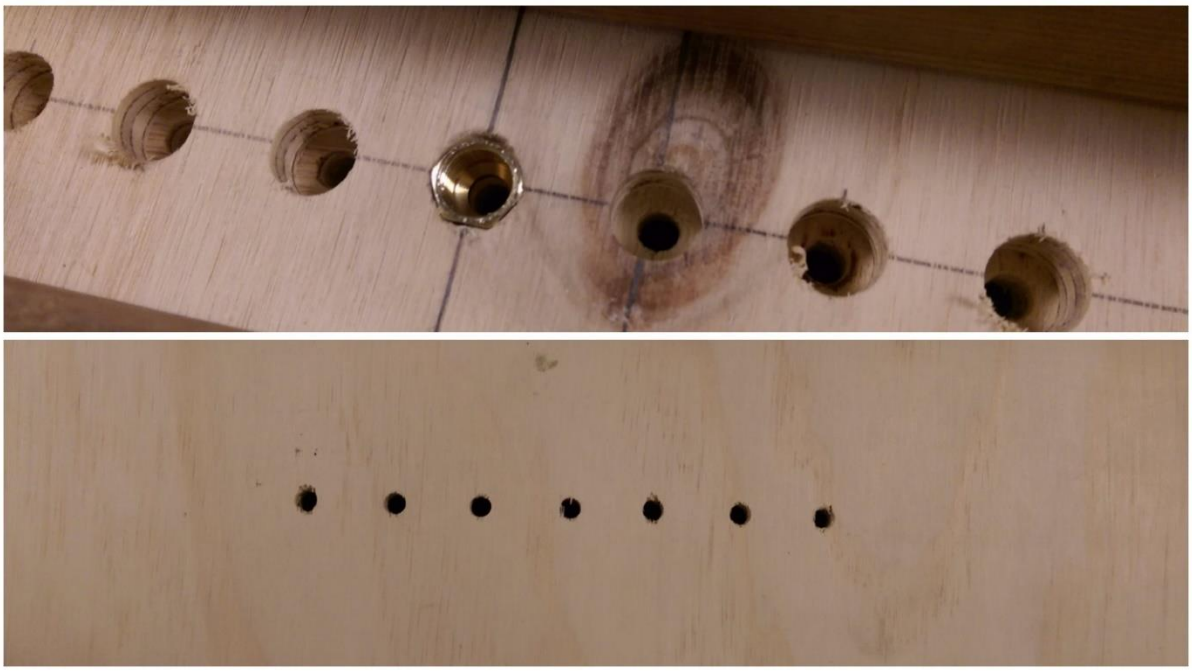

Figure 3-6 : Outside and inside view of the insertion ports for the microphones

The microphone was placed at a fixed reference position for all the experiments performed. Seven different positions on the top wall were tested to obtain the point of maximum acoustic pressure amplitude. Two points were tested upstream the cylinder, one point on top of the cylinder and four points downstream the cylinder. The maximum point of the trend line was found to be at a distance of *381 mm (15")* from the inlet of the test section,

which is *25.4mm (1")* downstream the cylinder. Therefore, this point was chosen to be the position of the microphone for all the experiments in this thesis. **Figure 3-7** shows the acoustic pressure amplitudes measured at each microphone location.

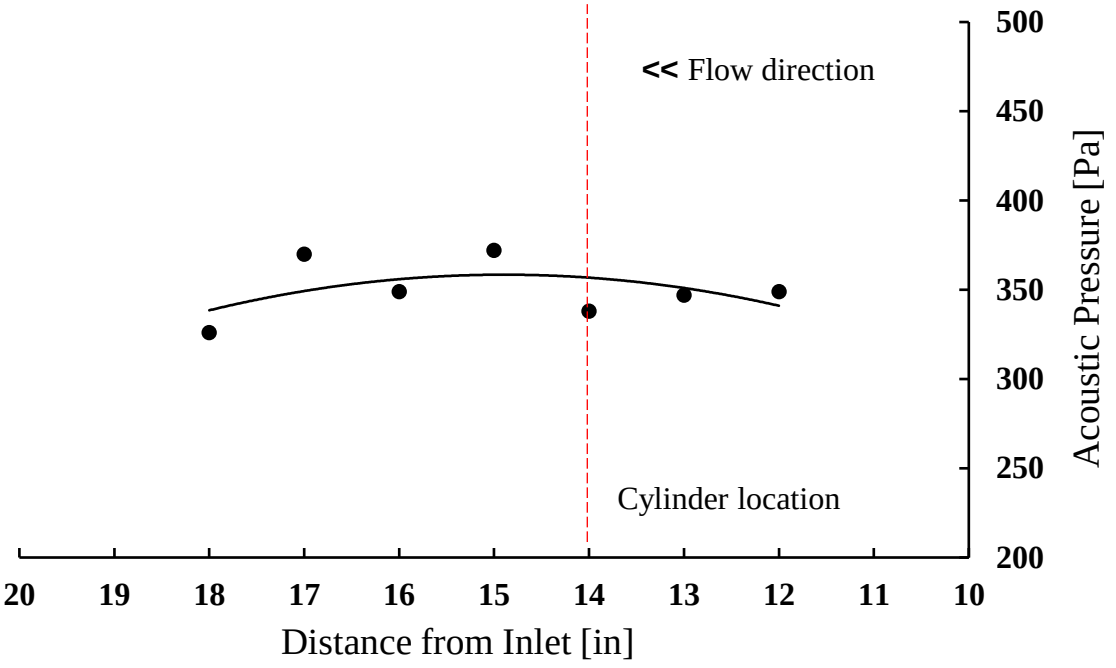

Figure 3-7 : Acoustic pressure amplitude measured from the top wall as a function of microphone position.

Piston-Phone / Calibrator: In order to ensure acoustic measurements accuracy, the microphones were calibrated using a sound calibrator before each experiment. The sound calibrator used is of type (42AB, Class 1) manufactured by G.R.A.S Sound & Vibration. Mainly, the sounds calibrator device consists of a sound source, an electronic control circuit, and a reference microphone. The calibrator works at a standard reference frequency of 1 kHz standard frequency at a calibration level of 114dB (*re 20 uPa*). The accuracy of calibration is **1000 Hz ±0.2 %** and **114 dB ±0.2 dB** as defined by the supplier.

Manometer: The manometer was used to measure the differential pressure inside the duct between two reference points. The manometer used is HT-1890 Digital Manometer and Differential Air Pressure Meter Gauge, manufactured by Specam. The manometer can report maximum, minimum, or time average pressure readings in 11 different formats. The manometer has an accuracy of ±0.3% full-scale output (FSO) at 25°, repeatability of ±0.2% (max ± 0.5% FSO), and works in the pressure ranges of -13.6kPa – 13.6kPa.

The static pressure across the cylinders inside the duct was measured through pressure taps drilled on the top wall of the test sections. For all the test sections, the pressure taps were drilled at the same location. The pressure taps were drilled at a distance of *254 mm (10")* upstream and downstream from the exact center of the duct. The distance from the inlet of the test section to the first pressure tap is *127 mm (5")* and the distance from the second pressure tap to the end of the test section is *127 mm (5")* as well. The positions were chosen carefully to account for the boundary effects at the test section inlet/outlet and to get the most accurate pressure drop reading possible.

Pitot tube: A pitot tube manufactured by Dwyer engineering (series 160 stainless steel) is used in order to calibrate the velocity inside different ducts with the motor frequency. The pitot tube and the manometer were used in a pitot-static arrangement to perform the calibration. The pitot tube was inserted to the centerline of the duct facing the incoming flow to get the most accurate mainstream velocity. The pitot tube compares the total pressure of the incoming flow from the hole in the front to the static pressure at the holes around the tube itself. The velocity inside the duct could then be related to the frequency of the motor using Bernoulli's principle to solve for velocity from the pressure drop according to the relation: -

$$V^2 = 2\frac{\Delta P}{\rho} \quad \textbf{(3.1)}$$

3.4 Experimental Procedure

The same systematic procedure is followed for all the experiments conducted throughout this study, to ensure that all obtained results are accurate and consistent. The following steps briefly describe the experimental procedure:

1) Test section velocity is calibrated using the pitot tube and manometer arrangement explained earlier. The velocity calibration is done every time the test section is changed to ensure that all the reported data is accurate.
2) Depending on the type of the performed experiment, the cylinder(s) is/are rigidly mounted at either the centerline of the test section or shifted away from the centerline. In the cases of tandem and side-by-side arrangements, two cylinders were rigidly mounted at the designated locations with respect to the spacing ratio (L/D or T/D).
3) The acoustic pressure amplitudes were measured using the pressure-field microphone that is flush-mounted on the duct top wall at the position of maximum acoustic pressure.
4) The static pressure drop across the cylinder is measured by means of a differential manometer, through the pressure taps on the top wall. The manometer device averaged samples over 2 minutes and reported the average reading in (inH20).
5) Measurement time for each signal was taken over 120 seconds, with a sampling rate of 20 kHz. FFT analysis was performed later on the data to obtain pressure and frequency spectra.
6) During experiments, velocity is increased by approximately 2m/s for every data point. However, before and after the lock-in regions the increments were reduced to 1m/s to accurately capture the full lock-in cycle.

Chapter 4

4 Aeroacoustic Response of Single Cylinder in Cross-Flow

4.1 Introduction

The aeroacoustics response of single cylinders in cross-flow is analyzed in this chapter. Seven cylinders of diameters; *10.56 (0.416"), 12.7 (0.5"), 15.875 (0.625"), 19.05 (0.75), 21.05 (0.829"), 25.4 (1"), and 28.575 (1.125") mm (inch)* are tested in three different test section heights of *203 (8"), 254 (10"), and 305 (12") mm(inch).* The effects of the cylinder diameter, the duct height, and the cylinder location on the aeroacoustic resonance excitation in ducts are addressed. The independent variation of both the height and diameter, allowed for a wide range of experiments to be done, as well as multiple parameters such as the height, the diameter or the combined effect of both (blockage ratio) to be varied independently. The Reynolds number of the experiments ranged from ($7.0 \times 10^3 - 3.0 \times 10^5$), and the Mach number ranged from (0.035 – 0.47).

Two sets of experiments were conducted for the single cylinder cases. The first set of experiments is conducted for single cylinders placed at the centerline of the duct (Y/H = 0). For the second set, the cylinders are shifted away from the centerline and placed at the position of Y/H = 0.25. The value Y/H refers to the cylinder position with respect to the duct height where H indicates the height of the duct and Y indicates the coordinate axis perpendicular to the cylinder's axis and flow direction. The position of the cylinder in the duct was chosen for the first and second set of measurements with respect to the first and

second acoustic mode distribution in the transverse direction along the duct height. This ensures that the first and second acoustic modes are excited respectively. **Figure 4-1** shows a schematic of the test section with the position of the cylinders relative to the height. The microphone is positioned at a distance of *25.4 mm (1")* downstream the cylinder since this position gives the maximum pressure amplitude reading. This position was determined in a separate experiment and the position of the microphone was fixed to $x = 25.4mm$ *(1")* downstream the cylinder for all the cases tested in this thesis. The experiment for determining the location of the microphone can be found in **Chapter 3: Experimental Set-up**. The pressure taps used to measure the static pressure across the cylinders were fixed at a distance of *508mm (20")* apart. The distance from the bellmouth to the first pressure tap is *254mm (10")*, and the distance from the last pressure tap to the end of the test section is *254mm (10")*. The positions of the upstream and downstream taps were carefully chosen to make sure that the pressure readings are not affected by the boundaries of the test section at inlet and outlet.

The first section of this chapter presents a typical response of a single cylinder in cross-flow experiencing resonance. This will help give an overview of the types of measurements done, the methodology used and the expected types of graphs from each test. The second section discusses the results obtained for the first set of measurements, where the cylinders were placed at Y/H = 0, to excite the first acoustic mode. Lastly, the measurements for the second set of experiments will be discussed, where the cylinders were placed at the relative position of Y/H = 0.25 to excite the second acoustic mode. The effects of the cylinder diameter, height, location and the combined effect of the diameter and height will be addressed for every section accordingly.

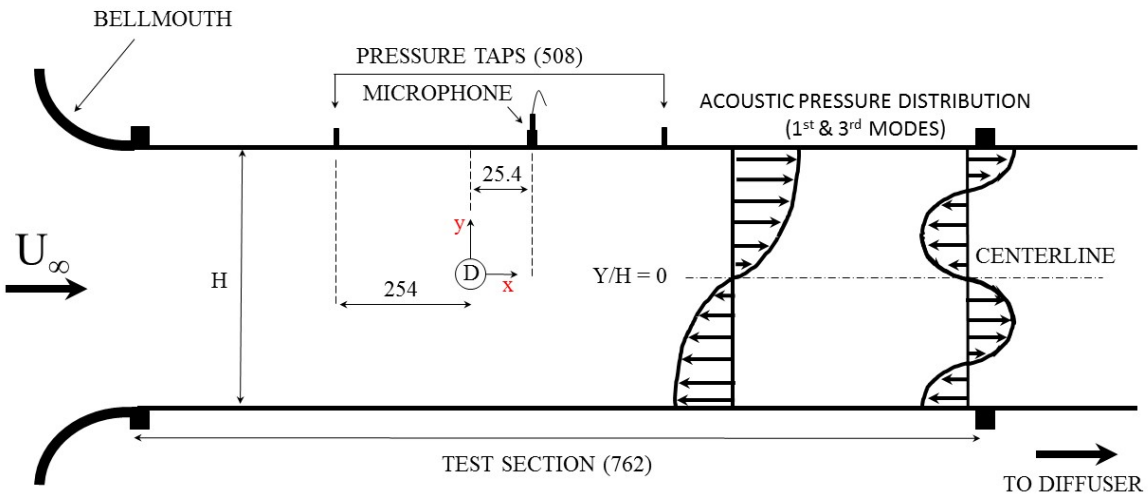

Figure 4-1 : Schematic of the test section used showing the position of measurement devices as well as the acoustic pressure distributions inside the duct (all dimensions in mm)

4.2 Typical Response

Figure 4-2 shows a typical microphone real time pressure spectrum signal from the experimental data at the off-resonance condition for specific velocity U. The FFT signal presented in the figure is for a *28.5mm (1.125")* cylinder in a duct of height *304mm (12")*. The vortex shedding frequency can be seen clearly at about $f_v = 200\ Hz$ and the fundamental frequency of the duct at $f_a = 563\ Hz$. The highest point of the vortex shedding peak is taken from each spectrum to form a complete aeroacoustic response for a certain case. The peak of the vortex shedding is usually sharp and easily distinguishable across the frequency spectrum. **Figure 4-3** shows the 3D waterfall plot for the same case, it can be seen that at the values of resonance the frequencies lock-in and the pressure amplitudes becomes very high. A waterfall plot constitutes a full experiment for a certain cylinder diameter.

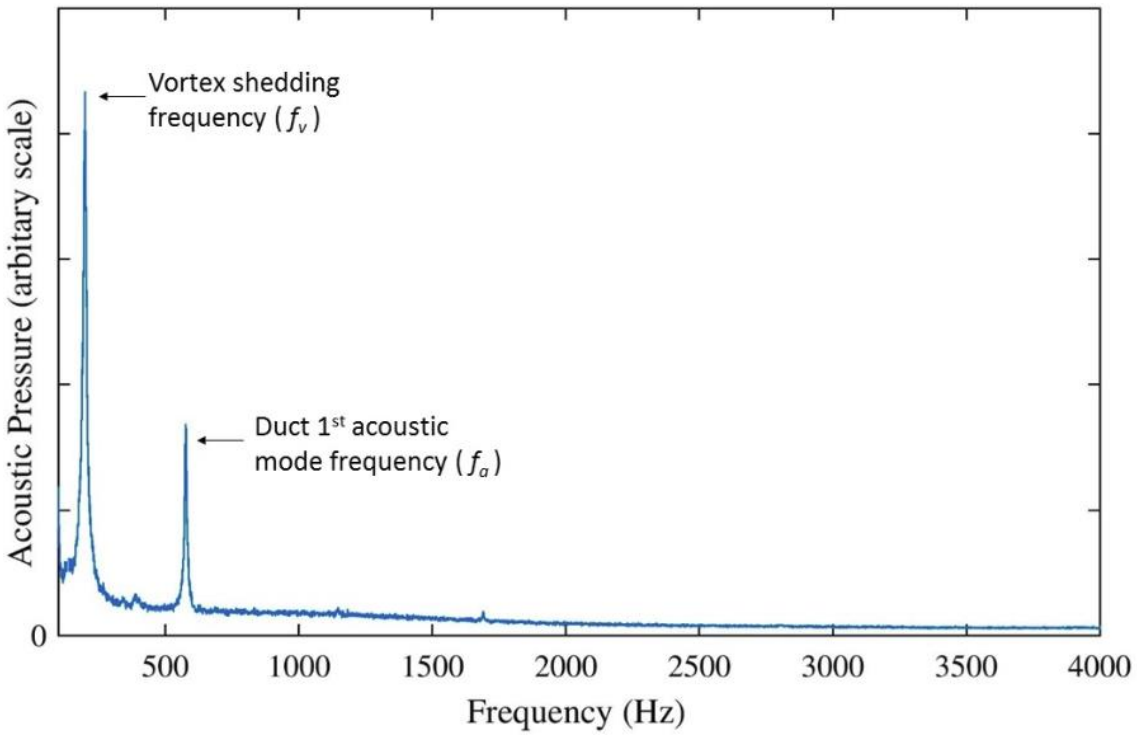

Figure 4-2 : Typical pressure spectrum (frequency domain) at any arbitrary velocity (U) , where U is any velocity at off-resonance condition, D=28.5 mm (1”), H=305mm (12”), Y/H=0

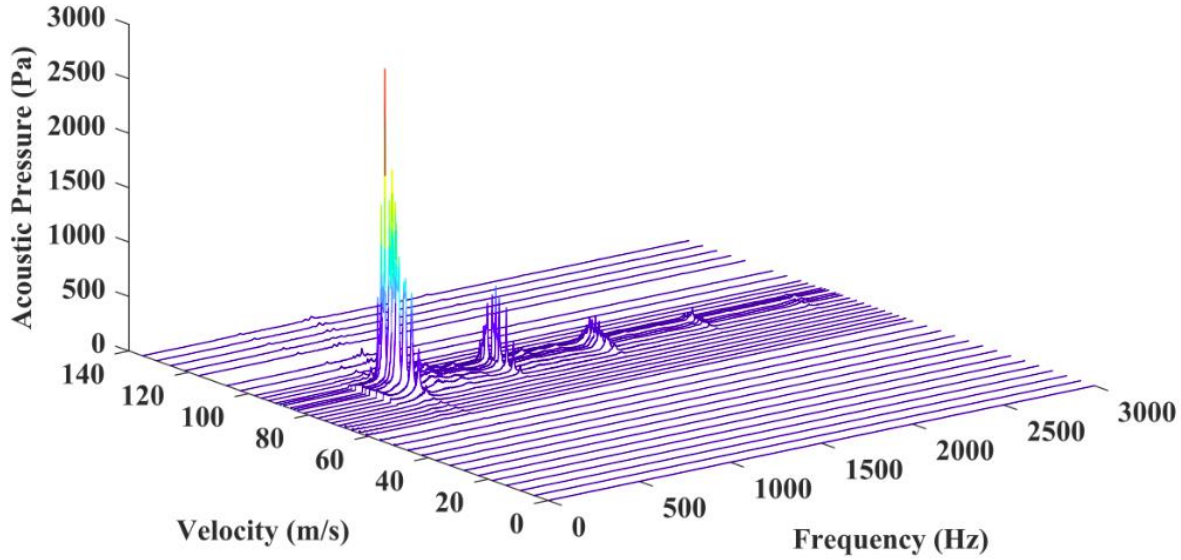

Figure 4-3 : 3D waterfall plot, D = 28. 5 mm (1.125”), H = 305mm (12”) for Y/H=0

Figure 4-4 and **Figure 4-5** shows the pressure and frequency response of a *10.56 mm (0.416")* cylinder in the *254 mm (10")* duct height. The frequency and pressure response graphs are together referred to as the aeroacoustic response. The acoustic pressure and frequency are plotted on the ordinate as a function of the upstream velocity in the abscissa. The Strouhal number for every case is calculated from the frequency response, based on the slope of the line drawn from the origin (shown in red).

The frequency of vortex shedding increases linearly with the upstream velocity up until it gets closer to the first fundamental frequency of the duct *(f_a ~ 675.00 Hz)*. Upon coinciding with the fundamental frequency of the duct, a "lock-in" region begins, where the vortex shedding frequency of the cylinder "lock-in" with the acoustic natural frequency of the duct. The lock-in region is usually easily observed in the frequency response and is characterized by a horizontal line at the value of the respective fundamental frequency of the duct. With the further increasing velocity, the lock-in remains until a certain point where it is broken and the vortex shedding frequency starts increasing again linearly with the velocity. *The lock-in region is a characteristic phenomenon of the flow-excited acoustic resonance.*

At higher velocities (U~100, U ~ 150 m/s), acoustic resonance occurs again and the vortex shedding frequency locks-in with the 3rd and 5th transverse acoustic modes (f_a ~ 2026, and f_a ~ 3378 Hz) respectively. The 2nd and 4th acoustic modes were not excited in this case; due to the relative position of the cylinder with respect to the acoustic pressure distribution along the duct height. Observing the higher order resonance modes was only possible for

a very small number of experiments where the diameter of the cylinders was small, namely the 10.56mm (0.416") diameter. This is expected since smaller diameter cylinders will experience the acoustic resonance at earlier velocities, thus with the capabilities of the given motor a wider range of fundamental frequencies, and subsequently resonance, could be covered.

Looking at the pressure and frequency responses it can be seen that during lock-in region the acoustic pressure amplitudes starts to instantly and rapidly increase until it reaches the highest point, ($P_{rms,\ max}$), at exactly the midpoint of the lock-in region. The maximum acoustic pressure point is of uttermost importance, as it usually represents the maximum sound pressure level that a system will experience at a specific acoustic mode.

For the small cylinders such as the one presented here, the first acoustic mode resonance amplitude is relatively weak. This is because the resonance occurred at a lower velocity so the energy in the flow is relatively low. The third mode acoustic pressure at resonance reaches a maximum value of 126 Pa, which is about an order of magnitude more than the first mode resonance.

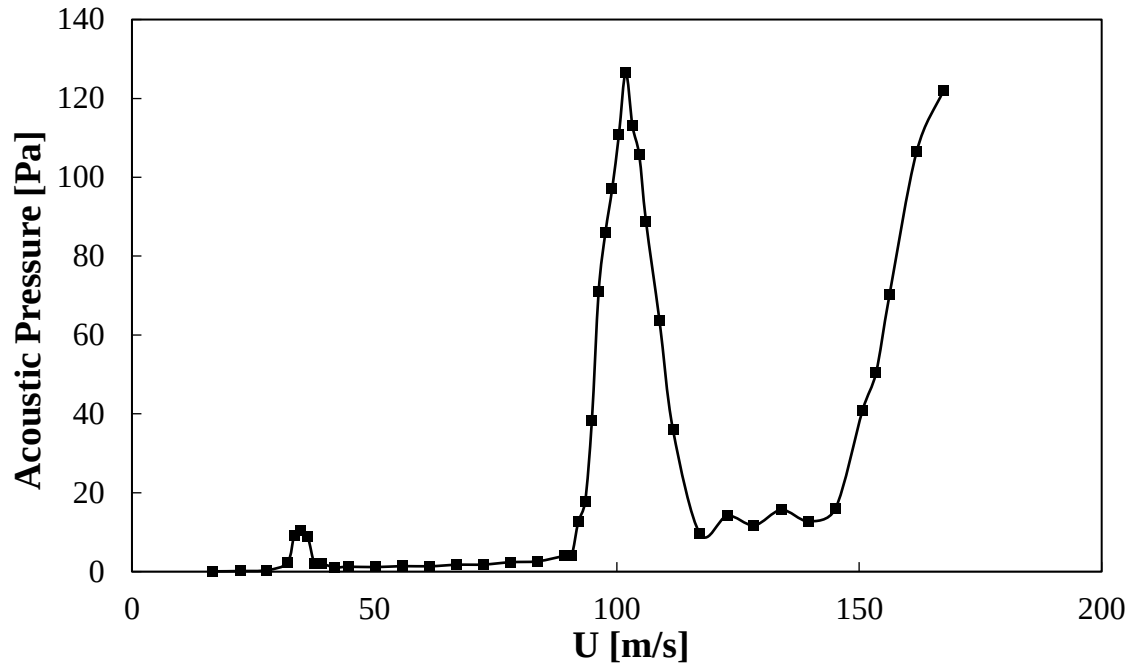

Figure 4-4 : Pressure response of single cylinder D = 10.5 mm (0.416") , H = 254mm (10"), Y/H = 0

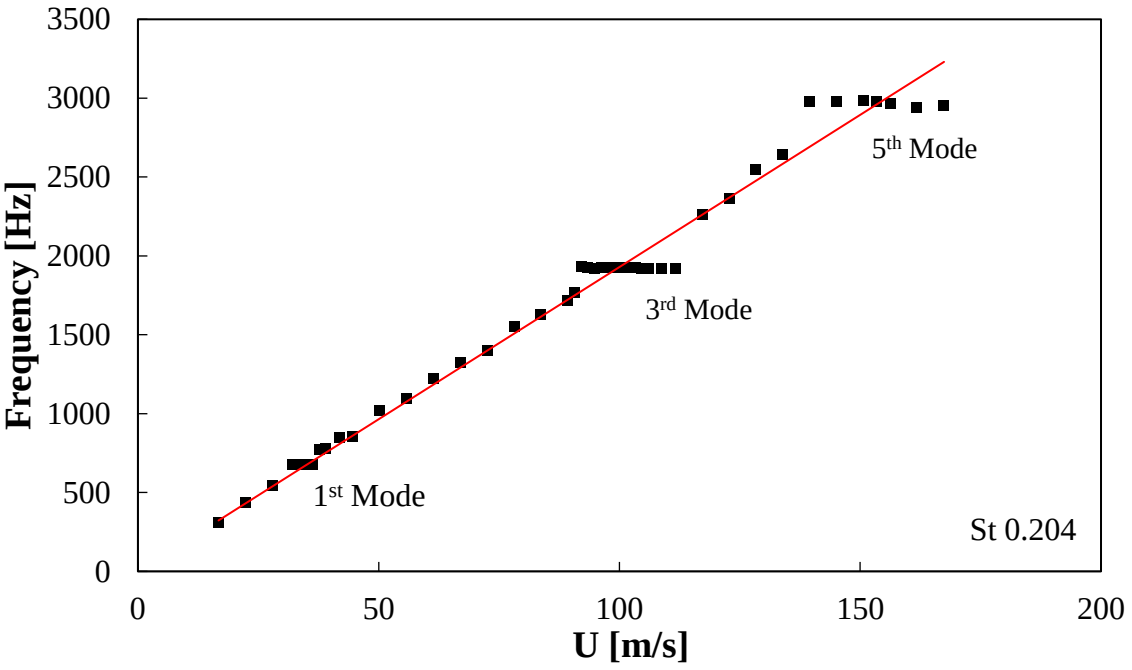

Figure 4-5 : Frequency response of single cylinder D = 10.5 mm (0.416") , H = 254mm (10"), Y/H = 0

4.3 Single Cylinder at Centerline (Y/H = 0)

4.3.1 Effect of Diameter

In order to study the effect of the diameter on the aeroacoustic response of single cylinders. The diameter of the cylinder was changed while keeping the height of the duct constant. Changing the diameter changed the velocity of the onset of acoustic resonance, the amplitude of the measured acoustic pressure and the pressure drop. This section helps to better understand the effect of the diameter alone on the excitation mechanism for cylinders. The normalized velocity used in all graphs (U_R) based on the first acoustic mode frequency and the diameter of the cylinder, U_R is calculated according to **Equation 4.1**.

$$U_R = \frac{f_i D}{U} \quad \textbf{(4.1)}$$

Figure 4-6 shows the acoustic pressure response for three different diameters namely *12.7 (0.5"), 19.05 (0.75")* and *28.575 (1.125") mm(inch)* in the duct height *203(8")*. The three diameters were used to demonstrate the full range of cylinders tested. The smallest diameter *(12.7mm)* produced a maximum acoustic pressure of *65.48 Pa* for the 1st mode and *424.24 Pa* for the 3rd mode. The middle diameter *(19.05mm)* produced a maximum acoustic pressure of 341.56 Pa for the 1st mode and no excitation for the 3rd mode. Lastly, the largest diameter *(28.575mm)* produced a maximum acoustic pressure of *813.8 Pa* for the 1st mode, and no excitation for the 3rd mode. The acoustic resonance of the middle and largest diameters could not be observed as they will theoretically occur at the flow velocities of U = *160 m/s* and *240 m/s* respectively, both of which are out of the motor range (160m/s).

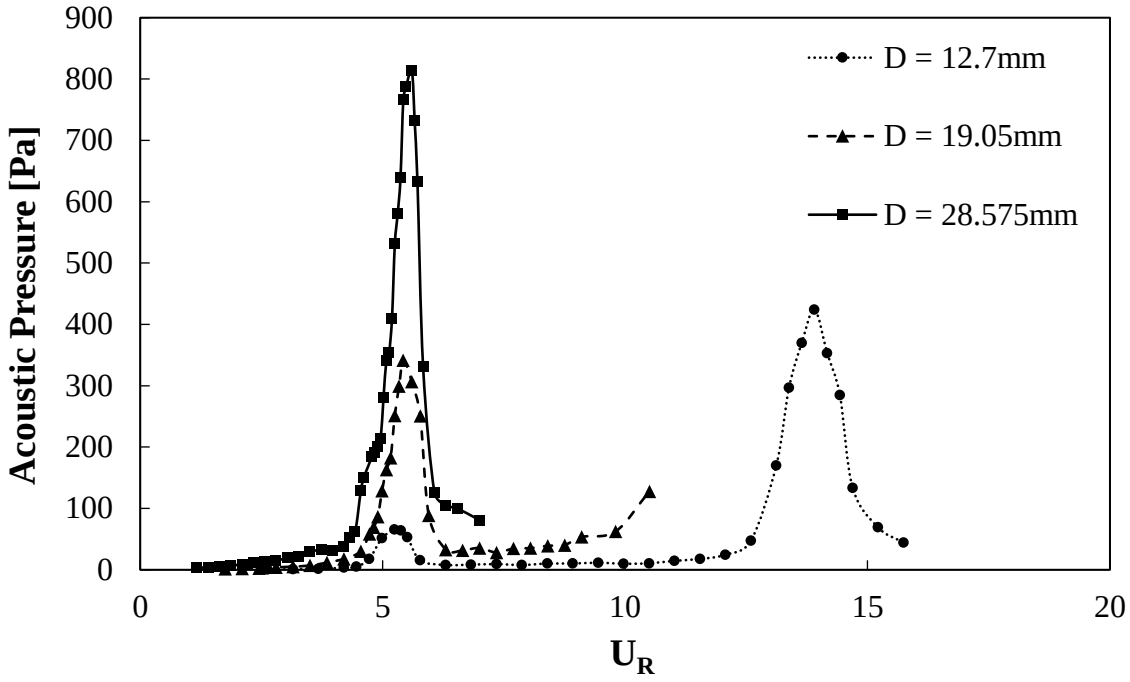

Figure 4-6 : Effect of diameter on acoustic pressure, H = 203mm (8"), Y/H = 0.

The onset of acoustic resonance for all cases occurred at the value of U_R = 4.5, with the maximum acoustic pressure being recorded at the reduced velocity of approximately U_R= 5.5. The maximum acoustic pressure reading should occur theoretically at the exact value of 5, since U_R is essentially the inverse of the Strouhal number, and at that point, the Strouhal number should be exactly 0.2.

In order to investigate the effect of the diameter on the variation of frequency at excitation, a numerical FEA simulation using ABAQUS software was performed. A simple case has been investigated where the diameter of the cylinder was varied inside a duct of a constant height *203 mm (8").* The resulting duct frequency was compared to the theoretical frequency value of *845 Hz*. **Figure 4-7** shows the outcome of this simulation. As the diameter increases the actual frequency at which resonance occurs compared to the duct

theoretical natural frequency decreases. This explains the slight variations in the U_R values at resonance. At higher acoustic modes where the frequency of coincidence is higher, this variation is usually amplified. The same trend was observed for all for all the tested cases. Mohany and Ziada (2009) reported similar effect for tandem cylinders and attributed this effect to the increasing in the path of acoustic particle velocity around the cylinder that occurs as a result of increasing the circumference of the cylinders; which results in the reduction of the acoustic resonance frequency.

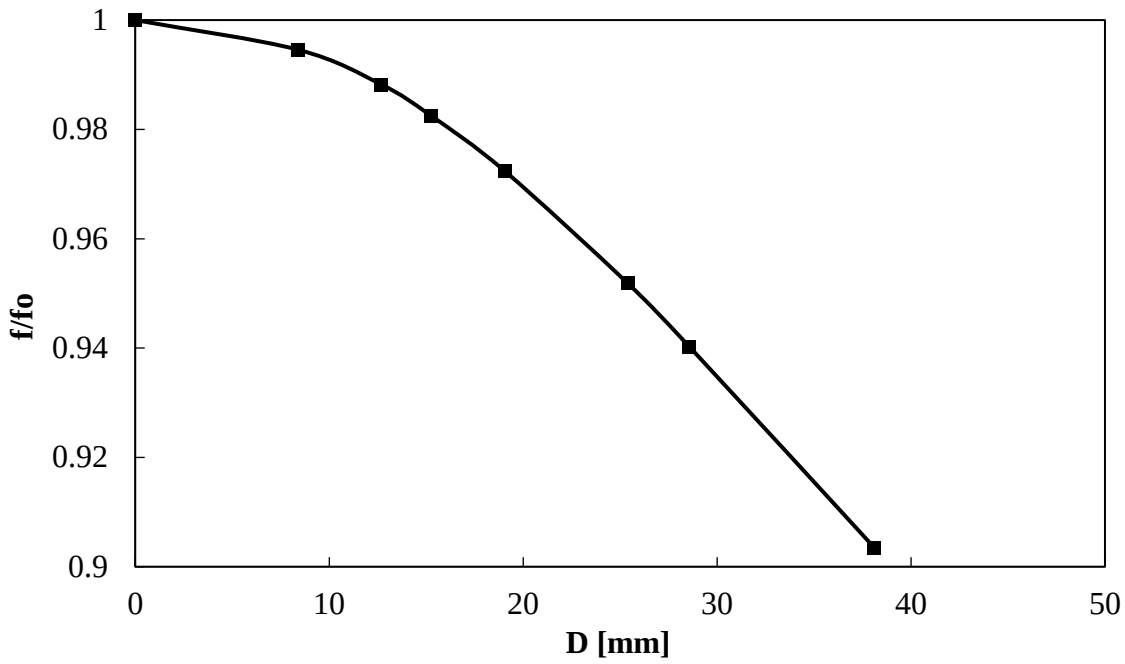

Figure 4-7 : Effect of diameter on the excitation frequency at resonance (numerical), H = 203 mm (8”), Y/H = 0.

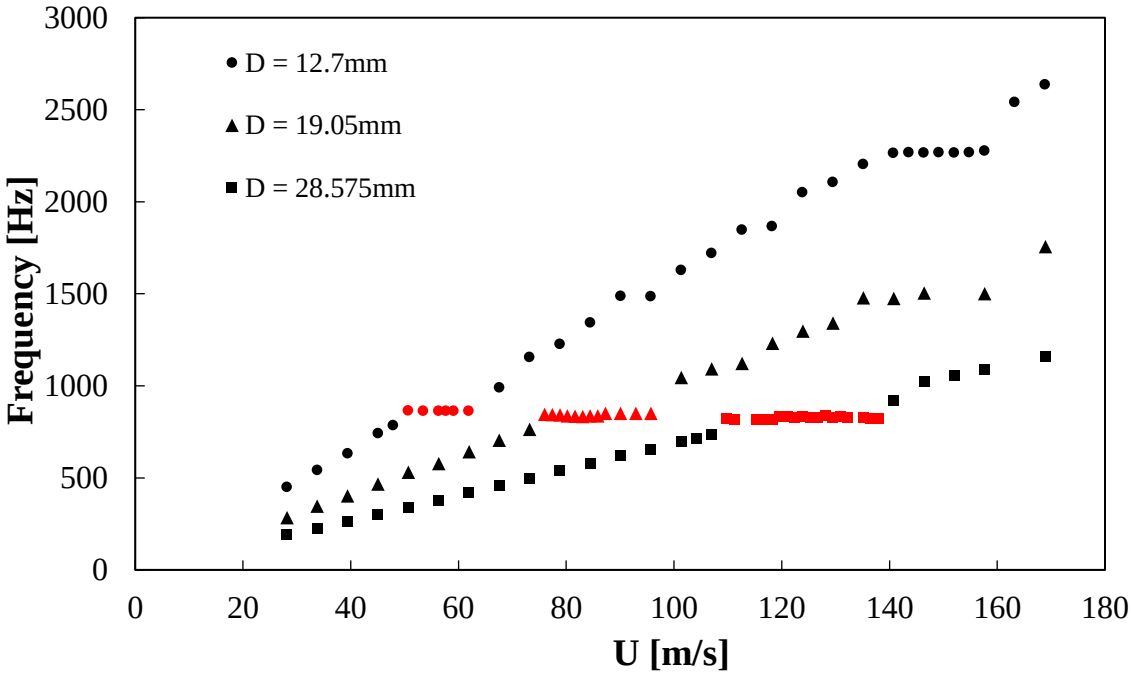

Figure 4-8 : Effect of diameter on frequency response , H= 203 mm (8"), Y/H = 0.

The frequency response of the before-mentioned diameters can be seen in **Figure 4-8**. The smallest diameter onset of acoustic resonance occurs at a velocity of *50m/s* while the middle and the largest diameters' onset occurs at *76* and *109 m/s* respectively. The onset of resonance is linearly shifted to higher velocities with the increasing diameter. The criteria for the onset of resonance is defined in this thesis as the point at which the lock-in region starts and the frequency suddenly jumps to a constant value equivalent to a reasonable range relative to duct natural frequency (f_a). For all the cases, the lock-in region and acoustic resonance occurred approximately at the expected theoretical frequency of the duct *(~ 844Hz.)*. The Strouhal number for all the tested diameters was 0.200 ± 0. 5%, which agrees well with the value of Strouhal number found in the literature for similar Reynolds number range. Table 2 summarizes the results of all cylinders in the duct height of *203mm*.

Table 2 : Comparison of Strouhal number, velocity at resonance and sound pressure level for single cylinder cases in duct height 203mm (8")

Cylinder diameter (mm)	**12.7**	**15.8**	**19**	**21**	**28**
Max SPL (db.)	138	140	144	147	152
Velocity @ P_{max} (m/s)	56	74	87	92	135
Strouhal Number	0.204	0.194	0.196	0.195	0.208

The pressure drop was recorded from two taps on the top wall over a fixed distance of *l = 504mm (20")* for all the test sections. **Figure 4-9** and **Figure 4-10** shows the static pressure drop for the *12.7 (0.5"), 19.05 (0.75"),* and *28.57 (1.125")* diameters and the corresponding dimensionless pressure coefficient C_p respectively. The C_p is the pressure drop normalized by the dynamic head of the flow, according to **Equation 4.2**

$$C_P = \frac{\Delta P}{\frac{1}{2}\rho U^2} \qquad \textbf{(4.2)}$$

Increasing the diameter of the cylinder increases the blockage inside the duct, this means that more energy would be required to excite the acoustic resonance. This explains why biggest diameter exhibits the largest pressure drop and produces the highest acoustic pressure amplitudes.

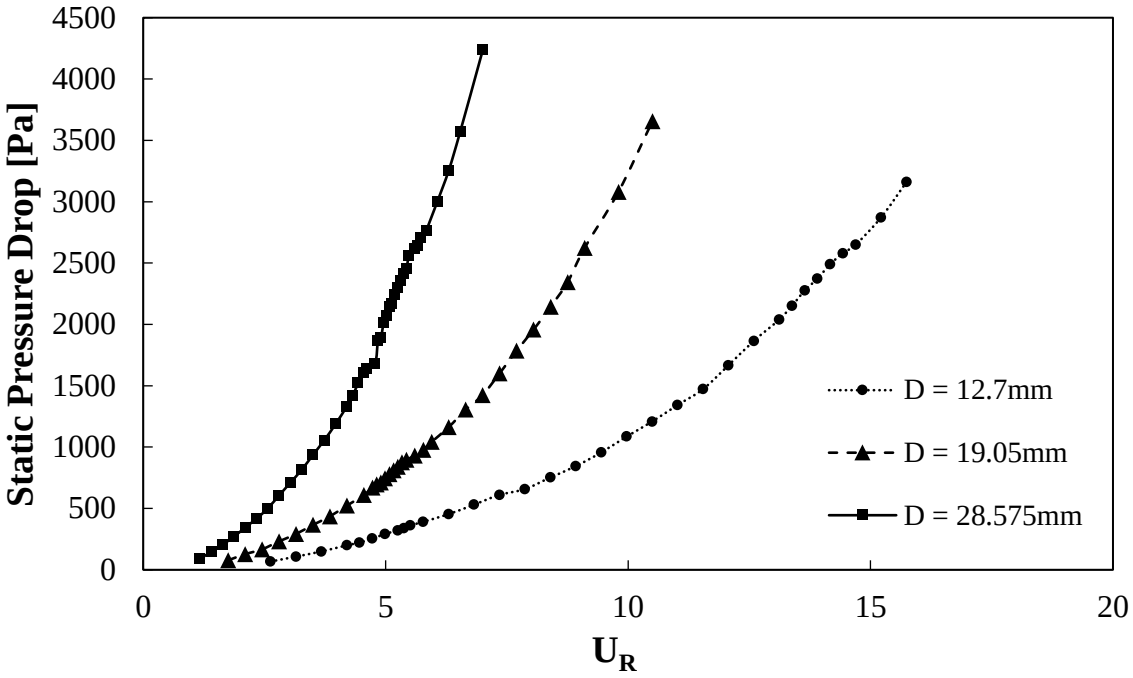

Figure 4-9 : Pressure drop measured across the cylinder over L = 504 (20”), H = 203 (8”), Y/H = 0.

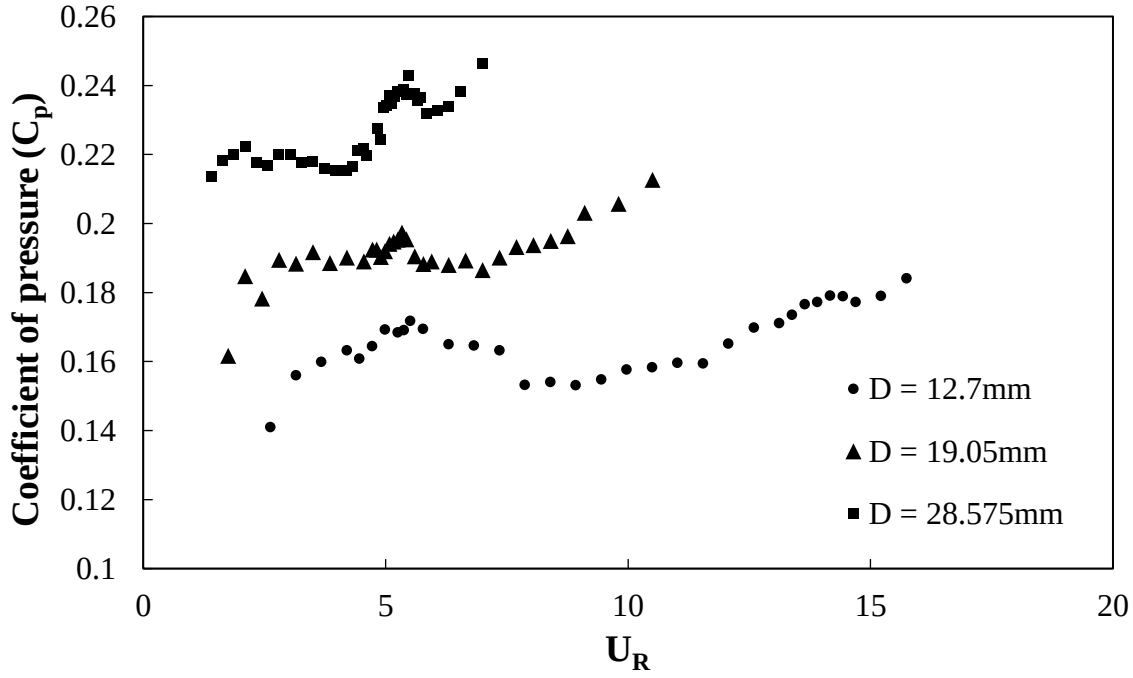

Figure 4-10 : Coefficient of pressure over L = 504 (20”), H = 203 (8”), Y/H = 0.

4.3.2 Effect of Height

In this section, the effect of varying the duct height on the aeroacoustic response is discussed. In order to do that, a set of cases will be compared were a single cylinder with a constant diameter is tested in the three different duct heights. The duct heights used are *203 (8), 254 (10), and 304 (12) mm(in)*. Changing the height of the test section changes both the aspect ratio (W/H) of the duct and the fundamental acoustic frequency (f_a). Flow-excited acoustic resonance tests on single cylinders in different duct heights have rarely been investigated in literature, and the exact effect of the height is not fully understood. Most cases in the literature have focused on either changing the diameter of the cylinder or the geometry of the cylinder, such as using finned cylinders. Understanding the effect of the duct height on the excitation mechanism of acoustic resonance for basic geometry such as that of a single cylinder can pave the road to fully understanding and characterizing the resonance phenomena in more complex configurations such as tube bundles of heat exchangers.

Figure 4-11 shows one of the cases where a single cylinder of diameter *21.05mm (0.8")* is tested in different test section heights. It is observed that the acoustic pressure amplitude produced by the cylinder is proportional to the duct height. The cylinder in the tallest duct height produced an acoustic pressure of *1108 Pa*, while when the same cylinder was placed in the middle and shortest duct heights it produced acoustic pressure amplitudes of *654 Pa*, and *565 Pa* respectively.

Figure 4-12 shows the frequency response for all the cases. The resonance occurred for all cases over the reduced velocity range of U_R = 4.5 – 6. The cylinder in the tallest duct experienced the widest lock-in region. The tallest duct height did indeed produce the

highest acoustic pressure, which is counterintuitive as the tallest duct height had the lowest natural frequency. The lower the frequency of the duct the earlier it will experience resonance, thus it was expected to see a different effect in which the smallest duct height (with the highest frequency and onset of resonance) will produce the highest acoustic pressure amplitude, since it would have the highest dynamic head in the flow proportional to ($0.5\ \rho\ U^2$). The Strouhal number calculated based on the slope of the frequency lines for the cases was 0.197 ± 0.1%. Similar trends were observed for all the tested cases, and it was confirmed that increasing the duct height while maintaining the cylinder diameter, increases the acoustic pressure produced at resonance.

Tests performed with small diameters (*D < 19.05 mm*) showed a relatively different response. Compared to the tests performed with larger diameters, the effect of the height was not very pronounced on the first mode. For the third acoustic mode excitation, the effect of the height was better observed even for smaller diameters. **Figure 4-13** shows the acoustic response of the cylinder of diameter *15.9 mm (0.625")* in the three different duct heights. For the smaller diameters, it can be observed that the differences in maximum acoustic pressure are within a very small range of amplitudes. The margin of differences keeps increasing with the increasing of diameter until it is very much observed in the bigger diameters (*21.056, 25.4 and 28.575mm*). This shows that there seems to be a combined effect of both the diameter and the height. Further investigation on the effect of the combined parameter of the diameter and height on the value of the maximum acoustic pressure produced $P_{rms,max}$ is discussed in the next section.

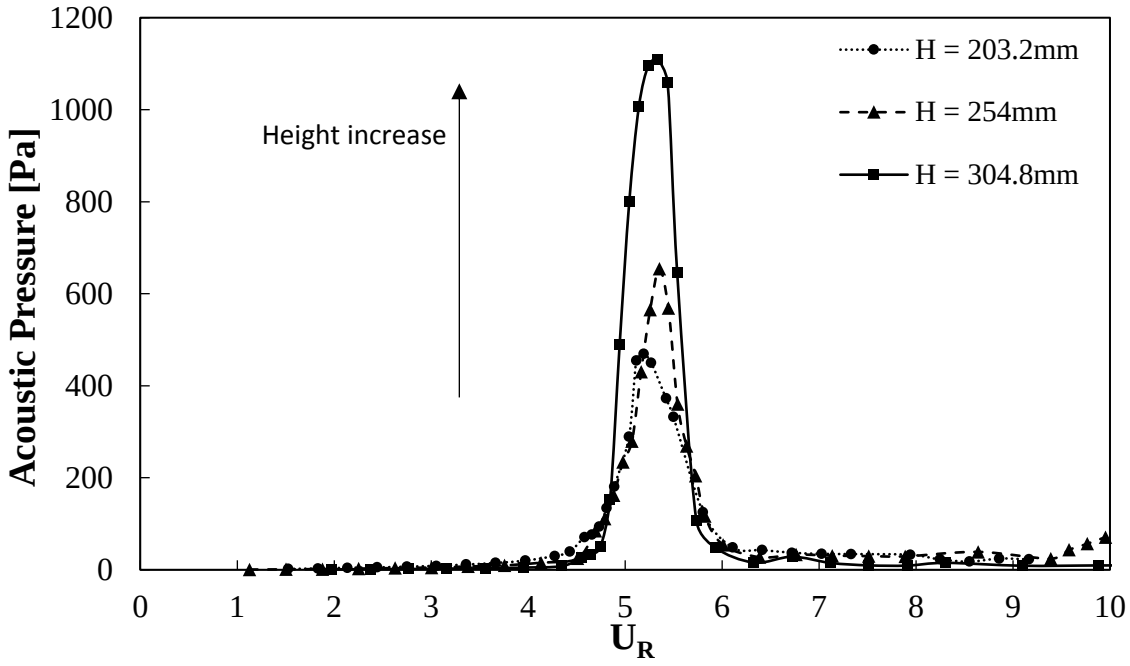

Figure 4-11 : Acoustic response of a single cylinder in different test section height, D = 21.05mm (0.8")

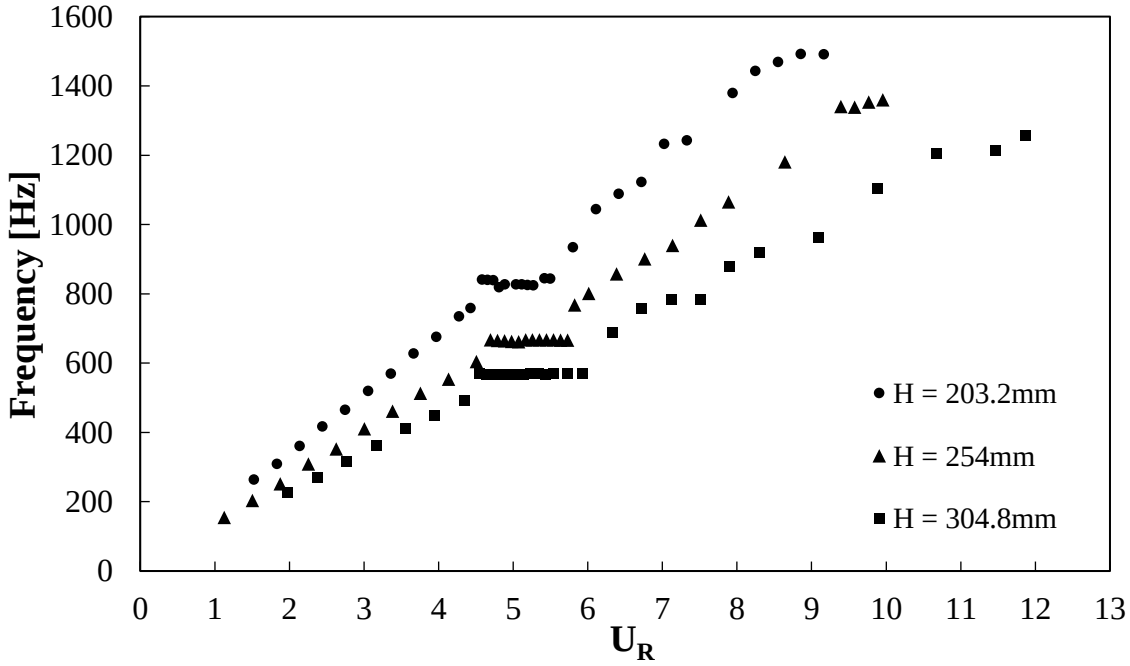

Figure 4-12 : Frequency response of a single cylinder in different duct heights D = 21.05mm (0.8")

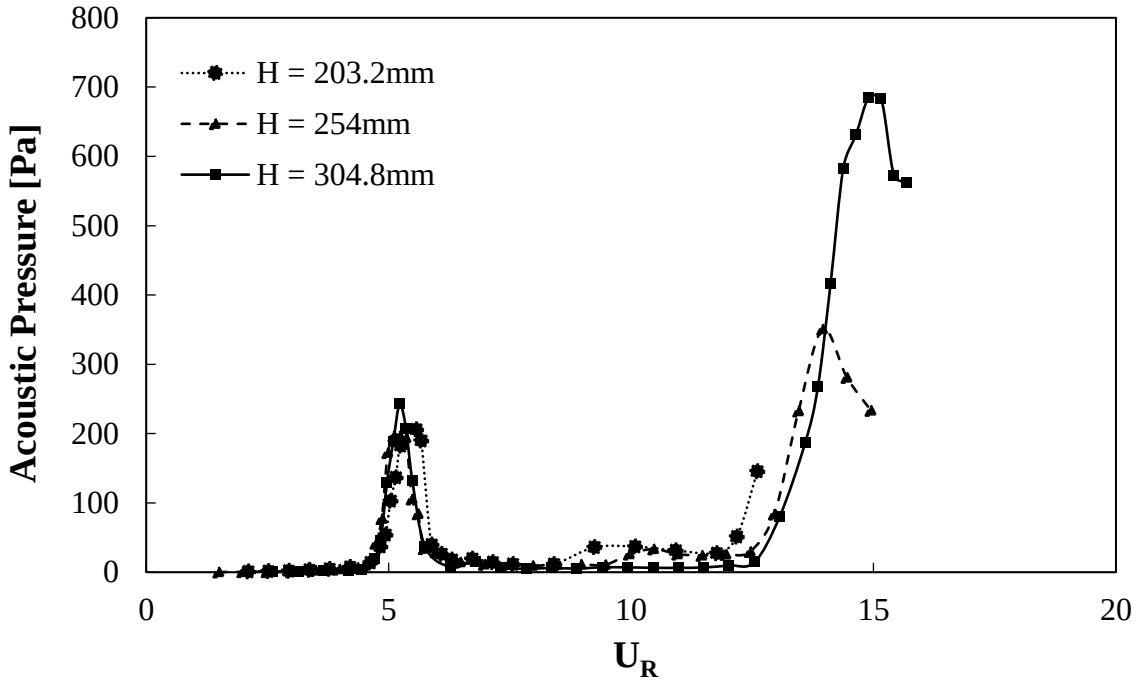

Figure 4-13 : Effect of height on acoustic pressure amplitude for small diameters, D = 15.9 mm (0.6")

4.3.3 Effect of Blockage Ratio (D/H)

Changing the duct height while maintaining the cylinder diameter or vice versa, changes the blockage ratio (D/H) of the duct. Results from the previous section seem to be counterintuitive, since changing the duct height while keeping the cylinder diameter constant is thought to be equivalent to changing the diameter of the cylinder while keeping the duct height constant, in terms of the blockage ratio (D/H) at least. However, they produce opposite effects in terms of the acoustic pressure amplitudes. For the case of constant duct heights, the acoustic pressure amplitudes seem to increase with the increasing cylinder diameter and decreasing blockage ratio (D/H). On the other hand, for the case of constant cylinder diameter, the acoustic pressure amplitudes seem to be increasing with the increasing height and blockage ratio (D/H). Moreover, it was found that theoretically for the same blockage ratio (D/H), the velocity at the resonance coincidence is the same.

Interestingly, when testing each parameter on its own (i.e. constant height or constant diameter) the same effect is not observed, and the velocity of coincidence seems to be shifted depending on the height or diameter of the case.

To better illustrate this consider **Figure 4-14** that shows a typical schematic of the theoretical frequencies of the duct mode (f_a) and the vortex shedding modes (f_v) for different diameters as a function of the upstream velocity U. The graph is the same for higher order acoustic modes, but for the sake of clarity only the first mode is shown here. Whenever a coincidence between the fundamental duct frequency and the vortex shedding frequency occurs, acoustic resonance occurs (Red dots), the velocity at which the resonance occurs is denoted as $U_{Resonance}$.

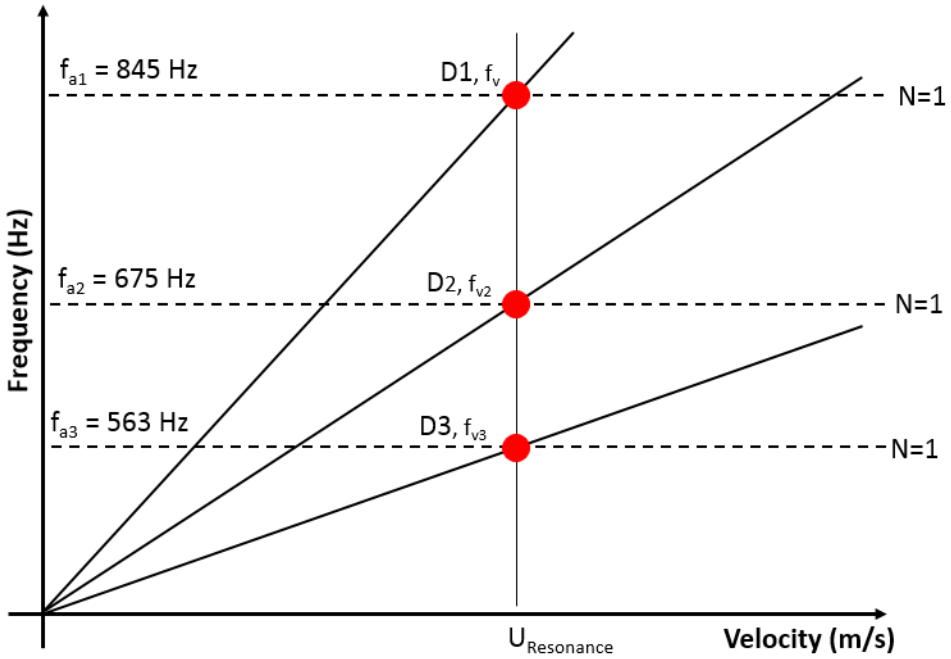

Figure 4-14 : Schematic of duct mode frequency and vortex shedding frequencies

The three different duct heights are shown in the figure in terms of their natural frequencies, and three different arbitrary diameters (D_1, D_2, and D_3) are shown in terms of their vortex

shedding frequencies. It must satisfy that $D_3 > D_2 > D_1$ in order to maintain the constant relationship of the Strouhal number value for the single cylinder (0.2). Thus depending on the value of the diameters, the slanted lines of the vortex shedding changes in slope and the coincidence of resonance may occur at the same instant of $U_{Resonance}$ for the three different heights. These points not only have the same velocity of coincidence but also have the same blockage ratio value (D/H). In other words, with the independent variation of both the diameter and the height, one can obtain the same blockage ratio with different heights and diameters. For example; combining the diameters of *12.7 mm (0.5"), 15.8 mm (0.62") and 19 mm (0.75")* with the heights of *203 mm (8"), 254 mm (10") and 304 mm (12")* respectively gives a constant blockage ratio of D/H ~ 0.0625 (6.25%). Theoretically, the three cases should have the velocity at the coincidence of *54 m/s*. Experimentally the three cases had the velocity at resonance coincidence at the values of *59 m/s, 56 m/s and 57 m/s* respectively.

Figure 4-15 shows the relationship between the blockage ratio (D/H) and the velocity at resonance from the experiments done for all of the tested cases. The figure shows all the velocities at coincidence for eighteen tests in which a different variation of D and H produced a constant value for D/H. For the set of cylinders and diameters tested, the same coincidence discussed here was possible for five cases at the blockage ratios of (4.16%, 6.25%, 7.5%, 9.4%, and 10%).

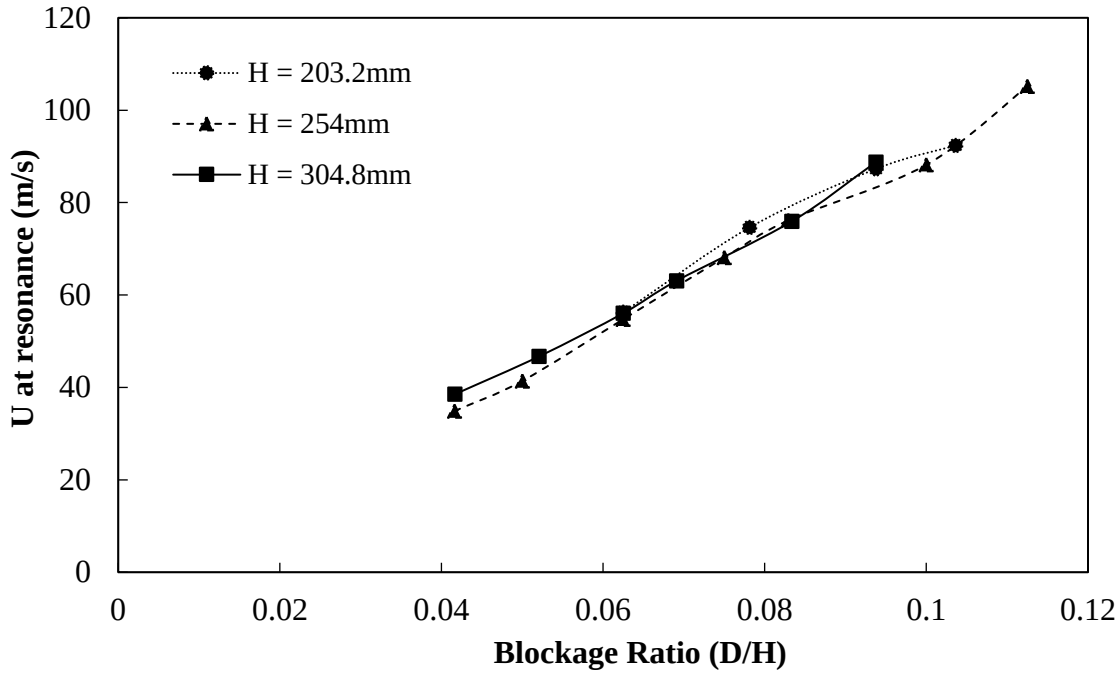

Figure 4-15 : Effect of blockage ratio (D/H) on the velocity at coincidence

The velocity at coincidence shows a strong correlation with the blockage ratio term (D/H) and not the diameter or height alone. This means that for a combination of an infinite number of diameters and heights that yield the same D/H ratio, the point of maximum velocity will essentially be the same.

Figure 4-16 shows the pressure response of a case in which three different combinations of cylinder diameters and ducts gave the same blockage ratio (6.25%). In this case the three diameters *12.7 mm (0.5"), 15.8 mm (0.62") and 19 mm (0.75")* are combined with the heights *203 mm (8"), 254 mm (10") and 304 mm (12")* respectively to give a constant blockage ratio of D/H ~ 0.0625 (6.25%).

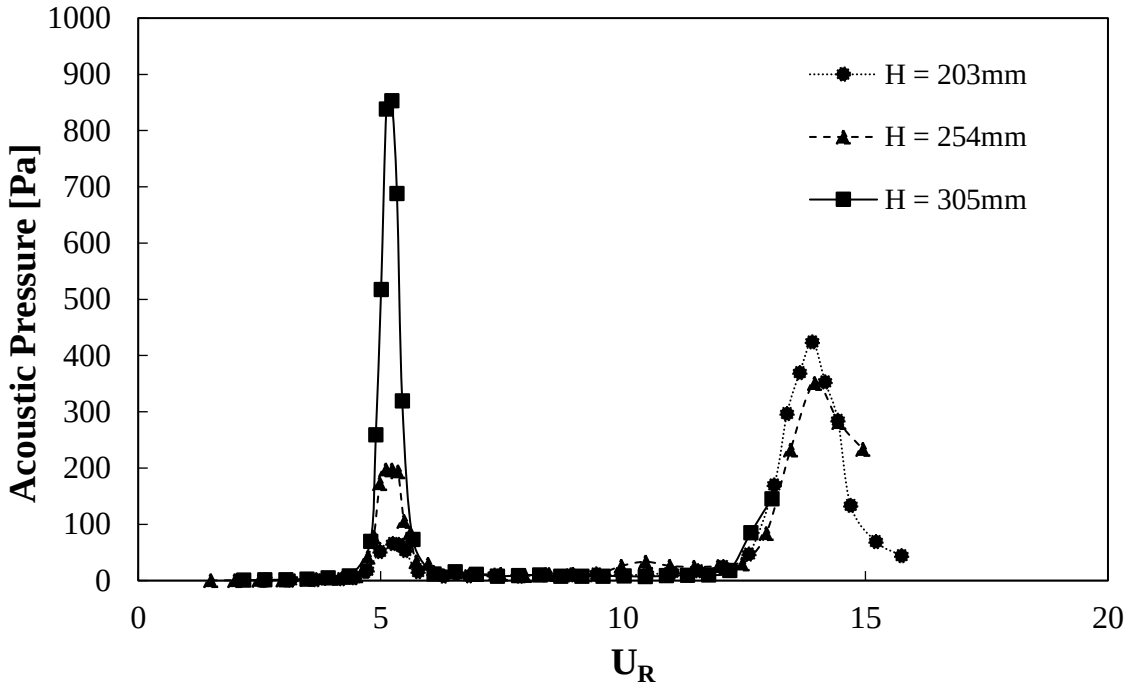

Figure 4-16 : Pressure response for blockage ratio (D/H) of 6.25%

The three cases seem to behave in a typical manner in terms of the onset and offset of acoustic resonance, for the 1st and 3rd modes respectively. The acoustic pressure amplitude, however, increases with the increasing duct height and diameter, despite the constant blockage ratio and velocity of coincidence. The acoustic pressure produced by the biggest diameter *(19mm)* and height duct *(304mm)* was 853 *Pa*, then *197 Pa* for the medium duct height and cylinder diameter *(15.8mm, 254mm)*, and finally *53 Pa* for the smallest cylinder diameter and duct height *(12.7mm, 203mm).*

Figure 4-17 summarizes all the cases with similar blockage ratio (D/H) as a function of the maximum acoustic pressure produced. The same trend is observed for all the cases, and the increasing of the blockage ratio seems to further increase the differences between the amplitudes of the maximum acoustic pressure. The only fundamental difference between the similar blockage ratio cases is the natural acoustic frequency of the duct. The frequency

of excitation was different in each case since the duct height has changed. The Strouhal number calculated for the cylinders, in this case, was 0.201.

In conclusion, for all the special cases tested at equal blockage ratios, the blockage ratio (D/H) and the velocity of coincidence (U) were equal but the maximum pressure amplitude at resonance ($P_{rms,\ max}$) and the frequency at resonance were different. The difference is proportional to the height of the duct.

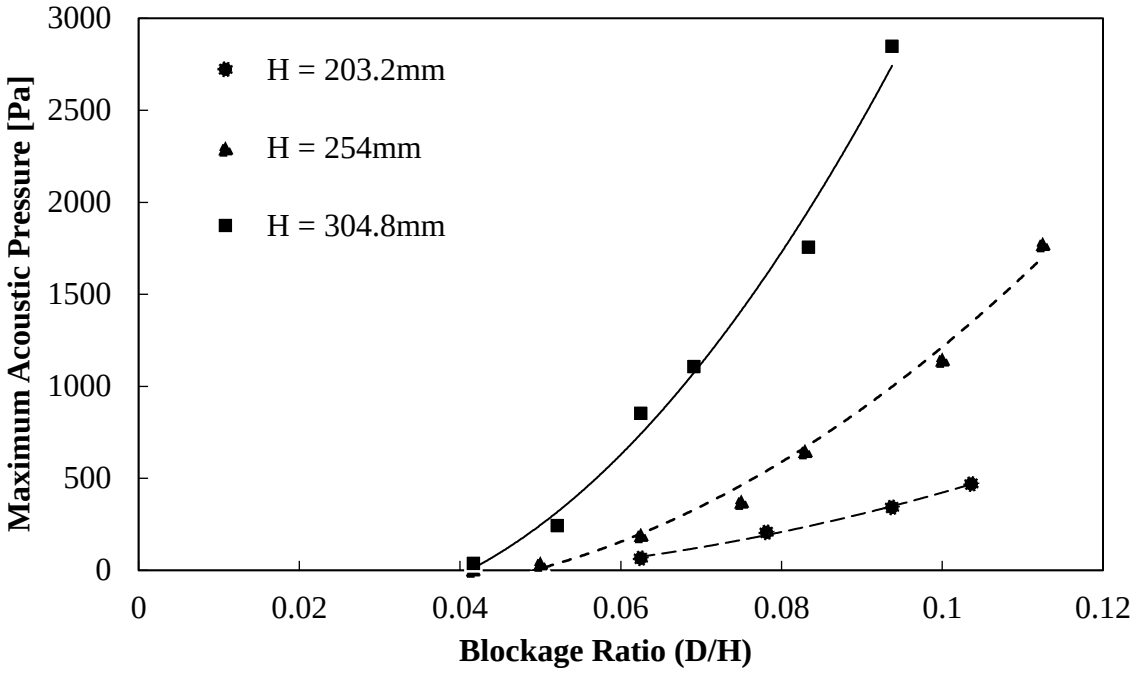

Figure 4-17 : Effect of blockage ratio (D/H) on the maximum acoustic pressure for single cylinder, 1st acoustic mode (Y/H = 0)

4.3.4 Comparison with the Literature

Blevins and Bressler (1993) performed similar experiments on single cylinders in variable duct heights. They performed sixteen experiments on single cylinders and fitted their data to correlate the maximum acoustic pressure amplitude to the dynamic head, the Mach number, blockage ratio, static pressure drop and the input energy parameter (MΔP).

They suggested that the maximum acoustic pressure can be calculated using **Equations 2.12a** and **2.12b**, for a single cylinder. The equations, according to the authors, work within 26% error margin in the range of $0.02 < M < 0.5$, $5 < \Delta P_{static} < 50$ (inH20) and $2000 < Re < 300000$.

The cases presented in the last section seems to be in no agreement with the equations suggested by Blevins and Bressler. Although all of the tested cases are within the range specified for the Mach number, Reynolds number, and static pressure drop. In the cases of similar blockage ratios (D/H) tested, the Mach number and velocity at resonance were almost equal in all the cases, however, the produced acoustic amplitudes were substantially different, and not even within the 26% error margin defined for the equations.

The maximum acoustic pressure amplitudes recorded for the cases of single cylinders are compared to the two empirical formulas suggested by Blevins and Bressler (1993). **Figure 4-18** shows the comparison with the equations in terms of the geometry of the duct (D/H), the dynamic head of the flow ($0.5\ \rho\ U^2$) and the Mach number.

Blevins and Bressler conducted their experiments in three different test sections of varying heights, however, the equations that they suggested seem to greatly under-predict and over-predict the maximum acoustic pressure amplitudes (sometimes with more than 26% error). The same difference is observed as well when comparing the data from the experiments to the other correlation suggested between the input energy parameter ($M\Delta P$) and the maximum acoustic pressure at resonance. **Figure 4-19** shows the comparison with the current data. The data seems to agree in terms of the linear relationship, however, the

suggested empirical relation seems to over-predict and under-predict the maximum acoustic pressure amplitudes.

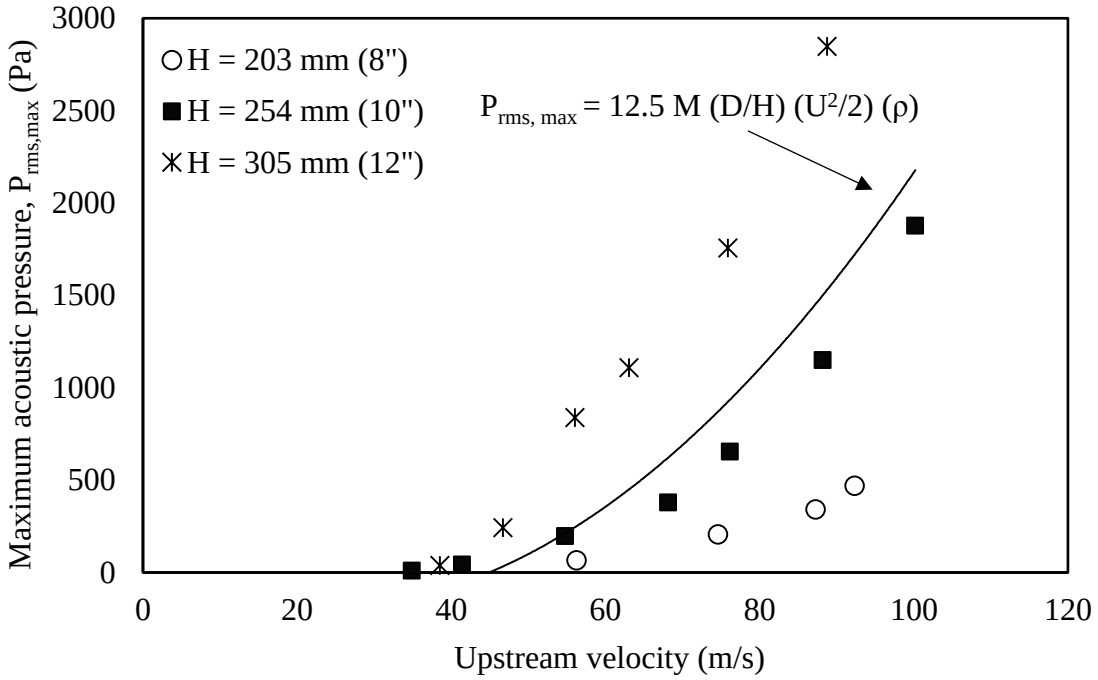

Figure 4-18 : Comparison with empirical formula related to duct geometry and dynamic head of the flow for 1st cross-mode, (Y/H = 0)

This major difference in the results might be due to various reasons. The test sections used for this thesis were different in the duct dimensions from those used by Blevins and Bressler. In this thesis, the width was fixed to *127mm* and the height was varied *203, 254 and 305mm*. For Blevins, the width was fixed to *127mm* and the height was varied *114, 228 and 457 mm*. Blevins and Bressler however, claimed that the equations are accurate within the specified ranges of Mach number, Reynolds number, and static pressure drop. All the experiments done were within this range, thus the suggested formulas should have agreed with the results, at least within the 26% error margin.

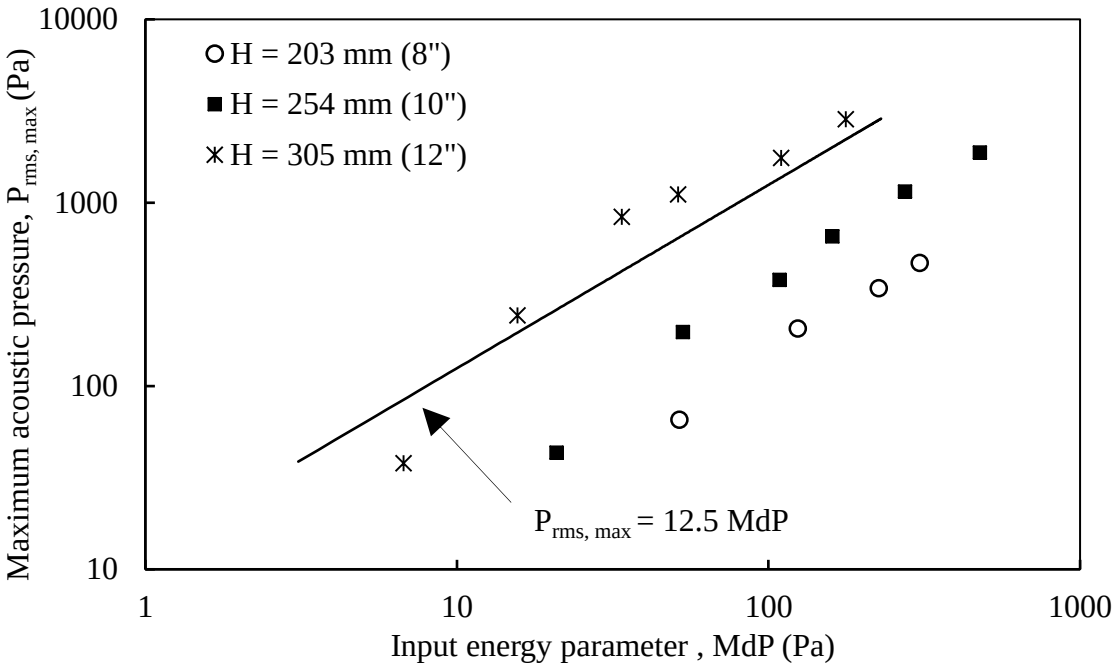

Figure 4-19 : Comparison with empirical formula related to input energy parameter, for 1st cross-mode, (Y/H = 0)

Other studies, such as that conducted by Fenestra et al. (2006), investigated the applicability of these equations in full-size tube-bundles. The equations also did not predict accurately the acoustic pressure amplitude at resonance. Moreover, the capabilities of the motor that was used by Blevins and Bressler, enabled them to only test for first acoustic mode resonance. No claims were made about the applicability of these equations for the second or higher order modes. In conclusion, the empirical equations suggested by Blevins and Bressler are very generalized and seem to exclude important parameters that affect the acoustic pressure amplitudes, and that is why they are highly unreliable and do not produce accurate results even for simple cases such as single cylinder cases.

4.3.5 Analogy Between Mechanical & Acoustic Systems

Surprisingly, the cylinder in the highest duct produced the highest acoustic pressure amplitude despite occurring at the lowest velocity and with the lowest dynamic head

(energy). Moreover, in cases where the blockage ratio of the duct (D/H) and the velocity of coincidence (U_{max}) are the same, the highest duct seems to always result in the highest acoustic pressure amplitude. This is counterintuitive as the acoustic pressure amplitude was always thought to be proportional to the dynamic head in the flow ($0.5\rho U^2$). In order to try and understand this relationship, and perhaps answer the question of why the variation between experimental results exists compared to the empirical relation suggested for the single cylinder cases. An analytical approach has been made to relate the acoustic system response of the cylinder in cross-flow (during resonance condition) to a single degree of freedom damped oscillator. Comparing complex acoustic systems to simpler systems such as mass-damping-spring mechanical or electrical resistor-inductor-capacitor systems to better understand their behaviors is a valid method that is adapted by many, Kinsler (2000).

Consider a single degree of freedom mechanical system such as mass-spring system undergoing a simple harmonic motion due to an external force f(t) being applied. The mass-spring-damper system in **Figure 4-20** consists of a mass, a spring, a viscous damper, and a sinusoidal force that varies harmonically with time f(t). The mechanical system will respond in a harmonic manner similar to the applied force. The equations for the amplitude and velocity of the system can be written as: -

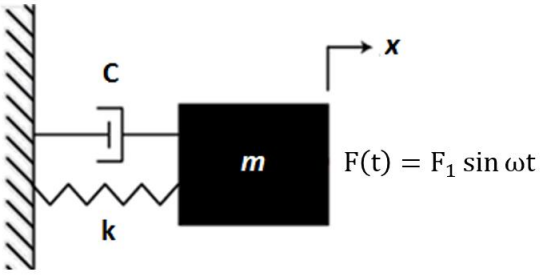

Figure 4-20 : schematic of a damped Mass-Damper-Spring (MDS) system

$$\text{Displacement } x(t) = A\sin(\omega t) \quad \textbf{(4.2a)}$$

$$\text{Velocity } v(t) = \frac{dx}{dt} = A\omega\cos(\omega t) \quad \textbf{(4.2b)}$$

Where A is the amplitude, ω is the angular frequency, and φ is the phase angle. The value *K* represents the stiffness of the system measured in (N/m), and *C* represents the damping coefficient of the system and is measured in (N.s/m). The *stiffness* of the system refers its rigidity and ability to resist the motion or deformation. The *damping* on the other hand refers to the ability of the system to reduce or restrict the motion or change, once it has been already imposed, the damping is usually related to the dissipation of energy and losses within the system. The stiffness and damping forces (F_s and F_d) for a simple MSD system is defined by

$$F_s = -kx \quad \textbf{(4.3a)}$$

$$F_d = -c\dot{x} \quad \textbf{(4.3b)}$$

Where *k* and *c* are the coefficients of stiffness and damping, and *x* and $\dot{x}$ refers to the displacement and the velocity of the mass system. The negative signs imply that both forces are restrictive to the motion. from Newton's second law the equation of motion for such system can be written as

$$\sum f = ma \rightarrow \quad -c\dot{x} - kx + F_1\sin\omega t = m\ddot{x} \quad \textbf{(4.4)}$$

Rearranging the equation and dividing by (*m*) yields the following 2nd order differential equation.

$$\ddot{x} + \frac{c}{m}\dot{x} + \frac{k}{m}x = F_1 \sin \omega t \quad \textbf{(4.5)}$$

The complete solution to the differential equation described above contains a steady-state and a transient response terms, and the dimensionless form to relate the amplitude of oscillation to the applied force and other parameters such as damping and stiffness can be expressed as follows: -

$$\frac{Xk}{F_o} = \sqrt{\left[1 - \left(\frac{\omega}{\omega_n}\right)^2\right]^2 + \left[2\zeta\left(\frac{\omega}{\omega_n}\right)\right]^2} \quad \textbf{(4.6)}$$

This equation indicates that the amplitude of oscillation is a function of only the frequency and the damping factor. The relation between the amplitude of oscillation and the frequency ratio and damping can be seen in **Figure 4-21.**

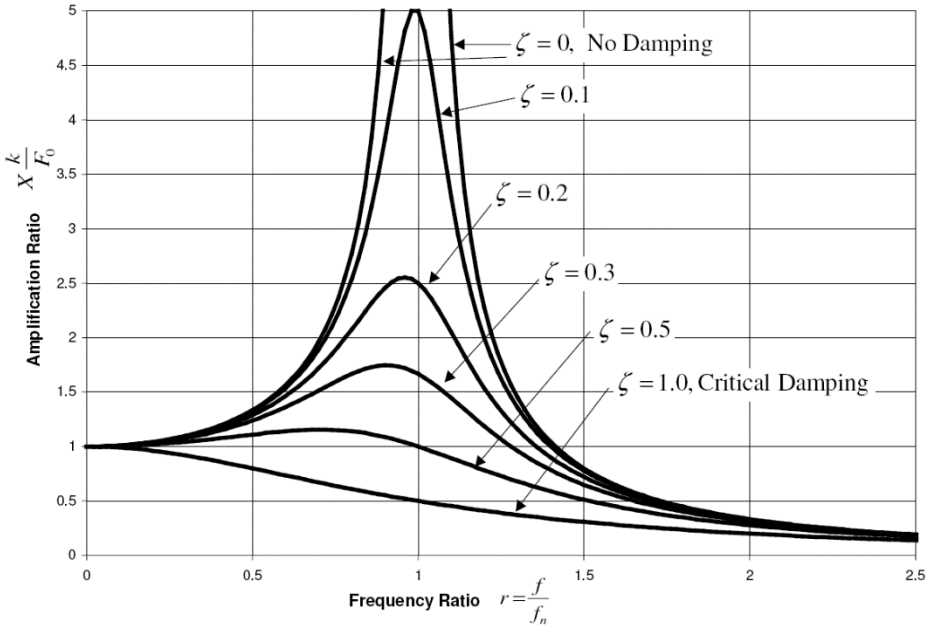

Figure 4-21 : Amplitude response as a function of the frequency ratio and amplification ratio

In short, the amplitude of the response of the mechanical system described above depends greatly on the natural frequency of the system, which is related to the stiffness of the spring and the whole system. The lower the natural frequency of the system, the less stiff it is, thus it becomes easier to excite.

At acoustic resonance, a standing wave transverse to the flow direction is created in the duct. The standing wave can be treated as a 1-D plane sound wave undergoing a simple harmonic motion similar to the one described for the mechanical system. With applying the proper state equations and assuming validity *only* at resonance it is valid to assume that the acoustic pressure amplitude becomes analogous to the displacement of the mechanical system and the acoustic particle velocity becomes analogous to the velocity, Blevins (2015). At resonance, the acoustic pressure wave follows a sinusoidal motion similar to the response of the mass-spring system. Thus quantities like stiffness and damping, which changes the response of the mass-spring system, may be applied also to the acoustic system and provide similar behaviors.

With the current analogy, it can be explained why the system with the lower natural frequency (i.e. highest duct) produced the highest acoustic amplitude, even though the resonance occurred at a lower velocity (dynamic head). The duct height dictates the natural frequency of the duct according to the equation of (f_a) thus the higher the duct is the lower the natural frequency will be. Comparing this with the damped oscillator system described above, it can be concluded that lowering the natural frequency of the system decreases its stiffness, which makes it more susceptible to excitation and progressively resonance. Thus for the cases of variable duct heights and constant cylinder diameters, the highest duct was

the least stiff of all systems, and therefore with the least amount of energy resonance materialized with higher amplitudes.

4.3.6 Damping of The Acoustic Systems

For the cases where the blockage ratio (D/H) and velocity of excitation (U) were equal. The situation is different since the same velocity implies that the same dynamic head is present in the system. The only difference, in this case, might, therefore, be related to the acoustic damping of each system.

The damping has the ability to reduce the total acoustic energy within the system by means of energy dissipation such as heating, radiation or turbulence. The damping has a direct effect on the acoustic pressure attenuation, Sanna et al. (2016). In the ducts, the acoustic damping is mainly due to the visco-thermal losses within, Peters et al. (1993). Quantifying the visco-thermal losses at the duct walls when a sound wave is propagating can be measured with the first order model of Kirchoff, expressed by **Equation 4.7**., Sanna et al. (2016)

$$\alpha_o(\text{Kirchoff Damping}) = \frac{l}{2A_s c_o}\sqrt{\frac{\pi f \mu_{dynamic}}{\rho}}\left(1+\frac{\gamma-1}{\sqrt{Pr}}\right) \qquad \textbf{(4.7)}$$

Where l is the length of the duct , A_s is cross-sectional area, c_o is speed of sound, f is frequency , μ is dynamic viscosity , ρ is density , γ is the ratio of specific heats (c_p/c_v), and Pr is the Prandtl number. Under standard pressure and temperature conditions, the values of c_o, μ, ρ, γ, and Pr are constant for all cases. The values at absolute temperature of 300 Kelvin are c_o =343.21 m/s, μ = 1.846 x (10^5), ρ = 1.2041 Kg/m^3, γ = 1.40 [-], Pr = 0.7 [-]. The length of the duct also is constant for all the three test sections , l = 0.762 m

(30”). The difference between the test sections would be in the cross-sectional area A_s and the natural acoustic frequency f.

Figure 4-22 shows the theoretical Kirchhoff visco-thermal damping coefficient as a function of the frequency and duct heights. The trend is general in all the cases, where the visco-thermal damping coefficient varies in proportional to the square root of the frequency. However, it is observed that the duct cross-sectional area also has a major effect on the damping. As the duct height and thus the cross-sectional area is increased, the damping of the system decreases.

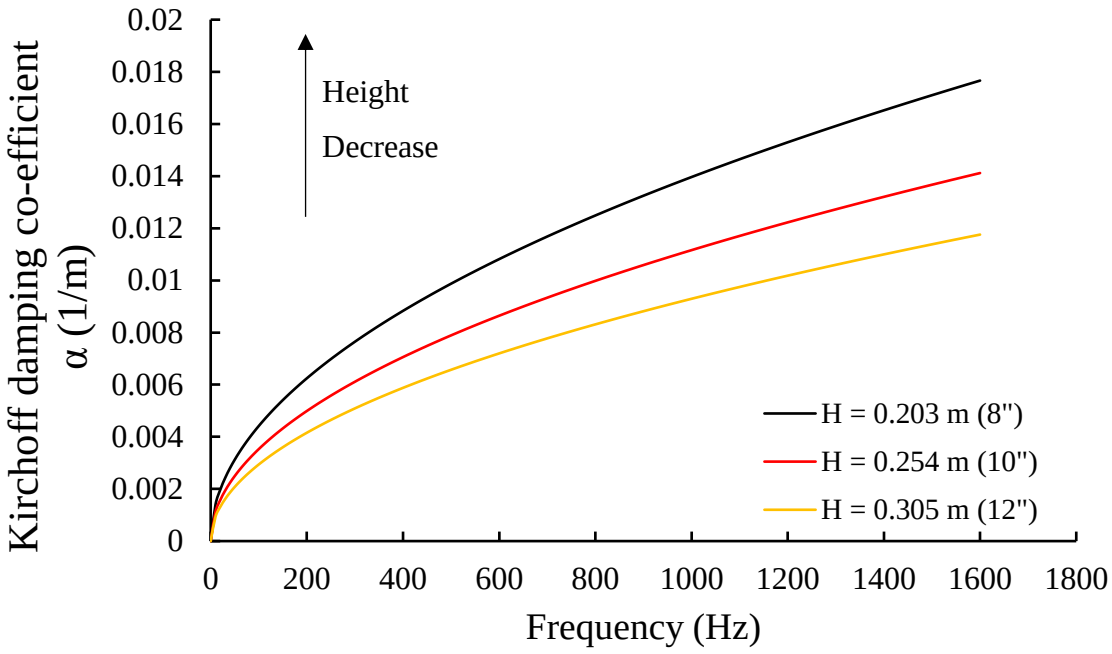

Figure 4-22 : Theoretical Kirchhoff damping coefficient (α) as a function of the frequency and duct height

The theoretical damping coefficient does not account for the velocity of the air in the duct, nor it discriminates between how the noise was initially generated. However, it can still be used to give a good approximation of the total damping of the duct. Ingard (1974)

performed experiments on visco-thermal damping in ducts containing turbulent flows for velocity ranges of 0 to 170 m/s. He reported that the visco-thermal damping in ducts is almost independent of the Mach number at low Reynolds numbers, however, at high Reynolds numbers, the effect is quite pronounced. This explains why for the smaller diameters cases the changes between the amplitudes were not very pronounced. It is due to the fact that it occurred at lower Mach numbers, where the effect of the duct damping was not very observable.

4.3.7 Effect of the Constant Parameters on the Acoustic Damping

The constant values assumed in the previous section greatly affects the visco-thermal damping coefficient. The constants related to the speed of sound, temperature and the pressure of the air are constant in all the experiments since the solidity ratio and the temperature variations were minimal. However, if applied to tube bundles of heat exchangers, many of the parameters would change.

For example, the constant value of the speed of sound would be substituted by the effective speed of sound which is related to the solidity ratio σ. The effective speed of sound can be expressed using **Equation (4.8)** proposed by Parker (1978).

$$c_{effective} = c_o\sqrt{(1+\sigma)} \qquad \textbf{(4.8)}$$

The solidity ratio can be calculated by **Equation (4.9)** based on the fraction of space occupied by (*n)* number of tubes to the enclosed duct volume.

$$\sigma = \frac{n\,V_{cylinder}}{V_{duct}} \qquad \textbf{(4.9)}$$

Where $V_{cylinder}$ is the volume of the cylinder, and V_{duct} is the volume of the duct. For the current cases, the volumes of the three ducts of heights 0.*203, 0.254 and 0.305 m* are *0.0196, 0.0246 and 0.0295* m^3 respectively. Calculating the effective speed of sound for the extreme case (maximum blockage ratio) when the biggest diameter *0.02857m (1.125")* is placed in the in the smallest duct *0.203m (8")*, the solidarity ratio will be 0.4% and the speed of sound will change by only *0.2%*. Therefore, the speed of sound is assumed constant for the current cases as the solidity ratio is minimal. It is generally accepted that the speed of sound remains unchanged for small blockage ratios (<10%), Arafa & Mohany (2016). In the case of tube-bundles however, the number of the cylinders is sometimes in hundreds, and thus the effective speed of sound will definitely change. **Figure 4-23** shows the effect of changing the speed of sound on the theoretical acoustic damping inside the duct.

The figure is constructed from calculating the values of the damping and effective speed of sound for a case of diameter of *0.127m (0.5")* enclosed in a duct of height *0.254m (10").* The speed of sound was changed by increasing the number of cylinders from n = 1 to 100 and evaluating the effective speed of sound based on the solidity ratio as per Equations 4.8 and 4.9. The acoustic damping is normalized by the value of the damping calculated for an empty duct of height *0.254m (10")* as per **Equation 4.8**.

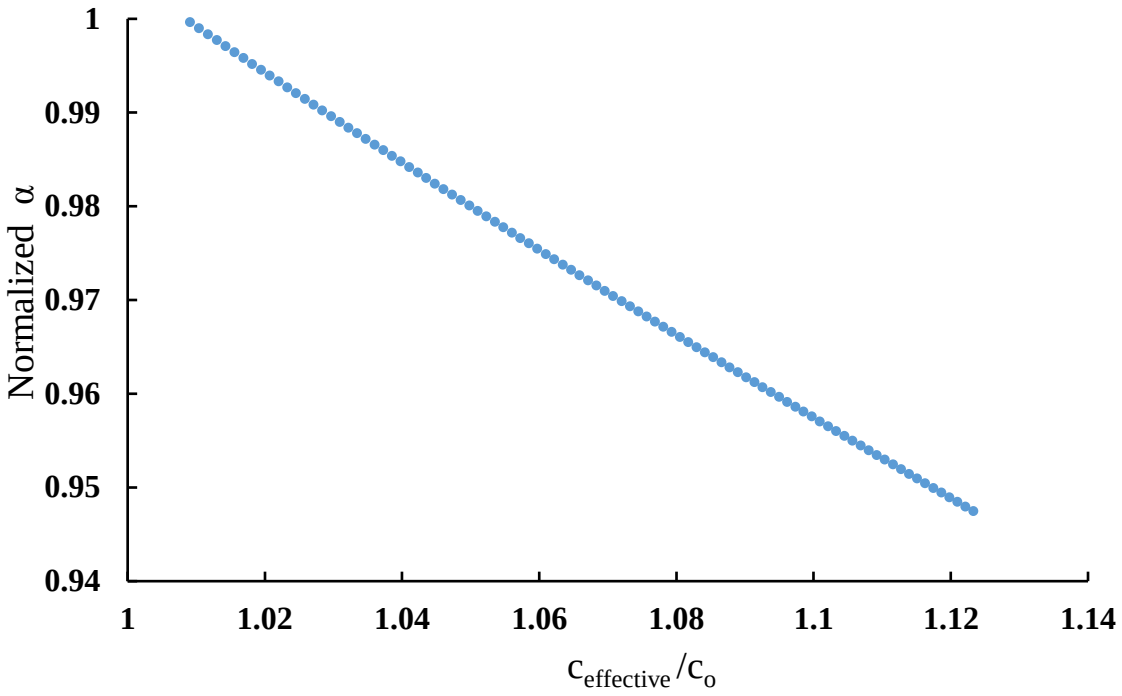

Figure 4-23 : Effect of the speed of sound on the damping coefficient for the case of D = 0.5", H = 10" (theoretical).

It can be seen that the acoustic damping of the duct decreases as the effective speed of sound is increased (i.e. increasing the number of tubes). This is because changing the speed of sound changes the natural frequency of the duct, which in turn affect the acoustic damping.

Other parameters that will affect the acoustic damping of the system are parameters such as the Prandtl number, specific heat ratios, and the dynamic viscosity. These parameters are related to the temperature and pressure of the fluid and the system in general. Any slight variation in one or more of these parameters could result in a completely different acoustic behavior.

Although the effect of the visco-thermal damping is a good indicator of the overall damping of the duct, it cannot be applied directly to the acoustic pressure amplitude of each case. There are other factors such as the radiation losses, and turbulent losses that also have an effect on the final acoustic pressure amplitude produced. Therefore, incorporating a damping parameter in the equations is not by any means an easy task, care should be taken when trying to formulate a comprehensive damping parameter.

In conclusion, the higher the acoustic damping of the system the more energy is required to produce noise. Since resonance in all cases has already materialized, it means that the energy supplied to the system was sufficient enough to overcome the acoustic damping of all the ducts. However, the duct with the highest damping will dissipate the energy faster. The resonance in the highest duct (lowest stiffness and lowest damping) will occur faster and with minimal energy, and will also dissipate energy slower than the other two ducts. This agrees with the experimental data in this thesis.

4.3.8 Normalization Scheme and Important Scaling Parameters

Comparing the experimental results with the suggested empirical relations in literature showed great discrepancy for the simple case of single cylinders. It has been shown that both the dynamic head of the flow and/or the input energy parameter suggested by Blevins and Bressler (MdP) cannot be used as scaling parameter on their own, especially when comparing ducts of different cross-sectional areas.

The acoustic damping and the stiffness of the system plays an important role in the onset of acoustic resonance as well as the range over which the resonance is sustained, as well as its amplitude. However, it is not very clear how the damping and/or stiffness of the

system affect the maximum acoustic pressure amplitude at resonance, at least for the cases in which the blockage ratio and the velocity of coincidence are equal. This is due to the complexity of the phenomena, as for in order to maintain a certain blockage ratio (D/H), one would have to change both the diameter of the cylinder and the height of the duct accordingly. Changing both parameters simultaneously introduce complexities to the system as changing the height changes the frequency of excitation, the acoustic particle velocity and the damping of the system while changing the diameter of the cylinder changes the acoustic source itself and affects the intensity of the radiated noise.

Therefore, equations that predict the maximum acoustic pressure amplitude at resonance based solely on geometrical characteristics such as the diameter of the cylinders or spacing ratios seems to be inaccurate as they do not include the effect of the acoustic damping and stiffness of the system.

In order to come up with a comprehensive damping parameter, the effect of geometrical parameters such as the height of the duct, and the number of cylinders enclosed should be included. These parameters change the frequency of excitation and the speed of sound inside the duct, both of which affects the acoustic damping in a nonlinear fashion. Moreover, the effect of the temperature and pressure of the flow affects quantities such as the Prandtl number and the specific heat capacities, which also affects the acoustic damping of the system.

4.4 Single Cylinder Shifted from Centerline (Y/H = 0.25)

4.4.1 Effect of Location

In this section, a number of tests similar to the ones discussed in the previous section are performed, however, the position of the cylinders relative to the duct height was changed. The cylinders were placed at a relative position of Y/H = 0.25 from the duct height. For the medium height at *0.25*(254) = 63.5mm (2.5")* and for the largest height the cylinders were placed at *0.25*(304.8) = 76.2mm (3")*. **Figure 4-24** shows a schematic of the test section with the new relative position of the cylinder. These positions were chosen to coincide with the nodes of the 2nd acoustic mode pressure distribution. Thus it is expected that placing the cylinders at these positions will excite the 2nd acoustic resonance modes in all the ducts.

The smallest duct height *203mm (8")* was not included in this analyses for two reasons. The first reason is that the second acoustic mode resonance was not possible for this duct except for only the three (3) smallest cylinders in the range of the cylinders tested, namely the *10.5 (0.4"), 12.7 (0.5")* and *15.8 (0.6") mm (inch)*. The 2nd acoustic mode for the rest of the cylinders was not excited due to the limitations of the motor (max velocity 160m/s). The second reason is that for the smallest duct the cylinders are marginally near the wall of the duct relative to the other two ducts. This wall proximity may affect the normal vortex shedding phenomena, especially at high Reynolds numbers. The proximity may impose an asymmetric vortex shedding or even completely suppress the vortices from shedding at the region closer to the wall. All these effects may change the whole resonance mechanism under investigation. Therefore, the smallest duct height was ruled out and not tested in the coming section and only the medium and the tallest ducts were used.

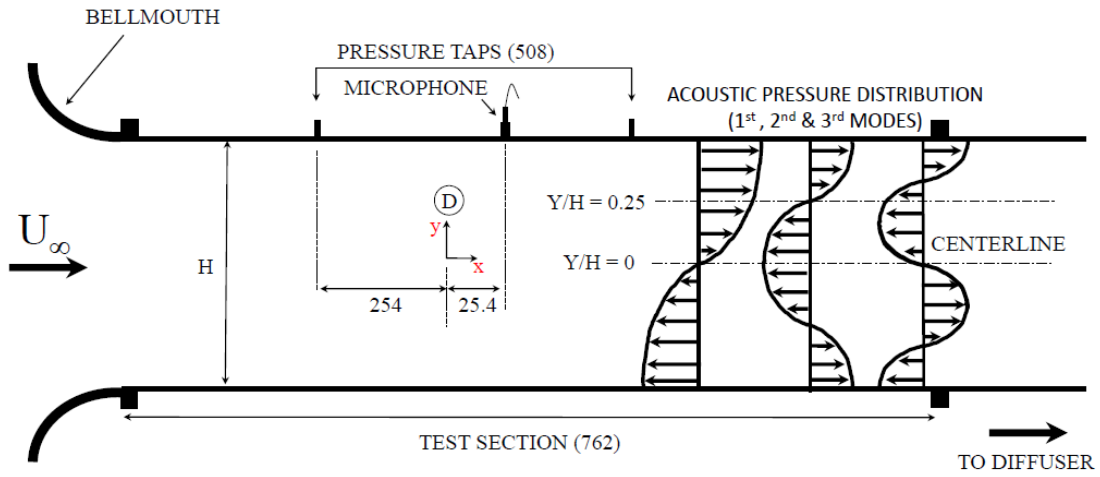

Figure 4-24 : Schematic of the test section showing relative position of cylinder away from centerline at Y/H = 0.25

First, the effect of the cylinder location on the excitation mechanism and frequency response relative to the base case will be analyzed. Two cases are compared where the diameter of the cylinder and the duct height are kept constant, while the location of the cylinder is shifted away from the centerline. The diameter chosen for this case is the *15.8mm (0.62")* diameter, and the height *254mm (10").* The same trend was observed for all the cases, however, this specific diameter and duct dimension were chosen carefully to show the most pronounced effect over the full spectrum for both cases. The range covers fully the first, second and third acoustic modes. **Figure 4-25** shows the acoustic response of the two cases. Placing the cylinder at Y/H = 0, fully excited the first and third acoustic modes as expected. The second mode, however, was completely suppressed. This is because the cylinder at the centerline is exactly placed at both the node of the acoustic pressure distribution for the 1st and 3rd modes and the anti-node of the 2nd mode. The pressure and acoustic particle velocity distributions lags by 90 degrees, therefore a pressure anti-node on the pressure wave constitutes a zero (node) acoustic particle velocity. The

anti-node on the acoustic pressure will thus give a zero pressure reading, according to Howe's (1975, 1980) triple product for instantaneous acoustic power.

When the cylinder was placed at the location of Y/H = 0.25, the second mode was fully excited, as seen on the red graph, and was the dominant mode across the spectrum. The first and third acoustic modes were still excited, however at a less amplitude than the dominant mode (2^{nd}). The difference in amplitude is found to be equal to the relative change of the position of the cylinder on the acoustic particle velocity distribution, Arafa & Mohany (2016).The vortex shedding frequency normalized by the first fundamental frequency of the duct is shown in **Figure 4-26** against the reduced velocity. The first three fundamental modes for this duct are calculated to occur as per $f_a = nc/2H$. At $n = 1,2\ and\ 3$ the corresponding frequencies are *675, 1351 and 2026 Hz* respectively. The behavior of both cases is almost identical, and the Strouhal number was calculated to be 0.199 for both, which agrees well with the values found in literature. There is no reason for the Strouhal number to change with the change in the location of the cylinder. The same trend is observed for the excitation frequency as expected from the numerical simulation presented in the previous section. This variation is well pronounced in the third mode where the resonance occurred at a frequency of *1820 Hz* which is about *10%* less than the theoretical frequency. The first acoustic mode occurred at a frequency of *675 Hz* which is *0.09%* less than the theoretical frequency, and the second mode occurred at a frequency of *1281 Hz* which is *5.3%* less than the theoretical frequency. Another representation of the acoustic pressure amplitudes for this case in sound pressure levels can be observed in **Figure 4-27.** It is clear that the second mode is entirely suppressed when the cylinder is located at Y/H = 0.

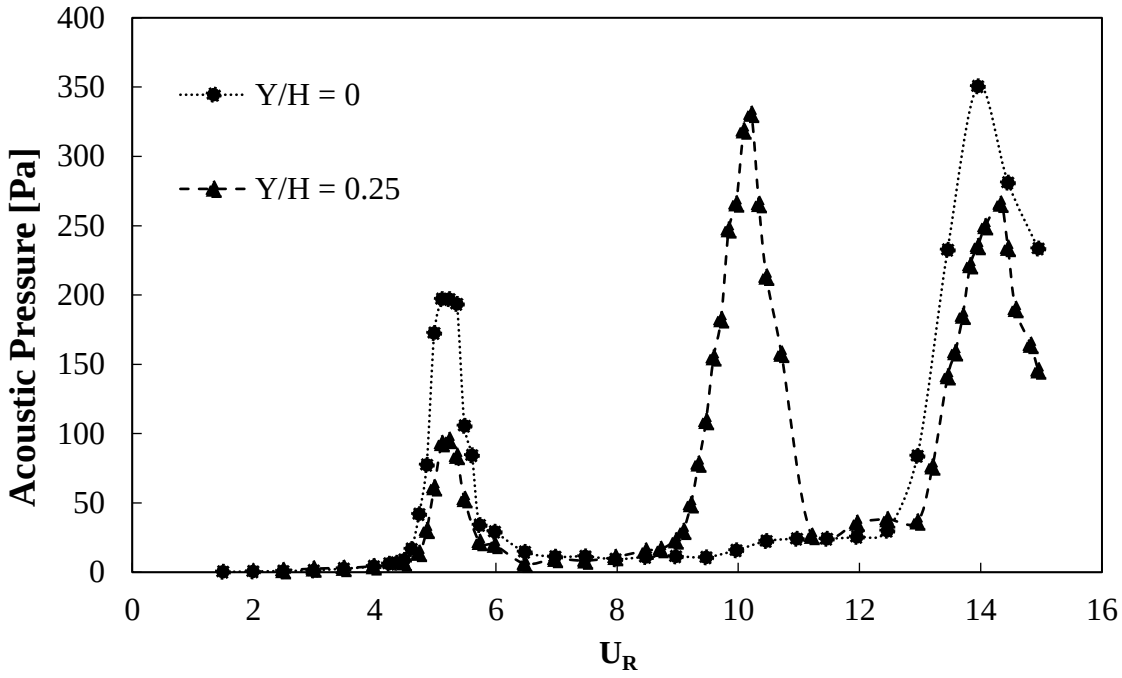

Figure 4-25 : Acoustic pressure response of single cylinder at two different locations, D = 15.9 mm (0.6") , H = 254 mm (10")

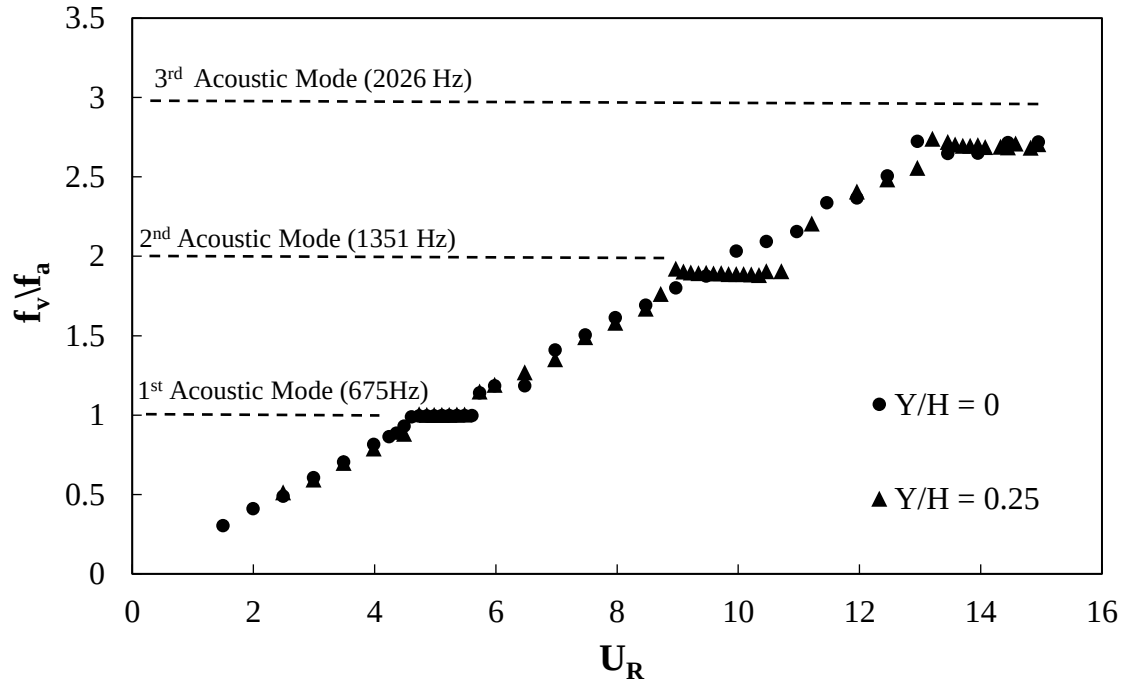

Figure 4-26 : Frequency response of single cylinder at two different duct locations D = 15.9mm (0.6"), H = 254 mm (10")

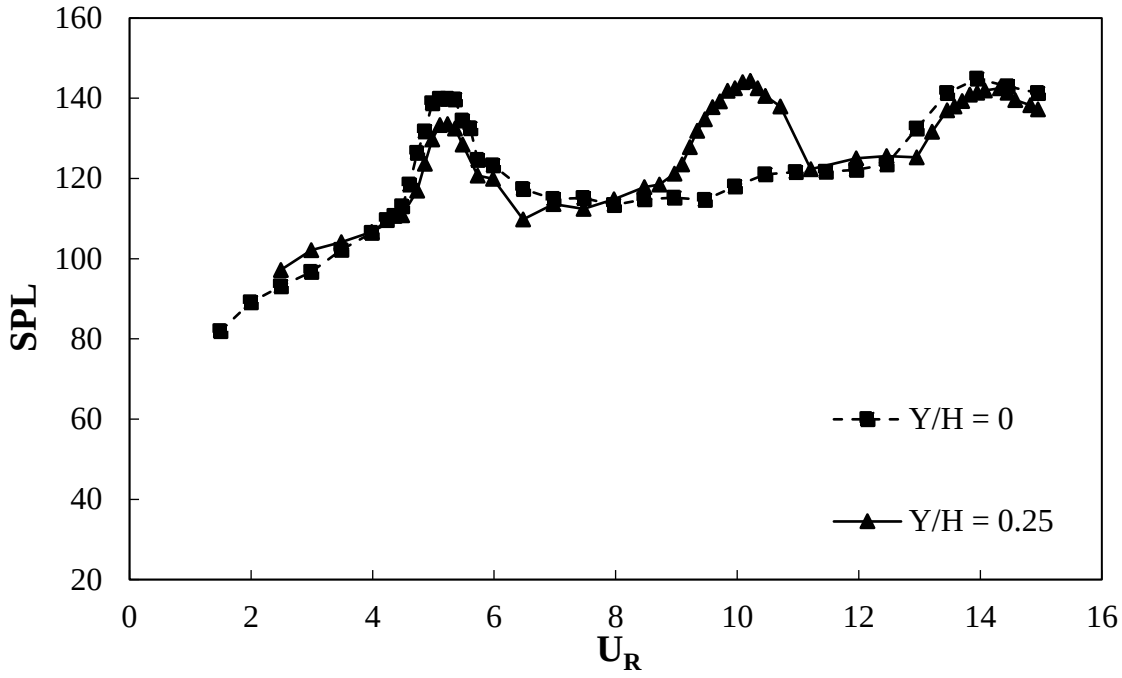

Figure 4-27 : Sound pressure levels of single cylinder at two different duct locations D = 15.9mm (0.6"), H = 254 mm (10")

Figure 4-28, Figure 4-29, and **Figure 4-30** show the pressure drop across a cylinder of diameter *15. 9mm (0.416")* at the two different duct locations. The pressure drop is shown for all the different duct heights *254mm (10"), 305mm (12")* and *203mm (8")* respectively. It is observed from the three figures that the pressure drop is not greatly affected by the position of a single cylinder inside the duct. This is reasonable since the actual blockage ratio is independent of the location of the cylinder. A similar trend was observed for all the other cases. The static pressure drop across the cylinder seems to only vary with the blockage ratio of the diameter relative to the duct height and the velocity of the flow.

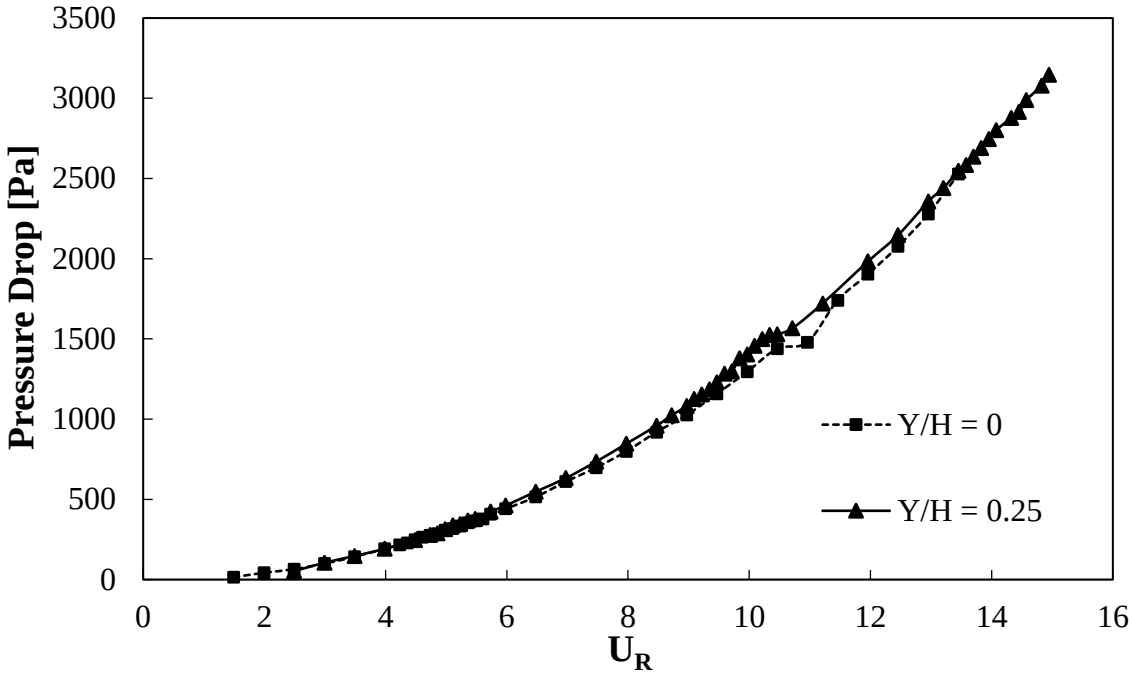

Figure 4-28 : Static pressure drop of single cylinder at two different duct locations D = 15.9mm (0.6”), H = 254 mm (10”)

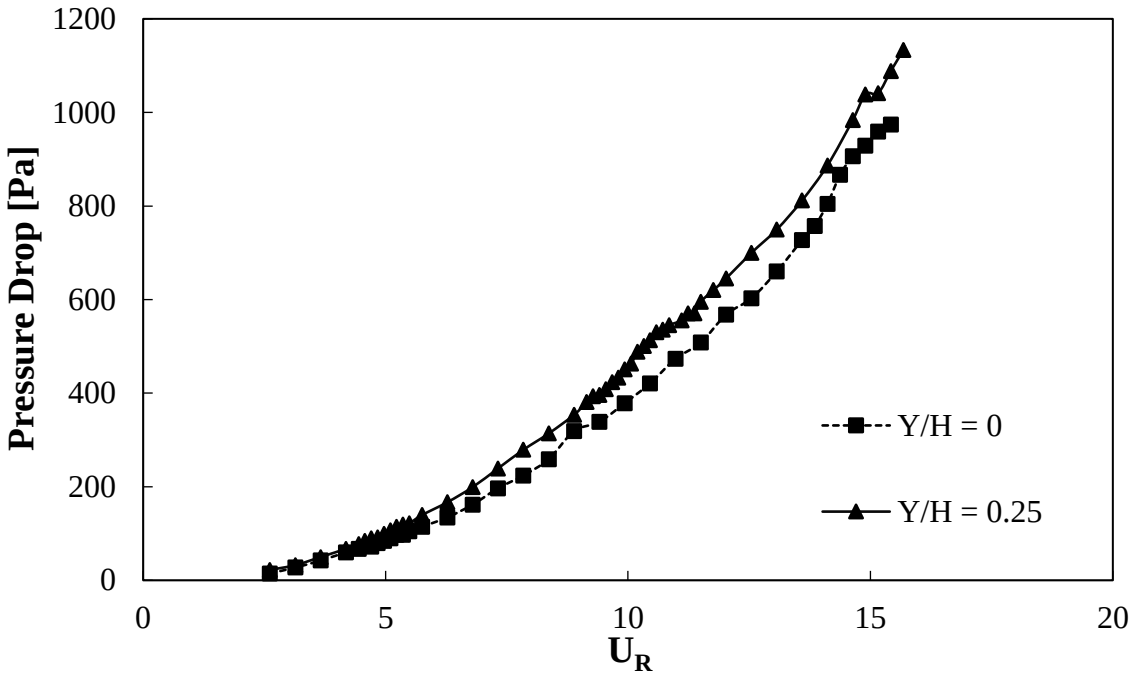

Figure 4-29 : Static pressure drop of single cylinder at two different duct locations D = 15.9mm (0.6”), H = 305 mm (12”)

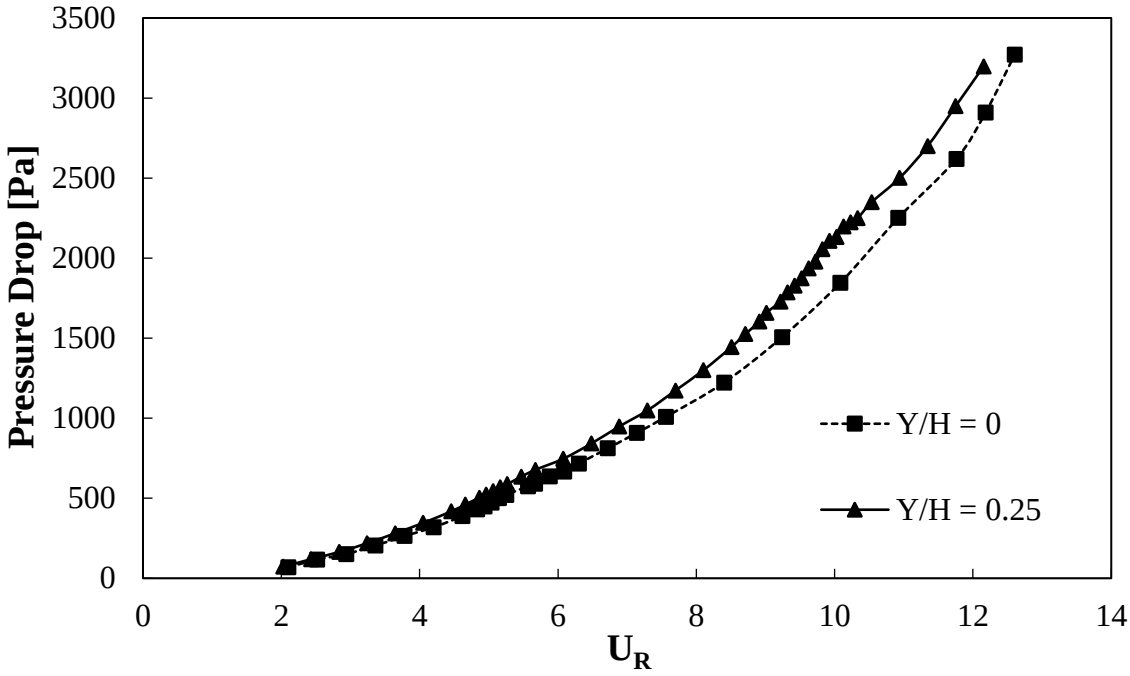

Figure 4-30 : Static pressure drop of single cylinder at two different duct locations D = 15.9mm (0.6”), H = 203 mm (8”)

The only difference that is observed with regards to the changing of the cylinder location in the duct, while marinating the cylinder diameter constant, seems to be in the excitation of different acoustic cross-modes and the acoustic pressure amplitudes of the excited modes. Placing a cylinder at the acoustic pressure node of a particular cross-mode tends to excite this particular cross-mode. The excitation seems to occur for other cross-modes too if the location of the cylinder is not at the extreme position of the mode’s acoustic pressure anti-node. The difference in amplitude is relative to the position of the cylinder on the sinusoidal acoustic pressure distribution along the duct height.

4.4.2 Effect of Height

The height of the duct has been shown to have a significant effect on the acoustic pressure amplitudes produced. As the height increased the amplitude of acoustic pressure also increased. **Figure 4-31** shows the acoustic pressures response for the diameter *12.7mm (0.5")* in the two duct heights of *254mm (10") and 305mm (12").* The same trend is observed for the second acoustic mode, where the highest duct produced the highest acoustic pressure. The second mode is excited at the reduced velocity of about U_R = 9 for both cases. The first mode is still excited at the reduced velocity range of U_R = 4.5-6, however with a lower amplitude due to the position of the cylinder relative to the acoustic particle velocity distribution.

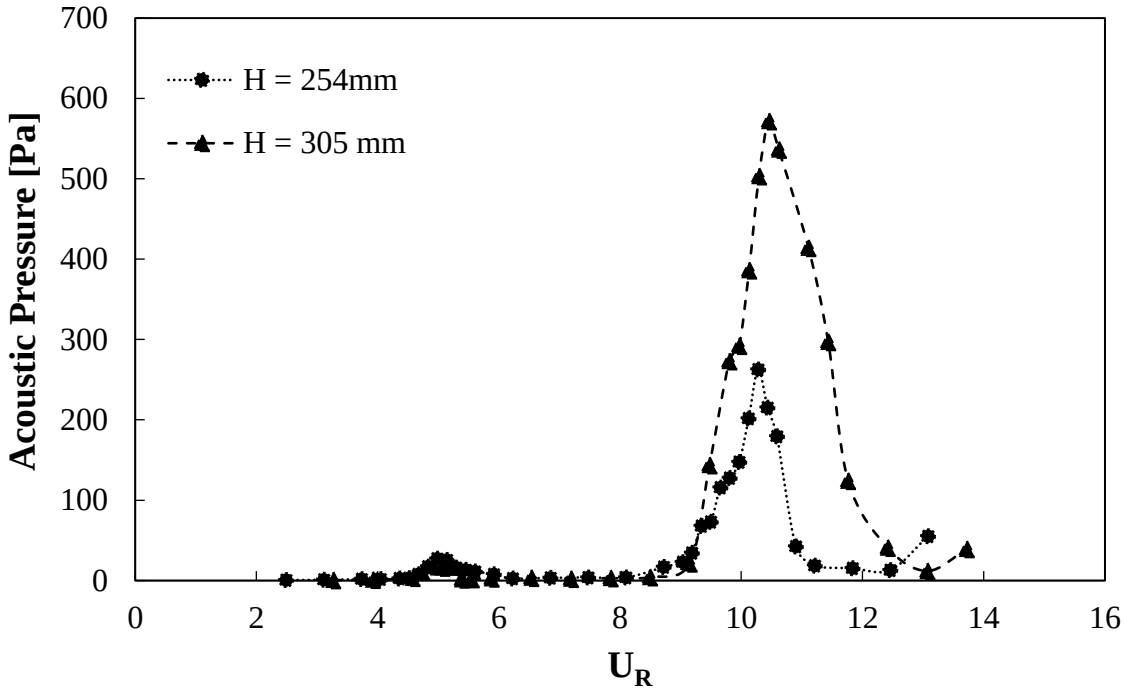

Figure 4-31 : Acoustic pressure response of D = 12.7mm (0.5") in different duct heights

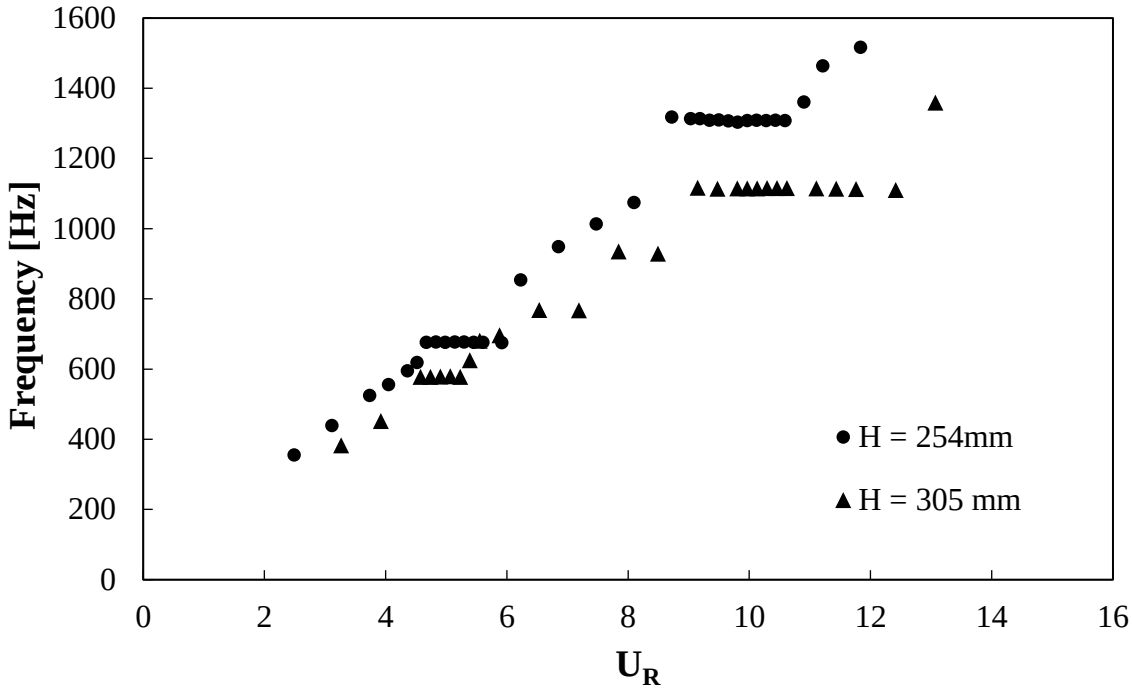

Figure 4-32 : Frequency response of D = 12.7mm (0.5") in different duct heights

The frequency response of the two cases is shown in **Figure 4-32**. It clearly shows two lock-in regions at the first and second acoustic modes respectively for the two ducts. The lock-in region of the second acoustic mode for the *305mm (12") duct* seems to be significantly wider than that of the 254mm (10") duct. The Strouhal number for the two cases was 0.202, which agrees well with the values of the Strouhal number found in the literature for single cylinders in cross-flow. **Figure 4-33** summarizes all the cases done in this set of experiments. The same trend is observed for the cylinders at the 2nd acoustic cross mode compared to the first location (Y/H = 0). The pressure amplitude is always higher for the highest duct *305mm (12").* The difference keeps increasing with the increase in the diameter of the cylinder enclosed. The excitation of the second cross-mode was not possible for the largest diameter namely *28.5mm (1.125")* because of the capabilities of the motor (max velocity 160 m/s).

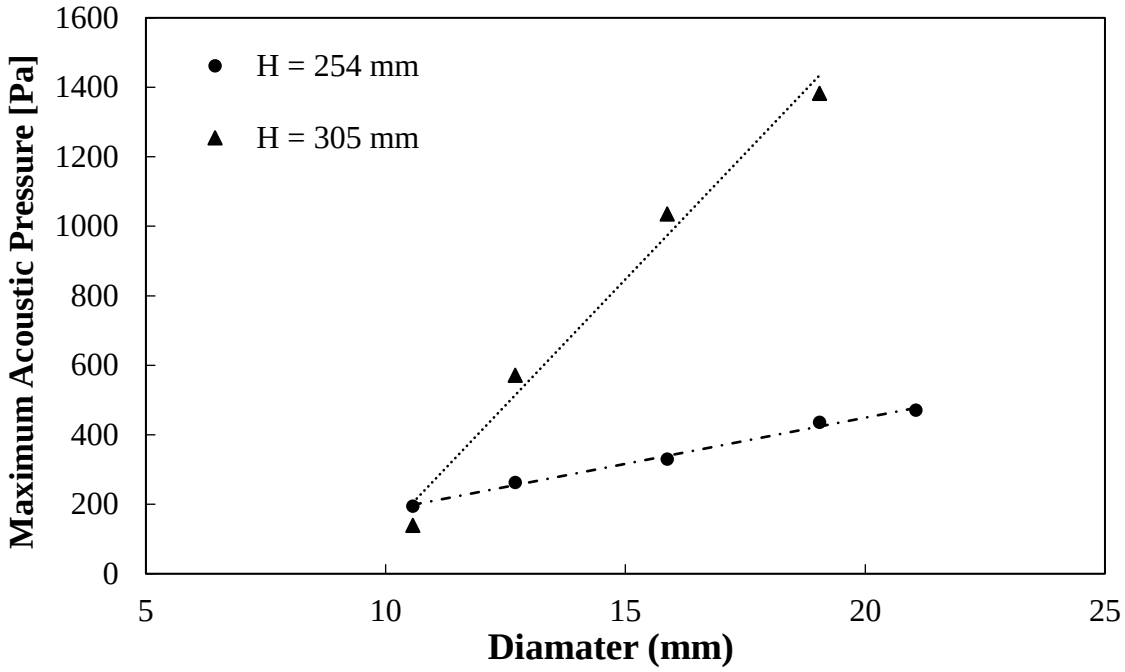

Figure 4-33 : All diameters tested for location (Y/H = 0.25), 2nd mode

When the cylinder is shifted away from the centerline, the first acoustic mode is still excited for all cylinders but at a lower level of amplitude. This is confirmed with the observed trends in the cases discussed. Shifting the location of the cylinder inside the duct not only changes the excitation frequency of resonance but also alters other parameters and might excite different duct modes.

4.4.3 Effect of Blockage Ratio (D/H)

Cases have been discussed in which the blockage ratio (D/H) and the velocity of coincidence were equal but the amplitude of pressure and the frequency of excitation were substantially different. When the cylinder is placed at the 2nd acoustic mode position, the response seems to be similar. **Figure 4-34** shows a case in which two different diameters *12.7mm (0.75")* and *21mm (0.82")* are placed in duct heights *254mm (10")* and *305mm*

(12") to obtain a constant blockage ratio of D/H = 0.075. The first acoustic mode was still excited in both cases and at approximately *64m/s* and 68 *m/s*. While for the second acoustic mode the velocity of coincidence was at *128m/s* for both. The cylinder in the highest duct produced higher acoustic pressure amplitude at both the first and second acoustic modes *392 Pa* and *1375 Pa* compared to *215 Pa* and *431 Pa* respectively.

The resonance in both acoustic modes seems to occur over a broader range of velocities compared to the similar cases when the cylinder was placed at the centerline of the duct (Y/H = 0). The other cases of similar D/H ratios are summarized in **Figure 4-35** and the trend seems to be the same for all the cases. This trend confirms that location of the cylinder in the duct and the acoustic damping are both very important parameter that greatly affects the aeroacoustics response of single cylinders.

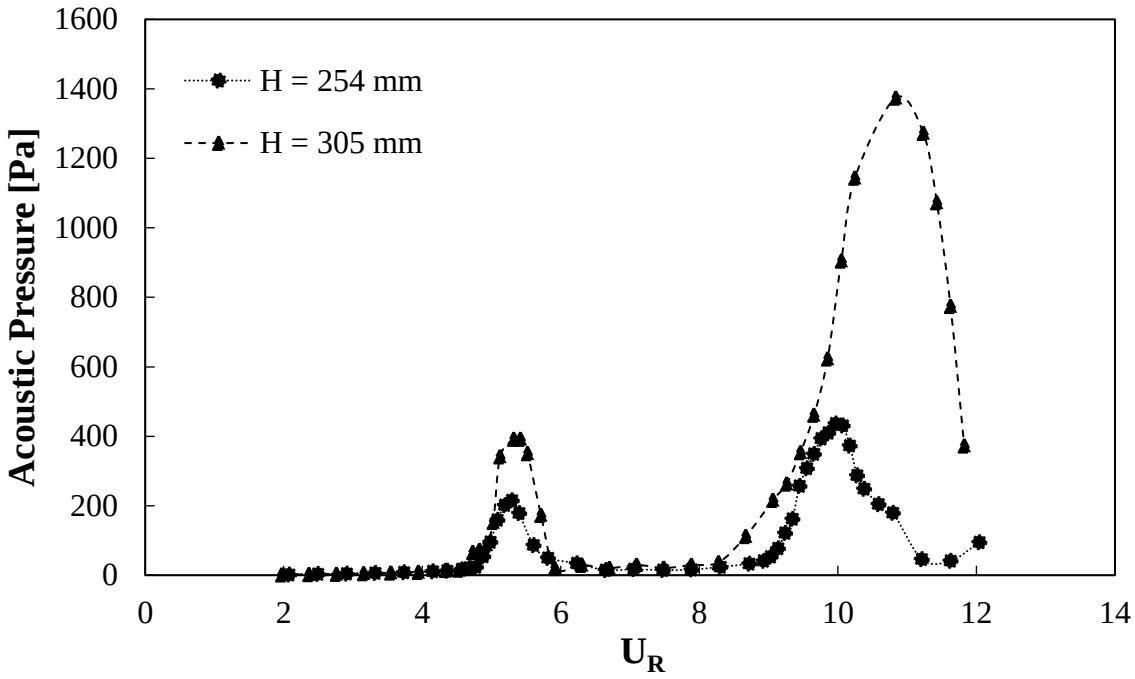

Figure 4-34 : Pressure response of D/H = 0.075 for different diameters and cylinders at Y/H = 0.25, 2nd mode

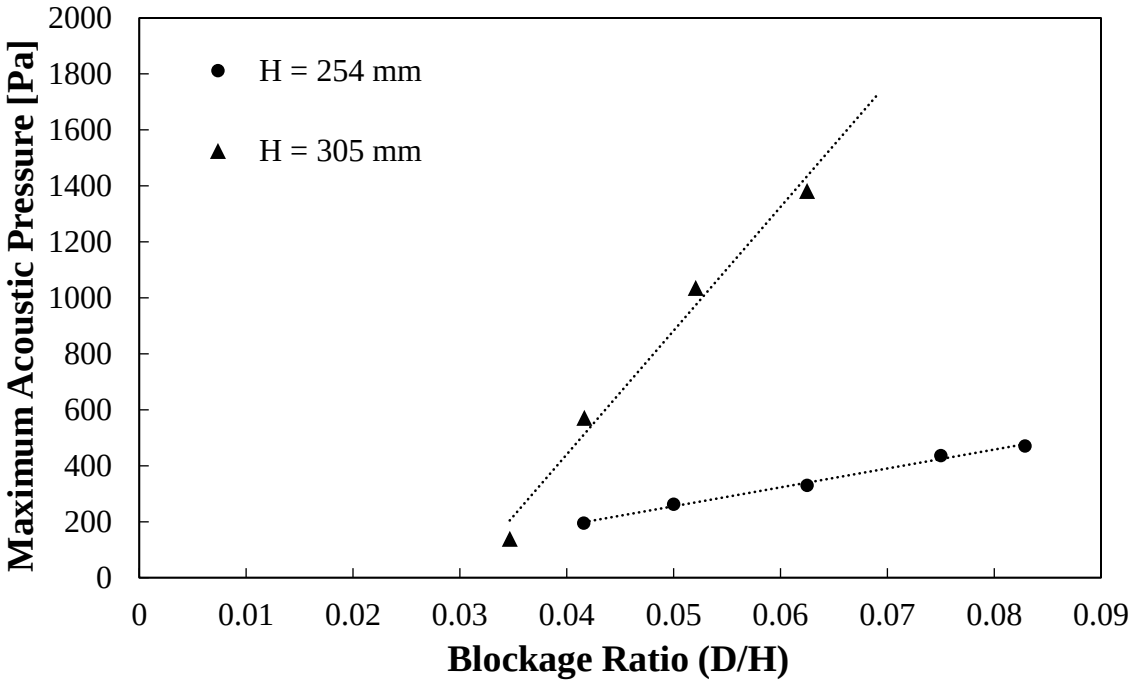

Figure 4-35 : Effect of blockage ratio (D/H) on the acoustic pressure response for single cylinders at Y/H = 0.25, 2nd mode

4.4.4 Comparison with the Literature

The tested cases for the second set of measurements, when the cylinder is placed at location Y/H = 0.25, are plotted against the equations suggested by Blevins and Bressler to predict the maximum acoustic pressure amplitude as a function of the Mach number multiplied by the static pressure drop. Although Blevins and Bressler did not do any experiments for single cylinders in the higher acoustic modes (2nd mode), they suggested that the empirical equation is valid for all modes. **Figure 4-36** shows the data of the current experiments, for both the first and the second acoustic cross-modes, against the empirical equation suggested. The equation may seem to capture the correct linear trend of the data, however, it highly over-predicts the maximum acoustic pressure point ($P_{rms,\,max}$) for all the cases.

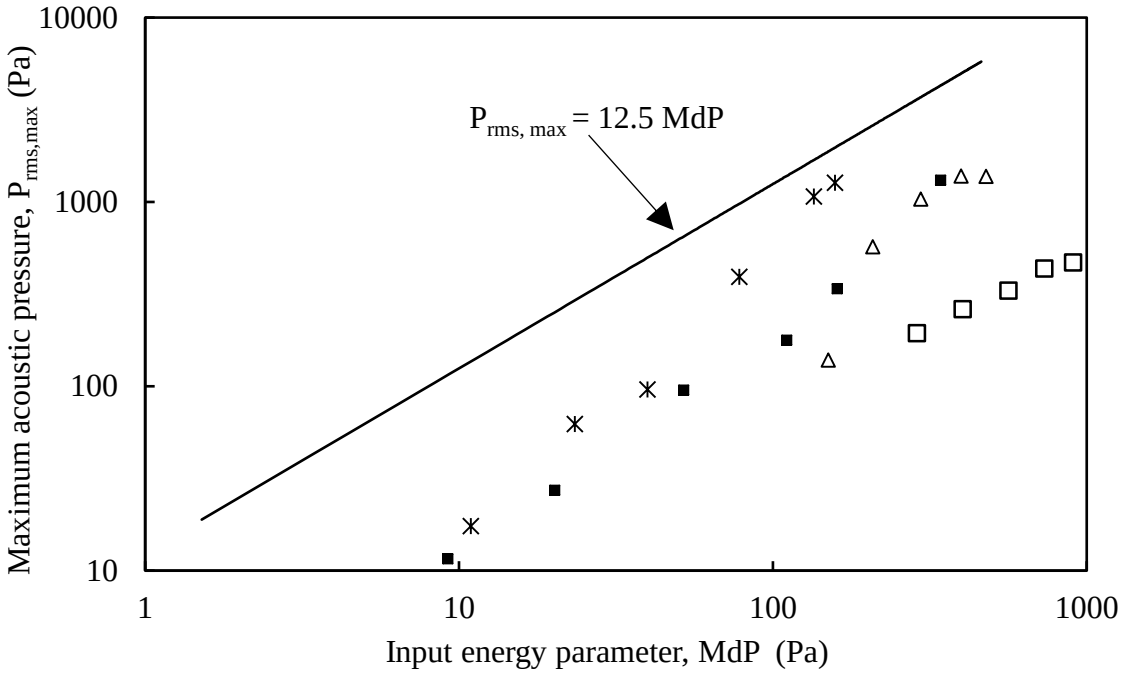

Figure 4-36 : Comparison with empirical formula related to input energy parameter for 2nd acoustic mode (Y/H = 0.25)

4.5 Special Case: Isolated Cylinders (Y/H = -0.25 and 0.25)

This section discusses the case of side-by-side cylinders at very large spacing ratios (*5.33 < T/D < 14.4*). Although physically there are two cylinders present in the duct, they are included as a special case of single cylinders because at this very large spacing the two cylinders are said to be hydrodynamically isolated, Arafa and Mohany (2016). The wake of each cylinder is not affected by the wake of the other cylinder, therefore both cylinders are expected to shed vortices in a similar fashion to the single cylinder, Sumner (1999b).

The purpose of this section is to analyze the aeroacoustic response of two isolated cylinders in one of the duct heights, namely *H = 305mm (12"),* for different cylinder diameters and at different pitch-to-diameter ratios. The cylinders are placed at the locations of Y/H = 0.25

and -0.25 as shown in **Figure 4-37**. The transverse pitch (T) is fixed to *152 mm (6")*, while the diameter of the cylinder is varied between *10.5 - 28.5 (0.416 – 1.125) mm(inch).* This change results in seven pitch-to-diameter ratios (T/D) within the parallel vortex shedding streets region, to be tested. The parallel vortex shedding region is defined at *T/D > 2.2* where the cylinders regain their symmetry of shedding and both undergo Karman vortex shedding at the same frequency, Sumner (2010).

Cases presented in this section are compared to the cases of single cylinders shifted away from the centerline at position (Y/H = 0.25) since in both cases the cylinders are placed at the same position relative to the acoustic pressure cross-mode distribution.

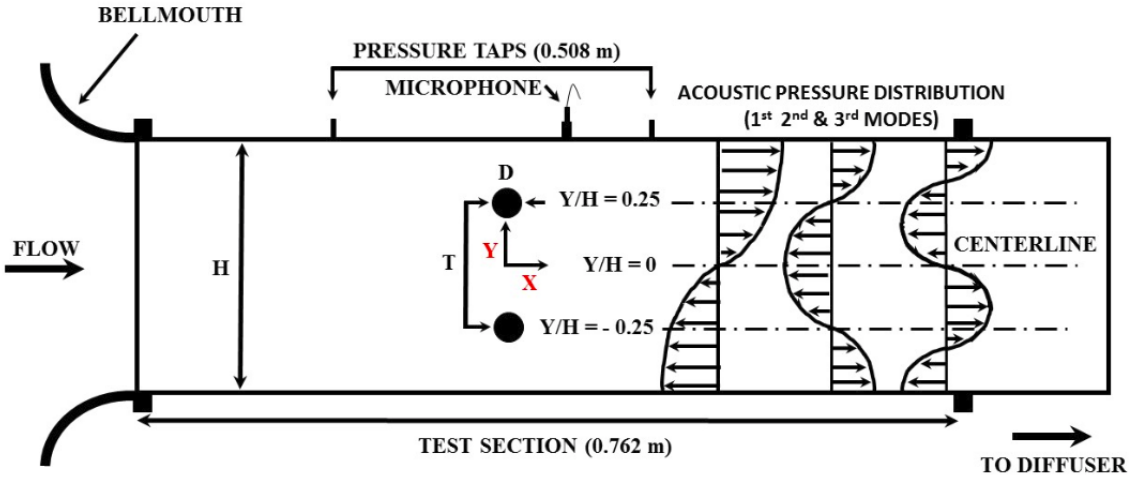

Figure 4-37 : Schematic of wind-tunnel for side-by-side experiment

The position of the cylinders at Y/H = 0.25 and Y/H = -0.25 is at the acoustic pressure **node** and the **anti-node** of the acoustic particle velocity distribution for the theoretical 2nd cross-mode distribution of the duct. Thus this position will excite the second acoustic mode

resonance, in addition to the first and the third acoustic cross-modes if the flow velocity is high enough.

Figure 4-38 and **Figure 4-39** shows the pressure response and the frequency response of cylinder diameter *19mm (0.75")* in duct height *305 mm (12")* for the different positions relative to Y/H. The pitch-to-diameter ratio for the cylinders placed at Y/H = -0.25 and 0.25 is T/D = 8. Since the cylinders at locations Y/H = 0.25 and Y/H = -0.25 and 0.25 are placed at the location of the pressure node of the second acoustic cross-mode, they excited the 2nd acoustic mode resonance at the frequency of *1126 Hz.* The two cases behave exactly the same in terms of the onset and offset of acoustic resonance at both the first and the second modes. All the cases were able to excite the first acoustic cross-mode, however, the case of the single cylinder at Y/H = 0, excited the first mode with the highest amplitude (*838 Pa)* of all. The Strouhal numbers for the cases were 0.193 and 0.194 respectively. Which agrees well with the literature since at this very long pitch to diameter ratio the side-by-side cylinders act as isolated cylinders.

Comparing the cases of the single cylinder at Y/H = 0.25 and two cylinders at Y/H = -0.25 and 0.25, it can be observed that placing two cylinders simultaneously at the acoustic pressure node of a certain mode excites the resonance at that mode with higher acoustic pressure amplitudes compared to one cylinder. The first and second acoustic cross-modes were excited with pressure amplitudes of *96Pa* and *1382Pa* respectively for the single cylinder at Y/H = 0.25. While for the two side-by-side cylinders the first and second acoustic cross-modes were excited with pressure amplitudes *332Pa* and *2783Pa* respectively. The change in the amplitude seems to be exactly doubled for the dominant cross-mode. A similar trend was observed for all the other diameters tested

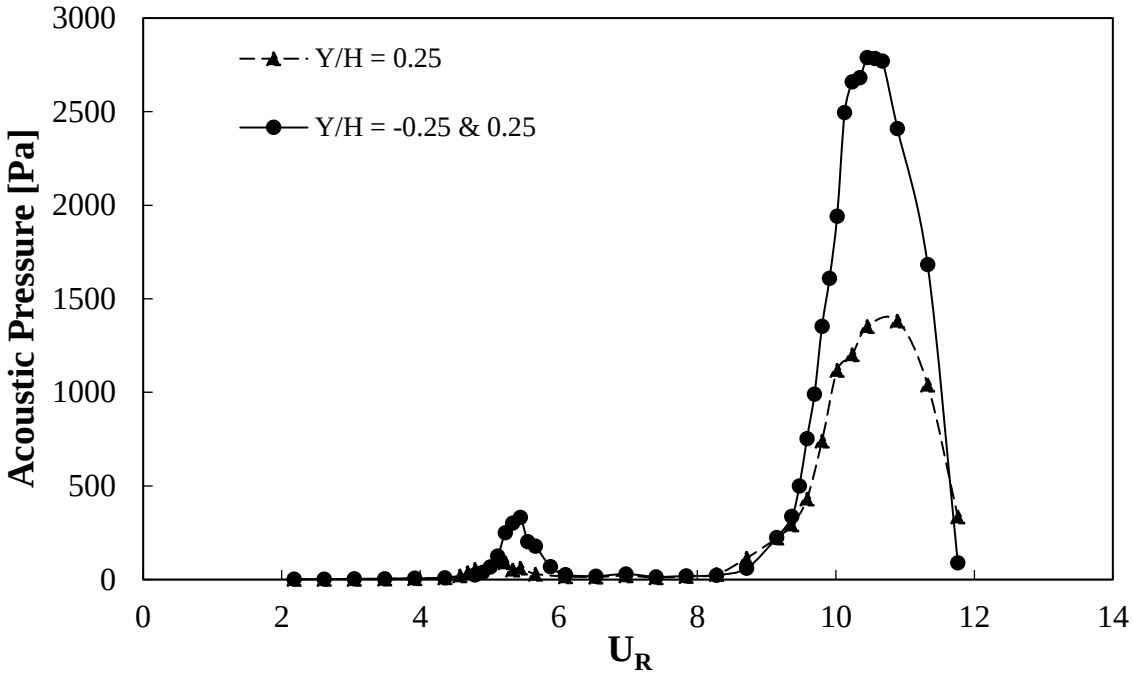

Figure 4-38 : Pressure response of diameter 19 mm (0.75") in H = 305 mm (12") relative to the cylinder position in duct.

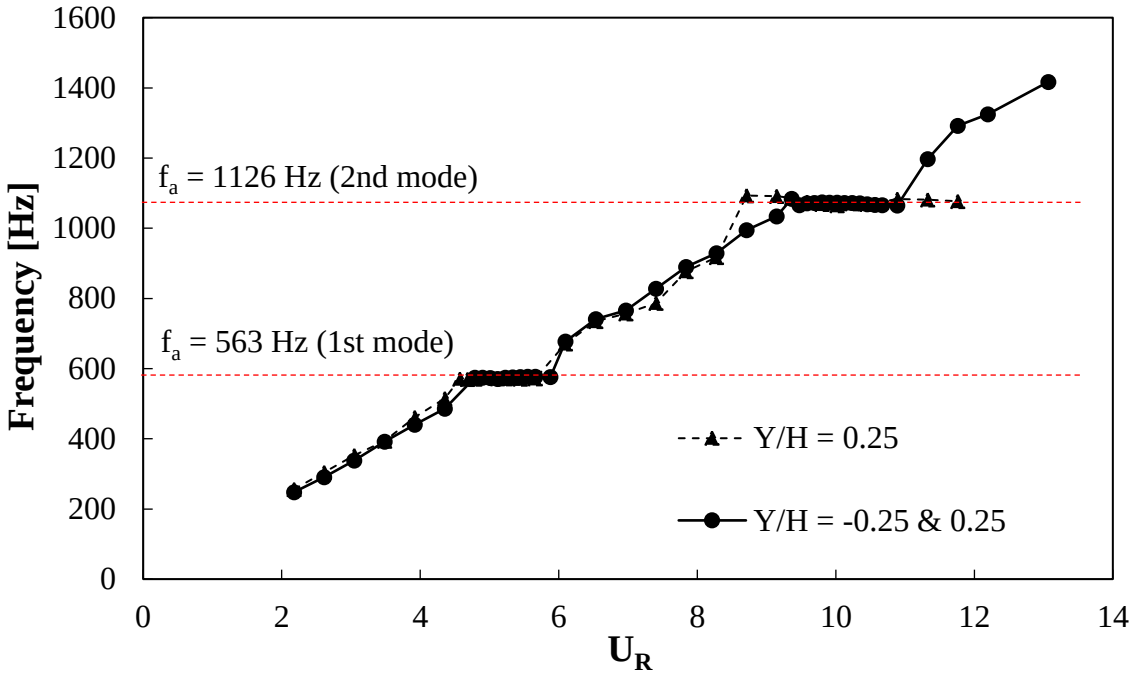

Figure 4-39 : Frequency response of diameter 19 mm (0.75") in H = 305 mm (12") relative to the cylinder position in duct.

Figure 4-40 shows the pressure drop of the two cases. As expected the pressure drop of the case of side-by-side cylinders is higher since the blockage ratio is greater. In fact, the change is pressure is almost exactly doubled. A similar trend was observed for all the other cases in this set as well.

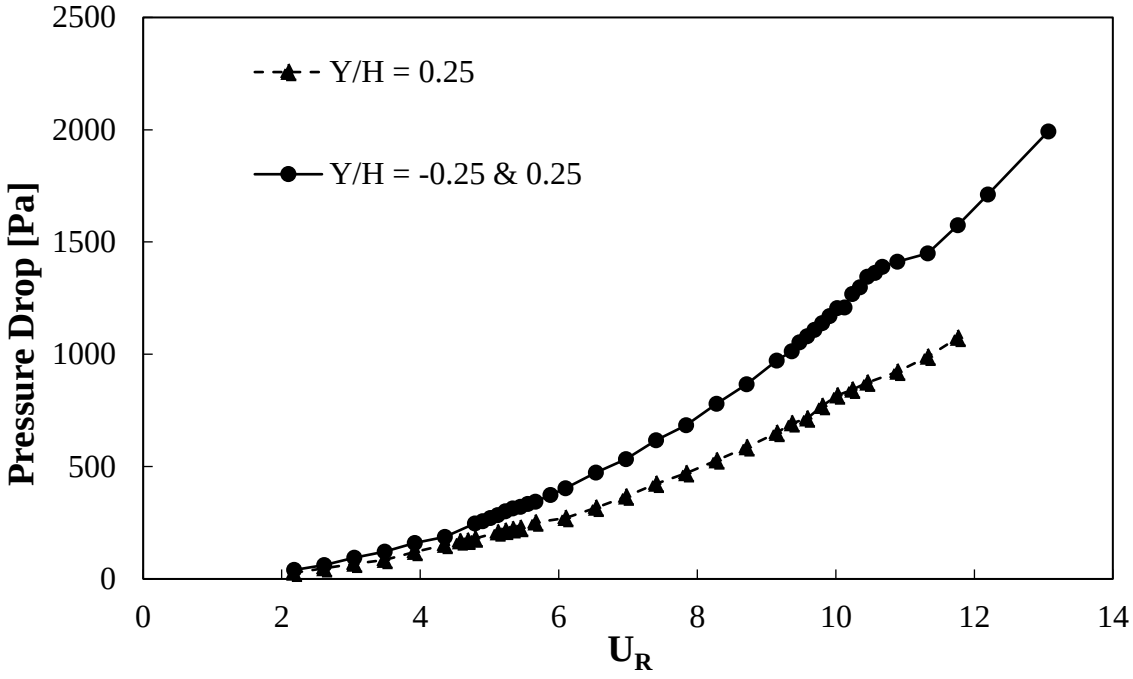

Figure 4-40 : Pressure drop of diameter 19 mm (0.75") in H = 305 mm (12") relative to the cylinder position in duct.

4.5.1 Effect of Diameter and T/D

The effect of diameter (and T/D) on the acoustic pressure and the frequency response of side-by-side cylinders is shown in **Figure 4-41** and **Figure 4-42** respectively. Tested cylinders are *12.7 (0.5), 19 (0.75)* and *28.5 (1.125) mm (inch)* with relative spacing ratios of T/D = *12, 8 and 5.33* respectively. The effect of the diameter seems to be similar to that of the single cylinder at the center line (Y/H = 0) and single cylinder at 2nd acoustic

cross-mode (Y/H = 0.25). Increasing the diameter of the enclosed cylinder increases the pressure drop and the acoustic pressure amplitude at resonance. The onset of acoustic resonance is shifted to higher velocities as the diameter is increased as well. The Strouhal number for the tested cases is 0.195, 0.194 and 0.201 receptively. The values of the Strouhal numbers are equal to that of the single cylinder because of the large spacing ratio value of T/D.

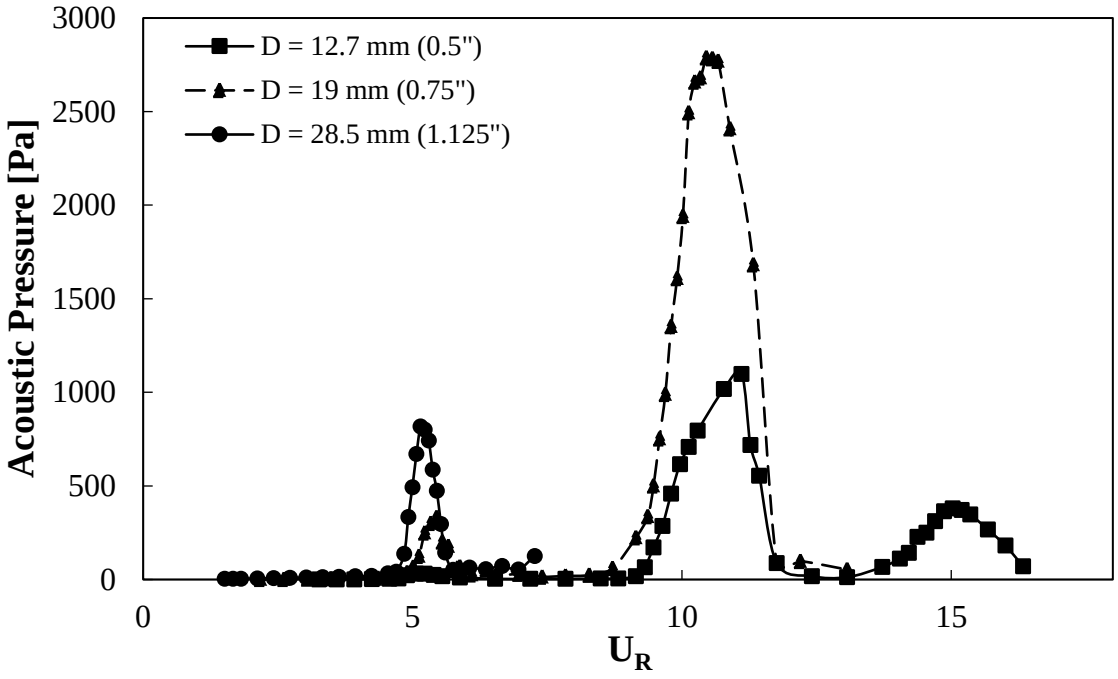

Figure 4-41 : Effect of diameter on acoustic pressure of side-by-side cylinders; H = 305 mm (12")

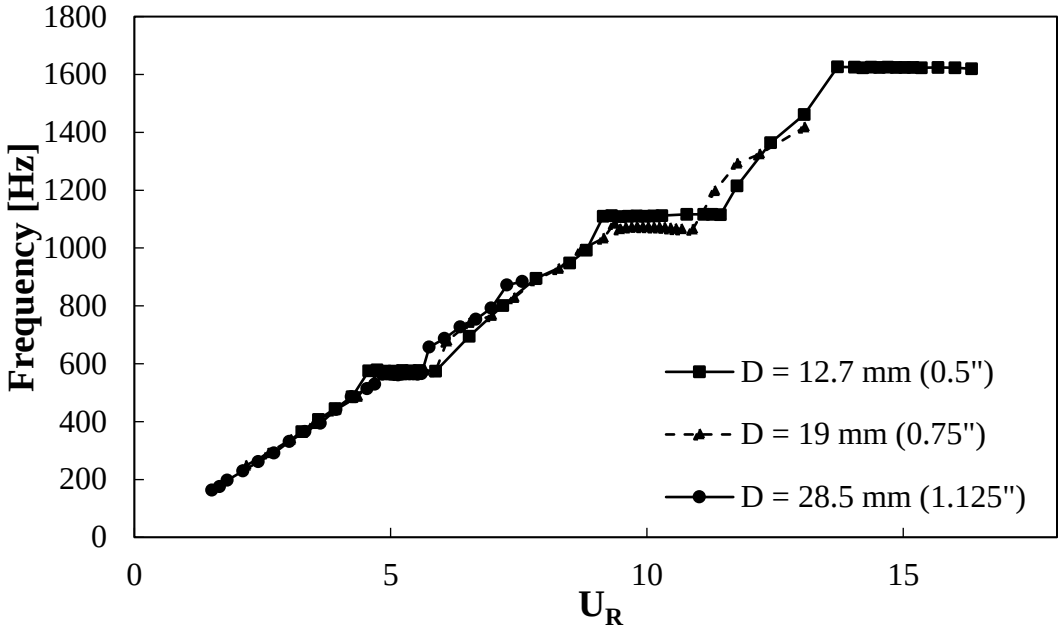

Figure 4-42 : Effect of diameter on frequency response of side-by-side cylinders , H = 305 mm (12")

4.6 Conclusion

This chapter analyzed the aeroacoustic response of single cylinders in cross-flow, under variable conditions. Seven different cylinders in the range of *[10 ~ 25 mm]* were tested in three different test sections with heights *203 (8), 254 (10) and 304(12) mm (inch).* All the cylinders were tested at two different locations (*Y/H = 0 and Y/H = 0.25*) inside the duct. These locations were carefully chosen to excite the first and second acoustic cross-modes of the duct respectively. The independent variation of the cylinder diameter, the duct height and the location of the cylinder within the duct allowed for a wide variety of variables to be changed as well as for various testing conditions. The effect of each parameter was tested independently as well as the combined effect of the diameter and the height (blockage ratio). The results were compared to the available literature.

For the first acoustic mode (cylinder placed at Y/H = 0), it was found that increasing the diameter while keeping the test section height constant, increases the acoustic pressure amplitudes and delays the onset of acoustic resonance to higher velocities. Moreover, changing the height of the duct was found to change the stiffness and damping of the system making it more or less susceptible to acoustic resonance. Placing the cylinder in a shifted position away from the center line (Y/H = 0.25) excites different acoustic modes. The height seems to have the same effect for cylinders at both locations. From the results of the side-by-side cylinder configuration at very large spacing ratios, it can be concluded that the cylinders behave exactly as for single cylinders in terms of the vortex shedding, thus predicting the acoustic resonance onset is not different from single cylinders. However, the amplitude of the acoustic pressure is higher than single cylinders and is not easily predictable from the similar single cylinder cases.

The empirical equation (in both forms) suggested by Blevins and Bressler failed to predict the acoustic pressure at resonance in the simple case of single cylinder presented. The equation over and under-predict the maximum acoustic pressure values for nearly all the cases. It is believed that the empirical equation fails to predict the maximum acoustic pressure because it does not take into account the effect of the system acoustic damping. The results obtained from comparing the current data with the data in literature shows that scaling the acoustic pressure amplitude with the dynamic head of the flow ($0.5\rho U^2$) might give inaccurate results. This was clearly observed when the special cases of D/H where tested. Since resonance occurred for all the cases at the same velocity which implied the same energy is found in the flow. However, the acoustic pressure response was different depending on the diameter.

Chapter 5

5 Aeroacoustic Response of Tandem Cylinders in Cross-Flow

5.1 Introduction

Cylinders in tandem configuration represent the simplest case of shear layer separation and reattachment between cylinders' wakes. It was found that the cylinders in tandem configurations tend to behave in a similar manner to the in-line tubes of heat exchangers. The case of tandem cylinders in cross-flow under *self-excited* resonance conditions has been investigated only by Mohany (2007), and Shaaban and Mohany (2015). No research has exclusively investigated the effect of the duct height on the aeroacoustic response of tandem cylinders.

The aeroacoustic response of tandem cylinders is complex in nature as it depends on many interacting parameters such as the diameter of the cylinders, the longitudinal length between the cylinders, (which affects the wake interference), the Reynolds number of the flow and other parameters. In the case of single cylinders, the acoustic resonance usually occurs at a reduced velocity range of U_R = 4.5 - 6.0. Cylinders in a tandem configuration like the ones shown in **Figure 5-1** experience a different resonance phenomenon referred to as "*dual-resonance*"; where the acoustic resonance occurs over two different ranges of velocities instead of one.

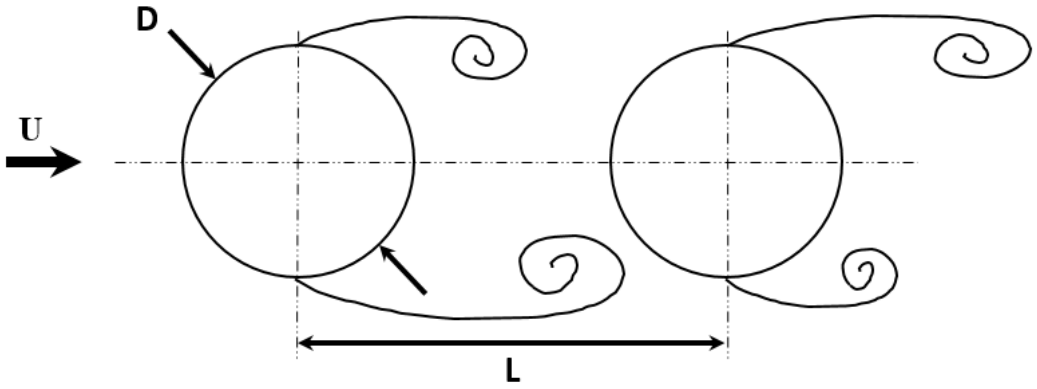

Figure 5-1 : Schematic of cylinders in tandem arrangement (L) is the length between the center of the two diameters and (D) is the diameter of the cylinder.

The first resonance in the case of tandem cylinders is called the "*pre-coincidence*" resonance which occurs at a reduced velocity range of about U_R = 3. 5. The pre-coincidence resonance is thought to occur due to, or at least is triggered by, the instability of the shear layers in the gap between the cylinders, Mohany and Ziada (2005). The second resonance is called the "*coincidence*" resonance, which takes place at the reduced velocity of U_R = 6. The coincidence resonance occurs at a Strouhal number similar to that of normal vortex shedding for single cylinders (0.2), which implies that it is indeed a result of von Karman vortex shedding behind the downstream cylinder.

The pre-coincidence resonance occurs earlier and exhibits characteristics similar to those of self-excited resonance in in-line tube bundles, thus it is important to be able to accurately predict the occurrence of the pre-coincidence resonance. No criterion to date is reliable in predicting acoustic resonance excitation in tube bundles. In fact, in 30-40% of the cases, the expected acoustic resonance never occurs, Blevins and Bressler (1993). Using the current prediction methods (damping criteria) may result in dangerously inaccurate

predictions when applied to tube bundles of different diameters and/or ducts of different sized. It is more important to be able to predict the pre-coincidence resonance occurrence rather than the actual acoustic pressure amplitude. That is because; if the occurrence of the pre-coincidence resonance is accurately predicted, countermeasures (such as operating at different velocity ranges) may be easily adapted resulting in the resonance being avoided altogether with all its consequences. On the other hand, being able to predict the acoustic pressure amplitude at resonance without knowing whether or not the resonance will initially materialize is not be very useful.

This chapter, therefore, aims to investigate the effect of the duct height and the cylinders' diameter on the aeroacoustic response of tandem cylinders in cross-flow. Special attention is given to the effect of the parameters under investigation on the occurrence of the pre-coincidence resonance rather than the coincidence resonance. For the purpose of analysis of the current chapter, seven cylinders within the range of *10.56 – 28.5 mm (0.416 – 1.125")* are tested in three different duct heights *203, 254 and 305 mm (8, 10, and 12").* Two sets of experiments are conducted at two different spacing ratios (L/D) below the critical spacing of 3. The two spacing ratios lie within the proximity region as specified by Zdravkovich (1985), in which the cylinders are expected to interact with one another, in terms of wake vortex shedding. The first spacing ratio is in the *alternate re-attachment* region of the shear layers (L/D = 1.5), and the second spacing ratio is in the *quasi-steady re-attachment* region of separated shear layers (L/D = 2). The outcome of this chapter shall help in developing better and more reliable criteria to predict acoustic resonance occurrence in full-sized heat exchangers.

5.2 Typical Response

Prior to resonance, the pressure spectrum signal of the tandem cylinders is not very different from that of signal cylinder case. At resonance, however, whether it is the pre-coincidence or the coincidence resonance, the tandem cylinders' frequency response is not very clear, in terms of peaks, due to the complexity of the phenomena. The acoustic pressure at resonance is also usually way higher in the case of tandem cylinders than the case of single cylinders with similar diameters.

Figure 5-2 shows the pressure spectrum at the pre-coincidence resonance for a tandem configuration with diameter *28.5 mm (1.125")*, spacing ratio *L/D = 2*, and *305 mm (12")* duct height. **Figure 5-3** shows the 3D waterfall plot of the same case but for the full velocity range. The waterfall plot shows both the pre-coincidence and coincidence resonance occurrences. The resonance, in this case, occurred at the natural duct acoustic frequency (*563 Hz*) as expected with an acoustic pressure value of around *6000* Pa. Due to the sharpness and intensity of the peak, the higher harmonics of the resonance could be clearly identified at *1126* and *1689* Hz respectively. The sound pressure levels in the case of tandem cylinders can reach values of up to 175 dB (11,000 Pa).

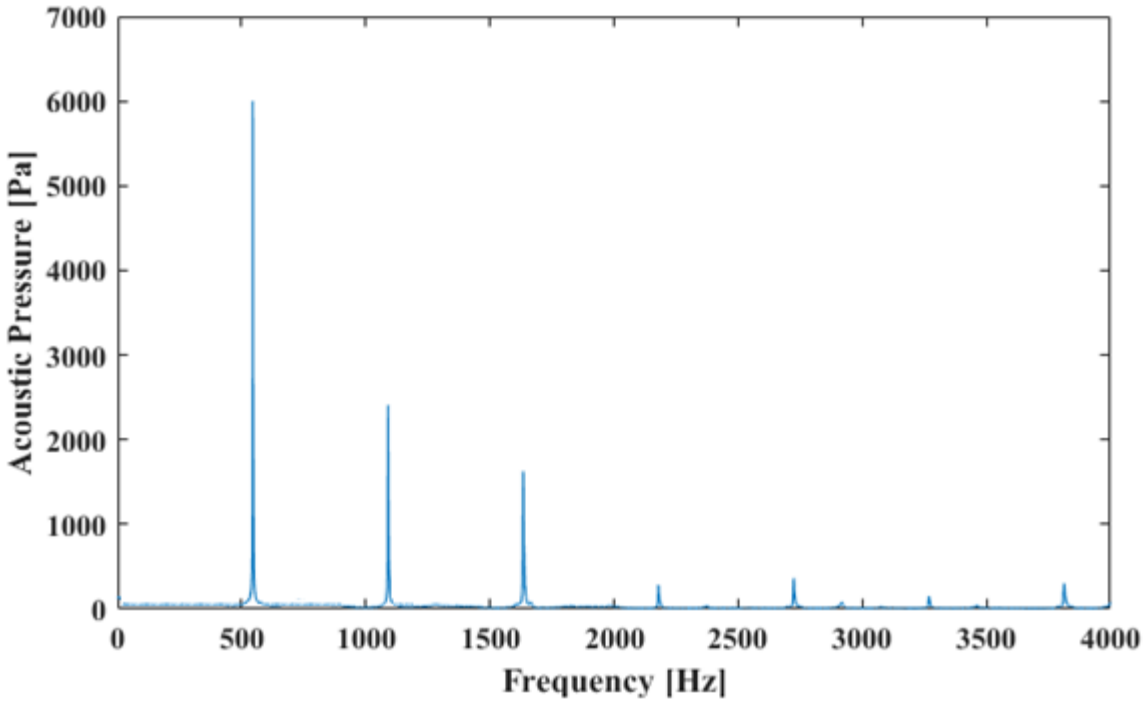

Figure 5-2 : Pre-coincidence resonance for tandem configuration (D = 28.5mm , L/D = 2.0, H = 305mm)

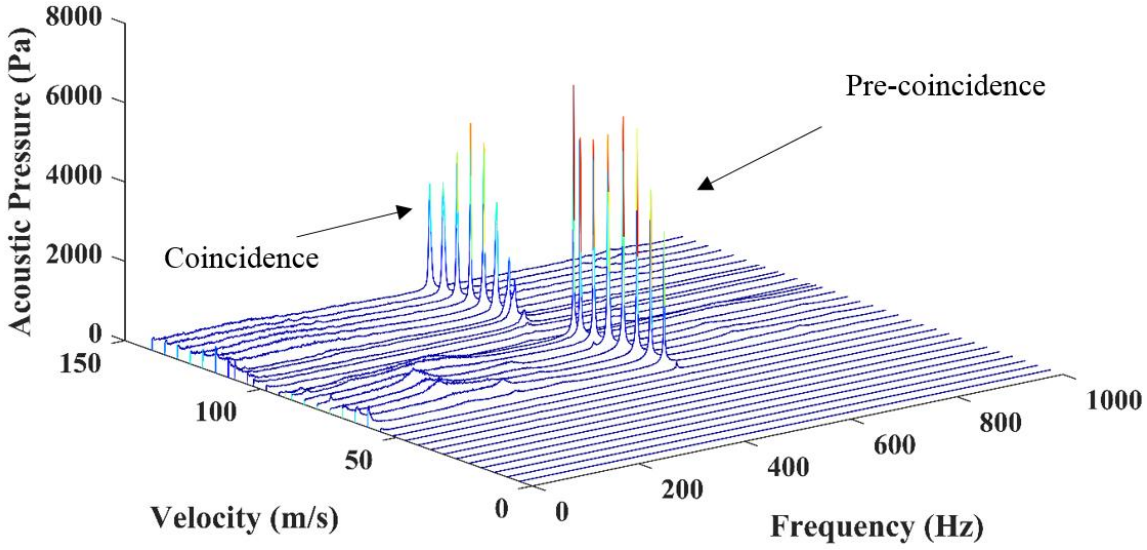

Figure 5-3 : 3D waterfall plot of cylinders in tandem arrangement (D = 28.5mm , L/D = 2.0, H = 305mm)

The aeroacoustic response of tandem cylinders (**Figure 5-4** and **Figure 5-5**) is also complex and harder to analyze compared to the case of single cylinders. For example; sometimes the lock-in regions at the pre-coincidence and the coincidence resonances are merged together in one wide lock-in region that spans across both velocity ranges. In the acoustic pressure response, this would appear as two pressure peaks separated by a smaller acoustic pressure in-between them exactly at the velocity of the frequency of coincidence, Mohany, and Ziada (2005). The Strouhal number for the case of tandem cylinders is also very different from the single cylinder cases. It is not constant and is highly dependent on both the spacing ratio between the cylinders and the Reynolds number.

The Strouhal number for the case in **Figure 5-5** is 0.15, which agrees well with the defined Strouhal number for the case of tandem cylinders in this flow range and spacing ratio, Igarashi (1981). The Strouhal number for all the cases tested in this thesis are within the ranges of 0.14 – 0.17. The frequency response of tandem cylinders, **Figure 5-5** shows two lock-in regions at the velocity ranges of the *pre-coincidence* and the *coincidence* resonance. In cases where the pre-coincidence resonance does not materialize, the frequency response shows one lock-in region representing the coincidence resonance at the reduced velocity range of around $U_R = 6$.

At low velocities, the frequency response of tandem cylinders is similar to the single cylinder frequency response; where the vortex shedding increases linearly with the increasing velocity. At the onset of pre-coincidence, the vortex shedding peak instantly lock-in with the natural duct frequency. Further increasing the upstream velocity causes the natural duct frequency to resonate more and the peak starts getting sharper until the pre-coincidence resonance breaks. Upon breaking, the vortex shedding frequency is seen

to increase linearly again with the increasing velocity up until it lock-in and merges with the natural duct frequency again to initiate the coincidence resonance.

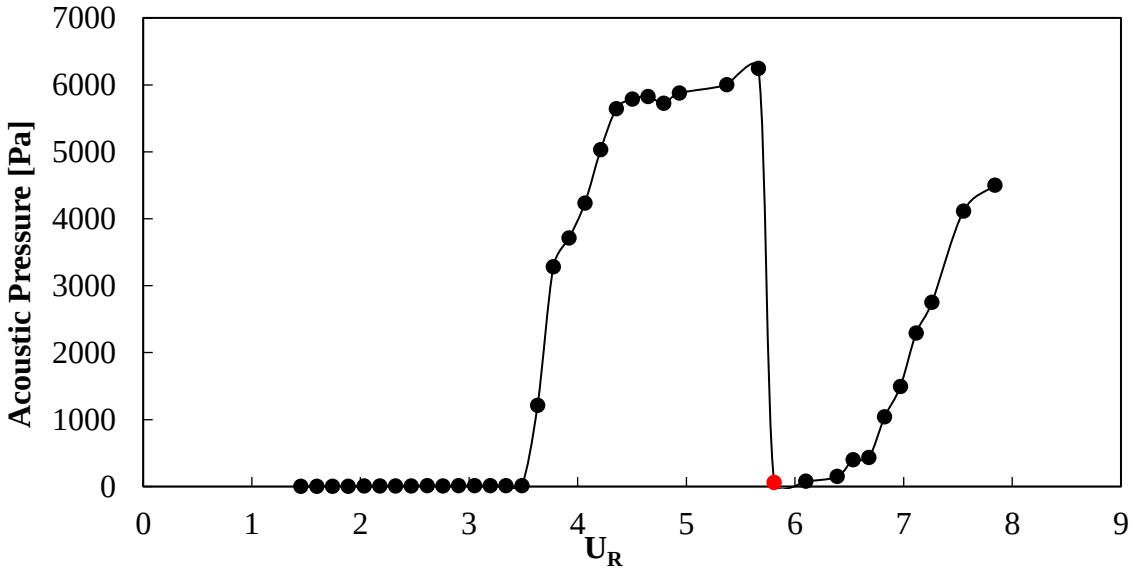

Figure 5-4 : Pressure response of two tandem cylinders for D = 28.5mm , L/D = 2, H= 305mm

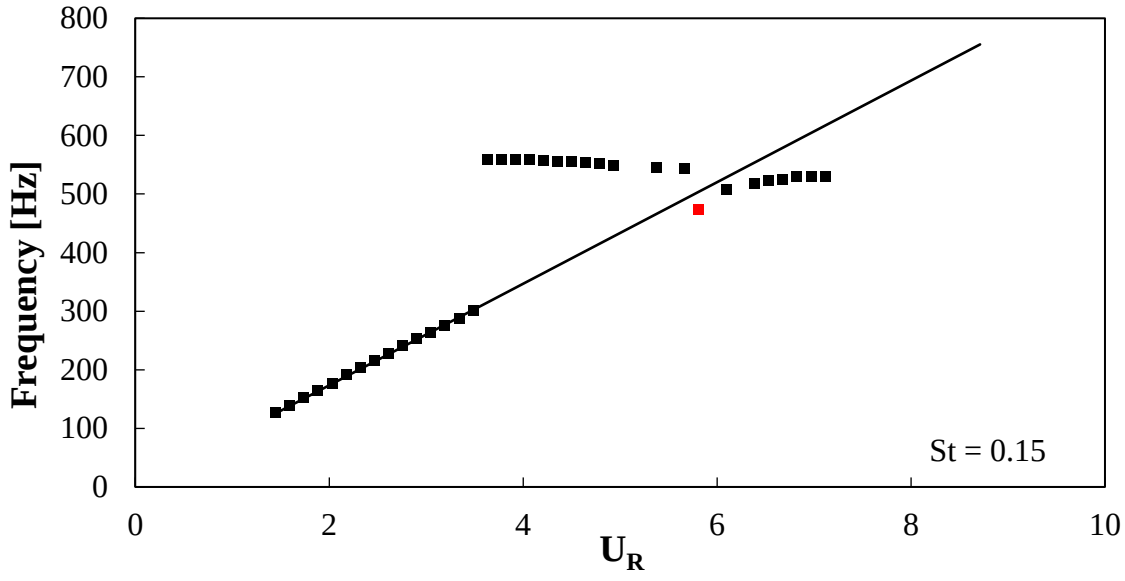

Figure 5-5 : Frequency response of two tandem cylinders for D = 28.5mm , L/D = 2, H= 305mm

5.3 Origin of Pre-Coincidence Resonance

The pre-coincidence resonance is thought to occur due to, or at least is triggered by, the instability of the shear layers in the gap between the cylinders, Mohany and Ziada (2005). **Figure 5-6** shows a comparison between the current experiment Strouhal number values at pre-coincidence, coincidence and vortex shedding to the experimental values found in the literature. The Strouhal number is calculated based on the longitudinal spacing (L) between the cylinders' centers instead of the cylinders' diameter.

The Strouhal number values from the current experiments show excellent agreement with the results obtained by Mohany and Ziada (2005) for spacing ratios of L/D = 1.5 and 2. The value of the Strouhal number at the pre-coincidence increases with the increasing spacing ratio between the values of 0.4 to 0.6, which is substantially higher than the Strouhal number at the onset of coincidence and vortex shedding Strouhal number. The excellent agreement between the present data and the data provided in the literature, confirms that the *pre-coincidence* resonance for the cases encountered in the thesis is also a result of the shear layer instabilities between the gaps of the cylinders. Moreover, since the value of between the Strouhal number of vortex shedding (based on the length between the cylinders) is almost equal to the value of the Strouhal number at the coincidence, it can be concluded that the *coincidence* resonance occurs due to the normal vortex shedding phenomena like the one observed for single cylinders.

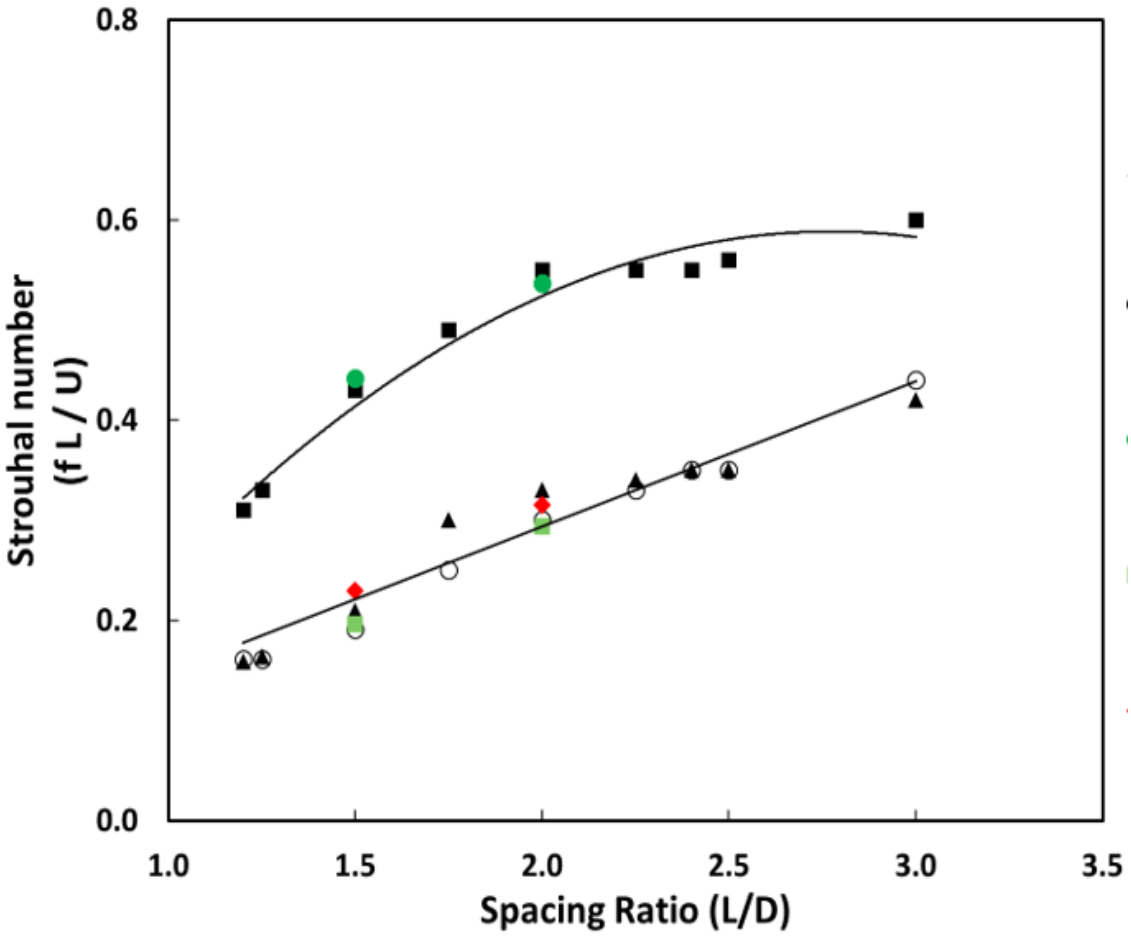

Figure 5-6 : Strouhal numbers for pre-coincidence, coincidence, and vortex shedding. ■, St. number for pre-coincidence, ▲, St. number for coincidence, ○, St. number for vortex shedding, (Mohany and Ziada, 2005). ■, St. number for coincidence, ●, St. number for pre-coincidence, ♦, St. number for vortex shedding, Current study. All Strouhal numbers are based on the frequency of vortex shedding and the spacing (L) between the cylinders.

The pre-coincidence resonance is more important than the coincidence resonance for industrial practices. That is because the tandem cylinders behave as in-line tube bundles of heat exchangers and most of the "unpredicted" acoustic resonance that occurs in tube bundles of heat exchangers occurs due to the pre-coincidence resonance. The problem with the pre-coincidence resonance is that its occurrence is unexpected as it is excited over a lower velocity range. The pre-coincidence resonance may sometimes produce higher

acoustic pressure levels compared to coincidence resonance. **Figure 5-7** shows a comparison of the sound pressure levels between the current experimental results and those found in the literature for in-line tube bundles with the same spacing ratios, Ziada & Oengoren (1992). Excellent agreement is observed between the current results and the literature data. This trend confirms the similarity between the tandem configuration and the in-line tube bundles, in terms of the severity of the noise, and subsequently, vibrations produced.

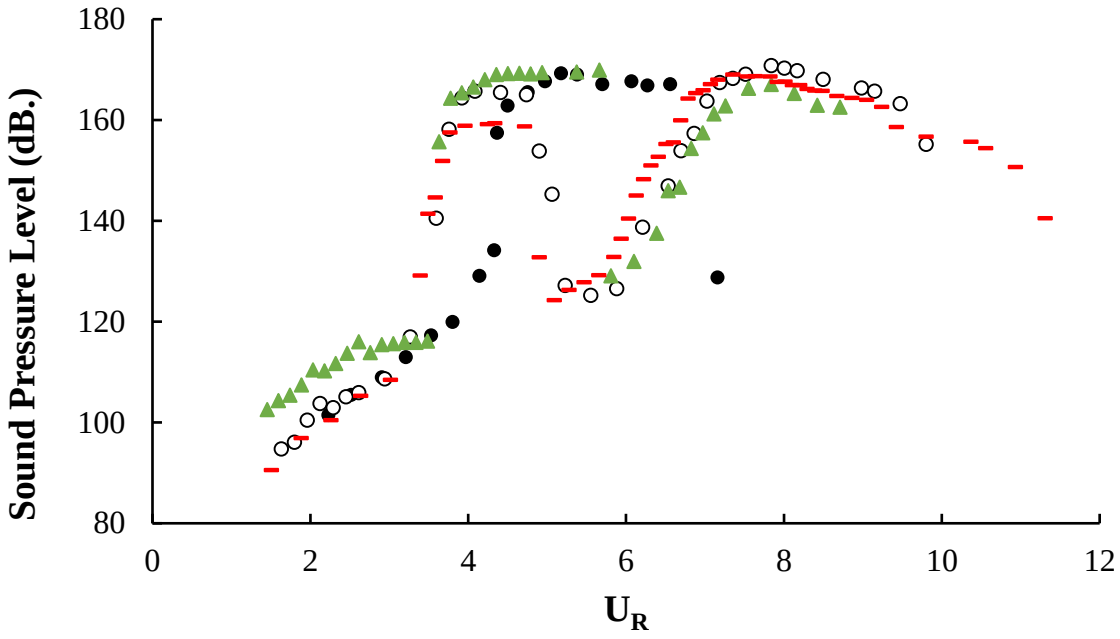

Figure 5-7 : Comparison between the sound pressure level for tandem cylinders with spacing ratio L/D = 2.0 and in-line tube bundles with X_L (L/D) = 2.0. ●, Ziada & Oengoren (1992) in-line tube bundle X_L = 2.0. ○, Current experiment L/D = 2.0, D = 25.4 mm, H = 305 mm. ▲, Current experiment L/D = 2.0, D = 28.5mm, H = 305 mm. —, Current experiment L/D = 2.0, D = 21 mm, H = 254 mm.

5.4 Effect of Reynolds Number on Strouhal Number

The effect of Reynolds number on the Strouhal number of vortex shedding from two tandem cylinders compared with literature values is shown in **Figure 5-8**. Excellent

agreement is observed between the current experiment and those provided in the literature for the Reynolds number at a range of *20,000 – 80,000*. At high Reynolds number, the Strouhal number for all the cases seems to asymptote at the value of 0.15, This relationship is only valid for the spacing ratios below the critical spacing ratio L/D = 3.0, Mohany and Ziada (2005). After the critical spacing ratio, the two cylinders start acting as single cylinders and no interaction is observed between their wakes.

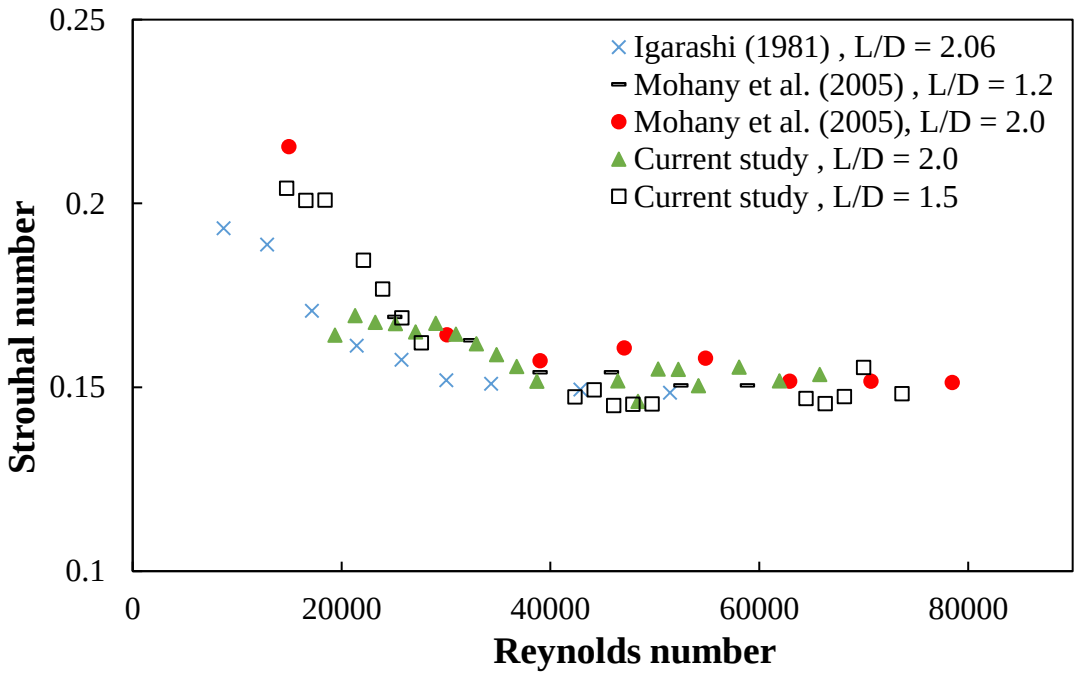

Figure 5-8 : Effect of Reynolds number on the Strouhal number of vortex shedding from two tandem cylinders for spacing ratios of L/D = 1.5 and 2.0. ×, Igarashi (1981) L/D = 2.06. ▬, Mohany et al. (2005), L/D = 1.2. ●, Mohany et al. (2005), L/D = 2. 0. ▲, Current experiments L/D =2.0, H = 305mm. □, Current experiments L/D = 1.5, H = 254mm.

5.5 Effect of Diameter and Height on Pre-Coincidence Resonance

It has been established by Mohany (2007), that the diameter of the cylinder in case of tandem configuration plays an important role in the occurrence of the pre-coincidence resonance. Moreover; Mohany and Ziada (2009) performed a parametric study to

investigate the effect of the cylinder diameter on the acoustic resonance mechanism for tandem cylinders in cross-flow. Six different cylinders with diameters ranging from *7.6 – 27.5 mm* were tested in three different spacing ratios within the interference proximity region. Mohany and Ziada found that changing the diameter of the tandem cylinders has a significant effect on the aeroacoustic response of the cylinders in terms of the pre-coincidence occurrence and intensity and coincidence resonance intensity. Large cylinder diameters were found to experience the dual-resonance phenomenon, while small diameter cylinders were found to act similar to single cylinders in terms of the single range of acoustic resonance. A minimum diameter was found to initiate the pre-coincidence resonance at every spacing ratio. As the spacing ratio is increased, the minimum required diameter to generate the pre-coincidence resonance decreased (for example at L/D = 1.5, D_{min} is *18.4 mm*, while at L/D = 2.0, D_{min} is *10. mm*). Lastly, it was also concluded that as the diameter of the cylinders increased the pre-coincidence resonance becomes more intense and occurs over a wider lock-in region.

The effect of the diameter of the cylinders and the height of the duct on the aeroacoustic response of tandem cylinders are investigated in the coming section. In order to do that; several diameters are tested in the ducts at two different spacing ratios L/D (1.5 and 2.0). First, the effect of the diameter on the pre-coincidence and coincidence resonances is analyzed then the effect of the height is analyzed.

Figure 5-9 and **Figure 5-10** show the aeroacoustic response of two tandem cylinders of diameter *15.8 mm (0.625)* in duct height *254 mm (10")* and the spacing ratio *L/D = 1.5*. Similarly, **Figure 5-10** and **Figure 5-11** shows the aeroacoustic response for the same spacing ratio and duct but for a larger diameter of *25.4 mm (1").* It is observed, as suggested

by Mohany (2007), that the diameter of the cylinders has a great effect on the intensity and occurrence of the *pre-coincidence* resonance, and the intensity of the *coincidence* resonance. The pre-coincidence intensity increases with the increase in diameter, and in some cases can reach the same order of magnitude as the coincidence resonance itself. This shows that the pre-coincidence might have the same destructive effect in terms of noise and vibration as the coincidence resonance. The onset of pre-coincidence and coincidence for all the cases was recorded at average values of U_R = 3.1 and 6.2 respectively.

The Strouhal number for the tested cases was 0.168, 0.148, 0.148 and 0.14 respectively from the smallest to the largest diameter. This agrees well with the Strouhal number reported in the literature for tandem cylinders' configuration in the same range of Reynolds number and spacing ratio, Igarashi (1981). It is interesting to note that in the case of the smallest cylinder the Strouhal number approaches 0.2, which implies that as the cylinder diameter decreases the vortex shedding starts to get back to the normal shedding process.

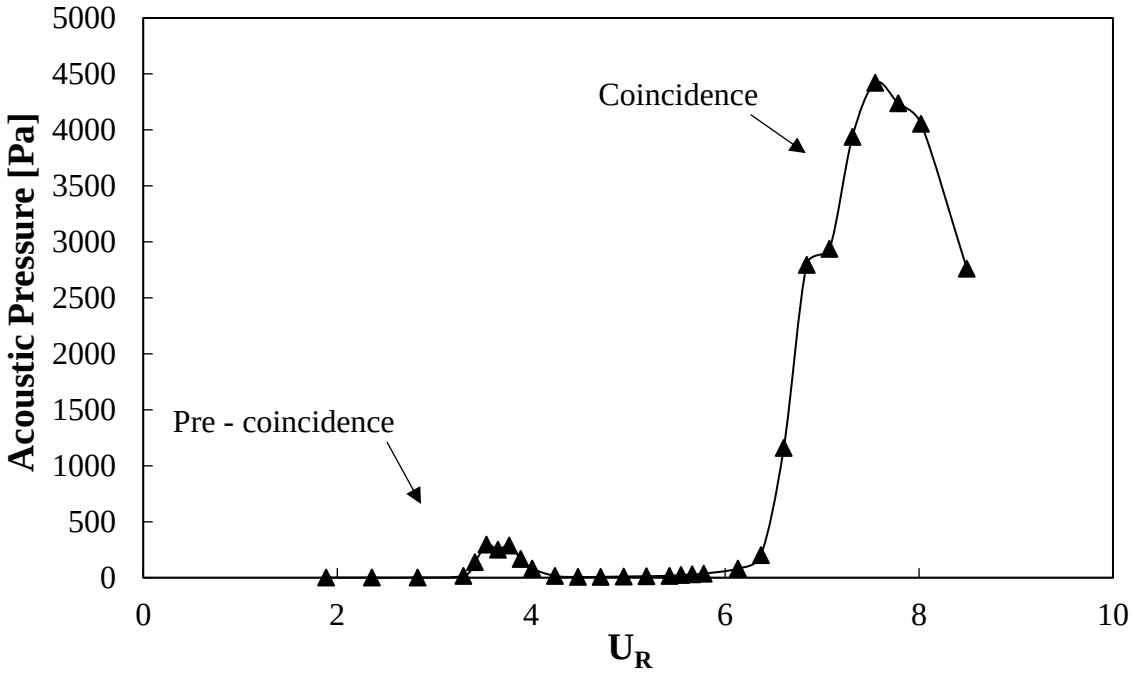

Figure 5-9 : Acoustic pressure response of two tandem cylinders D = 15.8 mm (0.625") in H = 254 mm (10") - L/D = 1.5

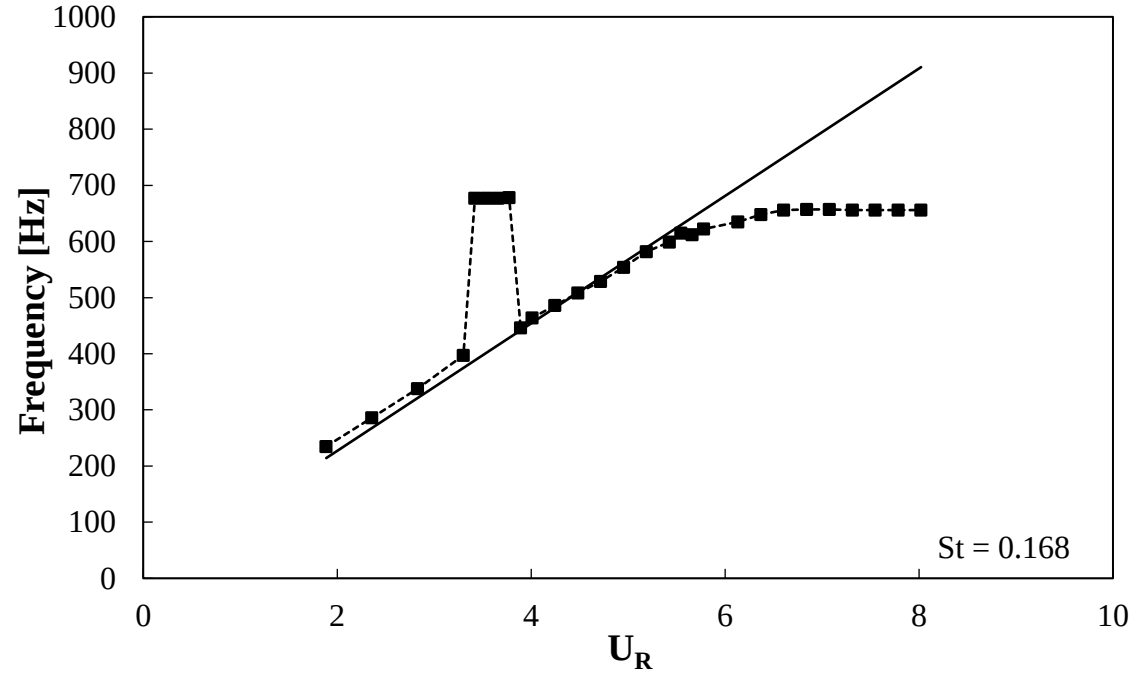

Figure 5-10: Frequency response of two tandem cylinders D = 15.8 mm (0.625") in H = 254 mm (10") - L/D = 1.5

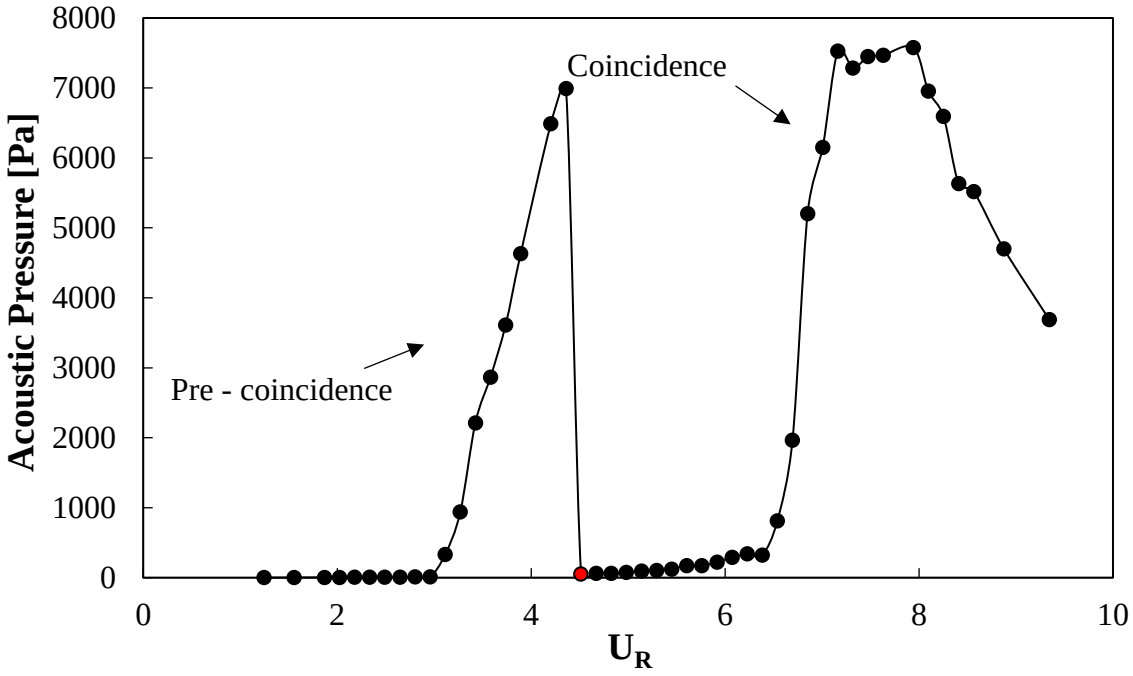

Figure 5-11 : Acoustic pressure response of two tandem cylinders D = 25.4 mm (1") in H = 254mm (10") - L/D = 1.5

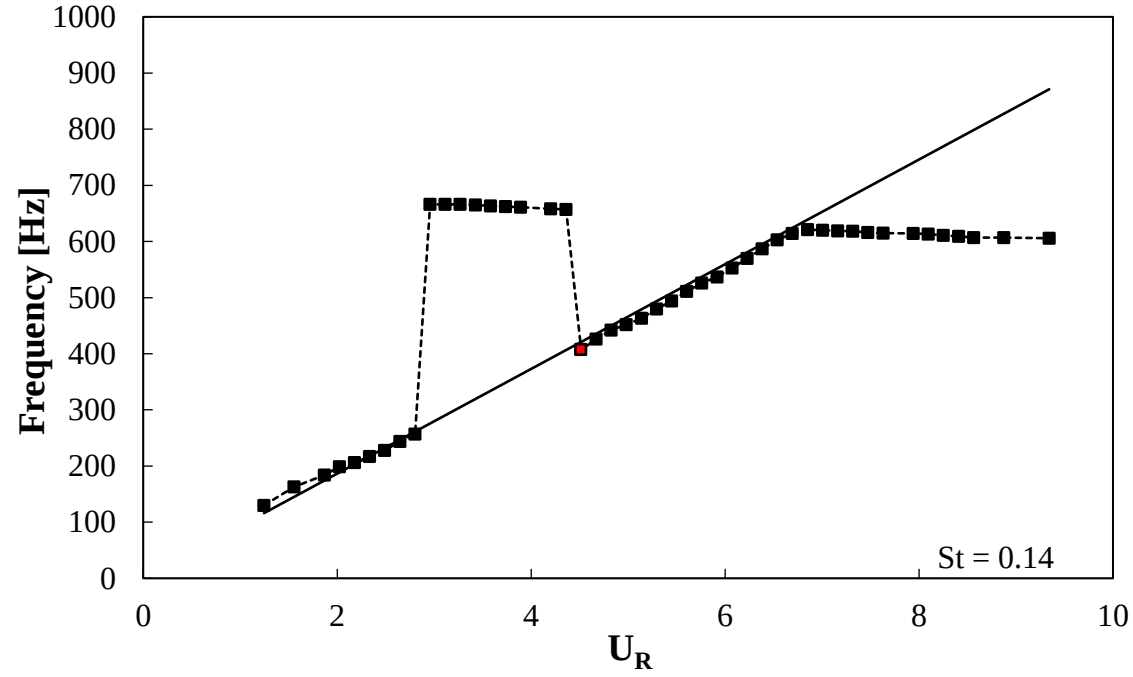

Figure 5-12 : Frequency response of two tandem cylinders D = 25.4 mm (1") in H = 254 mm (10") - L/D = 1.5

The static pressure drop across the cylinders in the above-mentioned cases is shown in **Figure 5-13**. The trend seems to be similar to the single cylinder cases, where the larger diameter has a higher pressure drop. The similarity between the single and tandem cylinders in pressure drop measurements is expected as the tandem cylinders are placed in front of each other facing the incoming flow, thus the frontal area experienced by the flow does not physically change.

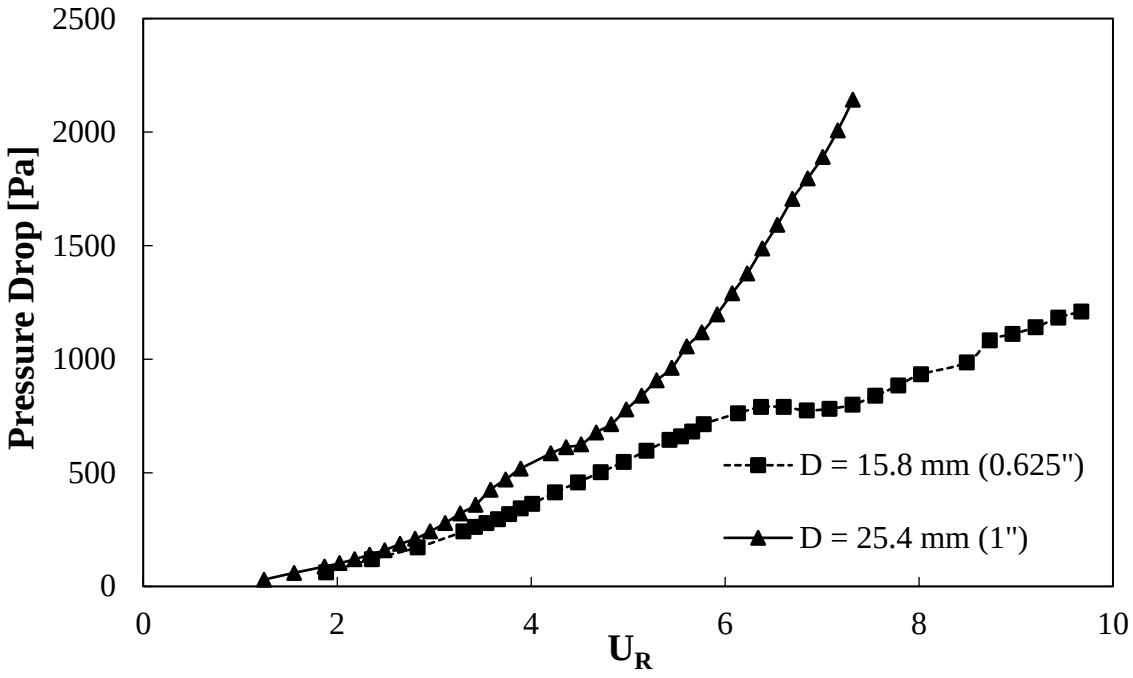

Figure 5-13 : Static Pressure Drop Across Tandem Cylinders at H = 254mm, L/D = 1.5

Similar trends were observed in all other test sections and spacing ratios; however, the difference seems to be in the intensity and occurrence of the pre-coincidence resonance with respect to the diameter of the cylinder and the height of the duct.

Figure 5-14 shows the effect of diameter for the same height but in with a larger spacing ratio of 2.0. It can be observed that the effect of the increasing the spacing ratio from 1.5 to 2 on the acoustic pressure response is not very significant. This is expected as both spacing ratios lie in the close proximity region where the wake interaction between the two cylinders is expected to behave similarly.

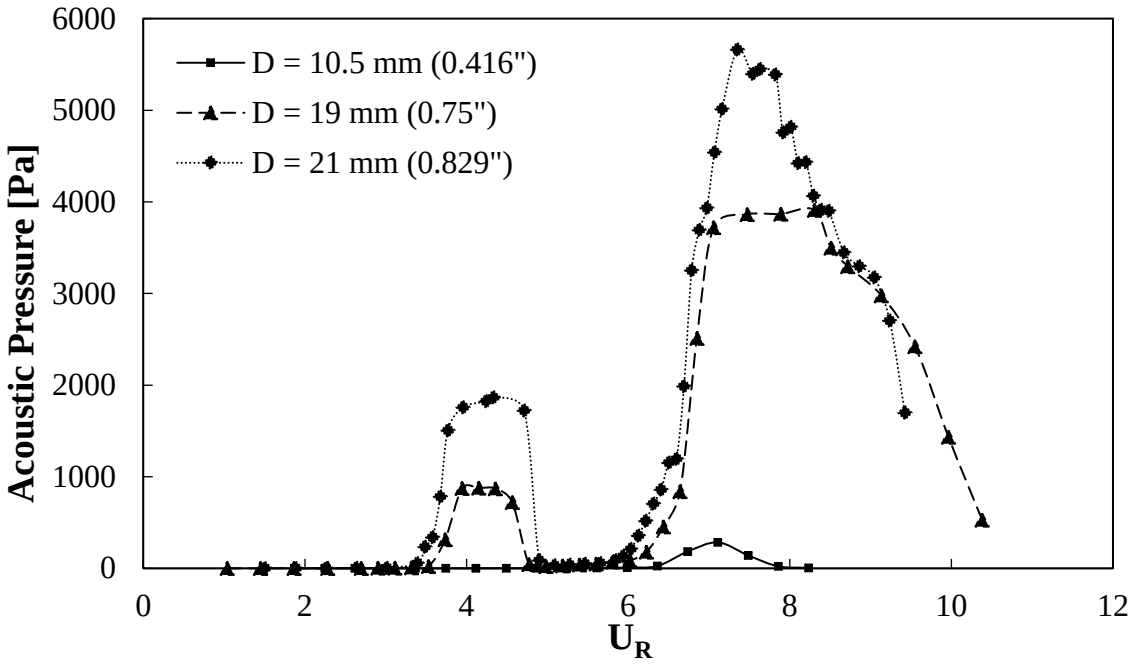

Figure 5-14 : Acoustic response of different cylinders in H = 245 mm (10") - L/D = 2.0

The effect of the duct height on the occurrence of the pre-coincidence resonance was tested for all the cases. The results showed that for the smallest duct height *305mm (8")*, all the cylinders tested did excite both the pre-coincidence and coincidence resonance. It is believed that smaller cylinders, diameter less than *8 mm (0.316")*, will not excite the pre-coincidence resonance in the same height.

At the duct height *254mm (10”)*, four diameters of *10.5 (0.416), 19.05(0.75), 21.05(0.829)* and *25.4(1) mm(inch)* were tested. The critical diameter, below which pre-coincidence occurred, was found to be *19.05mm (0.75”).* **Figure 5-15** and **Figure 5-16** shows the aeroacoustic response of the case of diameter *10.5mm (0.416”)* in duct height *254mm (10”)*. It can be seen that for this case the pre-coincidence resonance did not materialize and the cylinders acted as single cylinders with one range of resonance occurring at the reduced velocity of $U_R = 6$. The Strouhal number for this case is 0.17.

Lastly for the highest duct *305mm (12”)* four diameters of *12.7(0.5), 19.05(0.75), 25.4(1)* and *28.5(1.125) mm(inch)* were tested. The critical diameter for this height was found to be *12.7mm (0.5”).* Beyond this diameter, the pre-coincidence resonance was excited for all the cases. The aeroacoustic response of the diameter *12.7mm (0.5”)* in duct height *305mm (12”)* is shown in **Figure 5-17** and **Figure 5-18**. The coincidence resonance was excited at the reduced velocity of $U_R = 5.8$ and the Strouhal number was 0.168.

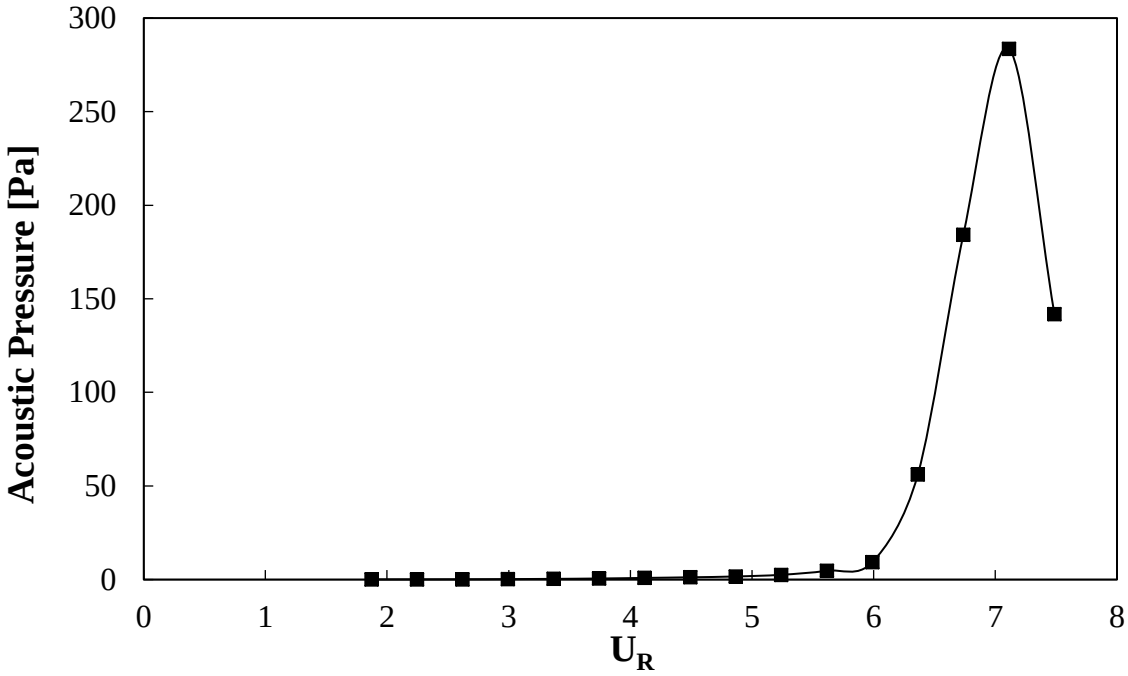

Figure 5-15 : Pressure response for D = 10.56 mm (0.416") , H = 254 mm (10"), L/D = 2.0

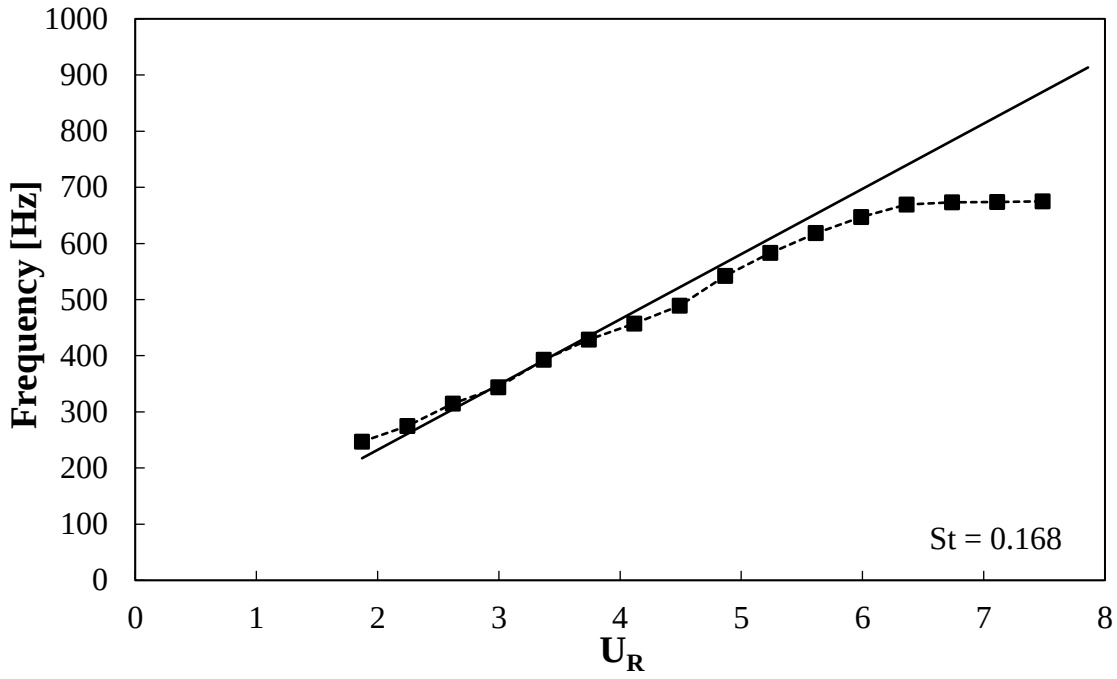

Figure 5-16 : Frequency response for D = 10.56 mm (0.416") , H = 254 mm (10"), L/D = 2.0

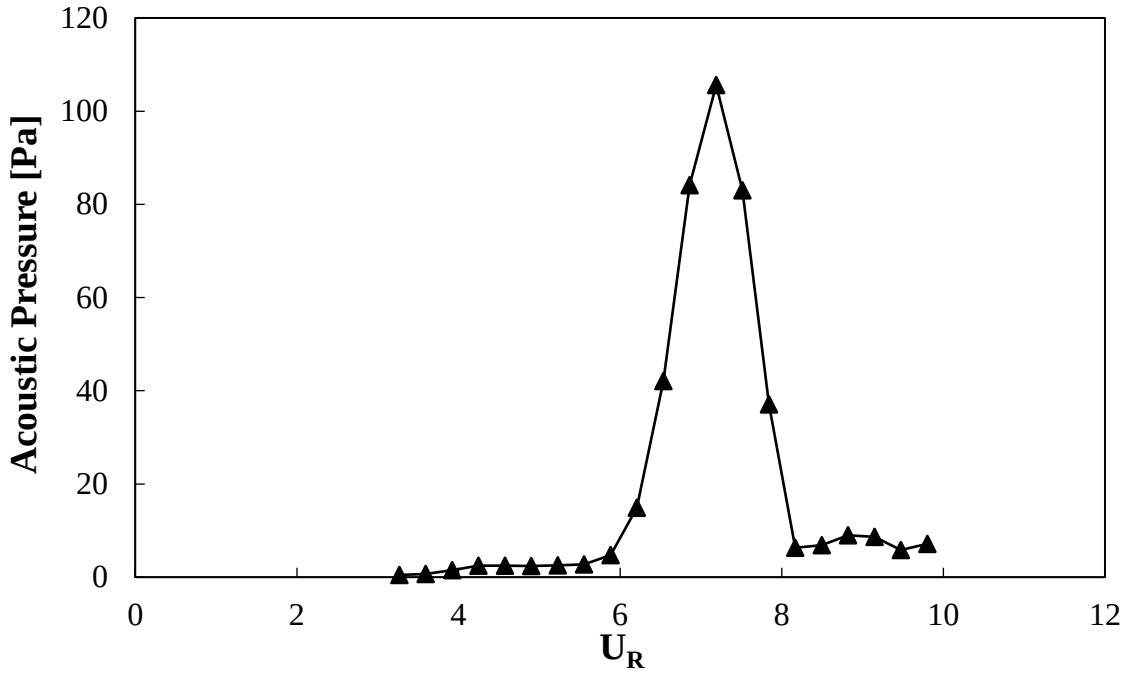

Figure 5-17 : Acoustic pressure response of two tandem cylinders D = 12.7 mm (0.5”) in H = 305mm (12") - L/D = 1.5

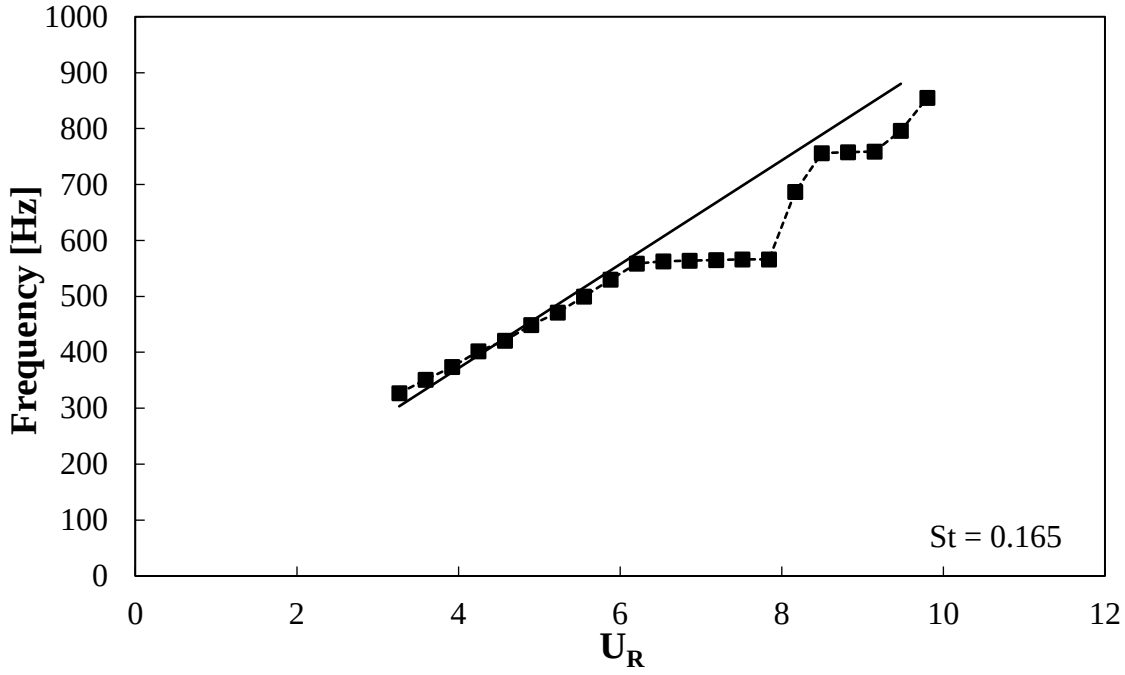

Figure 5-18 : Frequency response of two tandem cylinders D = 12.7 mm (0.5”) in H = 305mm (12") - L/D = 1.5

The effect of the height on the pre-coincidence and coincidence resonances is similar to the trend found by Mohany and Ziada (2009). It was found from the cases discussed in this section that there exists a critical diameter for each height beyond which the *pre-coincidence* resonance occurred. In fact, through analyzing all the cases of the tandem cylinders, a critical blockage ratio value (D/H) of 0.0416 was found. Any combination of diameters and duct heights above 0.416 experienced pre-coincidence resonance.

5.6 Effect of Height on Intensity of Resonance

The height of the duct plays an important role in the amplitude of the acoustic pressure at resonance. However, in the case of tandem cylinders, the trend seems to be reversed. **Figure 5-19** and **Figure 5-20** shows the aeroacoustic response of diameter *19mm (0.75")* at a spacing ratio of *L/D = 2*.0 in all three test sections. For the single cylinder cases, the higher duct produced higher acoustic pressure amplitude. But in the case of the tandem cylinders, and for all the cases tested the pre-coincidence (if occurred) and the coincidence resonance seem to occur with higher amplitude as the height of the duct is decreased.

This trend is observed regardless of the spacing ratio L/D between the cylinders. A similar trend was observed in the literature by Mohany and Ziada (2009) for tandem cylinders. Mohany and Ziada found that increasing the diameter of the tandem cylinders while keeping the duct height constant decreased the acoustic attenuation due to radiation losses, and thus made the system more prone to acoustic resonance.

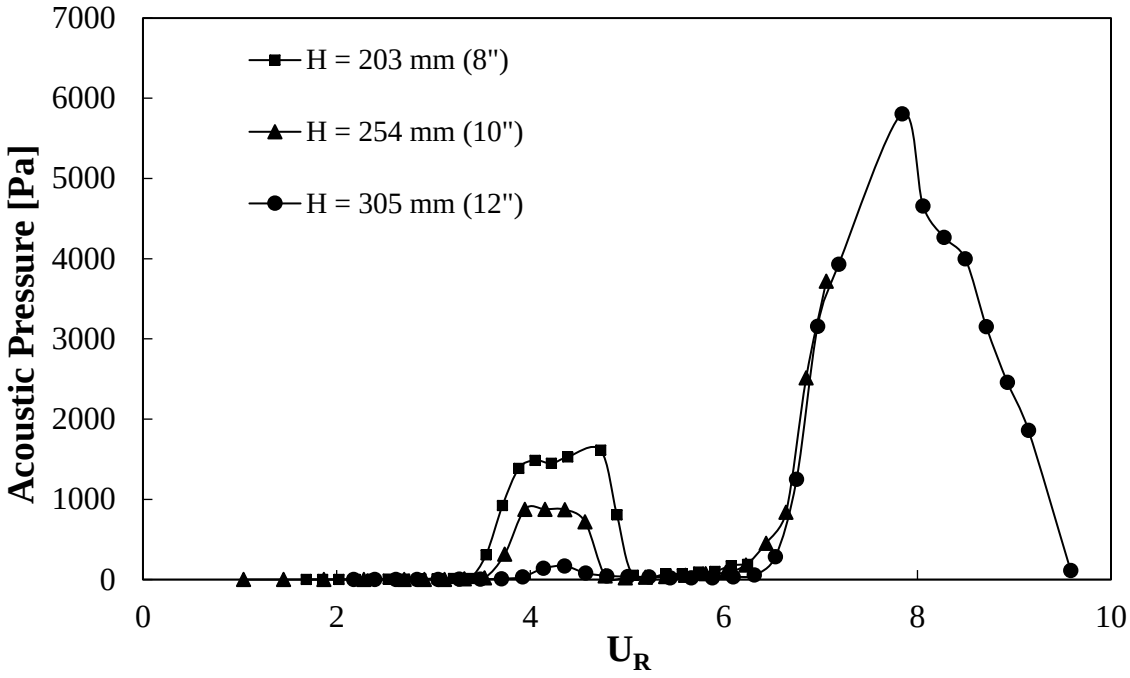

Figure 5-19 : Acoustic pressure response of diameter D = 19 mm (0.75") in different duct heights – L/D = 2.0

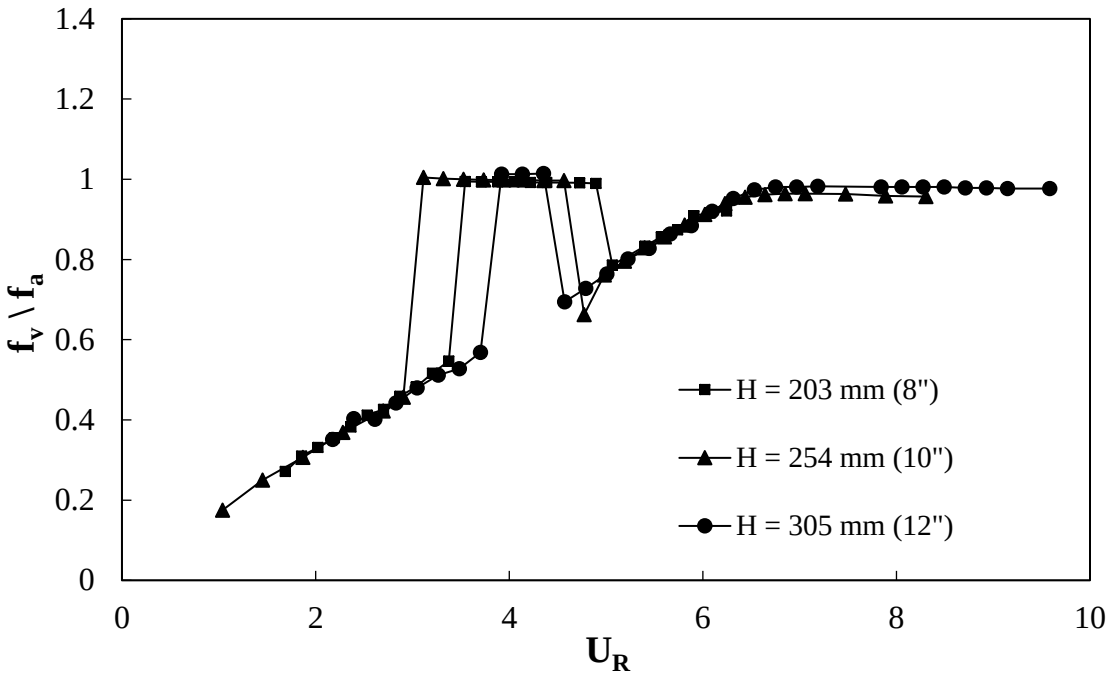

Figure 5-20 : Frequency response of diameter D = 19 mm (0.75") in different duct heights – L/D = 2.0

To see if the effect observed in the cases presented below is due to the radiation losses of the duct, an acoustic simulation similar to the one performed by Mohany and Ziada (2009) was done using ABAQUS software. Two cylinders with constant diameters of *19 mm (0.75")* were simulated in two ducts *203 mm (8")* and *305 mm (12").* The acoustic modes of the duct at resonance oscillate in a time-variant simple harmonic motion, therefore the acoustic pressure fields at the resonating modes can be expressed as, Kinsler (2000).

$$p = \emptyset \,.\, \exp i(2\pi f)t \qquad \textbf{(5.1)}$$

Where $\emptyset$ is a function defined by the Helmholtz equation

$$\nabla^2\emptyset + k^2\emptyset = 0 \qquad \textbf{(5.2)}$$

The pressure boundaries at the inlet and outlet of the duct were set to zero acoustic pressure, and the spacing ratio used was L/D = 1.5. The length of the simulated duct was long enough (l = 20D) downstream and upstream the cylinders to minimize boundary effects. The results of the numerical simulation can be seen in **Figure 5-21**.

The simulation results show a similar trend to that observed by Mohany and Ziada (2009), where decreasing the height of the duct makes the acoustic energy more trapped around the cylinders. This results in higher amplitudes of acoustic pressure at the pre-coincidence and coincidence resonance. In other words, for tandem cylinders' cases examined it was found that increasing the duct height (H) while maintaining the diameter (D) of the enclosed cylinders is equivalent in response to changing the cylinder's diameters while maintaining the duct height constant.

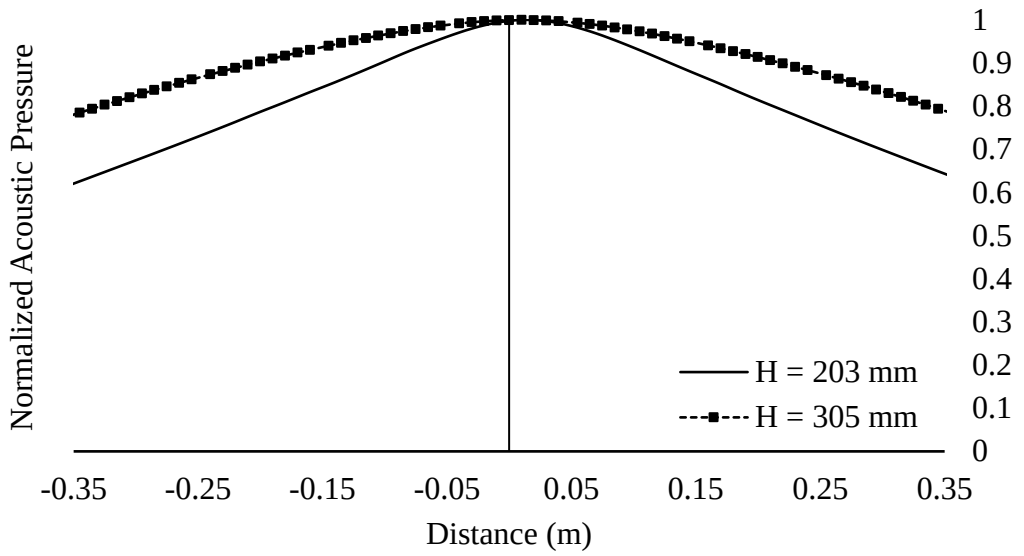

Figure 5-21 : Normalized acoustic pressure distribution for the first mode along the top wall of the duct , tandem cylinders of diameter D = 19 mm (0.75") , H = 203 mm (8") and 305 mm (12") - L/D = 1.5

The difference in trend between the tandem cylinders and the single cylinder cases for variable duct heights is complex to analyze, and the stiffness and damping analogies adapted for single cylinder cases could not be used to describe the tandem cylinders' responses. That is because the mechanism by which acoustic resonance occurs in tandem cylinders is different in nature compared to the mechanism of resonance for single cylinder cases, especially for pre-coincidence resonance. Moreover, the complexity of the interaction between the cylinders' wakes in tandem configuration, makes it hard to relate the damping and the stiffness of the system directly to the acoustic pressure amplitudes at resonance. Other mechanisms involved could be overcoming the effect of damping and stiffness.

5.7 Effect of Blockage Ratio (D/H)

For the case of a single cylinder in cross-flow, cases have been discussed in which the blockage ratio (D/H) and the velocity of coincidence were equal but the amplitude of pressure and the frequency of excitation were substantially different. For tandem cylinders, this coincidence also occurs. **Figure 5-22** shows the pressure response for a blockage ratio of D/H = 0.0937, for two tandem cylinders of diameters *19.05 (0.75)* and *28.5 (1.125) mm(inch)* in test sections of heights *203 (8)* and *305 (12) mm(inch)* respectively at a spacing ratio of L/D = 1.5. Similar to the cases of the single cylinders, the pre-coincidence resonance, and the coincidence resonance occurred for the two diameters at almost the same velocities. For the diameter of *19.05mm (0.75")* the pre-coincidence and the coincidence resonances occurred at the velocities of *59 m/s* (U_R = 3.7) and *127 m/s* (U_R =7.9) respectively. As for the larger diameter of *28.5 (1.125),* the pre-coincidence and the coincidence resonances occurred at *60 m/s* (U_R = 3.7) and *128 m/s* (U_R = 7.9) respectively.

Additional coincidence of velocities was obtained at other blockage ratios of D/H = 0.0416 and 0.0625 for this spacing ratio. A similar trend was observed for all the other cases as follows: - for the blockage ratio of D/H = 0.0416 the pre-coincidence and the coincidence resonance occurred at average velocities of *53.5 m/s* and *84 m/s* respectively. As for the case of blockage ratio D/H = 0.0625, the pre-coincidence and coincidence resonances occurred at an average velocity of *41 m/s* and *88 m/s*.

It is observed that the diameter in the larger test section produced higher acoustic resonance for the pre-coincidence. The trend seems to be reversed for the coincidence resonance, where the diameter in the smaller duct produced higher pressure amplitude. The acoustic pressure amplitude at the pre-coincidence resonance for the case of blockage ratio of 0.093

shows a value of *2190 Pa* and *250 Pa* for the diameter *28.5mm (1.125") and 19.05mm (0.75")* respectively. For the coincidence resonance, however, the smaller diameter shows *9255 Pa* while the larger diameter *5343 Pa.* In the other similar D/H cases, no specific trend could be reported in terms of the pressure amplitudes at the pre-coincidence and coincidence resonance. **Figure 5-23** and **Figure 5-24** shows the frequency response and the static pressure recorded for the case of D/H = 0.093. In terms of the pressure drop the highest duct always reported less static pressure drop regardless of the diameter of the cylinders, the blockage ratio or the spacing ratio L/D. For the larger spacing ratio of L/D = 2.0, a similar trend is observed for the velocity ranges of pre-coincidence and coincidence resonance. That is, for the same blockage ratio, the pre-coincidence, and the coincidence resonances occurred at the same velocity. Moreover, the static pressure drop across the cylinders was always higher in the smaller ducts. No specific trend was could be reported for the acoustic pressure amplitudes. The results obtained in this section suggests that the combined parameter of the diameter and the height, (i.e. the blockage ratio) could be a very important parameter in the prediction of the acoustic resonance in tube bundles.

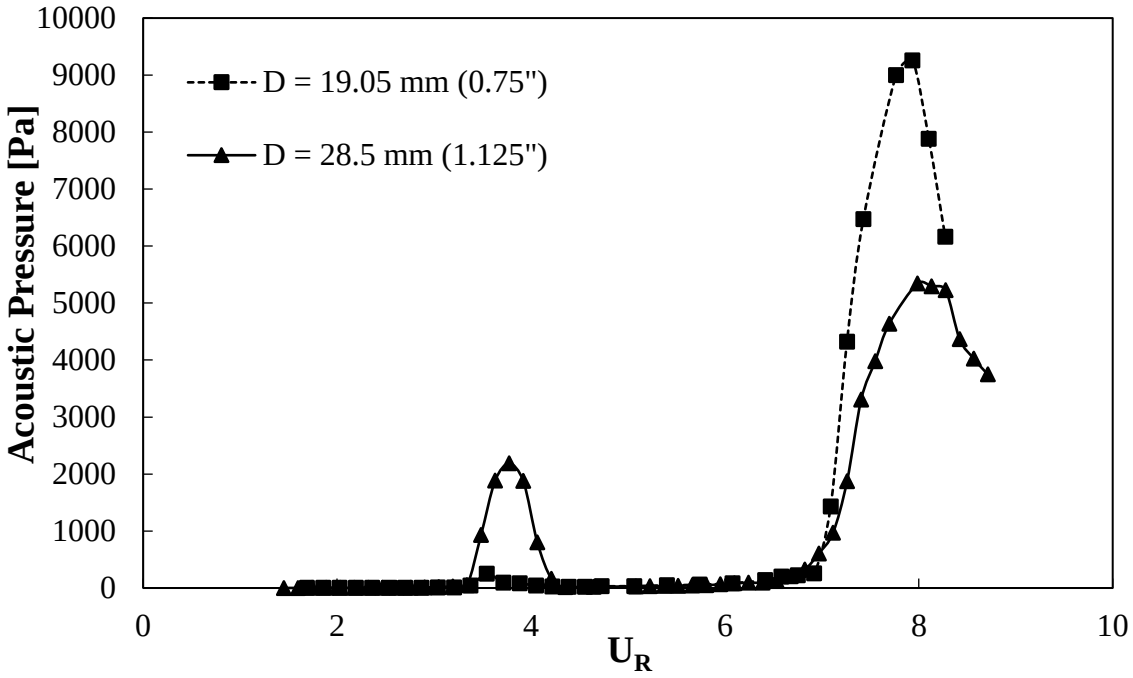

Figure 5-22 : Acoustic response for D/H = 0.093 , L/D = 1.5, ▲, H = 305 mm (12"), ■, H = 203 mm (8")

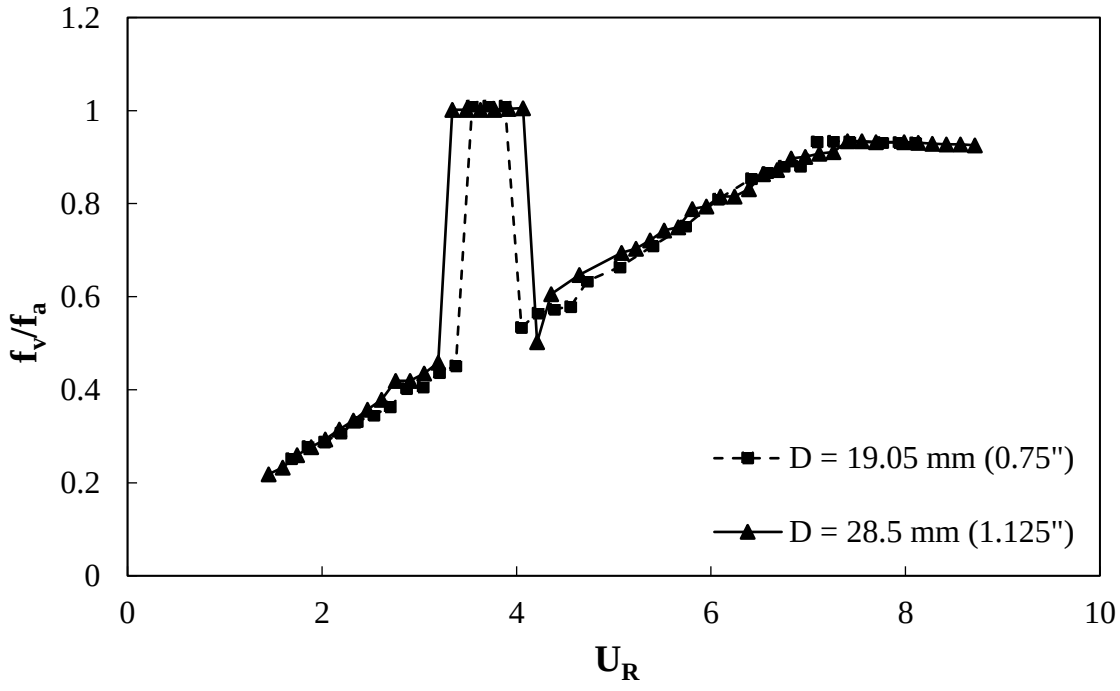

Figure 5-23 : Frequency response for D/H = 0.093 , L/D = 1.5, ▲, H = 305 mm (12"), ■, H = 203 mm (8")

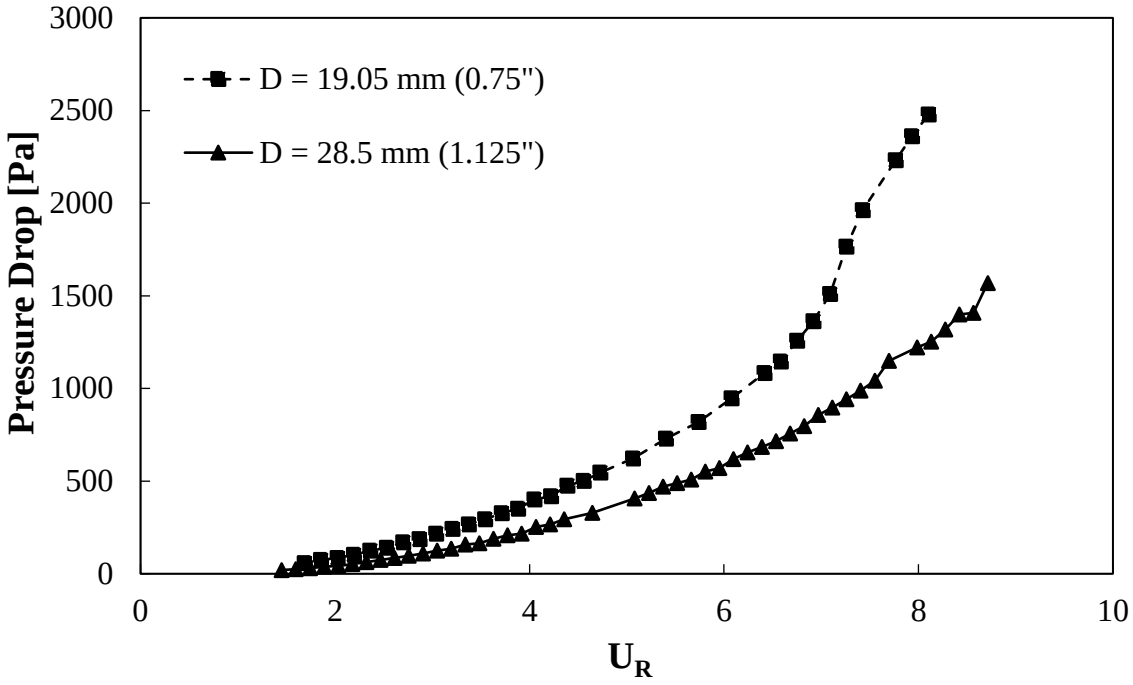

Figure 5-24 : Static pressure drop across the cylinders, for D/H = 0.093 , L/D = 1.5, ▲, H = 305 mm (12”), ■, H = 203 mm (8”)

5.8 Comparison with the Literature

One of the proposed criterion in literature to predict the acoustic resonance occurrence in in-line tube bundles is that proposed by Grotz and Arnold in (1956). The criterion is expressed by **Equation 2.13**. The application of the prediction criterion to the case of the tandem cylinders should be valid since the tandem cylinders are known to exhibit similar characteristics as in-line tube bundles. However, the Grotz and Arnold criterion seem to fail in predicting the resonance of the two cases in which the pre-coincidence did not occur. Namely for the case of diameter *12.7mm (0.5”)* in the *305mm (12”)* height and the diameter of *10.56mm (0.416”)* in *254mm (10”)*. For those cases at both spacing ratios of L/D = 1.5 and 2.0 the criterion predicts that resonance should occur (i.e. $\Gamma = 48 < 62$ or 80) however, in reality, resonance did not. All the damping criteria

found in literature does not distinguish between the pre-coincidence and the coincidence resonances, which is reasonable because the dual resonance phenomenon was just recently discovered in 2005, Mohany and Ziada (2005), while the last developed criterion was that developed by Ziada et al. (1989). Moreover; besides failing in almost 30-40% of the time to predict the actual occurrence of resonance, none of the criteria provides an estimation of the acoustic pressure amplitude at resonance. The only proposed criterion that allegedly provides such estimation, is the criterion developed by Blevins and Bressler (1993). The empirical formula suggested by Blevins and Bressler was previously discussed for single cylinder cases at different duct location. The formula failed to predict the amplitude of acoustic pressure at resonance for nearly all the cases, although the trend was conservatively predicted (see **Figure 4-18**, **Figure 4-19** and **Figure 4-36**).

For the case of row(s) of cylinders, Blevins and Bressler (1993) provided similar empirical formula to predict the maximum acoustic pressure ($P_{rms,\ max}$) at resonance. The formula is expressed by **Equation 2.14.**

Where dP is the static pressure drop across the cylinders in the bank. For the row of cylinders, Blevins and Bressler suggest the static pressure drop across the tubes is co-related with a different **Equation 5.3** as follows: -

$$\Delta_{p,row} = \ 0.45\ (0.5\ \rho U^2) \qquad \textbf{(5.3)}$$

Lastly, in terms of prediction, the only criterion that was suggested by Blevins and Bressler was that, if the spacing ratio L/D between the cylinders is less than 1.4 (closely packed cylinders), the resonance will not materialize. Although this hypothesis was criticized by Ziada et al., who reported cases of closely packed cylinders experiencing acoustic

resonance. For the current cases of tandem cylinders both spacing ratios (L/D = 1.5 and 2), where above the criterion set by Blevins and Bressler, thus it is supposed that all the cases will excite the resonance. The criterion also does not distinguish between pre-coincidence and coincidence resonances. In terms of maximum acoustic pressure prediction, **Figure 5-25** shows a comparison between the prediction formula suggested by Blevins and the current experimental data for spacing ratio L/D = 1.5 at all heights. It can be observed that the empirical criterion does not predict most of the acoustic pressure amplitudes, nor did it capture a specific trend. Similar poor agreement was observed for the larger spacing ratio L/D = 2.0. The points that were predicted by the equation (i.e. the black line), are all points of coincidence resonance. The coincidence resonance occurs at the normal frequency coincidence thus its prediction is easier than the pre-coincidence resonance. The equation does not predict any of the pre-coincidence resonance cases.

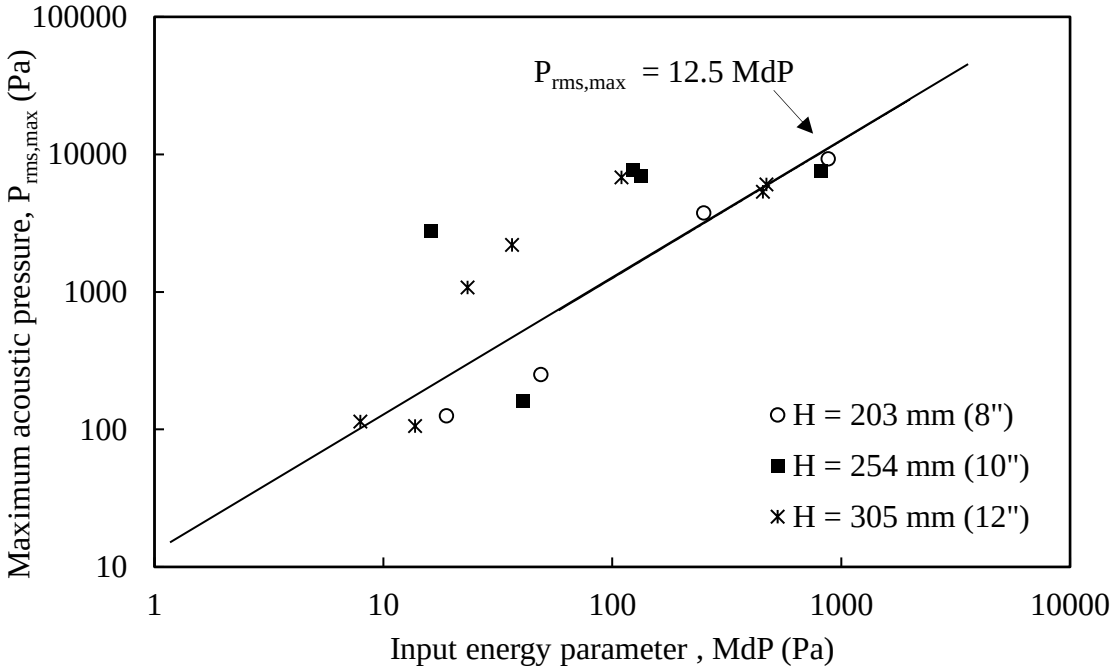

Figure 5-25 : Comparison of tandem cylinder cases at L/D = 1.5 with the empirical formula suggested by Blevins and Bressler in terms of input energy parameter.

5.9 Conclusion

In this chapter, the effect of the cylinder diameter and the duct height on the flow-sound interaction mechanism of two tandem cylinders in cross-flow was experimentally investigated. Seven cylinders within the range of *10.56 – 28.5 mm (0.416 – 1.125")* are tested in three different duct heights *203, 254 and 305 mm (8, 10, and 12").* Two sets of experiments are conducted at two different spacing ratios (L/D) below the critical spacing of 3. The first spacing ratio is in the *alternate re-attachment* region of the shear layers (L/D = 1.5), and the second spacing ratio is in the *quasi-steady re-attachment* region of separated shear layers (L/D = 2). The outcome of this chapter shall help in developing better and more reliable criteria to predict acoustic resonance occurrence in full-sized heat exchangers.

It was shown that in the case of the tandem cylinders, a dual resonance phenomenon may occur over two distinct velocity ranges. The first resonance "Pre-coincidence" is triggered by the instability of the shear layers between the cylinders, while the second resonance "coincidence" is triggered by the normal Karman vortex shedding downstream the cylinders. The pre-coincidence resonance is very similar, in mechanism and magnitude to the in-line tube bundles resonance.

The experimental results showed that, as suggested by Mohany (2007), the diameter of the cylinders (not only the spacing ratio) in the case of tandem configurations is a key parameter in determining whether or not the pre-coincidence resonance will occur even with the changing of the height. Changing the height of the duct in case of the tandem cylinders showed a similar trend as the changing the diameter. It was found that changing the height while keeping the enclosed cylinder diameter constant is equivalent in response

to changing the diameter while keeping the duct height constant. For each of the duct, heights tested, a critical diameter was identified beyond which the pre-coincidence resonance occurred. As the duct height is increased the minimum diameter required to initiate the pre-coincidence resonance is decreased. In fact, a critical blockage ratio (D/H) = 0.416 was identified, beyond which pre-coincidence resonance occurred. This suggests that the height of the duct as well plays a very important role in the occurrence of the pre-coincidence resonance, and should be included in any damping criteria for tube bundles of heat-exchangers.

Moreover, for the cases in which the blockage ratio (D/H) is equal, it was found that the pre-coincidence and coincidence resonances occurred at almost the same velocities for both spacing ratios. However, no specific trend for the amplitudes of resonance could be established. This suggests that the blockage ratio could be an important parameter that should be included in the prediction criteria for acoustic resonance in tube bundles of heat exchangers.

Lastly, comparing the current experimental data with the damping (prediction) criteria found in literature showed poor agreement. None of the damping criteria proposed is able to distinguish between the types of resonances (pre-coincidence or coincidence), and most of the criteria fail to predict the non-occurrence of the pre-coincidence resonance. For example, the Grotz and Arnold criterion imply that the diameter of 12.7mm (0.5”) in the height of 305mm (12”) should experience resonance, where in fact it did not experience pre-coincidence resonance when tested. Moreover, in terms of prediction of the maximum acoustic pressure amplitude, the only criterion found in literature to predict the amplitude is suggested by Blevins and Bressler (1993), however upon comparing the criteria against

the current experimental data, poor agreement was observed, and the criterion failed to predict pre-coincidence resonance, as well as the amplitude of coincidence resonances.

The analyses performed in this chapter suggests that the inclusion of the duct height as well as the cylinder diameter as parameter in the damping criteria could be promising, and could subsequently lead to producing a better and more reliable damping criteria.

Chapter 6

6 Conclusions & Recommendations

6.1 Conclusions

In this study, a parametric experimental investigation has been performed on a number of test sections with variable duct heights. The main objective of the research is to identify the effect of multiple critical parameters on the flow-sound interaction mechanism of circular cylinders in cross-flow under self-excited acoustic resonance conditions. In particular, the effects of the diameter of the cylinders, the location of the cylinder in the duct, and the duct height were analyzed for single, tandem and side-by-side configurations. The research presented is motivated mainly by the gap found in literature in predicting the flow-excited acoustic resonance in tube bundles of heat exchangers and in simple cases of single cylinders.

For the single cylinder cases, changing the diameter of the cylinder at constant duct height was found to delay the onset of acoustic resonance to higher velocities and cause higher pressure amplitudes at resonance. Changing the location of the cylinder within the duct was found to excite different acoustic modes depending on the relative location of the cylinder with respect to the acoustic pressure and acoustic particle velocity cross-mode distributions. Shifting the cylinder to a quarter of the duct height excited the second acoustic cross-mode of the duct, because the cylinder at this location is placed at the pressure node of the second acoustic cross-mode. More than one mode could be excited if the cylinder is not placed at the location of acoustic particle velocity node of a particular

mode. If more than one mode is excited, the dominant mode was found to always experience the highest pressure amplitudes. It was found that the acoustic particle velocity is the main triggering agent for the acoustic resonance and the acoustic pressure distribution was found to be the scaling agent of the amplitude.

For the case of side-by-side cylinders at very large spacing ratios it was found that the cylinders behave exactly as single cylinders in terms of the vortex shedding (i.e. Strouhal number similar to single cylinders), due to the non-interacting wakes. However, during resonance, the vortex shedding process is synchronized and enhanced between both cylinders and the produced acoustic pressure amplitude is almost exactly doubled. Tests performed for tandem arrangements showed that as suggested by Mohany (2007), the diameter of the cylinders (not only the spacing ratio) in the case of tandem configurations is a key parameter in determining whether or not the pre-coincidence resonance will occur. For different coincidence cases in which the blockage ratio (D/H) is equal, it was found that the pre-coincidence and coincidence resonances occurred at almost the same velocities.

Changing the duct height was found to have a significant impact on the acoustic pressure amplitude at resonance. The duct height dictates the acoustic natural frequency which is directly related to the acoustic damping and stiffness of the duct. The higher the duct height is the lower acoustic damping and stiffness capabilities it will have. If the stiffness of the system is low, it is prone to get easily excited even with the lowest energy. If the damping of the system is low, it responds with a higher acoustic pressure amplitude compared to a system with higher damping, under similar excitation forces. The system with lower damping capabilities also dissipates acoustic energy slower. Thus when placing the same

diameter in different duct heights the tallest duct will experience resonance first and with higher amplitudes due to the weak stiffness of the system. Moreover, if the resonance occurs at the same velocity and blockage ratio, the tallest duct height will produce the greatest acoustic pressure amplitudes due to the lower acoustic damping of the system. The effect of the height was pronounced in all the tested configurations, which implies its importance. Comparing experimental data to the literature showed that the height of the duct (and the damping) could be a significant parameter that has been over-looked in the past. The damping capacity of the duct should be included in the prediction (damping) criteria of acoustic resonance in tube bundles.

6.2 Future Work and Recommendations

The work presented in this thesis is a result of extensive experimental and parametric work performed. The outcome of the research shall help enrich the fundamental understanding of the flow-sound interaction mechanism that occurs between circular cylinders for simple configurations. The following are recommended future work that were not addressed in this thesis but, to the authors best of knowledge, could help further in the advancement in this field.

1) The effect of the width of the test section should be analyzed in the same manner, to know if the width has the same effect as the height in terms of the aeroacoustic response of simple geometries.

2) A reliable, experimental, method should be performed to capture the damping and stiffness capabilities of different ducts with and without mean flow inside the duct. Moreover, with and without bodies enclosed.

3) Particle image velocimetry (PIV) technique and/or validated fluid-acoustic coupled simulations should be performed on side-by-side arrangements to further investigate the vortex shedding interactions before, during and after resonance.

4) Fluctuating forces acting on the cylinders (i.e. fluctuating lift) should be measured for single, tandem and side-by-side configurations at different heights, to see the effect of the height on the fluctuating forces.

5) More experimental work should be done on tube-bundles of heat exchangers for full sized models, at different duct geometries (height, width) and under different room temperatures.

6) Further analyses should be done regarding the acoustic/mechanical analogy presented in this thesis.

References

[1] M. M. Alam and H. Sakamoto, "Investigation of Strouhal frequencies of two staggered bluff bodies and detection of multistable flow by wavelets," *Journal of Fluids and Structures*, vol. 20, no. 3, pp. 425–449, Apr. 2005.

[2] N. Arafa and A. Mohany, "Flow-Excited Acoustic Resonance of Single Finned Cylinder in Cross-Flow," 2014, p. V004T04A069.

[3] N. Arafa and A. Mohany, "Flow-Excited Acoustic Resonance of Isolated Cylinders in Cross-Flow," *Journal of Pressure Vessel Technology*, vol. 138, no. 1, p. 11302, Aug. 2015.

[4] N. Arafa and A. Mohany, "Aeroacoustic Response of a Single Cylinder with Straight Circular Fins in Cross-Flow," *Journal of Pressure Vessel Technology*, vol. 137, no. 5, p. 51301, Oct. 2015.

[5] M. Arie, M. Kiya, M. Moriya, and H. Mori, "Pressure Fluctuations on the Surface of Two Circular Cylinders in Tandem Arrangement," *Journal of Fluids Engineering*, vol. 105, no. 2, p. 161, 1983.

[6] G. Baylac and J. P. Gregoire, "Acoustic phenomena in a steam generating unit," *Journal of Sound and Vibration*, vol. 42, no. 1, pp. 31–48, Sep. 1975.

[7] W. K. Blake, *Mechanics of flow-induced sound and vibration Volume I, Volume I,* Orlando, Fla.: Academic Press, 1986.

[8] R. D. Blevins and M. M. Bressler, "Acoustic Resonance in Heat Exchanger Tube Bundles—Part II: Prediction and Suppression of Resonance," *Journal of Pressure Vessel Technology*, vol. 109, no. 3, p. 282, 1987.

[9] R. D. Blevins and M. M. Bressler, "Experiments on Acoustic Resonance in Heat Exchanger Tube Bundles," *Journal of Sound and Vibration*, vol. 164, no. 3, pp. 503–533, Jul. 1993.

[10] R. D. Blevins, *Formulas for dynamics, acoustics, and vibration*. Chichester, West Sussex ; Hoboken, NY: John Wiley and Sons, Inc, 2015.

[11] Y. N. Chen and W. C. Young, "The Orbital Movement and the Damping of the Fluidelastic Vibration of Tube Banks Due to Vortex Formation: Part 3—Damping Capability of the Tube Bank Against Vortex-Excited Sonic Vibration in the Fluid Column," *Journal of Engineering for Industry*, vol. 96, no. 3, p. 1072, 1974.

[12] Y. N. Chen, “Flow-Induced Vibration and Noise in Tube-Bank Heat Exchangers Due to von Karman Streets,” *Journal of Engineering for Industry*, vol. 90, no. 1, p. 134, 1968.

[13] N. Curle, “The Influence of Solid Boundaries upon Aerodynamic Sound,” *Proceedings of the Royal Society A: Mathematical, Physical and Engineering Sciences*, vol. 231, no. 1187, pp. 505–514, Sep. 1955.

[14] P. O. A. L. Davies, “Practical flow duct acoustics,” *Journal of Sound and Vibration*, vol. 124, no. 1, pp. 91–115, Jul. 1988.

[15] M. Eid and S. Ziada, “Vortex shedding and acoustic resonance of single and tandem finned cylinders,” *Journal of Fluids and Structures*, vol. 27, no. 7, pp. 1035–1048, Oct. 2011.

[16] F. L. Eisinger, J. T. Francis, and R. E. Sullivan, “Prediction of Acoustic Vibration in Steam Generator and Heat Exchanger Tube Banks,” *Journal of Pressure Vessel Technology*, vol. 118, no. 2, p. 221, 1996.

[17] E. J. English, “A measurement-based study of the acoustics of pipe systems with flow,” Thesis (Doctoral), University of Southampton, Institute of Sound and Vibration Research, 2010.

[18] B. Etkin, “Acoustic Radiation from a Stationary Cylinder in a Fluid Stream (Aeolian Tones),” *The Journal of the Acoustical Society of America*, vol. 29, no. 1, p. 30, 1957.

[19] P. A. Feenstra, D. S. Weaver, and F. L. Eisinger, “A Study of Acoustic Resonance in a Staggered Tube Array,” *Journal of Pressure Vessel Technology*, vol. 128, no. 4, p. 533, 2006.

[20] J. A. Fitzpatrick and I. S. Donaldson, “A Preliminary Study of Flow and Acoustic Phenomena in Tube Banks,” *Journal of Fluids Engineering*, vol. 99, no. 4, p. 681, 1977.

[21] J. A. Fitzpatrick, “Acoustic resonances in in-line tube banks,” *Journal of Sound and Vibration*, vol. 85, no. 3, pp. 435–437, Dec. 1982.

[22] J. A. Fitzpatrick, “The prediction of flow-induced noise in heat exchanger tube arrays,” *Journal of Sound and Vibration*, vol. 99, no. 3, pp. 425–435, Apr. 1985.

[23] J. H. Gerrard, “Measurements of the Sound from Circular Cylinders in an Air Stream,” *Proceedings of the Physical Society. Section B*, vol. 68, no. 7, pp. 453–461, Jul. 1955.

[24] J. Golliard, S. Belfroid, O. Vijlbrief, and K. Lunde, “Direct Measurements of Acoustic Damping and Sound Amplification in Corrugated Pipes with Flow,” 2015, p. V004T04A037.

[25] B. J. Grotz and F. R. Arnold, “Flow-induced vibrations in heat exchangers,” Stanford University, Department of Mechanical Engineering, Technical Report, 1956.

[26] R. Hanson, A. Mohany and S. Ziada, "Flow-excited acoustic resonance of two side-by-side cylinders in cross-flow", *Journal of Fluids and Structures*, vol. 25, no. 1, pp. 80-94, 2009.

[27] M. Hiwada, I. Mabuchi, and H. Yanagihara, “Fluid Flow and Heat Transfer around Two Circular Cylinders,” *Bulletin of JSME*, vol. 25, no. 209, pp. 1737–1745, 1982.

[28] M. S. Howe, “Contributions to the theory of aerodynamic sound, with application to excess jet noise and the theory of the flute,” *Journal of Fluid Mechanics*, vol. 71, no. 4, p. 625, Oct. 1975.

[29] M. S. Howe, “The dissipation of sound at an edge,” *Journal of Sound and Vibration*, vol. 70, no. 3, pp. 407–411, Jun. 1980.

[30] M. S. Howe, *Theory of vortex sound*. New York: Cambridge University Press, 2003.

[31] T. Igarashi, “Characteristics of the Flow around Two Circular Cylinders Arranged in Tandem: 1st Report,” *Bulletin of JSME*, vol. 24, no. 188, pp. 323–331, 1981.

[32] T. Igarashi, “Characteristics of a Flow around Two Circular Cylinders of Different Diameters Arranged in Tandem,” *Bulletin of JSME*, vol. 25, no. 201, pp. 349–357, 1982.

[33] U. Ingard, “Sound attenuation in turbulent pipe flow,” *The Journal of the Acoustical Society of America*, vol. 55, no. 3, p. 535, 1974.

[34] L. E. Kinsler, Ed., *Fundamentals of acoustics*, 4th ed. New York: Wiley, 2000.

[35] L. S. G. Kovasznay, “Hot-Wire Investigation of the Wake behind Cylinders at Low Reynolds Numbers,” *Proceedings of the Royal Society A: Mathematical, Physical and Engineering Sciences*, vol. 198, no. 1053, pp. 174–190, Aug. 1949.

[36] K. M. Lam, P. T. Y. Wong, and N. W. M. Ko, “Interaction of flows behind two circular cylinders of different diameters in side-by-side arrangement,” *Experimental Thermal and Fluid Science*, vol. 7, no. 3, pp. 189–201, Oct. 1993.

[37] J. H. Lienhard, “Synopsis of lift, drag, and vortex frequency data for rigid circular cylinders,” Washington State University, College of Engineering, Research Division, 1966.

[38] M. J. Lighthill, “On Sound Generated Aerodynamically. I. General Theory,” *Proceedings of the Royal Society A: Mathematical, Physical and Engineering Sciences*, vol. 211, no. 1107, pp. 564–587, Mar. 1952.

[39] M. J. Lighthill, “On Sound Generated Aerodynamically. II. Turbulence as a Source of Sound,” *Proceedings of the Royal Society A: Mathematical, Physical and Engineering Sciences*, vol. 222, no. 1148, pp. 1–32, Feb. 1954.

[40] M. Mahbub Alam, M. Moriya, and H. Sakamoto, “Aerodynamic characteristics of two side-by-side circular cylinders and application of wavelet analysis on the switching phenomenon,” *Journal of Fluids and Structures*, vol. 18, no. 3–4, pp. 325–346, Sep. 2003.

[41] M. Mahbub Alam and Y. Zhou, “Strouhal numbers, forces and flow structures around two tandem cylinders of different diameters,” *Journal of Fluids and Structures*, vol. 24, no. 4, pp. 505–526, May 2008.

[42] N. Mahir and D. Rockwell, “Vortex Formulation From a Forced System of Two Cylinders. Part II: Side-By-Side Arrangement,” *Journal of Fluids and Structures*, vol. 10, no. 5, pp. 491–500, Jul. 1996.

[43] N. Mahir and D. Rockwell, “Vortex Formulation From a Forced System of Two Cylinders. Part I: Tandem Arrangement,” *Journal of Fluids and Structures*, vol. 10, no. 5, pp. 473–489, Jul. 1996.

[44] A. Mohany and S. Ziada, “Flow-excited acoustic resonance of two tandem cylinders in cross-flow,” *Journal of Fluids and Structures*, vol. 21, no. 1, pp. 103–119, Nov. 2005.

[45] A. Mohany and S. Ziada, “A Parametric Study of the Resonance Mechanism of Two Tandem Cylinders in Cross-Flow,” *Journal of Pressure Vessel Technology*, vol. 131, no. 2, p. 21302, 2009.

[46] A. Mohany and S. Ziada, “Numerical Simulation of the Flow-Sound Interaction Mechanisms of a Single and Two-Tandem Cylinders in Cross-Flow,” *Journal of Pressure Vessel Technology*, vol. 131, no. 3, p. 31306, 2009.

[47] A. Mohany and S. Ziada, “Effect of acoustic resonance on the dynamic lift forces acting on two tandem cylinders in cross-flow,” *Journal of Fluids and Structures*, vol. 25, no. 3, pp. 461–478, Apr. 2009.

[48] A. Mohany and S. Ziada, “Measurements of the dynamic lift force acting on a circular cylinder in cross-flow and exposed to acoustic resonance,” *Journal of Fluids and Structures*, vol. 27, no. 8, pp. 1149–1164, Nov. 2011.

[49] A. Mohany, D. Arthurs, M. Bolduc, M. Hassan, and S. Ziada, "Numerical and experimental investigation of flow-acoustic resonance of side-by-side cylinders in a duct," *Journal of Fluids and Structures*, vol. 48, pp. 316–331, Jul. 2014.

[50] A. Mohany, "Flow-Sound Interaction Mechanisms of a Single and Two Tandem Cylinders in Cross-flow," Doctor of Philosophy, McMaster University, Canada, 2007.

[51] P. M. Morse and K. U. Ingard, *Theoretical acoustics*. Princeton, N.J: Princeton University Press, 1986.

[52] M. Naguib Mikhail and M. R. El-Tantawy, "Effect of the medium viscosity on sound propagation and attenuation in ducts," *Journal of Computational and Applied Mathematics*, vol. 45, no. 3, pp. 283–298, May 1993.

[53] A. Oengören and S. Ziada, "Vorticity shedding and acoustic resonance in an in-line tube bundle part II: Acoustic resonance," *Journal of Fluids and Structures*, vol. 6, no. 3, pp. 293–309, May 1992.

[54] A. Oengören and S. Ziada, "An In-depth Study of Vortex Shedding, Acoustic Resonance and Turbulent Forces In Normal Triangle Tube Arrays," *Journal of Fluids and Structures*, vol. 12, no. 6, pp. 717–758, Aug. 1998.

[55] A. Okajima, "Flows around Two Tandem Circular Cylinders at Very High Reynolds Numbers," *Bulletin of JSME*, vol. 22, no. 166, pp. 504–511, 1979.

[56] P. R. Owen, "Buffeting excitation of boiler tube vibration," *ARCHIVE: Journal of Mechanical Engineering Science 1959-1982 (vols 1-23)*, vol. 7, no. 4, pp. 431–439, Dec. 1965.

[57] R. Parker, "Acoustic resonances in passages containing banks of heat exchanger tubes," *Journal of Sound and Vibration*, vol. 57, no. 2, pp. 245–260, Mar. 1978.

[58] M. C. A. M. Peters, A. Hirschberg, A. J. Reijnen, and A. P. J. Wijnands, "Damping and reflection coefficient measurements for an open pipe at low Mach and low Helmholtz numbers," *Journal of Fluid Mechanics*, vol. 256, no. 1, p. 499, Nov. 1993.

[59] A. Powell, "Theory of Vortex Sound," *The Journal of the Acoustical Society of America*, vol. 36, no. 1, p. 177, 1964.

[60] Lord Rayleigh, "LXI. *Acoustical observations*," *Philosophical Magazine Series 5*, vol. 3, no. 20, pp. 456–464, Jun. 1877.

[61] E. F. Relf, “XVII. *On the sound emitted by wires of circular section when exposed to an air-current*,” *Philosophical Magazine Series 6*, vol. 42, no. 247, pp. 173–176, Jul. 1921.

[62] O. Reynolds, “An Experimental Investigation of the Circumstances which determine whether the Motion of Water shall be Direct or Sinuous, and of the Law of Resistance in Parallel Channels.,” *Philosophical Transactions of the Royal Society of London*, vol. 174, pp. 935–982, 1883.

[63] E. Rodarte and N. R. Miller, “Flow-Induced Noise in Heat Exchangers,” University of Illinois, 2001.

[64] E. Rodarte, G. Singh, N. R. Miller, and P. Hrnjak, “Sound Attenuation in Tubes Due to Visco-thermal Effects,” *Journal of Sound and Vibration*, vol. 231, no. 5, pp. 1221–1242, Apr. 2000.

[65] A. Roshko, “On the Drag and Shedding Frequency of Two-dimensional Bluff Bodies,” California Institute of Technology, National Advisory Committee for Aeronautics, Technical, 1954.

[66] A. Roshko, “Experiments on the flow past a circular cylinder at very high Reynolds number,” *Journal of Fluid Mechanics*, vol. 10, no. 3, p. 345, May 1961.

[67] F. Sanna, “Acoustical Damping in a Circular Pipe with and Air-Water Mixture Flow: A New Design Setup,” in *11th Conference on Flow-Induced Vibration and Noise*, The Hague, The Netherlands, 2016.

[68] M. Shaaban and A. Mohany, "Parametric Investigation of the Flow-Excited Acoustic Resonance From Multiple In-Line Cylinders in Cross-Flow”, *Proceedings of the ASME 2015 Pressure Vessels and Piping Conference, Volume 4: Fluid-Structure Interaction*, 2015.

[69] V. Strouhal, “Ueber eine besondere Art der Tonerregung,” *Annalen der Physik und Chemie*, vol. 241, no. 10, pp. 216–251, 1878.

[70] D. Sumner, S. S. . Wong, S. . Price, and M. . PaïDoussis, “Fluid Behaviour of Side-by-side Circular Cylinders in Steady Cross-flow,” *Journal of Fluids and Structures*, vol. 13, no. 3, pp. 309–338, Apr. 1999.

[71] D. Sumner, “Two Circular Cylinders in Cross-Flow: A Review,” *Journal of Fluids and Structures*, vol. 26, no. 6, pp. 849–899, Aug. 2010.

[72] C. H. K. Williamson and A. Roshko, “Vortex formation in the wake of an oscillating cylinder,” *Journal of Fluids and Structures*, vol. 2, no. 4, pp. 355–381, Jul. 1988.

[73] M. M. Zdravkovich, "REVIEW—Review of Flow Interference Between Two Circular Cylinders in Various Arrangements," *Journal of Fluids Engineering*, vol. 99, no. 4, p. 618, 1977.

[74] M. M. Zdravkovich, "Flow-induced oscillations of two interfering circular cylinders," *Journal of Sound and Vibration*, vol. 101, no. 4, pp. 511–521, Aug. 1985.

[75] M. M. Zdravkovich, "The effects of interference between circular cylinders in cross-flow," *Journal of Fluids and Structures*, vol. 1, no. 2, pp. 239–261, Apr. 1987.

[76] M. M. Zdravkovich, *Flow around circular cylinders: a comprehensive guide through flow phenomena, experiments, applications, mathematical models, and computer simulations*. Oxford; New York: Oxford University Press, 1997.

[77] S. Ziada, A. Oengören, and E. T. BÜhlmann, "On acoustical resonance in tube arrays part I: Experiments," *Journal of Fluids and Structures*, vol. 3, no. 3, pp. 293–314, May 1989.

[78] S. Ziada, A. Oengören, and E. T. Bühlmann, "On acoustical resonance in tube arrays part II: Damping criteria," *Journal of Fluids and Structures*, vol. 3, no. 3, pp. 315–324, May 1989.